AD-A069 727 SYSTEMS SCIENCE AND SOFTWARE LA JOLLA CALIF F/G 8/11
SYNTHESIS OF REGIONAL GROUND MOTION FROM WESTERN U. S. EARTHQUA--ETC(U)
MAR 79 W L RODI, T C BACHE, H J SWANGER F19628-77-C-0004
UNCLASSIFIED SSS-R-79-3988 AFGL-TR-79-0080 NL

1 OF 3
AD
A069727

LEVEL II

12

AFGL-TR-79-0080

SYNTHESIS OF REGIONAL GROUND MOTION FROM WESTERN U. S. EARTHQUAKES

W. L. Rodi
T. C. Bache
H. J. Swanger
T. G. Barker
J. T. Cherry

Systems, Science and Software
P. O. Box 1620
La Jolla, California 92038

Final Report
November 1977 - December 1978

Approved for public release; distribution unlimited

29 March 1979

Air Force Geophysics Laboratory
Air Force Systems Command
United States Air Force
Hanscom AFB, Massachusetts 01731

UNCLASSIFIED

SECURITY CLASSIFICATION OF THIS PAGE (When Data Entered)

REPORT DOCUMENTATION PAGE

READ INSTRUCTIONS BEFORE COMPLETING FORM

1. REPORT NUMBER: AFGL-TR-79-0080	2. GOVT ACCESSION NO.
3. RECIPIENT'S CATALOG NUMBER	
4. TITLE (and Subtitle): SYNTHESIS OF REGIONAL GROUND MOTION FROM WESTERN U. S. EARTHQUAKES.	5. TYPE OF REPORT & PERIOD COVERED: Final Report. Nov 1977-Dec 1978
	6. PERFORMING ORG. REPORT NUMBER: SSS-R-79-3988
7. AUTHOR(s): W. L. Rodi, T. C. Bache, H. J. Swanger, T. G. Barker and J. T. Cherry	8. CONTRACT OR GRANT NUMBER(s): F19628-77-C-0004
9. PERFORMING ORGANIZATION NAME AND ADDRESS: Systems, Science and Software, P. O. Box 1620, La Jolla, California 92038	10. PROGRAM ELEMENT, PROJECT, TASK AREA & WORK UNIT NUMBERS: 61102F 2309G1AC
11. CONTROLLING OFFICE NAME AND ADDRESS: Air Force Geophysics Laboratory, Hanscom AFB, Massachusetts 01731, Monitor/Henry Ossing/LWH	12. REPORT DATE: 29 March 1979; 13. NUMBER OF PAGES: 204
14. MONITORING AGENCY NAME & ADDRESS (if different from Controlling Office): 286 p.	15. SECURITY CLASS. (of this report): Unclassified
	15a. DECLASSIFICATION DOWNGRADING SCHEDULE

16. DISTRIBUTION STATEMENT (of this Report)

Approved for Public Release; Distribution Unlimited

17. DISTRIBUTION STATEMENT (of the abstract entered in Block 20, if different from Report)

18. SUPPLEMENTARY NOTES

19. KEY WORDS (Continue on reverse side if necessary and identify by block number)

Earthquake ground motion
Synthetic seismograms

20. ABSTRACT (Continue on reverse side if necessary and identify by block number)

Synthetic displacement, velocity and acceleration seismograms and the resulting response spectra are computed and analyzed for earthquake ground motions in the western United States. A source model for the 1975 Pocatello Valley earthquake (developed under this contract and reported by Day, et al., 1978) is used with plane layered earth models to estimate the ground motions at Minuteman Wing V which is at a range of about 700 km. (continued)

→ next page

DD FORM 1 JAN 73 1473 EDITION OF 1 NOV 65 IS OBSOLETE

388 507

UNCLASSIFIED

SECURITY CLASSIFICATION OF THIS PAGE (When Data Entered)

20. ABSTRACT (continued)

The 1975 Yellowstone earthquake was a similar event at the same range from Wing V. However, the ground motions are estimated to be an order of magnitude smaller due to three effects: (1) the two earthquakes were the same size at long periods but the Yellowstone event appears to be a factor of 2 to 4 smaller at short periods; (2) the sources are oriented such that radiation pattern differences between the two events are nearly maximum; (3) the Yellowstone caldera and, perhaps, other highly attenuating structures to the south cause the Wing V ground motions from the Yellowstone event to be much smaller than otherwise expected.

Synthetic seismograms are also computed for typical western U. S. events at ranges of 150 and 250 km. Comparisons are made to show the effects of crustal structure, radiation pattern, focal depth and magnitude. Results from the synthetic seismogram calculations spanning ranges from 150 to 768 km are compared to empirical estimates of the attenuation with range of peak displacement, velocity and acceleration. The two are found to be in reasonable agreement.

The report also includes brief discussions of the effects of site topography on earthquake ground motions and the similarity between earthquake and surface burst induced ground motions. These discussions summarize results in the literature and identify areas requiring further investigation.

TABLE OF CONTENTS

I. INTRODUCTION AND SUMMARY

1.1 INTRODUCTION

The objectives of this contract may be summarized as follows:

1. Determine a source model for the 1975 Pocatello Valley earthquake.
2. Compute the likely ground motion at the Wing V Minuteman site due to the Pocatello Valley event and determine those features of the source or propagation path that may have caused this ground motion to be peculiar or untypical of western U. S. earthquakes.
3. Compute synthetic seismograms for typical western U. S. earthquakes using appropriate earth models and determine the important characteristics of the ground motions at ranges of 150-250 km.
4. Provide initial estimates of the similarities and differences between the surface motions generated by earthquakes and large surface nuclear explosions.

In a previous report, "A Source Model for the 1975 Pocatello Valley Earthquake", by S. M. Day, T. C. Bache, T. G. Barker and J. T. Cherry, we determined a source model for the Pocatello Valley earthquake. We found the Pocatello Valley earthquake to be quite typical of the shallow thrust or normal faulting events that frequently occur in the western U. S., especially in the Basin and Range tectonic province. Thus, in our previous report, we were concerned with the first objective and a minor portion of the second.

In this report we intend to summarize our entire research program, but are primarily concerned with describing our work to accomplish the last three objectives listed. This introductory section may be read as a summary of the entire program and we have tried to include all the important conclusions. Detailed discussions of the results leading to these conclusions are presented in succeeding sections of the report.

A special feature of this research effort is the unified application of several techniques that have only recently, if ever, been attempted before. These include the following:

1. A fully three-dimensional finite difference simulation of relaxation earthquake faulting. One calculation allowed simple (elastic-plastic) nonlinear material behavior near the fault surface. These simulations were done on the ILLIAC IV computer.
2. The use of synthetic seismograms computed with a dynamic fault model to infer the source characteristics of a particular earthquake from teleseismic data.
3. The computation of regional (150-750 km) ground motions for a realistic earthquake fault model and a realistic plane-layered earth model.

We will be saying more about these techniques and their application to achieve our stated objectives in the next section.

1.2 OUTLINE OF THE RESEARCH PROGRAM

We begin by listing in outline form the various elements of our research program. The research results presented

in our previous report (Day, et al., 1978), and in this report conform closely to this outline.

I. Develop a Source Model for the 1975 Pocatello Valley Earthquake

A. Apply conventional methods to constrain the focal plane.

1. Construct a focal mechanisms solution from P wave first motion data.

2. Study the aftershock distribution.

B. Using a dynamic fault model (the Archambeau/Minster model), compare synthetic and observed seismograms to estimate dynamic fault parameters.

II. Confirm the physical parameter estimates of the Archambeau/Minster model by comparing with results from three-dimensional finite difference simulations of earthquake faulting. (The Archambeau/Minster model is cast in an unrealistic spherical geometry and the inferred parameters are therefore subject to some question. The finite difference simulations were as realistic as any ever done.)

A. Test the ILLIAC version of our earthquake modeling program by comparing to analytical results.

B. Compute two full-scale ILLIAC simulations of bilateral earthquake faulting using initial estimates of the source parameters for the Pocatello Valley earthquake. One simulation was fully elastic, the second included elastic-plastic material behavior near the fault plane.

C. For similar source parameters, compare the predicted ground motions for the finite difference and Archambeau/Minster models.

III. Estimate the ground motions at Wing V due to the 1975 Pocatello Valley earthquake.

A. Using published information, estimate the range of earth velocity and attenuation models likely to be encountered.

B. Compute the ground motions.

1. The source model is that deduced in I, the earth models are from A.

2. Displacement, velocity, acceleration and response spectra are computed and compared.

C. Discuss the potential effects of non-planar layering, particularly the ridge and valley topography at the Wing V site.

IV. Estimate the ground motions at Wing V due to the 1975 Yellowstone earthquake.

A. The Pocatello Valley and Yellowstone earthquakes are assumed to be the same except for known differences in the strike.

B. Known path differences are taken into account.

V. Estimate the likely ground motions at ranges of 150-250 km from typical Basin and Range earthquakes.

A. The source model for the Pocatello Valley earthquake and variations on this source are used to represent typical events.

B. Earth models representing the range of variations expected in the southwestern U. S. are used.

C. Synthetic displacement, velocity, acceleration and response spectra are computed and compared.

VI. Summarize the important similarities and differences between the ground motions induced by a large surface burst and shallow earthquakes.

In our previous report we were concerned with items I and II of this outline. The remaining four items are the subject of this report. Items III and IV of the outline are discussed in Sections II and III. Items V and VI are discussed separately in Sections V and VI.

The research program we have outlined here is based on the use of deterministic calculations of ground motions from earthquakes. Such a use of deterministic ground motion simulations to evaluate earthquake hazards is a method that must be described as being in its infancy. Our ground motion simulations include the following elements:

- Earthquake faulting on a single fault plane in a homogeneous material. Some variable rupture velocity/variable stress drop effects are included in a fairly simple fashion.
- Wave propagation in a laterally homogeneous, plane-layered earth.

Are the synthetic seismograms, when subjected to the above restrictions, sufficiently realistic to allow quantitative or even qualitative conclusions about ground motion characteristics of interest? We believe they are, but recognize that this assertion must be tested by comparison to observations. We will try to point out where we have most

confidence in our results, generally at the longer periods, and where we are less certain.

How important are the effects of multiple (on several fault planes) earthquake faulting, lateral inhomogeneity or non-planar layering on regional earthquake ground motion? These are questions that are properly addressed when we understand how well the data are explained with simpler assumptions. The work described in this report represents, we believe, the first attempt to study the characteristics of regional ground motion by direct simulation. The results demonstrate that there is much to be learned before it is necessary to include more complex models (which are only beginning to be developed anyway) than those we have used.

In the remainder of Section I we will summarize the important results. The format closely follows the outline given earlier in this subsection.

1.3 A SOURCE MODEL FOR THE 1975 POCATELLO VALLEY EARTHQUAKE

The source parameters of the earthquake were inferred in the following way:

- A focal mechanism solution was constructed from observations of P wave first motion.
- Results from a study of the aftershock sequence by Arabasz, et al. (1975) were examined to further constrain the fault plane orientation.
- Using the Archambeau/Minster earthquake source model (Archambeau 1968; Minster, 1973) and methods for computing synthetic seismograms in layered earth models (Bache and Harkrider, 1976), synthetic seismograms were computed for comparison to long and short period P wave observations.

- The model parameters were varied to obtain estimates for the source dimension, rupture velocity and stress drop as well as confirming the orientation. The main diagnostic features of the observations are the waveform and frequency content of the P and pP phases, their time delay and their relative amplitudes.

An important conclusion of this study is that no uniform stress drop, uniform rupture velocity model can simultaneously fit the long and short period data. We were led to the same conclusion in an earlier study of the 1971 San Fernando earthquake (Bache and Barker, 1978). To improve the fit to the data over a broad frequency range, variable stress drop and variable rupture velocity effects were introduced into the analytical source model. This was done in a rather ad hoc fashion and the results are far from unique. However, we claim that they are qualitatively correct. The new source model gives a reasonably good fit to the long and short period data for the first 5 to 8 seconds of faulting.

Our final model for the Pocatello Valley fault may be described as follows:

Strike:	N45°E
Dip:	39°W
Slip:	Up 53°N*, Unilateral toward the surface
Fault Length:	7 km
Focal Depth:	8.7 km

*This is normal faulting with a large left-lateral strike-slip component.

Rupture Velocity:	3 km/s	$0 \leq L \leq 4$,*
	$(21-3L)^{1/2}$ km/s	$4 \leq L \leq 7$,
Stress Drop:	160 bars,	$0 \leq L \leq 4$,
	$1.7\ (21-3L)^{3/2}$ bars	$4 \leq L \leq 7$.

The parameters of this source are given in very specific form. What confidence do we have in these values? We can say that the source specified by these parameters gives a reasonably good match to the first 5-8 seconds of the teleseismic records. The teleseismic recordings indicate that the source is certainly more complicated; the duration of motion is much longer than 5 to 8 seconds. Therefore, we can say with some confidence that we have, at least, an equivalent elastic source representation for the early, and largest, portion of the faulting.

How closely do the source parameters for our "equivalent source" correspond to the actual physical parameters of the earthquake? This depends on how well our model represents earthquake physics. This question is addressed in Section 1.5.

1.4 THREE-DIMENSIONAL FINITE DIFFERENCE SIMULATIONS OF EARTHQUAKE FAULTING

Two three-dimensional finite difference calculations, simulating faulting in a uniform whole space, were performed. The first calculation was for a linearly elastic medium; the second treated an elastic-plastic medium. The accuracy of the finite difference method was verified by comparing the results to analytical and numerical solutions of crack problems. The far-field displacements associated with the finite difference simulations were obtained using an elastodynamic representation theorem. This integral representation was applied in two different forms and the far-field results compared.

---

*L is position along the fault.

An important objective was to evaluate the near-field and far-field effect of nonlinear deformation in the fault zone. It was found that the initial portion of the slip time-function is unaffected by the admission of a simple form of plasticity. The large velocity peak at the crack tip, characteristic of elastic crack problems, persisted in the inelastic case. The stopping phase was modified somewhat, however. Yielding at the edge of the fault resulted in less abrupt stopping, reducing the high-frequency content of both the slip function and the far-field displacements, and increasing the average slip by 11 percent. Accumulation of plastic strain beyond the fault edge resulted in a 38 percent higher moment than in the elastic case.

These effects of plasticity depend upon our choice of the magnitude of prestress, the yield strength, the frictional stress, and the width of the nonlinear zone. The problem treated was an extreme case in the sense that the prestress level everywhere equaled the strength of the medium ($Y/\sqrt{3}$). With a moderate increase in the yield strength (26 percent), or a similar decrease in the prestress, there would have been no yielding, and the solution would have been identical to that of the elastic problem. On the other hand, we arbitrarily limited the extent of the plastic zone. Outside the plastic zone, a static shear stress concentration persisted which was nearly as large as that of the elastic case; had the plastic zone been larger, more plastic strain would have occurred, resulting in an even larger seismic moment.

1.5 COMPARISON OF ANALYTICAL AND FINITE DIFFERENCE MODELS

In Section 1.3 we described a model for the Pocatello Valley earthquake which was determined using the analytical relaxation model of Archambeau (1968) and Minster (1973). This analytical model is convenient to use because it is expressed in terms of relatively few parameters. However,

interpretation of these parameters in terms of earthquake physics is quite controversial because of the geometry in which the source model is formulated. The Archambeau/Minster source is a spherical volume of reduced shear strength which grows in a pure shear prestress field. The growth is asymmetric with a point on the boundary being fixed as shown below.

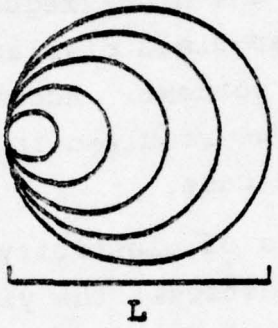

This model does include directionalized rupture, finite source dimension and finite rupture velocity effects, but in a geometry unlike conventional ideas of earthquake geometries.

The ILLIAC calculations of earthquake faulting described in Section 1.4 are close to the most detailed and realistic models of earthquake faulting that are currently available. The disadvantage of using such calculations to model a particular earthquake is, of course, the expense of varying the parameters. The parameters for our two calculations are not entirely fixed, however, because the fault dimension and stress drop can be scaled.

Taken together, the analytical models and the ILLIAC calculations can be used to define the earthquake source with considerable confidence. Questions about the physical significance of parameters of the analytical model can be resolved by comparing to the numerical model results.

Comparison of the finite difference and analytical models by means of synthetic seismograms appropriate for stations observing the Pocatello Valley event suports our conclusions about earthquake faulting reached with the analytical models. That is, we cannot simultaneously match the long and short period data with a single rupture velocity/ single stress drop source model.

Another interesting facet of the comparison is that source directivity effects can be seen in that data. The finite difference simulations are bilateral and give poorer agreement with the short period data than the unilateral analytical model.

Finally, we conclude that the variable rupture velocity analytical model is a good model for the initial few seconds of rupture of the Pocatello Valley earthquake. The long and short period teleseismic records show that the source is more complex and has longer duration. The later faulting is, however, considerably smaller as a source of seismic waves so our model should give a reasonable estimate for the peak ground motions at the regional ranges of ultimate interest.

1.6 ESTIMATED GROUND MOTIONS AT WING V FROM THE POCATELLO VALLEY EARTHQUAKE

An important objective of this contract was to estimate the likely ground motions at the Minuteman Wing V site from the Pocatello Valley earthquake. Observations of the ground motion were too sparse to allow direct inference of these motions. Therefore, our idea was to first infer the source parameters from the data that were available and then compute the ground motions at Wing V consistent with this source model.

In Section 1.3 we described our inferred source model for the Pocatello Valley event. This model is consistent with

the first 5 to 8 seconds of the teleseismic observations for periods of 0.5 seconds and longer. If we can properly account for path effects, we should be able to use this model to estimate the ground motions at the Wing V range (≃ 700 km). The important approximations are as follows:

- Our estimate for the source amplitude depends on our ability to correctly account for the path attenuation. An error of about a factor of two in the source amplitude is possible.
- We model the path from the earthquake epicenter to Wing V with a plane layered earth model intended to represent the average properties of the path. We have insufficient information to do this with full confidence. We compute with several models to define the range of effects.
- Our computations are accurate to about one hertz or a bit higher. At frequencies much above one hertz, neither the source model nor the propagation calculations are considered to be very accurate.

In Section II we describe our estimates of the ground motions at Wing V from the Pocatello Valley earthquake. Three-component displacement, velocity and acceleration seismograms are computed at two sites at either end of Wing V. Response spectra are also computed. We use a basic path model that represents our best estimate of the velocity and Q structure. Calculations are also done with a second velocity structure that has no sedimentary layer at the surface. This layer has a strong influence on the high frequency motions so the two earth models are intended to bracket this effect. We also compute with a second Q model in which all Q values are doubled. Thus, there are a total of four models that define a range of predicted ground motions.

An average of the peak motions obtained for the two sites and four path models gives an idea of the typical peak ground motion levels our calculations predict at Wing V. These averages are:

Average Peak Displacement: 0.08 cm

Average Peak Velocity: 0.13 cm/sec

Average Peak Acceleration: 0.35 cm/sec^2

Typical periods of the peak motions are 5 seconds for displacement, 3-4 seconds for velocity and 2-3 seconds for acceleration. In most cases the peak displacements are from the fundamental mode Rayleigh or Love wave and the peak accelerations are from the S or Lg phases. The average values given above may be high because the perturbations on our "best" estimate for the velocity and Q structure tend to increase the ground motions.

For our best estimate for the structure, the peak motions at the closer of the two Wing V sites are:

Peak Displacement: 0.05 cm (Tangential)

Peak Velocity: 0.12 cm/sec (Radial)

Peak Acceleration: 0.35 cm/sec^2 (Radial)

The corresponding values for the farther Wing V site are about half these. As noted, the largest motions are on the horizontal components.

These estimated peak ground motions are in reasonable agreement with estimates from empirically determined ground motion attenuation curves. We compare our values to those from nine different empirical studies in Table 3.

Our discussion of the Pocatello Valley earthquake ground motions is completed with a presentation of the range of estimated response spectra (Figures 7 through 9). The spectra are rather sharply peaked with maxima at periods

between 1.5 and 5 seconds. Typical maxima are 0.2 cm for relative displacements, 0.4 cm/sec for pseudo-relative velocity and 0.4 cm/sec^2 for absolute acceleration. The response curves decay rapidly for periods below 1 to 20 seconds. This is plausible for this range, but may be due, in part, to our failure to properly compute the ground motions at the higher frequencies.

1.7 COMPARISON OF GROUND MOTIONS FROM THE 1975 POCATELLO VALLEY AND YELLOWSTONE PARK EARTHQUAKES

The 1975 Pocatello Valley and Yellowstone Park earthquakes were superficially similar events at virtually the same range from Wing V. What were the likely ground motions from the two and how did they differ? The moment and M_s for the two events indicate no differences in the excitation of long period waves. There are two measures for the short period amplitude, M_L and m_b. The former is from two regional stations and is the same for both. The m_b is a measure of the downgoing P waves near 1 Hz. By this measure the Yellowstone event is about a factor of three smaller than the other. There are insufficient data to define the Yellowstone source in the same detail as we did the Pocatello Valley source. Therefore, our approach is to assume the two sources are identical. This means that we compute an upper bound estimate for the Yellowstone ground motion at 1 Hz. At longer periods the data indicate that the two sources are nearly the same.

Work by Pitt, Weaver and Spence (1979) allows a reasonably confident definition of the main fault plane of the Yellowstone event. The event was characterized by normal faulting on a plant dipping about 45°. The strike is well defined as being N50°W. The slip appears to be vertical, but there may have been some strike-slip component.

One important difference between the two events is that Wing V is at a different location with respect to the strike for the two events and thus sees a different portion of the

radiation pattern. Travel path differences can also cause differences in the ground motions. As far as we know, the two paths are the same except for the Yellowstone caldera which lies directly astride the path to Wing V. We expect this to sharply attenuate the motions.

There is independent evidence for the Wing V ground motions from the Yellowstone event being anomolously low. Isoseismal intensity maps for this and other historical earthquakes in the region show a distinct asymmetry with lows to the south. Pitt, et al. (1979) report some instrumental confirmation of the asymmetry for the Yellowstone event and its aftershocks.

We compare the ground motions for the two events, assuming they are identical except for two effects; the source orientation and the presence of the caldera. The Pocatello Valley event is oriented to focus high frequency energy toward Wing V. The Yellowstone event is on a low portion of the radiation pattern for high frequencies. These known differences in the radiation pattern cause differences in the peak accelerations of a factor of 3-5. The peak velocities and displacements differ somewhat less.

We account for the presence of the caldera in an ad hoc way by assuming the Q in that region, which makes up about 10 percent of the path, to be one-tenth the standard Q. The effect was to reduce the acceleration, velocity and displacement by 40 percent, 35 percent and 20 percent, respectively. We also computed with Q/20 in the caldera to show a range of effects.

Accounting for both radiation pattern and Q effects, our best estimates of the ratio of Pocatello Valley to Yellowstone peak motions are as follows:

	Q/10	Q/20
Peak Displacement	1.7	2.1
Peak Velocity	4.5	6.6
Peak Acceleration	7.9	13.7

In every case, the peak motions are from horizontal components. The dominant periods are 2-4 seconds for the accelerations and somewhat larger for velocities and displacements. Since these estimates take no account of the likelihood that the Yellowstone earthquake was a weaker source of energy near 1 Hz, we view these as lower bounds for the ratios.

We also compare the response spectra from the ground motion estimates for the two events. They are consistent with the ratios of peak motions given above, differing by about an order of magnitude.

Our conclusions about the relative ground motions from the two events may be summarized as follows. The ground motions at Wing V due to the Pocatello Valley event were probably a bit larger than usual because the event happened to be oriented to focus energy in that direction. More important is the near certainty that the Yellowstone ground motions were much smaller than usual for this size event. A small contributor was the source orientation which put Wing V or a low part of the radiation pattern. The most important factor is the Yellowstone caldera and, perhaps, other highly attenuating structures to the south of the epicenter. Also important is the probability that the Yellowstone earthquake source was a factor of 2-3 smaller at short periods.

1.8 EFFECTS OF SITE TOPOGRAPHY ON EARTHQUAKE GROUND MOTION

Our ground motion estimates discussed in previous sections were computed with plane-layered models for the earth. Thus, we estimate the "average" ground motion at the sites at Wing V; we take no account of local structure that may cause differences at sites in close proximity. In fact, the ground motions were significantly variable across Wing V (see Figure 22).

A general observation about the observed variation in ground motions across Wing V is that sites on plateaus had

larger motions than those in lower lying valleys (R. A. Gray, private communication). This leads naturally to the hypothesis that the differences were due to the surface topography. We discuss that possibility in Section IV.

The possible causes for ground motion differences between sites can be divided into four categories:

1. Source radiation pattern.
2. Deep structure (several kilometers and more) that focuses and channels the seismic waves.
3. Local site geology; for example, the depth to bedrock.
4. The local site topography, e.g., ridge versus valleys.

The first cause seems most implausible in this case. There is ample evidence in the literature for the importance of the second and third causes, particularly the latter. On the other hand, very little has been done with the fourth item listed. This is an area in which research is just beginning..

Published work has shown that topographic effects can amplify or deamplify ground motions by a factor of two or so. However, these effects are highly variable and depend upon local topographic details. More important, the topographic influence is not felt for wavelengths much larger than the scale of the topographic feature. Examination of topographic maps of the Wing V site indicates that sharp topographic changes occur on vertical scales of no more than a few hundred meters. We conclude that it is unlikely that the topography has much influence on periods longer than, say, 0.5 seconds.

More likely causes for the observed ground motion differences are items 2 and 3 of the above list. The deep structural effects are relatively difficult to quantify, though it could be done. However, there has been a great amount of work devoted to the effects of local site geology.

Given information about the local site geology, results from this work may be able to explain the observed ground motion differences.

1.9 GROUND MOTIONS AT 150 AND 250 KM FROM WESTERN U. S. EARTHQUAKES

To this point we have been concerned with the ground motions at Wing V for two specific events. Only a few ranges and azimuths have been considered, but the results seem to be rather good. A natural extension of this work is to estimate the ground motion at other locations. More generally we can determine the effect of the important source and path parameters on the earthquake ground motions.

In Section V we turn our attention to earthquake ground motions at ranges of 150 and 250 km. Our objective is to estimate these ground motions for "typical" western U. S. events and typical western U. S. crustal structure. We use our experience with the Pocatello Valley and Yellowstone earthquakes as a starting point. They represent, as far as we know, typical events. The path models used in Sections II and III are, once again, "typical" western U. S. crustal models. We add another crustal model which we know to be appropriate for the path from NTS to Tucson, Arizona.

An exhaustive study of the many source and path parameters controlling the ground motions was not attempted. Only a few variations were possible within the limits of this contract, but they are intended to illustrate the important trends. The comparisons presented in Section V include the following:

1. Seismograms were computed at two azimuths on high and low portions of the radiation pattern for the Pocatello Valley source model.
2. Seismograms were computed for three path models, Structures A and B which differ only in the

sedimentary layer and the NTS-TUC structure which is rather different from the other two.

3. The depth effect is investigated by computing seismograms with focal depths of 8.7 and 5 km. Both depths are, of course, quite shallow so we see the effect of small perturbations in this parameter.

4. Seismograms were computed for a source like the Pocatello Valley event, but with larger source dimension, giving an M_s that is about a unit larger.

For each case, comparisons are based on displacement, velocity and acceleration seismograms and on responsive a. Our conclusions may be listed item by item.

1. The radiation pattern effects are strongest at the higher frequencies. These effects are distance-dependent since energy leaving the source at many different angles interferes to make up the seismogram. On the vertical/radial motion the effects are small at 150 km and large at 250 km. On the tangential component, the effects are the same at both ranges. Differences between the response spectra at the azimuths compared are as much as an order of magnitude at high frequencies.

2. Path structure affects almost every feature of the seismogram. Most obvious is the effect on duration which strongly depends on the thickness of the sedimentary layer. In most cases, peak motions differ by about a factor of two among the structures. Differences larger than this occur when the peak is controlled by the P wave whose amplitude is more structure-dependent than for other phases.

3. The effect of depth is to change the frequency content and relative amplitude of different phases on the seismograms. The shallower depth causes greater excitation of short period fundamental mode surface-waves while reducing the amplitude of Lg and P. The response spectra are larger for the shallow source at longer periods and vice versa at short periods.

4. The larger magnitude source is characterized by a larger source dimension and, therefore, a lower corner frequency. Ground motion differences between the two are, as expected, greatest at the longer periods and are generally less at higher frequencies. Unexpected interference effects can, however, cause this general rule to be violated.

1.10 COMPARISON OF PEAK MOTIONS FROM THE SYNTHETIC SEISMOGRAMS WITH THOSE FROM EMPIRICAL ESTIMATES

Many of the synthetic seismograms presented in this report were computed with essentially the same source model. Seismograms were computed for ranges from 150 km to 768 km. In Section 5.6 we plot our peak displacements, velocities and accelerations together with the ground motion attenuation curves from as many as seven different studies.

Our synthetic seismogram estimates for the peak motions generally fall within the bounds outlined by the empirical curves. Figures 48, 49 and 50 show the comparison. Generally, our values plot in the lower portion of the range of empirical estimates. This agreement with the empirical data is as good as can be expected and greatly enhances confidence in the procedures used in this research program.

1.11 COMPARISON OF EARTHQUAKE AND SURFACE BURST INDUCED GROUND MOTIONS

One of the tasks of this contract was to provide some initial estimates of similarities and differences between the ground motions generated by earthquakes and large surface nuclear explosions. We also proposed to outline the steps required to develop a quantitative capability to link predictions of the energy coupling of nuclear weapons into the ground with the ground motion propagation techniques used in earthquake studies. The latter was done some time ago and resulted in a proposal to AFGL to actually complete and exercise the link between the coupling and propagation calculations. This proposal resulted in a contract (Contract No. F19628-79-C-0003) and the work is now in progress.

In Section VI we give a brief summary of the qualitative similarities and differences between ground motions from a large surface burst and its associated airblast and shallow earthquakes of moderate size. One difference is that the surface burst may be viewed as a sum of surface point loads while an earthquake is viewed as a series of shear dislocations. The radiation pattern of compressional and shear waves is then quite different. The surface burst is approximately axisymmetric while earthquakes exhibit strong azimuthal variations. Dislocation sources are very efficient generators of shear waves compared to surface bursts. Ideal models of the latter source indicate that no horizontal shear energy should be present.

Another difference between the two sources is associated with the depth of the energy release. Surface bursts should be much more efficient generators of short-period surface waves which can dominate the motion at close ranges.

As far as the source coupling is concerned, there is good evidence that the air-blast is most important for the

longer period ground motions (Auld and Murphy, 1979). There have been few calculations to fully explore the induced ground motions due to this kind of source. In Section 6.4 we describe how these calculations can be done.

The ground motion coupling of the surface explosion is even less well understood as far as its excitation of waves in the elastic regime is concerned. Our current AFGL contract is intended to study such things as the relative importance of the ground coupling and air-blast on the ground motions at various ranges. Earthquake coupling into ground motions is relatively well understood and other sections of this report include many pertinent results.

1.12 SUMMARY OF THE MATERIAL PRESENTED IN APPENDICES A, B AND C

In the main body of the report we show only enough seismograms to illustrate the important points. All synthetic seismograms computed for this study are plotted in Appendices A and B. In Appendix A are the displacement, velocity and acceleration records for the Pocatello Valley and Yellowstone Park earthquake induced ground motions at Wing V. The seismograms presented in Sections II and III are a subset of those in Appendix A.

The seismograms in Appendix B are the complete set for our ground motion calculations at 150 and 250 km. That is, the seismograms of Section V are a subset of those shown in Appendix C.

An important part of the ground motion for each synthetic seismogram is that due to the superposition of Rayleigh and Love wave modes. Generally, we include the first 6 to 7 modes up to frequencies of 2-4 Hz. The phase and group velocity dispersion for all modes used for the calculations in this report are plotted in Appendix C. In that Appendix we also plot

the velocity and density versus depth for the earth models considered.

1.13 CONTRIBUTING SCIENTISTS

The results presented in this report represent the work of a number of members of the Systems, Science and Software staff. J. T. Cherry was the Principal Investigator on the contract. The contributions of S. M. Day, T. C. Bache, T. G. Barker, J. T. Cherry, J. F. Masso, D. G. Lambert, B. F. Mason and E. J. Halda to the work presented in our earlier scientific report (Day, et al., 1978) were specified in that report. A somewhat different group accomplished the work described in this report.

The authors of the several sections of this report are as follows:

Section I : Introduction and Summary
T. C. Bache

Section II : Pocatello Valley Earthquake Motions at Wing V
W. L. Rodi

Section III: Comparison of Pocatello Valley and Yellowstone Events
W. L. Rodi and T. C. Bache

Section IV: Effects of Site Topography
H. J. Swanger and T. C. Bache

Section V: Ground Motions at 150 and 250 km
W. L. Rodi

Section VI: Comparison of Earthquake and Surface Burst Induced Ground Motions
J. T. Cherry and H. J. Swanger

The research reported here was directed by T. C. Bache as part of the Theoretical Geophysical Program at S^3. The contributions of W. L. Rodi and H. J. Swanger are reflected by the authorship indicated above. The model selection and design of the parameter variation studies was done in large

part by T. G. Barker. He also did all generalized ray theory calculations. B. F. Mason assisted with the computer programming in all stages of the effort. The manuscript was prepared by D. A. Roddy and E. Tessary.

II. ESTIMATED GROUND MOTIONS AT WING V FROM THE POCATELLO VALLEY EARTHQUAKE

2.1 INTRODUCTION

In Figure 1 we show the location of the Wing V site in the vicinity of the triple junction of Wyoming, Nebraska and Colorado. Two particular sites are identified on the figure and the direction to the Pocatello Valley earthquake epicenter from those sites is indicated. For Site 1, 680 km and 90° are the distance and azimuth from the epicenter and 768 km and 97° are these quantities for Site 2. We see that these two sites are reasonably representative of the variations in range and azimuth across the Wing V site.

In our previous work (Day, et al., 1978), summarized in Sections 1.3-1.5, we inferred a source model for the Pocatello Valley earthquake. In this section we use this model and a range of plausible path models to synthesize the ground motions at Sites 1 and 2. We compute synthetic displacement, velocity and acceleration seismograms and also compute the standard 5 percent damped response spectrum for each case.

2.2 COMPUTATIONAL METHOD

Synthetic regional seismograms were computed with a combination of two analytical wave-propagation techniques: generalized ray expansion, which was used for obtaining the early-arriving body waves, and modal superposition, used for S-wave arrivals and surface waves. Both techniques were implemented to accommodate an Archambeau-Minster relaxation source model (Archambeau, 1968; Minster, 1973) and a plane-layered elastic model of the structure along the source-receiver path. An approximate operator accounted for anelastic shear dissipation due to frequency-independent Q in the earth.

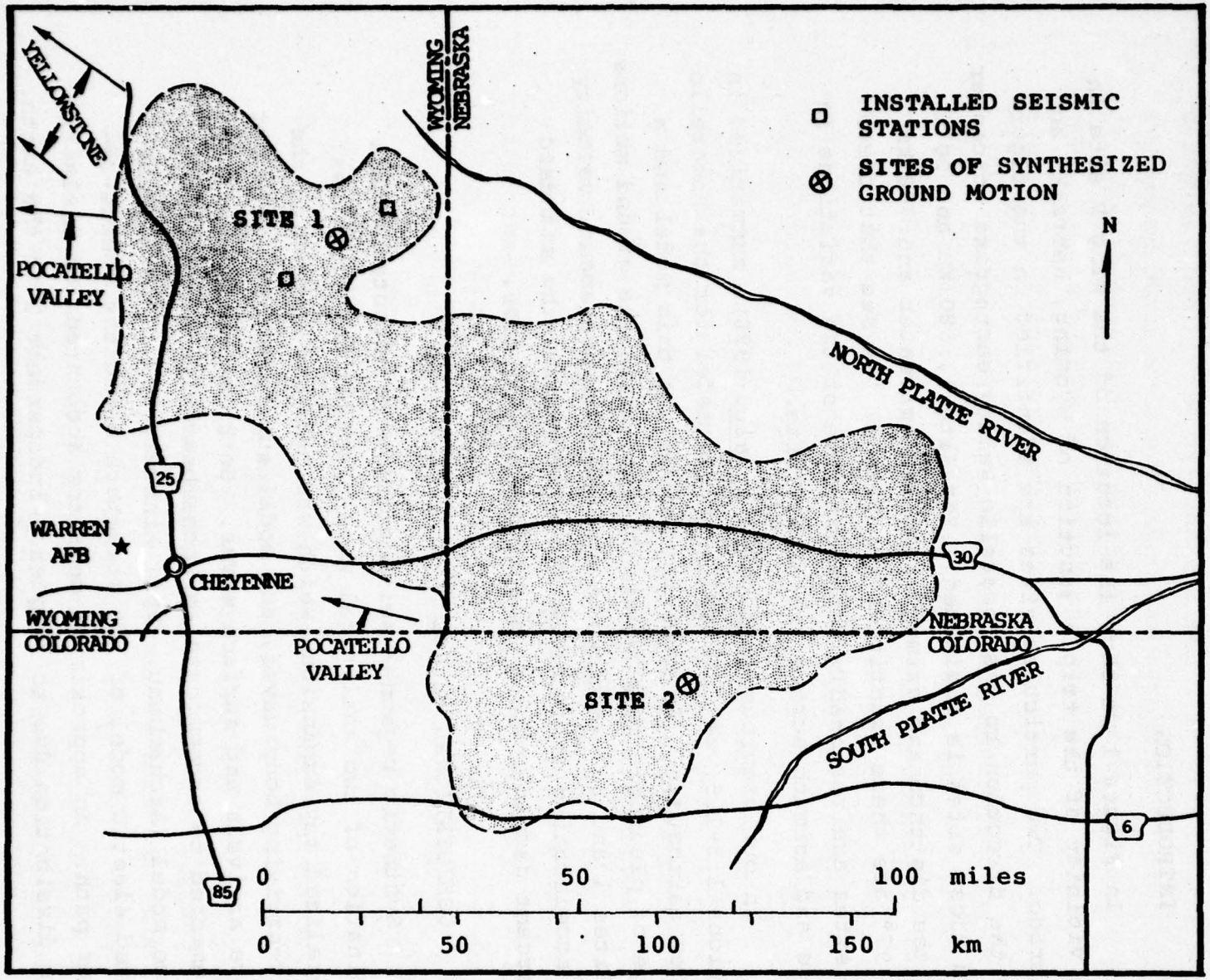

Figure 1. The locations of the two sites of synthesized ground motion at Wing V are shown, with the silo complex denoted by the shaded region. One of the two sites lies between two recently installed seismic stations shown as open squares. The travel paths from the Pocatello Valley and Yellowstone earthquakes are indicated by arrows pointing from Sites 1 and 2 to the earthquake epicenters. (Wing V location from R. A. Gray, private communication.)

The generalized ray method is discussed by Helmberger (1974) and our implementation of it with the Archambeau-Minster source is described by Bache and Barker (1978). The method employs a representation of the surface ground displacement in terms of an infinite sum, each term of which may be associated with a multiply reflected geometrical ray. The ray responses can be evaluated analytically in the time domain. From the geometrical travel time, reflection coefficients, and ray parameter of each ray, one can determine the subset of rays that are required to evaluate the motion in a given time and ray-parameter window.

In general, the number of rays required to evaluate a particular arrival or phase on a seismogram increases rapidly with its travel time and ray parameter. Therefore, we used the generalized ray method to obtain only the significant body-wave arrivals with faster travel times and smaller ray parameters than the earliest S-wave phase (Sn); namely, phases consisting mainly of near-horizontal P-wave rays. For the source-receiver distances considered in this report, the most important of these include direct P (Pg) and a family of Moho and Conrad discontinuity refracted P waves (Pn and P*) which are generated by both S and P from the source, including their free surface reflections, and are radiated back to the surface as both S and P waves. These phases comprise the earliest ten seconds of radial and vertical motion and required on the order of 300 rays to evaluate.

The effect of anelastic attenuation cannot be incorporated directly into the generalized ray expansion and must be accounted for with a final filtering operation. This was done by transforming to the frequency domain and applying Strick's (1970) operator

$$\exp \{-\Pi f t^* [1 + (2i/\pi) \log (f/1000)]\} \quad ,$$

where f is frequency and t* is the geometrical travel time of a ray divided by the average Q along its path. The largest ray contributions we evaluated had a relatively small range of travel times and had nearly the same average path Q. Therefore, a single t* was appropriate for the entire generalized ray solution at each distance.

In the modal superposition technique, the ground displacement at a given site is formed as a sum of surface-wave normal modes. Several examples of this technique are present in the literature; for example, Panza, et al. (1972), Knopoff, et al. (1973), Panza and Calcagnile (1975), Herrmann (1977), and Swanger and Boore (1978).

The modal superposition was done with methods due to D. G. Harkrider, California Institute of Technology. For elementary point forces the theory is presented in two papers (1964, 1970) by Harkrider. However, the earthquake source developed in our previous report (Day, et al., 1978) is described by the coefficients of an expansion in spherical harmonics. The transformation to the equivalent coefficients for an expansion in cylindrical harmonics was worked out by Harkrider (see Bache and Harkrider, 1976) as were the expressions for computing Rayleigh and Love waves for a source expressed in this way.

The seismograms to be presented were for the source being represented by the first seven terms of the spherical harmonic expansion ($\ell = 6$, see Equation (17) of Day, et al., 1978). Numerical experiments showed that this was adequate for representing source-dimension and directivity effects in the frequency range of interest (0.1 to 1 Hz). Anelastic attenuation due to a depth-dependent Q in the path structure was included to first order in Q^{-1} (Anderson and Archambeau, 1964).

Surface-wave modes form arrivals having a horizontal phase velocity (reciprocal ray parameter) less than the shear velocity of the deepest layer in the earth model, which in our models is the upper mantle shear velocity of 4.5 km/sec. The principal regional arrivals contained in the modal solution are the mantle refraction Sn (which is small at the distances of interest here), crustal body waves like Sg and S* and their reverberations in the sedimentary layer, crustal guided waves (Lg) and of course the fundamental mode Rayleigh and Love waves.

Our hybrid synthesis technique does not provide a complete solution to the elastic wave equation in a multilayered halfspace, but this does not present a serious problem in the computation of regional seismograms. The incompleteness of Love wave solutions for SH seismograms is reasonably well understood. An infinite sum of Love-wave modes ignores branch-line integral contributions (see Ewing, Jardetsky and Press, 1957) to the total motion. It is possible that these contributions are also provided by leaking modes (Laster, et al., 1965). At regional distances, the main consequence of omitting branch-line contributions is a slight acausality in the S-wave motion (Swanger and Boore, 1978) and perhaps a misrepresentation of the Sn phase, which is a small phase anyway. Herrmann (1977) presents informative examples of the deficiencies of Love-mode solutions and shows they are not serious at epicentral distances much larger than the source depth.

Rayleigh wave modal solutions for P-SV motion also omit branch-line contributions. As far as the representation of the S phases is concerned it is widely believed, though not proven, that the incompleteness of Rayleigh modes takes a similar form as in the SH case. However, the P-SV branch-line contributions also include the P-wave arrivals and these may be evaluated with generalized rays. Since generalized rays

and surface-wave modes do not exactly separate, though, one must be careful not to duplicate certain portions of the motion with the two techniques. For example, this would cause difficulty in computing S to P conversions which arrive as precursors to the direct S-wave. However, at the distances of interest here, the P-wave arrivals having significant amplitude differ in ray parameter from the Rayleigh modes sufficiently for duplication to be avoided.

A more serious deficiency of our solutions is caused by the truncation of the modal sums. We used the fundamental Love and Rayleigh modes and, depending on the earth models, five or six higher modes. Therefore, all of the surface-wave energy at frequencies less than about 0.5 Hz is included in our solutions, but an increasing percentage of the energy is absent as one goes to higher frequencies. For the source depths and source-receiver distances considered in this section of the report, a significant fraction of the surface-wave motion in the 0.5 to 1 Hz band is contained in the first six modes. Equally important, though, is the fact that the ground displacement, and in some cases even the velocity and acceleration, is dominated by frequencies less than 0.5 Hz. At distances in the 150 to 250 km range, which are considered in Section V, frequencies above 0.5 Hz are more important in the total motion, but it is also true that at these shorter distances more of the high frequency energy is concentrated in the six lowest order modes.

2.3 SOURCE AND PATH MODELS

2.3.1 Crustal Structure Models

The Pocatello Valley to Wing V propagation path extends east-west across southern Wyoming. There are no published models of the crustal structure along this path, but a model

of the nearby northern Colorado Plateau inferred by Keller, et al. (1976) provides a reasonable basis for our path models.

The model of Keller, et al. is listed as Structure A in Table 1 and is one of the models we used in our ground motion calculations. The crustal shear velocity was inferred from short period Rayleigh-wave dispersion, while the P velocity was constrained to give a Poisson's ratio of 0.25. The mantle velocities and crustal thickness were determined from seismic refraction data. We provided the density values, chosen to match the authors' theoretical dispersion curve, and the Q_β values.

Structure A has several advantageous features. Its crustal thickness of 40 km, an important parameter in ground motion estimation, is in agreement with estimates by Warren and Healy (1973) for average values along our paths. Furthermore, Structure A is derived primarily from short period Rayleigh waves, which are significant contributors to the regional ground motion from shallow earthquakes. Another good property of Structure A is its simplicity. It possesses no detailed features, like crustal low velocity channels, that might have a large effect on ground motion, but whose exact nature or even whose existence in our paths cannot be determined.

A structural parameter that is likely to vary significantly from region to region is the thickness of the surface sedimentary layer. The paths of interest intersect a wide variety of surface geology, much of which differs from the northern Colorado Plateau. Therefore, the 2 km sediment thickness in Structure A cannot be assigned a high degree of certainty. Due to the importance of this parameter on regional ground motion, we used a second path model in our calculations in which the sedimentary layer was replaced with basement material. This is Structure B in Table 1. In using

TABLE 1

CRUSTAL STRUCTURE MODELS USED IN POCATELLO GROUND MOTION CALCULATIONS

MODEL	LAYER THICKNESS (km)	DEPTH (km)	P VELOCITY (km/sec)	S VELOCITY (km/sec)	DENSITY (gm/cm^3)	Q_β
STRUCTURE A	2	2	3.15	1.81	2.00	75
Northern Colorado Plateau model from Keller, et al., (1976)	7	9	6.10	3.52	2.69	325
	15	24	6.40	3.69	2.78	375
	16	40	6.80	3.92	2.90	450
	∞	∞	7.80	4.50	3.20	650
STRUCTURE B	9	9	6.10	3.52	2.69	325
Structure A with no sedimentary layer	15	24	6.40	3.69	2.78	375
	16	40	6.80	3.92	2.90	450
	∞	∞	7.80	4.50	3.20	650

both models we hoped to estimate, and perhaps bracket, the sediment-thickness effect.

The least certain structural parameters of our paths to Wing V are the anelastic attenuation parameters Q_α and Q_β (the compressional and shear quality factors, respectively). Accurate regional estimates of crustal Q's are virtually nonexistent, due mainly to the difficulty of isolating the effect of intrinsic dissipation on seismic amplitudes. Nonetheless, previous studies do provide guidelines for selecting reasonable Q versus depth profiles for our paths.

Like most previous studies, we assume that dissipation in the earth occurs only with shear deformation, implying

$$Q_\alpha = (3\alpha^2/4\beta^2)\, Q_\beta$$

(Anderson and Archambeau, 1964), where α and β, respectively, are the P and S seismic velocities. Further, we assume Q_α and Q_β do not vary with frequency.

The Q_β structure in Structures A and B (Table 1) has the essential features of Q_β models inferred by Tsai and Aki (1969), Anderson and Hart (1978), and Mitchell (1975). In Tsai and Aki's model, Q_β increases with depth from 100 at the surface to 800 in the upper-most mantle. Anderson and Hart's model, based on free oscillations and long period surface waves, has a uniform crustal Q_β of 500. Both these models are essentially global estimates. Mitchell's model represents an average for the western United States, inferred as a perturbation to his eastern United States model (Mitchell, 1973) from short period surface waves. In it, Q_β varies between 100 and 200 in the upper half of the crust and between 800 and 2000 in the deep crust, these latter values being only poorly resolved by his data. Our Q_β of 75 in the sedimentary layer is suggested by observations of low Q's in sedimentary rocks (for

example, O'Neill and Healy, 1973) and may even be high for an average sedimentary value. We should also point out that the Q_β deeper than the topmost mantle has a very minor effect on our ground motion calculation, so it was not necessary to include mantle features, such as a low Q, low velocity zone, in our model.

Because of our uncertain knowledge of the Q for these paths, it is important to know what effect variations in Q can have on our ground motion estimates. The Q model in Table 1 represents our best estimate for the Q in this region. However, if it errs, it is probably on the low side. Therefore, we also did calculations for a high Q model obtained by simply doubling all Q values in Table 1.

In subsequent sections we will identify the Q model by a Q scaling factor we call f_Q. Thus, the standard Q model of Table 1 is characterized by $f_Q = 1$ and the high Q model has $f_Q = 2$. Although these two models do not necessarily bracket the true Q for the paths under study, they do represent a broad range of plausible Q structures.

Our four crustal models (with and without sediments, high and low Q) are suitable for estimating the plane-layered path effects on the Pocatello earthquake ground motions at Wing V. To a degree these models also account for the bulk effect of mild lateral variations in the path structure.

2.3.2 Pocatello Valley Earthquake Model

The source model for our ground motion synthesis is that derived by Day, et al. (1978) and described in Section 1.3 of this report. The model used in the computations is the Archambeau-Minster relaxation source. This is an analytical representation of an earthquake as a spherical volume of reduced shear strength growing asymmetrically in a pure shear

prestress field. The asymmetric growth simulates rupture propagation along a fault of finite dimension. The parameters that describe the model are the fault length, fault orientation (strike and slip), rupture or slip direction, focal depth, and the rupture velocity and stress drop as functions of position along the fault.

The final source parameters inferred by Day, et al. (1978) are given in Section 1.3. They describe a normal fault, intermediate between strike- and dip-slip, rupturing unilaterally toward the surface from a depth of 8.7 km. The rupture velocity and stress drop both decay to zero over the second half of the fault. This decay reduces the high frequency content of the source, compared to a uniform rupture rate and stress drop, and was required to simultaneously match the long and short period P-wave amplitudes.

2.4 GROUND MOTIONS AT WING V

Using the source and path models of Section 2.3, and the computational methods of Section 2.2, we computed synthetic displacement, velocity and acceleration seismograms and response spectra for stations in the northwest (Site 1) and southeast (Site 2) portions of Wing V. The location of these sites is shown in Figure 1. In this section we will discuss the results of those calculations and show selected seismograms to illustrate our important conclusions. All of the computed seismograms are plotted in Appendix A. The beginning of the Appendix describes the seismogram display format used throughout this report.

Our best estimates of the ground motions at Sites 1 and 2 are for Structure A (including a 2 km layer of sediments) with our standard Q model denoted by $f_Q = 1$. We also indicate a range of predicted ground motions by showing seismograms with no sedimentary layer (Structure B) and with a high Q model denoted by $f_Q = 2$.

Many of the important characteristics of the ground motion at Wing V are evident from the synthetics for Site 1 obtained with the $f_Q = 1$ version of Structure A. Figure 2 shows the three-component displacement, velocity and acceleration seismograms for this case. These seismograms represent unfiltered ground motion; they have not been passed through an instrument.

The most prominant phase on each component of displacement in Figure 2 is the fundamental mode surface wave. On the vertical (V) and radial (R) components, the Rayleigh wave can be seen from about 230 sec after origin time to the end of the time window shown. The period of dominant motion ranges from about 3.5 to 8 sec. The Love wave on the tangential (T) component begins earlier ($t \simeq 190$ sec) and is dominated by longer period motion (5 to 15 sec). Both of the surface waves exhibit a significant degree of dispersion, which is caused largely by the high velocity contrast between the sedimentary and granitic layers of Structure A. Because of this dispersion, many of the seismograms computed with Structure A actually continue beyond the 320 sec time window shown in the figures, but with a small amplitude.

The other major arrival on the displacement records in Figure 2 is the high frequency motion beginning at about $t = 195$ sec, corresponding to a group velocity close to the granitic shear velocity of 3.52 km/sec. This arrival is primarily the Lg phase but also includes the direct and refracted S waves. Lg and crustal S waves have similar velocities and are not computed separately in a modal solution, so they are difficult to distinguish. Other small S-wave arrivals appear on the vertical component between 160 sec and 190 sec. The crustal P waves on the vertical and radial components arrive at about $t = 105$ sec but are barely visible on the displacement records.

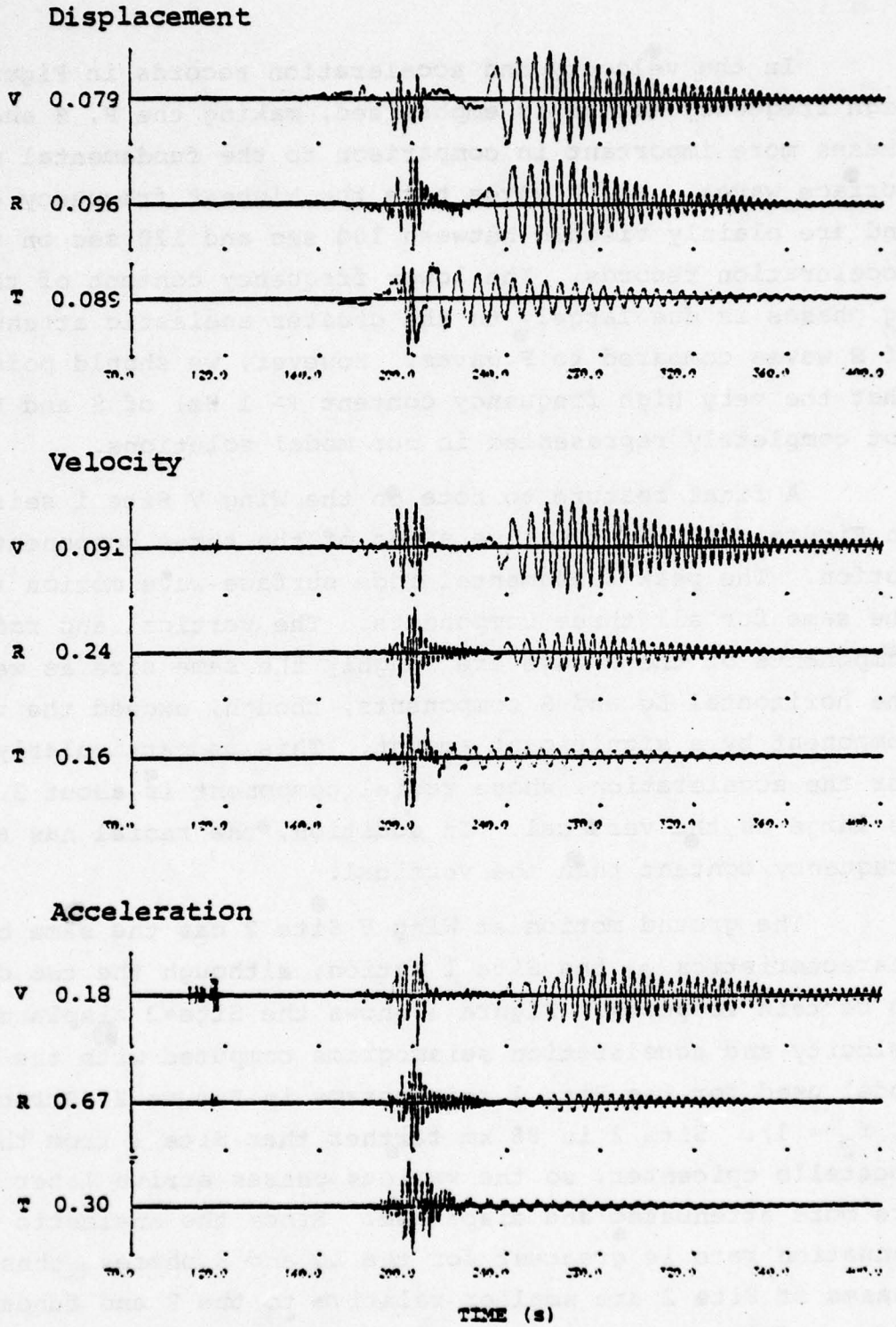

Figure 2. Pocatello seismograms at Wing V Site 1 for Structure A, standard Q (f_Q = 1). The time from the origin time is marked in 40 second increments. The height of the vertical axis is given for each seismogram in the appropriate units (cm, cm/sec or cm/sec^2).

In the velocity and acceleration records in Figure 2 the high frequency motion is emphasized, making the P, S and Lg phases more important in comparison to the fundamental mode surface waves. The P waves have the highest frequency content and are plainly visible between 100 sec and 120 sec on the acceleration records. The lower frequency content of the S and Lg phases is due largely to the greater anelastic attenuation of S waves compared to P waves. However, we should point out that the very high frequency content (> 1 Hz) of S and Lg is not completely represented in our modal solutions.

A final feature to note on the Wing V Site 1 seismograms in Figure 2 is the relative sizes of the three components of motion. The peak fundamental mode surface-wave motion is about the same for all three components. The vertical and radial components of the P wave are roughly the same size as well. The horizontal Lg and S components, though, exceed the vertical component by a significant amount. This is particularly true for the acceleration, whose radial component is about 3.5 times as large as the vertical. In addition, the radial has a higher frequency content than the vertical.

The ground motion at Wing V Site 2 has the same basic characteristics as the Site 1 motion, although the two differ in certain respects. Figure 3 shows the Site 2 displacement, velocity and acceleration seismograms computed with the path model used for the Site 1 seismograms in Figure 2 (Structure A, $f_Q = 1$). Site 2 is 88 km farther than Site 1 from the Pocatello epicenter, so the various phases arrive later and are more attenuated and dispersed. Since the anelastic attenuation rate is greatest for the Lg and S phases, these phases at Site 2 are smaller relative to the P and fundamental mode surface waves than they are at Site 1. In addition, radiation pattern effects also cause some differences between the ground motions at the two sites; in particular, the Love and Rayleigh wave ratio is lower at Site 2.

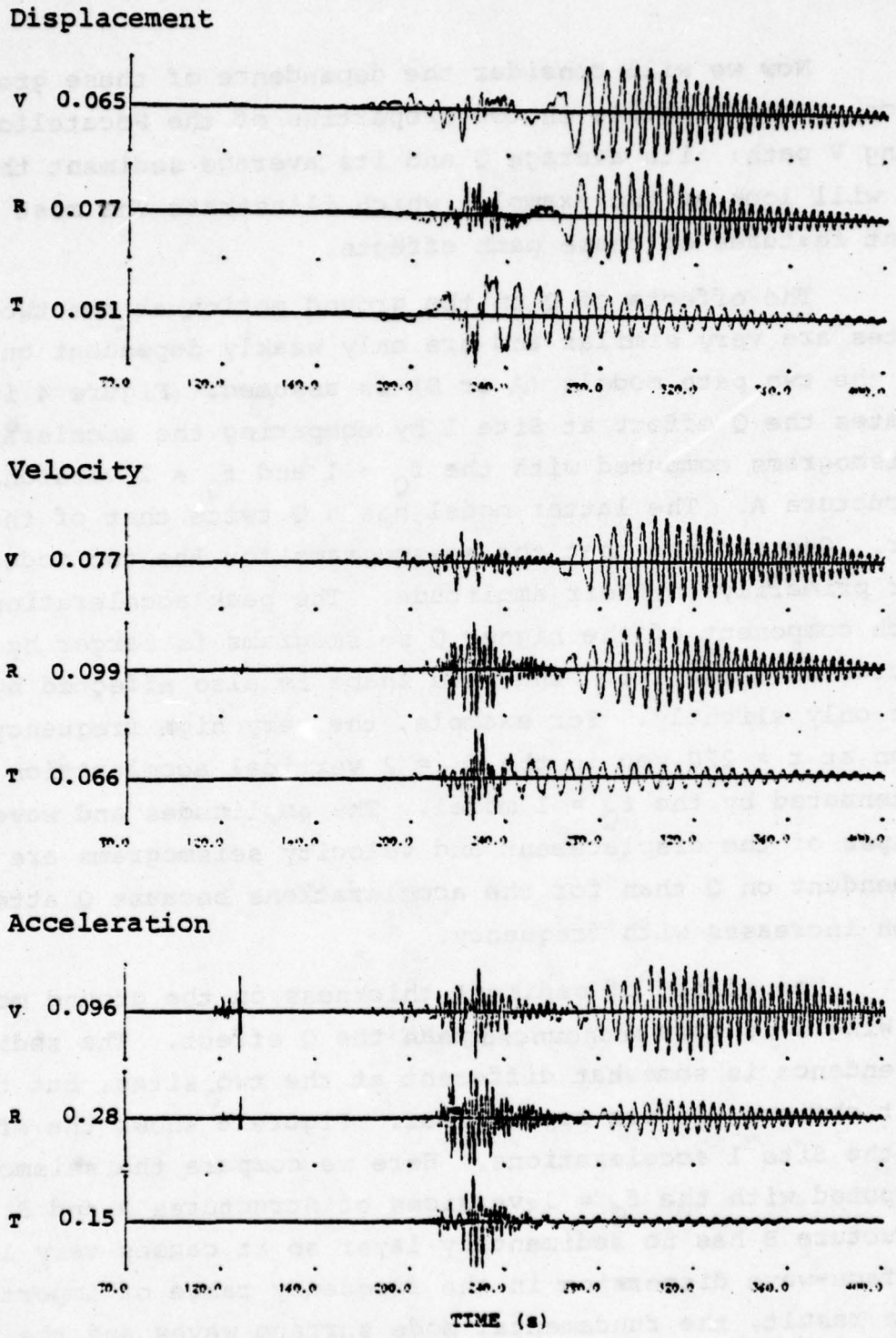

Figure 3. Pocatello seismograms at Site 2 for Structure A, $f_Q = 1$.

Now we will consider the dependence of these ground motion characteristics on two properties of the Pocatello Valley-Wing V path: its average Q and its average sediment thickness. We will look at two examples which illustrate the most important features of these path effects.

The effects of Q on the ground motion at the two Wing V sites are very similar and are only weakly dependent on which of the two path models (A or B) is assumed. Figure 4 illustrates the Q effect at Site 1 by comparing the acceleration seismograms computed with the $f_Q = 1$ and $f_Q = 2$ versions of Structure A. The latter model has a Q twice that of the former. One can see that the seismograms for the two models differ primarily in their amplitude. The peak acceleration on each component of the higher Q seismograms is larger by a factor of about 1.5. The wave shape is also affected by Q, but only slightly. For example, the very high frequency motion at $t \approx 220$ sec in the $f_Q = 2$ vertical acceleration is attenuated by the $f_Q = 1$ model. The amplitudes and wave shapes of the displacement and velocity seismograms are less dependent on Q than for the accelerations because Q attenuation increases with frequency.

The effect of sediment thickness on the ground motion at Wing V is more pronounced than the Q effect. The sediment dependence is somewhat different at the two sites, but the most obvious effects are similar. Figure 5 shows the effect on the Site 1 accelerations. Here we compare the seismograms computed with the $f_Q = 1$ versions of Structures A and B. Structure B has no sedimentary layer so it causes very little surface-wave dispersion in the frequency range of importance. As a result, the fundamental mode surface waves and the Lg phase are very impulsive in Structure B. On the tangential component, on which the Lg and Love wave arrival times are almost the same, significant motion lasts less than 20 sec.

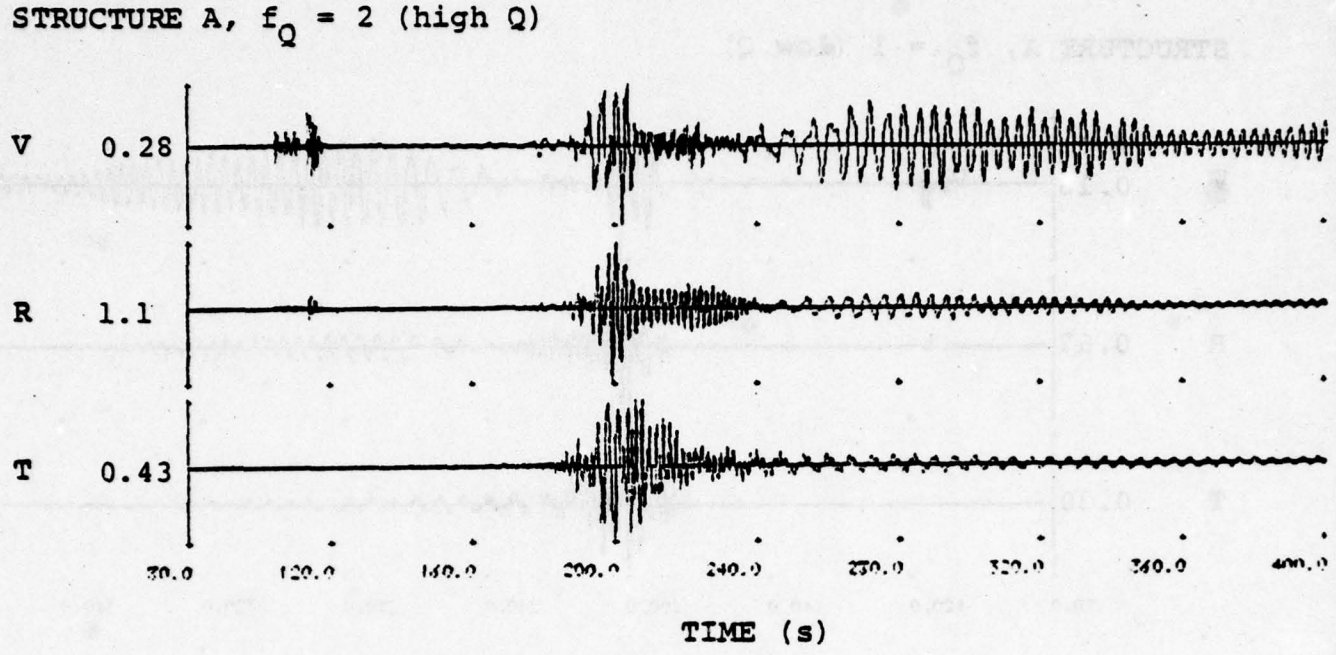

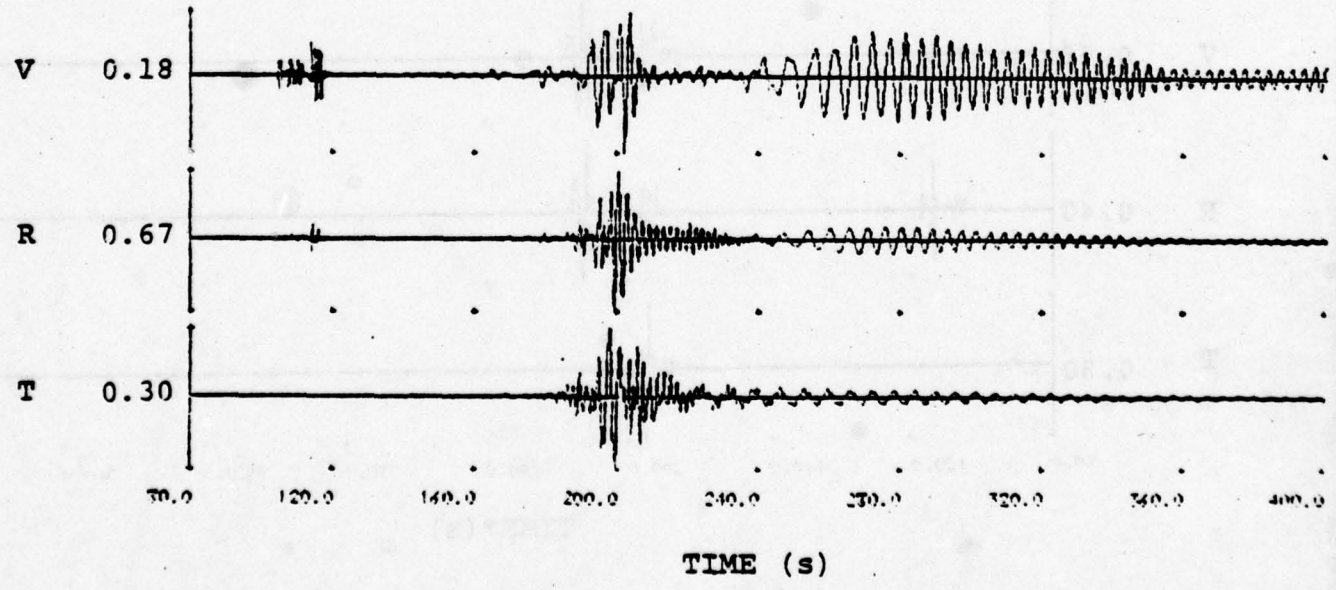

Figure 4. Comparison of Site 1 acceleration seismograms obtained with f_Q = 1 and 2 versions of Structure A.

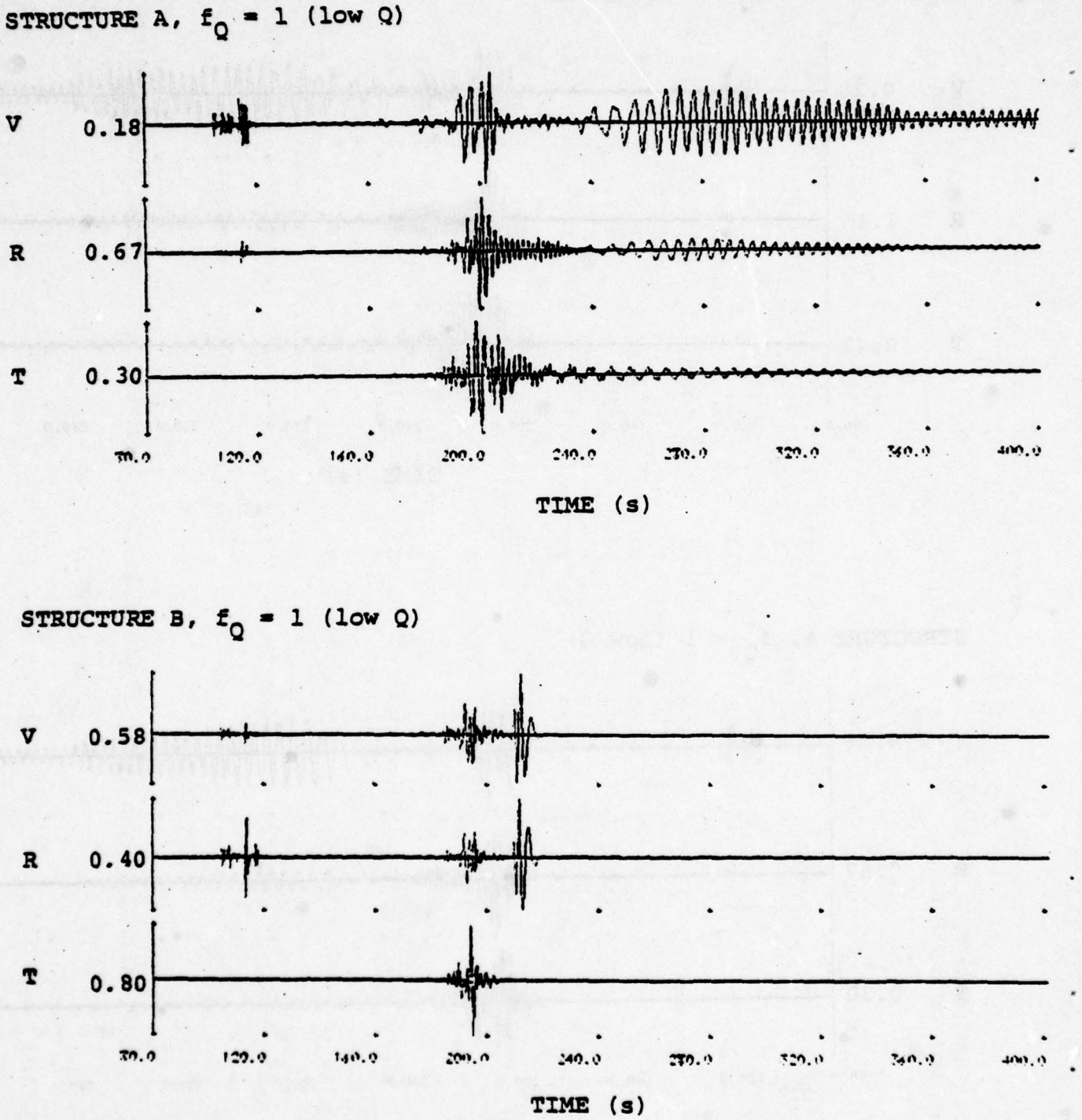

Figure 5. Comparison of Site 1 seismograms obtained with f_Q = 1 versions of Structures A and B.

In addition to the duration of the ground motion, its amplitude is also affected by the sedimentary layer. The peak displacements, velocities and accelerations for Structure B are roughly twice those for Structure A. However, the various phases and components of motion are affected differently. At both Site 1 and Site 2 the vertical surface-wave modes increase the most as a result of removing the sedimentary layer. The radial modes increase the least; at Site 1, the radial component actually decreases, as can be seen in Figure 5. This reflects a change in the Rayleigh wave ellipticity by a factor of about three.

Our inferred ground motion amplitudes at the two Wing V sites are summarized in Table 2. Here we have tabulated the peak time-domain displacements, velocities and accelerations of all our synthetic Pocatello earthquake seismograms. These peak values were interpolated between discrete sample points using a parabolic fit. Listed beside each amplitude value is its approximate period of motion, determined from the spacing between the zero crossings nearest the peak. The peak motions in Table 2 are shown graphically in Figure 6.

In Table 2 we see a wide variation in the peak ground motion values determined with the various path structure models. We also list a geometric average for each grouping of peak values. These averages have no statistical significance, but provide a useful reference for comparison to the individual values. If we consider the largest peak motions of the three components and average these for the two sites and four path models, we obtain the following estimates of peak motion at Wing V:

Average Peak Displacement: 0.08 cm

Average Peak Velocity: 0.13 cm/sec

Average Peak Acceleration: 0.35 cm/sec^2 (mgal)

TABLE 2

PEAK POCATELLO VALLEY EARTHQUAKE GROUND MOTIONS AT WING V FROM SYNTHETIC SEISMOGRAMS

	Path Structure		Displacement (cm)				Velocity (cm/sec)				Acceleration (cm/sec^2)			
			Site 1		Site 2		Site 1		Site 2		Site 1		Site 2	
Comp.	B or A	f_Q	A*	T*	A	T	A	T	A	T	A	T	A	T
V	B	2	.15	5	.13	5	.22	4	.19	3	.44	3	.38	3
	B	1	.13	5	.11	5	.17	4	.14	4	.32	3	.26	3
	A	2	.054	6	.045	6	.066	5	.058	5	.16	3	.086	3
	A	1	.041	6	.033	6	.047	5	.039	5	.099	3	.049	3
Geometric Average			.081		.068		.10		.088		.22		.14	
R	B	2	.098	4	.088	6	.14	3	.13	4	.31	2	.26	2
	B	1	.078	4	.073	6	.11	5	.098	4	.21	2	.17	3
	A	2	.074	2	.053	5	.19	2	.088	2	.58	2	.26	2
	A	1	.049	3	.039	6	.12	2	.050	2	.35	2	.14	2
Geometric Average			.073		.060		.14		.086		.34		.20	
T	B	2	.13	5	.078	6	.23	2	.13	3	.83	1	.38	2
	B	1	.11	5	.060	6	.16	2	.089	3	.40	2	.21	2
	A	2	.069	4	.037	9	.11	3	.057	3	.23	3	.20	2
	A	1	.054	4	.028	10	.080	4	.036	3	.15	3	.087	2
Geometric Average			.080		.047		.13		.070		.33		.19	

*A = Peak motion amplitude
T = Approximate period in seconds

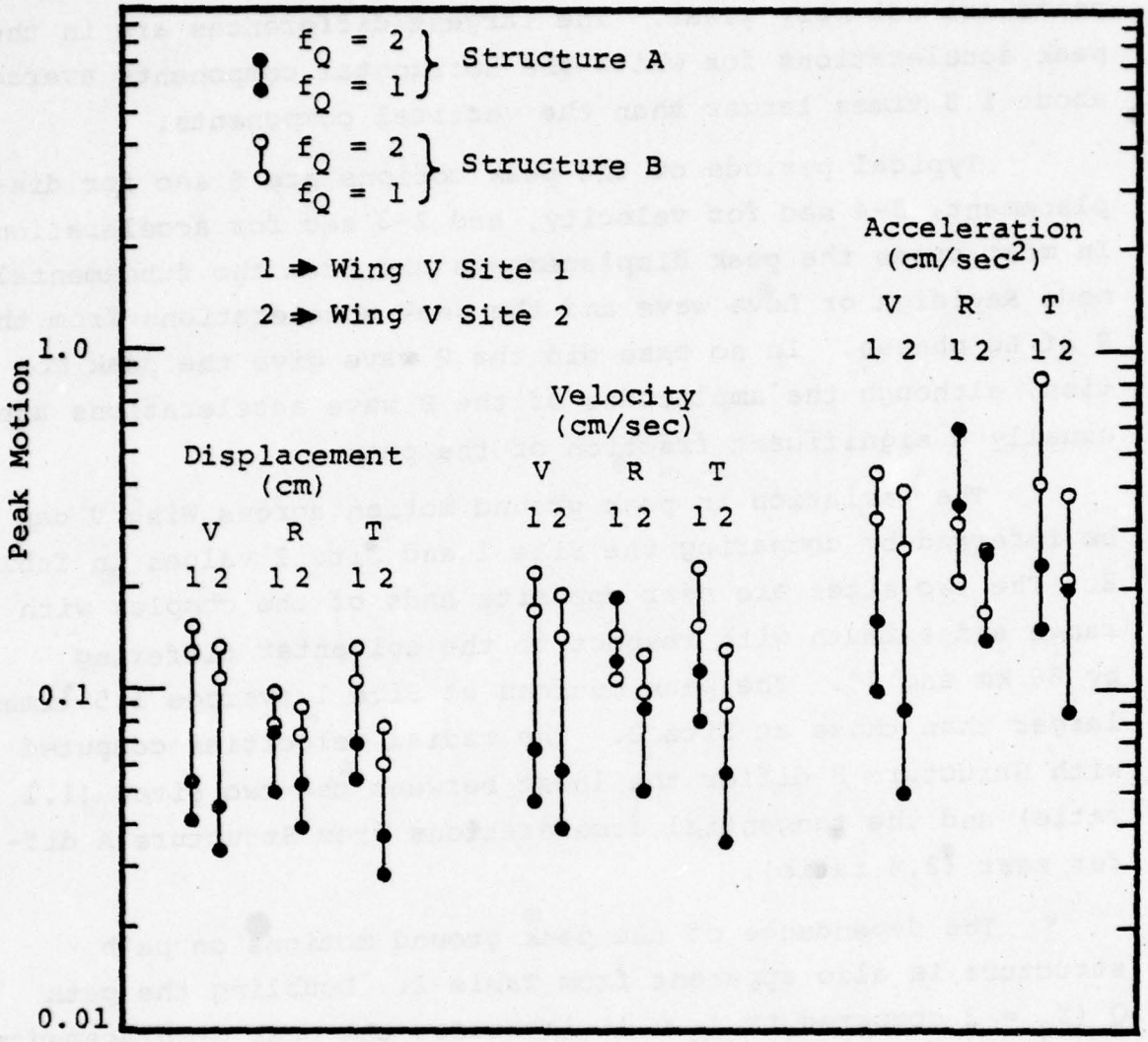

Figure 6. Peak Pocatello Valley earthquake ground motions at Wing V (from Table 2).

Differences between the peak motions of the different components are not very great. The largest differences are in the peak accelerations for which the horizontal components average about 1.5 times larger than the vertical components.

Typical periods of the peak motions are 5 sec for displacement, 3-4 sec for velocity, and 2-3 sec for acceleration. In most cases the peak displacements are from the fundamental mode Rayleigh or Love wave and the peak accelerations from the S of Lg phases. In no case did the P wave give the peak motion, although the amplitudes of the P wave accelerations are usually a significant fraction of the peak.

The variation in peak ground motion across Wing V can be inferred by comparing the Site 1 and Site 2 values in Table 2. The two sites are near opposite ends of the complex with range and azimuth with respect to the epicenter differing by 88 km and 7°. The peak motions at Site 1 average 1.5 times larger than those at Site 2. The radial velocities computed with Structure B differ the least between the two sites (1.1 ratio) and the tangential accelerations from Structure A differ most (2.4 ratio).

The dependence of the peak ground motions on path structure is also apparent from Table 2. Doubling the path Q ($f_Q = 2$ compared to $f_Q = 1$) increases the peak displacements by an average of 1.3, the velocities by 1.4, and the accelerations by 1.6. Also, the period of peak motion tends to be smaller for the $f_Q = 2$ models. The Q dependence is slightly larger at Site 2 than at Site 1, because of its greater epicentral distance, and slightly larger for Structure A than Structure B, because of the low Q sedimentary layer in Structure A. The biggest effect of Q for the cases we ran is on the Site 2 tangential acceleration computed with Structure A, for which the $f_Q = 2$ value is larger by a factor of 2.3.

The thickness of the low velocity sedimentary layer in the path structure can have a very big effect on the peak ground motions, as one can see by comparing the values in Table 2 for Structure B (no sedimentary layer) to the Structure A (2 km layer) values. The peak displacements, velocities, and accelerations for Structure B average twice those for A. The sediment effect is quite variable, however. The extreme cases are a B to A ratio of 0.6 for the radial accelerations at Site 1 and a ratio of 4.9 in the vertical accelerations at Site 2.

The combination of the Q and sediment effects leads to a variation in our peak ground motion estimates on the order of a factor of three, the variation being largest for the vertical component and smallest for the radial. However, we should point out that much of this variation is due to the sediment thickness effect, which we have examined with a rather extreme case. Although the effective thickness of sediments seen by seismic waves over the 700 km Pocatello-Wing V path may be much thinner than 2 km, it is not likely to be zero as it is in Structure B. Secondly, we should point out that the average structure of paths to different areas in Wing V cannot differ very much; the azimuthal window is only nine degrees. Thus, variations in the peak ground motions across the complex, which we found to be about 1.5, are not very dependent on the path effects we have examined. Likely to be more important for both absolute and relative motions at different locations within Wing V are the effects of lateral variations, which we have not modeled.

Because the Pocatello Valley earthquake was not recorded in the Wing V area, the accuracy of the peak motion estimates in Table 2 cannot be determined directly. However, a comparison of these estimates to estimates from empirical ground motion attenuation studies shows that our values are very reasonable. We make this comparison in Table 3.

TABLE 3

COMPARISON OF INFERRED PEAK GROUND MOTIONS FROM SYNTHETIC SEISMOGRAMS TO EMPIRICAL ESTIMATES

Source	Type of Estimate	Peak Motions		
		Displacement (cm)	Velocity (cm/sec)	Acceleration (cm/sec^2)
This study	Pocatello-Wing V Site 1 synthetic seismograms	0.054-0.15	0.12-0.23	0.35-0.83
McGuire (1974)	Empirically derived attenuation curves	0.47	0.54	4.49
Orphal & Lahoud (1974)		0.056	0.16	1.87
Esteva & Villaverde		--	0.19	1.31
Esteva & Rosenblueth (1963)		--	0.12	0.53
Donovan (1974)		--	--	3.77
Donovan (1973)		--	--	2.01
Esteva (1970)		--	--	0.30
Page, et al. (1972)		--	--	<1.0
Battis & Hill (1977)	LASA recording of Pocatello Valley earthquake	--	--	~0.005

Given for "this study" in Table 3 are the range of peak motions at Site 1 implied by the synthetics from our four path structure models, where the peak motion for a given path model is the largest of the peak amplitudes on the three components of motion. The estimates listed for most of the other authors are values predicted by attenuation formulas of the form

$$P = a_1 e^{a_2 M_L} (r + a_3)^{-a_4} ,$$

where P is the peak motion (displacement, velocity, or acceleration), M_L is local magnitude, r is epicentral distance, and a_1, a_2, a_3, a_4 are regression parameters fit to observed peak motion data from several earthquakes. We have used a summary given by Battis (1978) of the regression parameters determined by the authors listed in Table 3. The peak motion values in the table are obtained by inserting these parameters, $M_L = 6$, and r = 680 km (the Pocatello - Site 1 epicentral distance) into the above formula.

The estimate listed in Table 3 for Page, et al. (1972) is from their graph of observed peak horizontal acceleration versus distance for several California earthquakes having magnitudes between 5.0 and 6.9. They have no data for r > 500 km, but we have extrapolated an upper limit of 1.0 mgal acceleration for r > 500 km and $M_L = 6$. The last entry in Table 3 is based on an actual recording of the Pocatello earthquake at the LASA array in Montana, which is 700 km from the epicenter. Battis and Hill (1977) derived a peak vertical P-wave acceleration of 1.7 μg from the LASA seismograms. Then with the assumption that the SH wave had the largest acceleration and using an empirical SH to P acceleration ratio of 3, they determined an absolute peak acceleration of about 5 μgal.

Table 3 shows that the peak motions of our synthetic seismograms are consistent with a wide range of empirical estimates. However, our peak accelerations appear to be quite low compared to some of the empirical estimates, particularly in light of the fact that the Pocatello - Wing V azimuth is near a maximum in the high frequency radiation patterns for our Pocatello source model (see Section 3.4). One explanation for this is that our synthetic seismograms underestimate the true ground accelerations because of two factors. The first is the truncation of the surface-wave modal sums to six or seven modes, which deletes some of the energy above 0.5 Hz in our S-wave phases. The second is that our modeling procedure may not excite high frequencies strongly enough.

It is also possible that some of the empirical peak acceleration estimates are too high. Battis and Hill (1977) point out that most of the data used to determine the attenuation-distance relations they studied are from California earthquakes. There is some evidence that California earthquakes generally produce larger ground accelerations than earthquakes in the Rocky Mountain region. The small peak accelerations inferred for the Pocatello earthquake at LASA lends some validity to this argument. This estimate is very low compared both to the other empirical estimates and to our estimate. Battis and Hill deduced this peak acceleration from the P-wave peak acceleration and their procedure is subject to some doubt. However, the LASA observed P-wave acceleration itself is small compared to the P-wave acceleration on our synthetic seismograms.

Response spectra computed from our synthetic Pocatello - Wing V seismograms are shown in Figures 7, 8 and 9 for the vertical, radial and tangential components, respectively. In each figure, four response spectra, corresponding to the four path structure models used in the ground motion synthesis, are compared for each of the two Wing V sites. The response spectra were computed with 0.05 of critical damping.

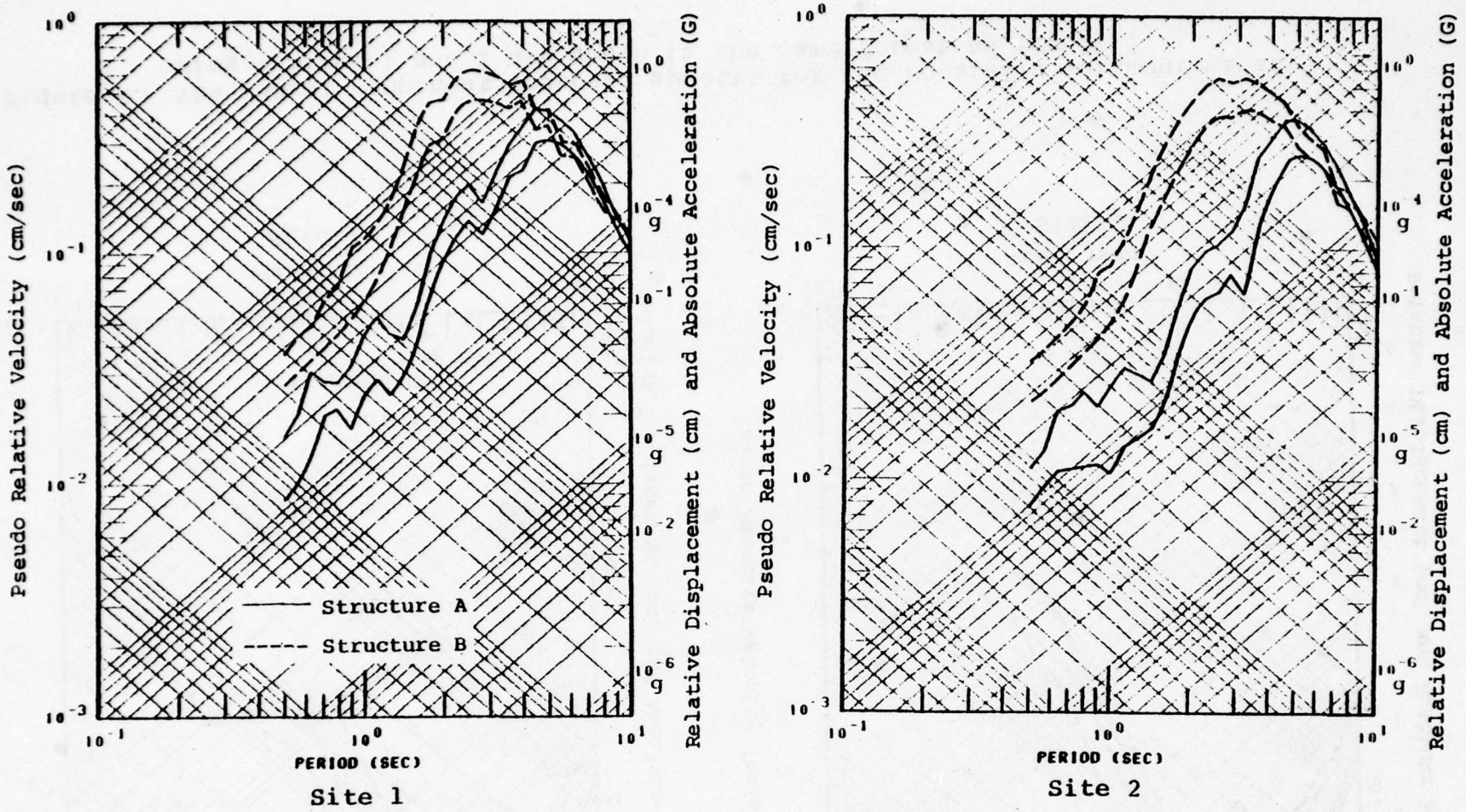

Figure 7. The vertical component response spectra for the Pocatello seismograms from four path models are shown for Sites 1 and 2 at Wing V. The two curves shown for each of Structures A and B correspond to the two Q models given by $f_Q = 1$ and $f_Q = 2$. For both structures, the $f_Q = 2$ (high Q) curve lies above the $f_Q = 1$ curve. The response spectra are for a damping factor of 0.05 of critical.

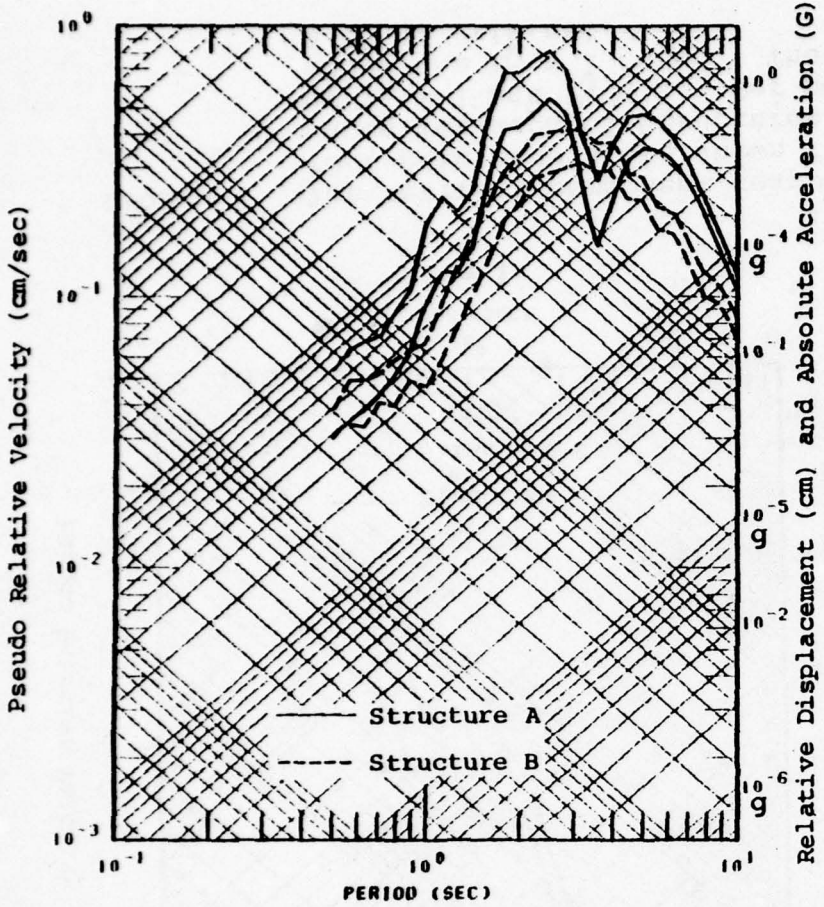

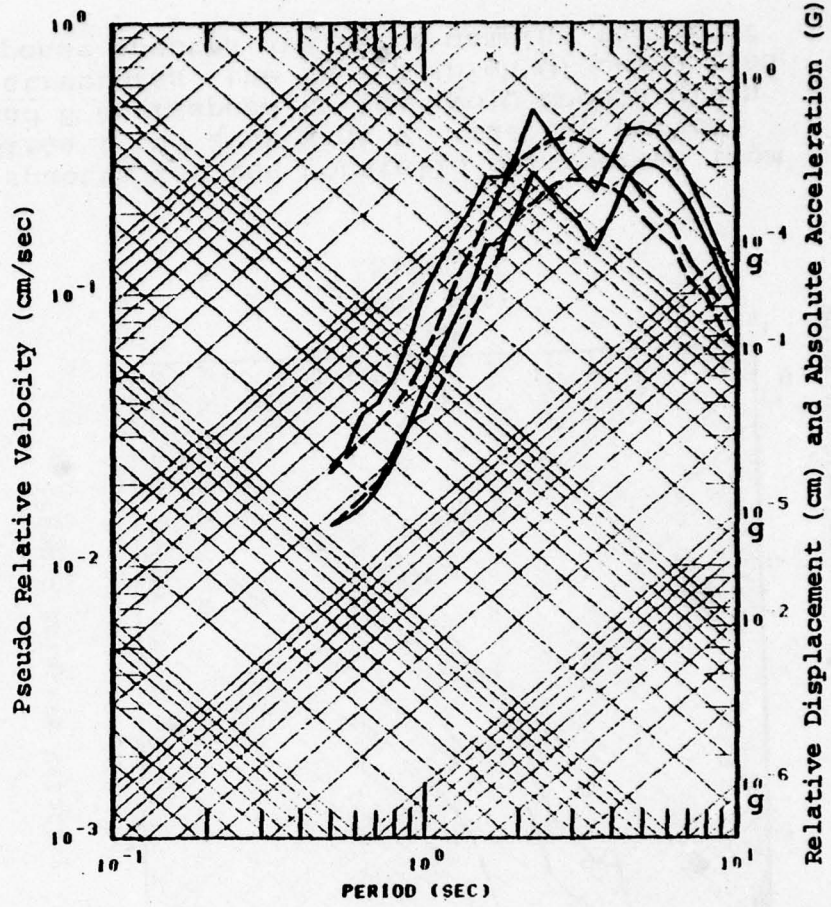

Figure 8. The radial component response spectra for the Pocatello seismograms at Wing V Sites 1 and 2 are shown in the same format as Figure 7.

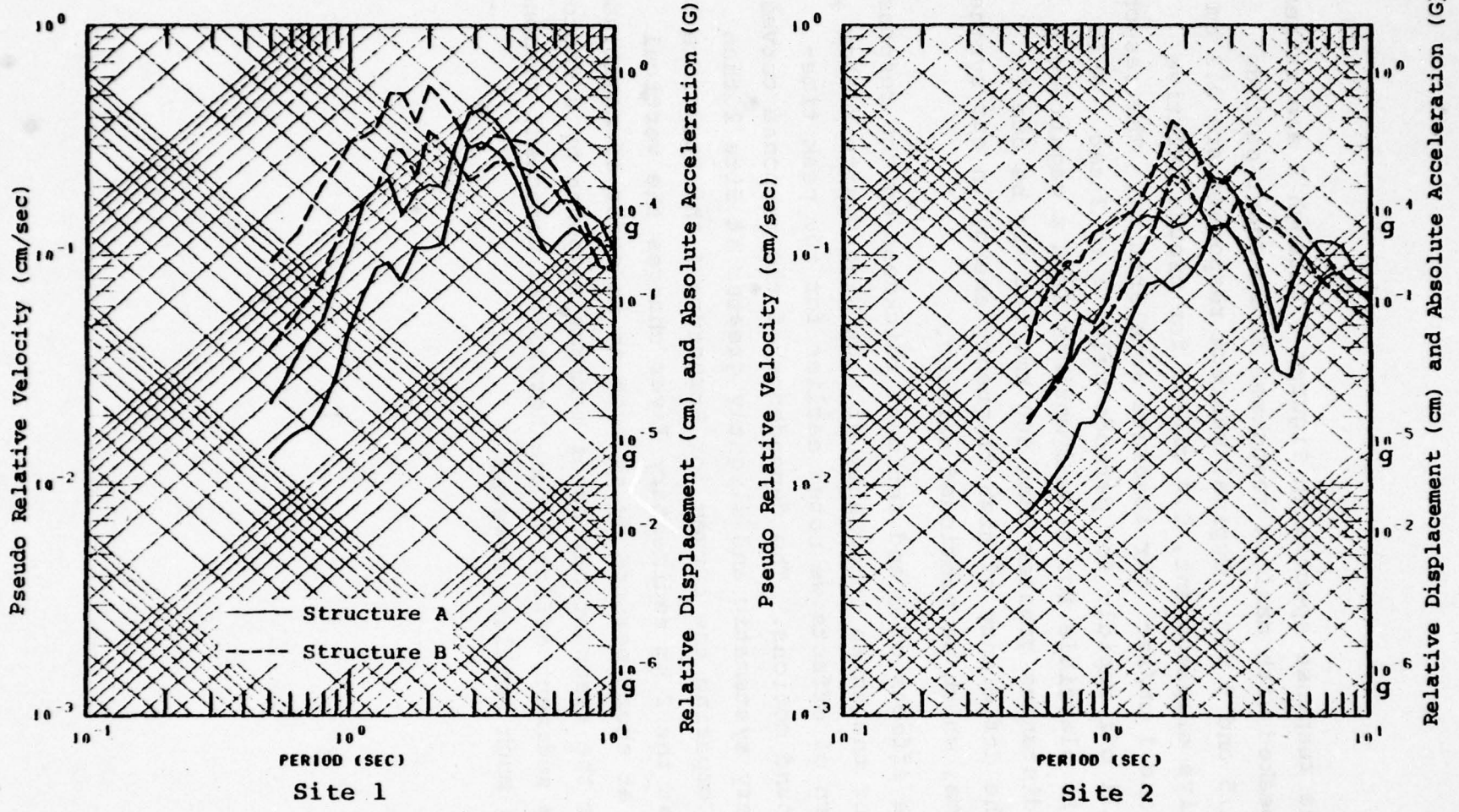

Figure 9. The tangential component response spectra for the Pocatello seismograms at Wing V Sites 1 and 2 are shown in the same format as Figure 7.

The response spectra in Figures 7 through 9 are rather sharply peaked with maximum responses at resonant periods between 1.5 and 5 sec. Typical maximum responses are 0.2 cm for relative displacement, 0.4 cm/sec for pseudo relative velocity and 1 cm/sec^2 for absolute acceleration. The response curves fall off rapidly for periods below 1 to 2 sec. This fall-off is plausible for ground motions from a magnitude 6 event at distances greater than 500 km, but may be due in part to the deficiency of high frequency energy in our synthetic seismograms, which we mentioned earlier.

The effects of Q and sediment thickness on the response spectra for the three components at each Wing V site follow the pattern of effects we noted earlier for the peak time-domain ground motions. The dependence of the response curves on Q is very systematic and slightly greater at Site 2 than Site 1. Comparing the curves for Structure A and Structure B, we see that the 2 km sedimentary layer changes the vertical responses at short periods by as much as an order of magnitude and shifts the resonant period of maximum response by a factor of 2. The sediment effect on the horizontal component response spectra is much smaller, however.

III. COMPARISON OF GROUND MOTIONS AT WING V FROM THE 1975 POCATELLO VALLEY AND YELLOWSTONE EARTHQUAKES

3.1 INTRODUCTION

The March 28, 1975 Pocatello Valley and June 30, 1975 Yellowstone Park earthquakes were quite similar events. They had nearly the same moment (M_0) and M_s which are measures of the long period amplitude of the source. Battis and Hill (1977) give $M_0 = 7.2 \times 10^{24}$ dyne-cm for the Pocatello Valley event and 7.5×10^{24} dyne-cm for the Yellowstone event. Our analysis of the long period body waves gave $M_0 = 7.1 \times 10^{24}$ dyne-cm for the first event. The USGS assigned M_s values are 6.0 and 5.9. A short period measure, the local magnitude (M_L) reported by BRK and PAS was 6.1 or 6.2 for both events. Based on this information one would conclude that the two events were the same. However, the USGS m_b values were 6.1 for the Pocatello Valley and 5.6 for the Yellowstone events. The m_b is a measure of the downgoing P waves near one hertz and this different indicates that this aspect of the Yellowstone earthquake was a factor of three smaller.

The direction from Sites 1 and 2 within Wing V to the Yellowstone earthquake epicenter is indicated in Figure 1 of Section 2.1. The location of Sites 1 and 2 with respect to both earthquakes is summarized below.

	Site 1		Site 2	
	Distance (km)	Azimuth	Distance (km)	Azimuth
Pocatello Valley	680	90°	768	97°
Yellowstone Park	610	121°	730	124°

These are similar events at similar locations with respect to the Wing V sites. What are the relative levels of

ground motion? In this section we synthesize the likely ground motions at Wing V for the Yellowstone earthquake. The available telseismic data for this event were of insufficient quality to resolve high frequency characteristics of the source. We simply assume that the two earthquakes are identical in all respects except the source orientation for which there is reliable information. We ignore the m_b differences but keep in mind that our ground motion estimates are then likely to be over-estimates near one hertz.

Differences in the character of the travel path between the earthquake epicenters and Wing V is another possible cause of ground motion differences. The most likely cause of such differences is a dramatic feature, the Yellowstone caldera, that lies astride the path to Wing V. We account for this feature, at least in an ad hoc fashion, in our ground motion synthesis.

A previous study of the Yellowstone Park earthquake (Pitt, Weaver and Spence, 1979) leads us to expect the ground motion at Wing V to be anomalously low for this event. Figure 10 shows the Modified Mercalli isoseismal map given by Pitt, et al. These authors comment on the pronounced asymmetry of the isoseismal map and state that "nearly every large historical earthquake in Montana has shown a distinctly larger felt area to the north of its epicenter than to the south." For the Yellowstone earthquake there is also some instrumental confirmation of this asymmetry. Pitt, et al. report that the M_L (local magnitude) of this earthquake and eight large aftershocks averaged 0.45 units (a factor of 2.8) lower at Logan, Utah than at Newport, Washington.

Our objective in this section is to use synthetic seismogram methods to quantify differences between the ground motions from the two events. The computed ground motions for the two events would be identical except for two effects. We account

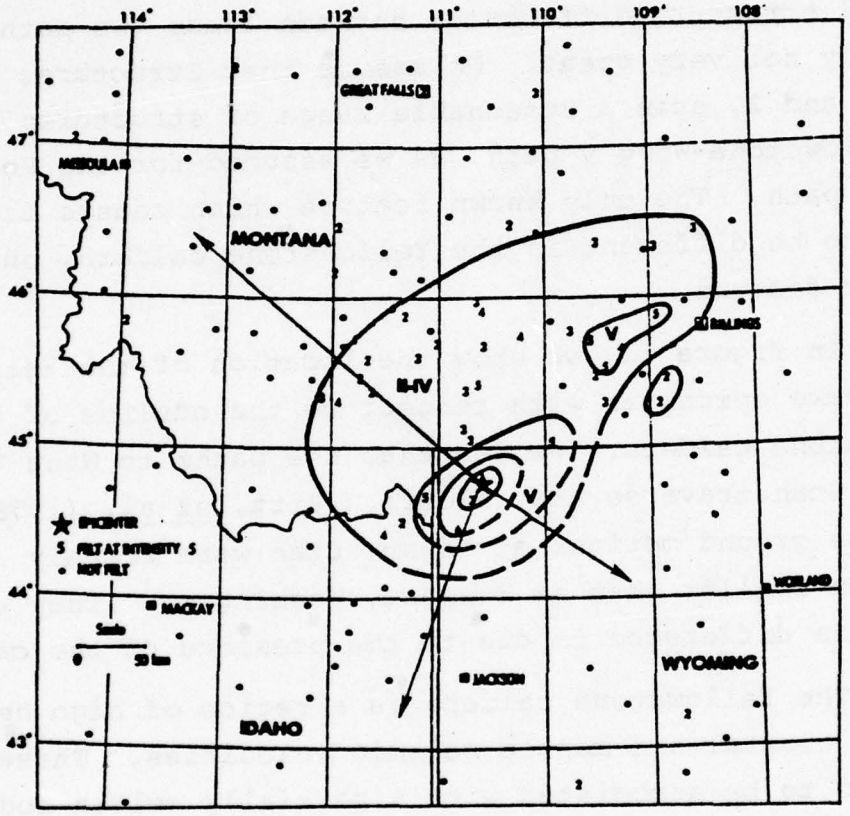

Figure 10. Modified Mercalli isoseismal map for the 1975 Yellowstone Park earthquake. The dashed lines indicate lines subject to some uncertainty (from Pitt, Weaver and Spence, 1979).

for the different source orientations and we account for the presence of the Yellowstone caldera.

3.2 MODELS OF THE YELLOWSTONE-WING V PATH STRUCTURE

Because of the proximity of the paths from Wing V to the Pocatello Valley and Yellowstone Park earthquakes, crustal structure differences between these two paths are probably not very great. We assume that Structures A and B, f_Q = 1 and 2, span a reasonable range of structures for most of Yellowstone-Wing V path, as we assumed for the Pocatello-Wing V path. The only known feature which causes the two paths to be different is the Yellowstone caldera, but this is a major feature.

In Figure 11, we show the location of the Yellowstone earthquake epicenter with respect to the outline of the Yellowstone caldera. We see that the paths to Wing V and to Logan, Utah traverse the caldera. Pitt, et al. (1979) found that the ground motions at Logan, Utah were roughly a factor of three smaller than at Newport, Washington. They suggest that this difference is due to the presence of the caldera.

The Yellowstone caldera is a region of high heat flow and low crustal and mantle seismic velocities. These are supposed to be associated with a partially molten body extending to mantle depth (Eaton, et al., 1975; Smith, et al., 1974; Evoy, 1978). Thus the attenuation (Q) within the caldera is likely to be extremely low. We would also expect the caldera boundaries to have a large impedance contrast with the surrounding medium, reflecting and scattering much of the energy traversing the region. This scattering effect can be roughly accounted for by lowering Q.

While we cannot directly model the effect of the caldera, we roughly account for its presence by using a special Q model for the Yellowstone-Wing V path. About ten percent of the latter path is influenced by the caldera. We suppose the Q in

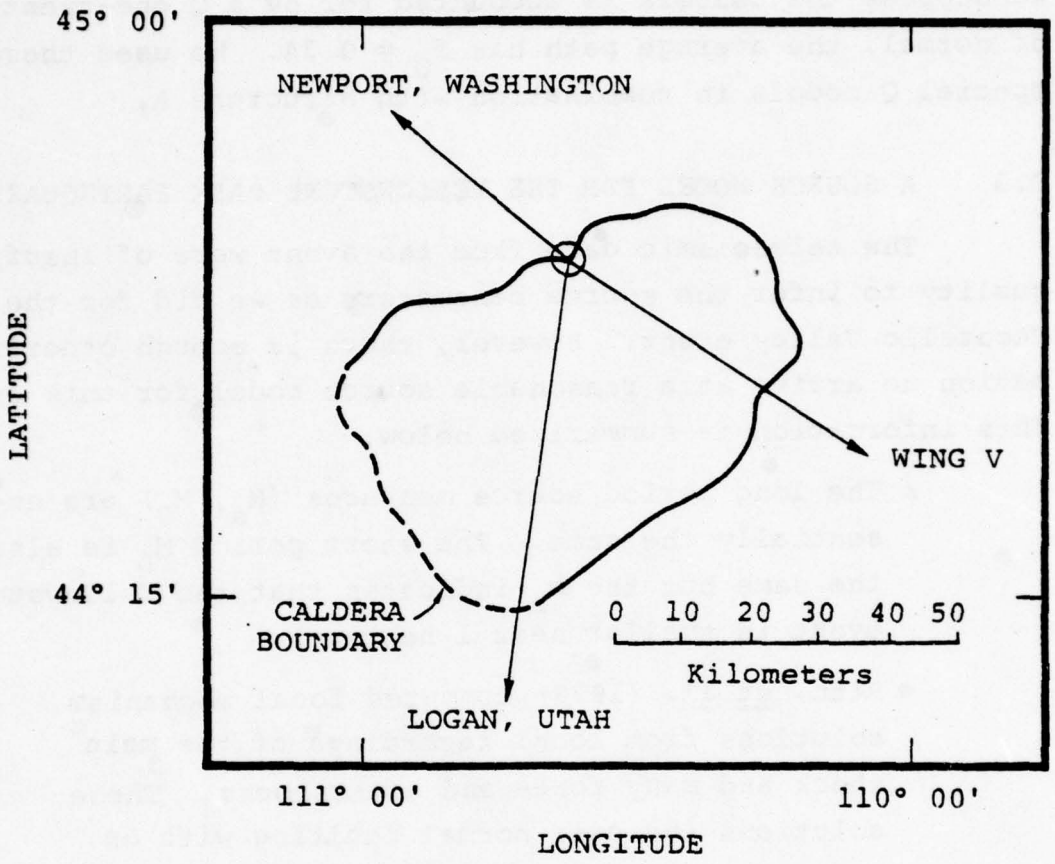

Figure 11. The epicenter location for the Yellowstone Park earthquake is shown with respect to the outline of the Yellowstone caldera. The directions to Wing V and two seismometer stations are indicated. (Adapted from Figure 1 of Pitt, Weaver and Spence, 1979.)

this region is one-tenth of its normal value. The average path Q is then obtained by setting the scale factor f_Q to 0.53. If we suppose the caldera is accounted for by a Q one-twentieth of normal, the average path has $f_Q = 0.34$. We used these special Q models in combination with Structure A.

3.3 A SOURCE MODEL FOR THE YELLOWSTONE PARK EARTHQUAKE

The teleseismic data from the event were of insufficient quality to infer the source parameters as we did for the Pocatello Valley event. However, there is enough other information to arrive at a reasonable source model for this event. This information is summarized below:

- The long period source measures (M_s, M_0) are essentially the same. The short period M_L is also the same but the m_b indicates that the Yellowstone event is smaller near 1 hertz.
- Pitt, et al. (1979) computed focal mechanism solutions from local recordings of the main shock and many fore- and aftershocks. These solutions indicate normal faulting with an approximate strike of N50°W. One solution dips 40° to the south and the depth distribution of the aftershocks suggests that this should be preferred over the orthogonal solution (the evidence is marginal). The slip appears to be vertical (up dip).
- Battis and Hill (1977) used a technique called far-field surface-wave amplitude spectral fitting (Turnbull, et al., 1973) to determine a focal mechanism. Their solution was poorly constrained, but seemed to agree with that of Pitt, et al. (1979).

In conclusion, we are reasonably certain that the earthquake was characterized by normal faulting with a strike of about N50°W. The dip and slip are less certain, but the evidence favors vertical slip (not much strike-slip component). The dip could be 40° to the south or 50° to the north. We prefer the former, though the evidence is not strong. Finally, if we assume the size and depth of the two events are the same, we should obtain an upper limit estimate for the Yellowstone source.

We will show synthetic seismograms with two orientations. These are:

Yellowstone Orientation 1

Strike	N50°W
Dip	39°S
Slip	Up 53°W

This is the Pocatello Valley fault orientation rotated to the known strike of the Yellowstone event.

Yellowstone Orientation 2

Strike	N50°W
Dip	40°S
Slip	Up 90°W

This is about the same as Orientation 1 except that the strike-slip component has been removed.

3.4 RADIATION PATTERNS OF THE POCATELLO VALLEY AND YELLOWSTONE PARK EARTHQUAKES

In Figure 12 we show the surface wave radiation patterns of the Pocatello earthquake source at four frequencies between 0.1 and 1 Hz. The amplitudes plotted are the Fourier spectral amplitudes of synthetic surface-wave displacement seismograms

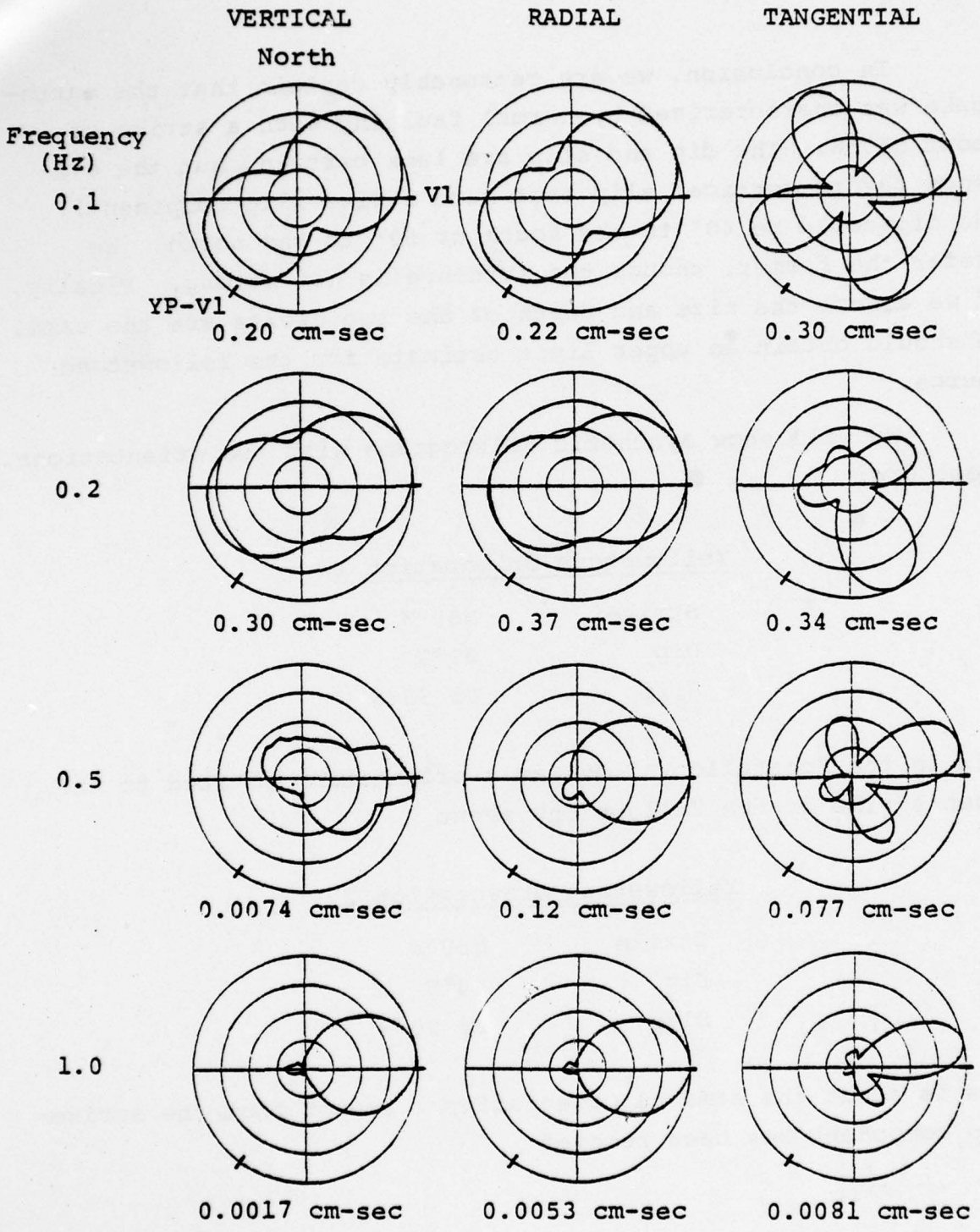

Figure 12. Surface wave radiation patterns for the Pocatello Valley earthquake source with Structure A, $f_Q = 2$ and a range of 650 km. The 90° azimuth to Site 1 of Wing V is indicated as V1. For Yellowstone Orientation 1, the portion of the pattern contributing to motions at Site 1 is indicated as YP-V1. The length of the radial axis is labeled below each plot.

(fundamental plus higher modes), computed as a function of azimuth for a fixed epicentral distance of 650 km. The computation used Structure A with $f_Q = 2$ (high Q) for the path structure. These amplitudes do not include the P-wave contributions, but at 650 km the surface-wave modes dominate the vertical and radial displacement spectra, at least for frequencies below 1 Hz, and essentially comprise the entire tangential spectrum.

On each radiation pattern plot in the figure we indicate the azimuth (90°) from the Pocatello Valley earthquake epicenter to Site 1 at Wing V. Thus the amplitudes at 90° are close to the spectral amplitudes (at the indicated frequencies) of the Site 1 displacement seismograms shown in Figure 2.

Now assume that the Yellowstone earthquake has the same orientation as the Pocatello Valley except for the strike (Yellowstone Orientation 1). Then the azimuth to Site 1 from the Yellowstone earthquake is the azimuth from the Pocatello Valley plus 95° (the difference in strike) plus 31° (the difference in source-receiver azimuth). This azimuth is also indicated on each radiation pattern in the figure.

The surface-wave radiation patterns at 0.1 Hz are close to double couple patterns. At higher frequencies they become highly skewed in the direction of slip. This is a source directivity effect associated with the direction of rupture propagation. The horizontal projection of the rupture direction, which in our model is the same as the slip direction, is one degree south of east.

Free-field radiation patterns for the Pocatello source are shown in Figure 13. The curves plotted for each frequency are the amplitudes of the far-field displacements in a whole-space as a function of azimuth for a fixed takeoff angle of 90° from vertical. The surface ground motion in a layered halfspace receives energy from all takeoff angles, of course, but the 90° case illustrates clearly the directivity of high

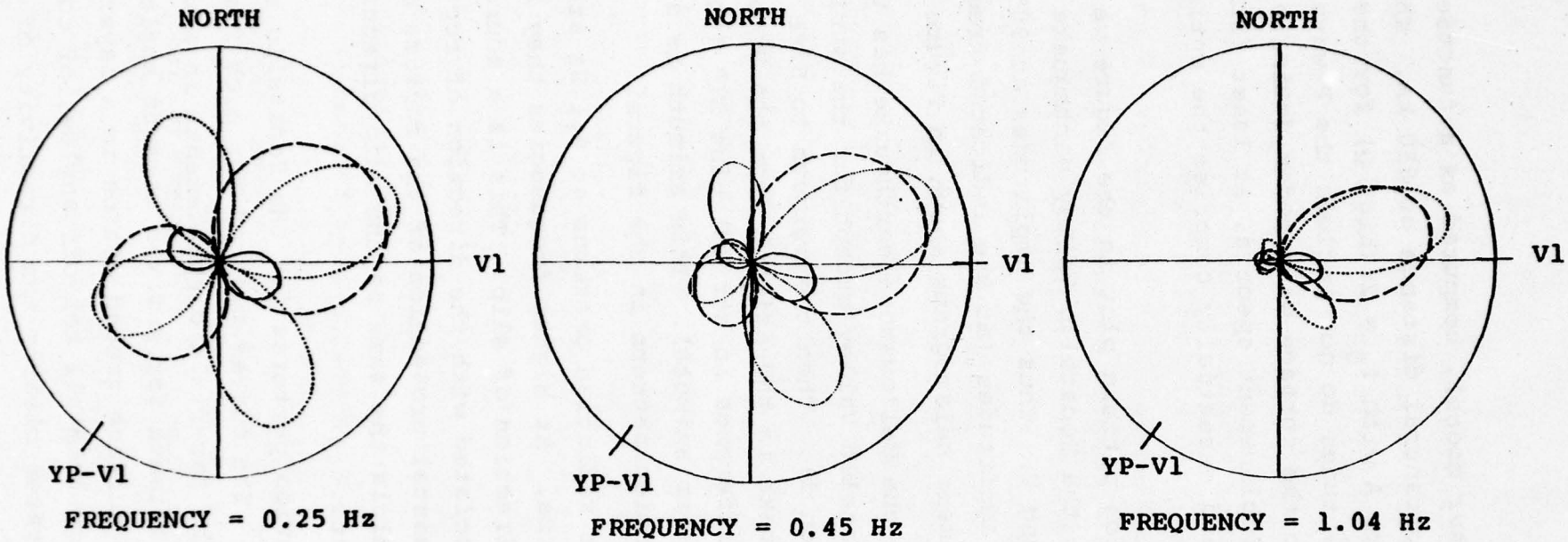

Figure 13. The free-field radiation patterns of the Pocatello Valley earthquake model at the horizontal takeoff angle are shown for three frequencies. On each plot, the amplitudes of the three components of displacement are drawn as a function of azimuth on a common arbitrary amplitude scale.

frequency energy. We might also point out that the radial component leaving the source with takeoff angle near 90° forms a large contribution to the regional P-wave arrivals.

The radiation pattern of the Pocatello earthquake has important implications for the ground motions at Wing V. From the Pocatello epicenter, Wing V subtends an azimuthal angle of about 89° to 98° from the north. The azimuth to Site 1 at Wing V is 90° and is labeled "V1" on the radiation plots in Figures 12 and 13. These plots imply that the high frequency energy from the Pocatello earthquake is directed toward Wing V. Therefore, peak ground accelerations would be higher at Wing V than at other azimuths from the Pocatello event. This is the case even allowing for uncertainty in our inferred fault orientation. A more subtle effect, apparent from the surface-wave radiation patterns, is a variation in both the low and high frequency ground motions across Wing V, decreasing as one goes from the northwest corner (89° azimuth) to the southeast corner (98° azimuth). This primarily affects the tangential component and the effect is reinforced by the variation in epicentral distance across the complex.

If Orientation 1 is appropriate for the Yellowstone earthquake, implying that this event has a significant left-lateral strike-slip component rupturing to the northwest, these radiation pattern effects would predict a significant difference in the Wing V ground motions from the Yellowstone and Pocatello events. Wing V Site 1 is 125° from the horizontal rupture direction of the Yellowstone Orientation 1 while being 1° from the Pocatello Valley earthquake rupture direction.

We did not construct radiation plots for Yellowstone Orientation 2, the orientation with no strike-slip component, but this orientation also directs the high frequency energy away from Wing V. The Wing V Site 1 is 81° from the rupture direction for Yellowstone Orientation 2. A reasonable approximation to the spectral amplitude at Site 1 for this orientation

is given by the radiation pattern values at 170° in Figure 12. At high frequencies the radiation at this azimuth is still much smaller than for the Pocatello Valley earthquake.

3.5 GROUND MOTIONS AT WING V

To quantify the effects of radiation pattern and caldera attenuation on the Yellowstone Park earthquake ground motions at Wing V, we computed Yellowstone-Wing V Site 1 seismograms with a number of different path models. We estimate the radiation pattern effect using seismograms computed with Structures A and B, f_Q = 1 and 2, which are the path models we used for the Pocatello ground motion calculations. With Structures A we computed seismograms with both Yellowstone fault orientations given in Section 3.3, while only Orientation 1 was used with Structure B. To estimate the combined radiation pattern and caldera effects, we computed seismograms using the Orientation 1 source with Structure A, f_Q = 0.53 and 0.34. As noted earlier, these values of f_Q, respectively, result from lowering Q in the caldera to one-tenth and one-twentieth the Q of the remaining 90 percent of the path, the latter Q being that for the f_Q = 1 model. Plots of all the synthetic Yellowstone earthquake seismograms are in Appendix A.

Figure 14 illustrates the radiation pattern effects on the Yellowstone ground motions by comparing synthetic Site 1 velocity seismograms from the Pocatello source and the two orientations of the Yellowstone source. The path model for all three sets of seismograms is Structure A, f_Q = 1. While the levels of low frequency motion at Site 1 from the two earthquakes are not very different, one can see that the high frequency motion (primarily the Lg phase) is much larger from the Pocatello event than from either orientation of the Yellowstone event.

In Figure 15 we make a similar comparison but with the low caldera Q included in the Yellowstone-Site 1 path. In

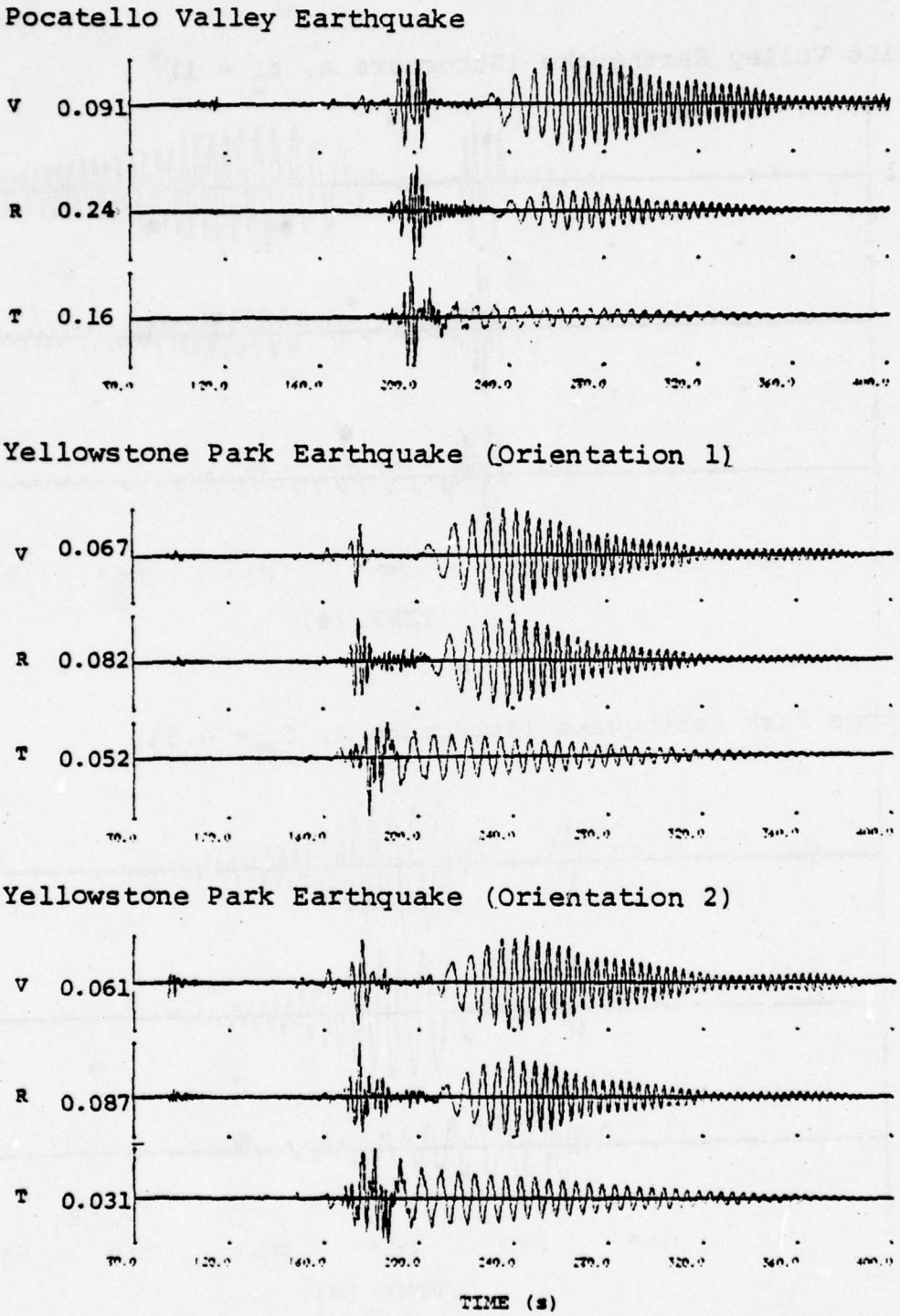

Figure 14. The effect of radiation pattern differences between the Pocatello Valley and Yellowstone Park earthquakes on the velocity seismograms at Wing V Site 1 is shown. The three sets of seismograms were computed with Structure A, $f_Q = 1$.

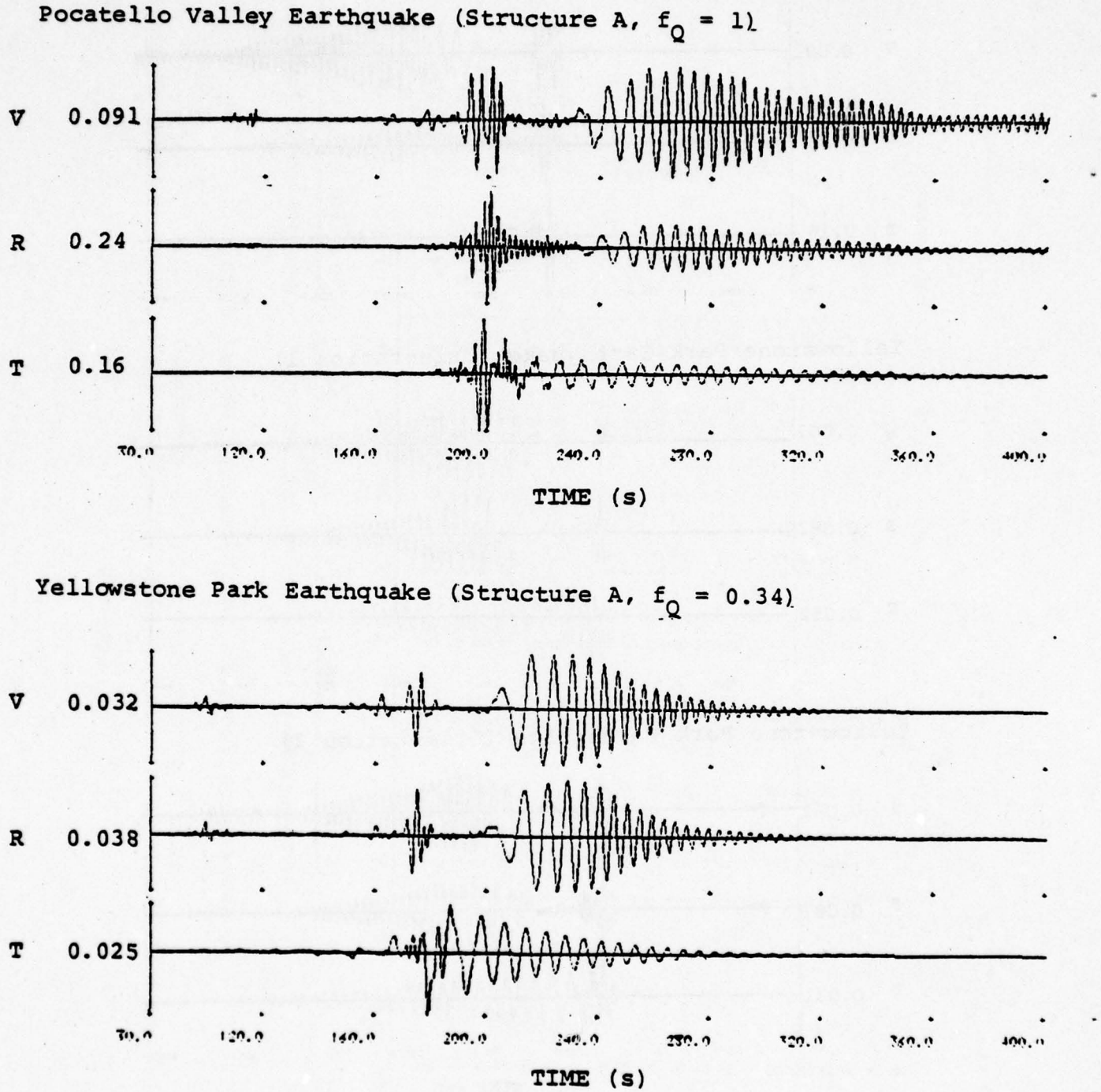

Figure 15. The velocity seismograms at Site 1 from the Pocatello Valley and Yellowstone (Orientation 1) earthquakes are compared. The attenuation due to Q/20 in the caldera has been included in the Yellowstone-Site 1 path model.

this figure, the Pocatello velocity seismograms from Figure 14 are compared to the Yellowstone velocity seismograms obtained with Structure A, f_o = 0.34. One can see that the radiation pattern differences and caldera attenuation cause the high frequency motion from the Yellowstone earthquake to be substantially smaller than for the Pocatello Valley earthquake. In addition, the caldera causes a reduction in the low frequency motion from the Yellowstone event.

Tables 4 and 5 compare the peak motions of our synthetic Yellowstone- and Pocatello-Wing V Site 1 seismograms. In Table 4 the Yellowstone earthquake peak motions obtained without a low caldera Q in the path model are compared to the corresponding Pocatello earthquake values. The Yellowstone peak motions given in Table 5 do include the effect of a low Q caldera. Figures 16 and 17, respectively, show the peak motion values from the two tables in graphical form.

From Table 4 we see that the variation in the peak Yellowstone-Site 1 ground motions for different path structures is about the same as the variation in the peak Pocatello motions: about a factor of 3. For each path structure, though, the peak motions from the Pocatello event are on the order of 2-3 times larger than those from the Yellowstone event. The horizontal accelerations differ the most, with Pocatello to Yellowstone ratios as large as 5. As we show for Structure A, the peak motion ratios between the two events are similar for both assumed Yellowstone fault orientations. Thus, we can infer from Table 4 that known differences between the orientations of the Pocatello Valley and Yellowstone Park earthquakes radiation patterns with respect to Wing V are likely to have caused differences on the order of a factor of 3 in the peak accelerations at Wing V from the two events.

In Table 5, we see that the effect of a low Q caldera in the Yellowstone-Wing V path increases the Pocatello to Yellowstone peak motion ratios to as much as 10. The caldera

TABLE 4

COMPARISON OF THE POCATELLO VALLEY AND YELLOWSTONE EARTHQUAKE PEAK GROUND MOTIONS AT WING V SITE 1 WITH NORMAL Q IN THE CALDERA

(* Denotes Yellowstone Earthquake Orientation 2)

			Displacement (cm)				Velocity (cm/sec)				Acceleration (cm/sec^2)			
			PV		YP		PV		YP		PV		YP	
Component	Structure	f_Q	A	T	A	T	A	T	A	T	A	T	A	T
V	B	2	.15	5	.12	6	.22	4	.14	4	.44	3	.20	3
	B	1	.13	5	.10	6	.17	4	.11	4	.32	3	.16	4
	A	2	.054	6	.041	8	.066	5	.043	5	.16	3	.059	5
	A	1	.041	6	.036	9	.047	5	.034	6	.099	3	.042	5
	A	2			.033*	6			.042*	5			.096*	1
	A	1			.026*	6			.031*	5			.071*	1
R	B	2	.098	4	.071	8	.14	3	.093	5	.31	2	.15	4
	B	1	.078	4	.060	9	.11	5	.078	5	.21	2	.12	4
	A	2	.074	2	.046	5	.19	2	.053	5	.58	2	.11	2
	A	1	.049	3	.039	8	.12	2	.041	5	.35	2	.074	3
	A	2			.040*	6			.067	3			.17*	2
	A	1			.032*	6			.050	3			.11*	2
T	B	2	.13	5	.045	14	.23	2	.10	3	.83	1	.21	2
	B	1	.11	5	.037	15	.16	2	.078	3	.40	2	.14	2
	A	2	.069	4	.027	15	.11	3	.043	3	.23	3	.082	3
	A	1	.054	4	.022	15	.080	4	.032	4	.15	3	.057	3
	A	2			.021*	15			.023*	3			.059	2
	A	1			.017*	15			.016*	3			.037*	2

TABLE 5

COMPARISON OF THE POCATELLO VALLEY AND YELLOWSTONE PARK EARTHQUAKE PEAK GROUND MOTIONS AT WING V SITE 1 WITH LOW CALDERA Q'S

(Path Model is Structure A)

Component	Description	f_Q	Displacement (cm) A	Displacement (cm) T	Velocity (cm/sec) A	Velocity (cm/sec) T	Acceleration (cm/sec^2) A	Acceleration (cm/sec^2) T
V	Pocatello Valley	1	.041	6	.047	5	.099	3
	Yellowstone Park, Q/10 Caldera	.53	.029	11	.023	6	.027	4
	Yellowstone Park, Q/20 Caldera	.34	.024	11	.016	8	.018	4
R	Pocatello Valley	1	.049	3	.12	2	.35	2
	Yellowstone Park, Q/10 Caldera	.53	.032	9	.028	6	.044	3
	Yellowstone Park, Q/20 Caldera	.34	.026	10	.019	7	.025	3
T	Pocatello Valley	1	.054	4	.080	4	.15	3
	Yellowstone Park, Q/10 Caldera	.53	.018	16	.021	7	.032	3
	Yellowstone Park, Q/20 Caldera	.34	.015	16	.014	8	.018	4

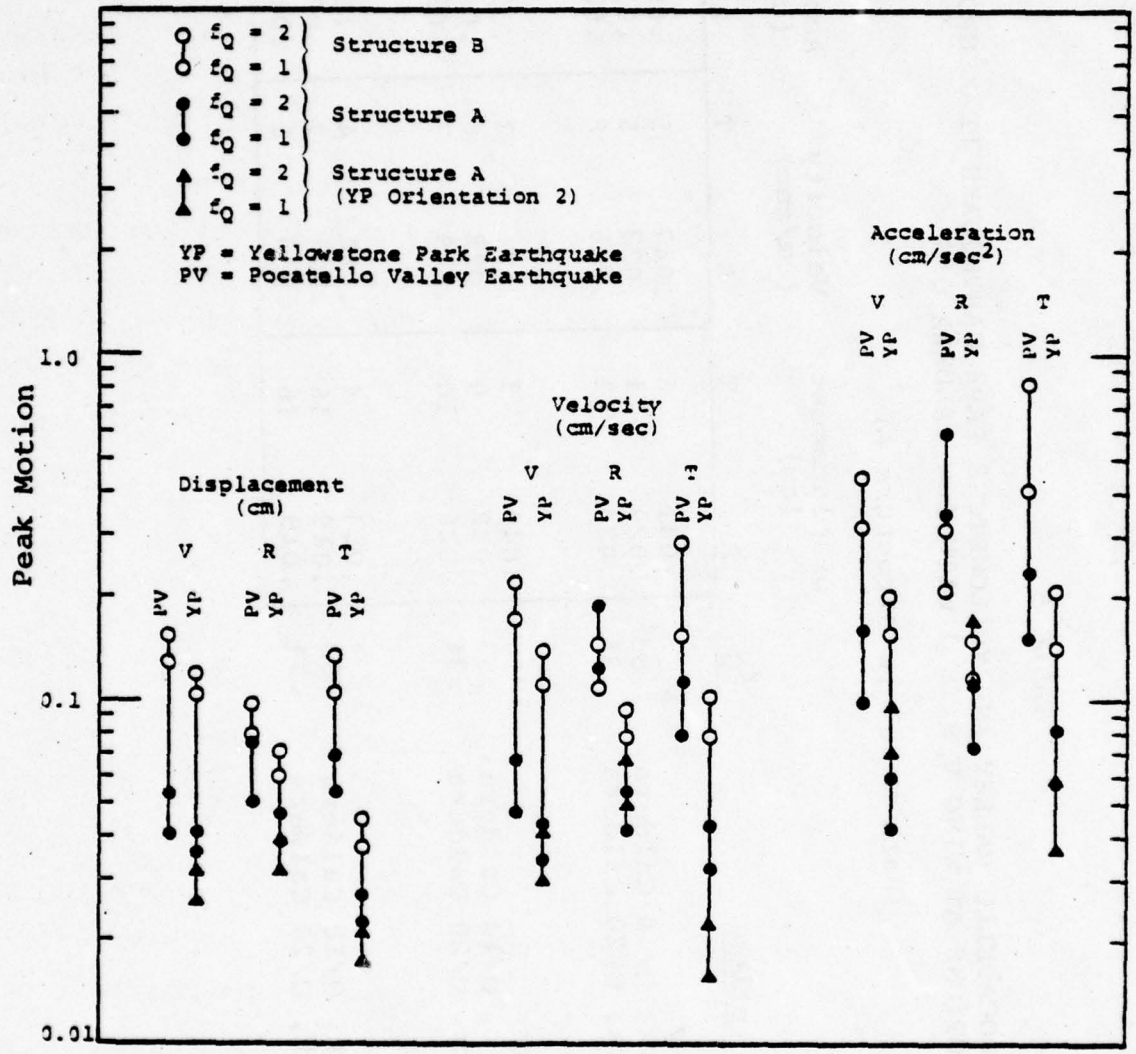

Figure 16. The peak Pocatello and Yellowstone-Wing V Site 1 ground motions from Table 4.

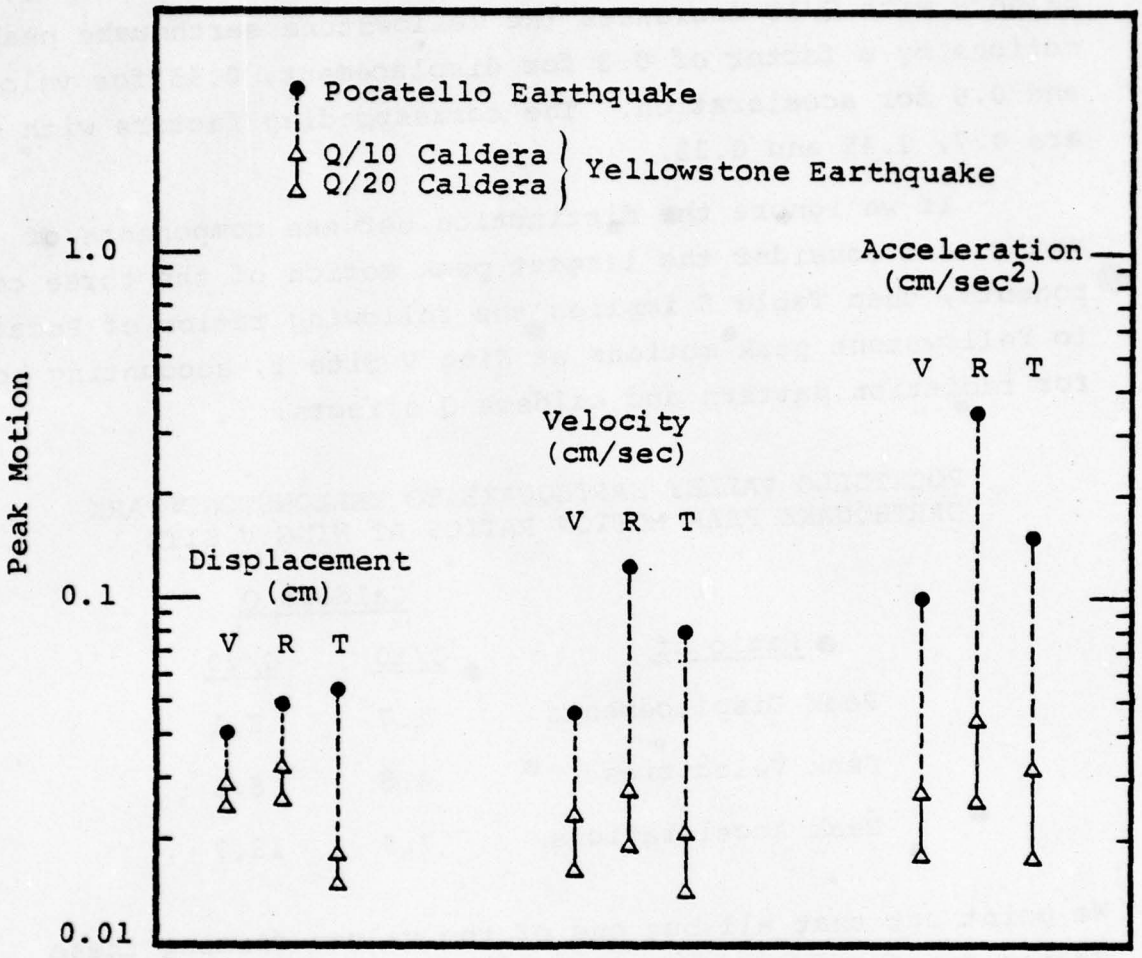

Figure 17. Peak ground motions at Wing V Site 1 from Pocatello and Yellowstone earthquakes accounting for low Q caldera (from Table 5).

Q affects the three components of the Yellowstone ground motion almost equally. Compared to a caldera with normal Q, a caldera with Q/10 decreases the Yellowstone earthquake peak motions by a factor of 0.8 for displacement, 0.65 for velocity, and 0.6 for acceleration. The corresponding factors with Q/20 are 0.7, 0.45 and 0.35.

If we ignore the distinction between components of motion and consider the largest peak motion of the three components, then Table 5 implies the following ratios of Pocatello to Yellowstone peak motions at Wing V Site 1, accounting both for radiation pattern and caldera Q effects:

POCATELLO VALLEY EARTHQUAKE TO YELLOWSTONE PARK EARTHQUAKE PEAK MOTION RATIOS AT WING V SITE 1

	Caldera Q	
Ratio of	Q/10	Q/20
Peak Displacements	1.7	2.1
Peak Velocities	4.5	6.6
Peak Accelerations	7.9	13.7

We point out that all but one of the values forming these ratios are for the radial component, the one exception being for the tangential component.

Because of the limitations in our source and path models, and in our synthesis procedures, the above ratios can only be considered crude estimates of the relative peak motions at Wing V from the Pocatello Valley and Yellowstone Park earthquakes. Had we used Structure B rather than Structure A to determine these ratios, they would probably be a little smaller since the radiation pattern effect by itself tends to be smaller for Structure B than Structure A (see Table 4). However, if we had to pick one model as the more likely structure along the Pocatello- and Yellowstone-Wing V paths, we would pick A. While we know of no substantial differences in

the average crustal structures for the two paths (other than the caldera), they could exist. Based on our experience with the two structures, A and B, studied here, such differences could cause our inferred Pocatello to Yellowstone peak motion ratios to increase or decrease by a factor of 2 or 3.

The remaining figures in this section show the response spectra for our synthetic Yellowstone earthquake seismograms and compare them to the Pocatello-Site 1 response spectra. All the response spectra have 0.05 of critical damping.

Figures 18 and 19 show the Yellowstone earthquake response spectra at Wing V Site 1 obtained with path models that do not include a low Q caldera: Structures A and B, f_Q = 1 and 2. The response spectra in Figure 18 are for Yellowstone Orientation 1 with each of the four path models. (The f_Q = 2 curve lies above the f_Q = 1 curve for both A and B.) The dependence on sediment thickness and Q we see is similar to that for the Pocatello Valley earthquake. In Figure 19 the response spectra obtained with the two Yellowstone fault orientations are compared. At the periods of greatest response, the curves for the two orientations are almost the same except that the tangential responses for Orientation 2 are somewhat lower.

Figures 20 and 21 compare the Wing V Site 1 response spectra from the Yellowstone Park earthquake to those from the Pocatello Valley earthquake. In Figure 20 the effect of the different radiation patterns of the two events is shown. The solid line outlines the four Pocatello response curves that result from the four path structure models (an outline of the Site 1 curves in Figures 7 through 9). The dashed line outlines the six independent Yellowstone response curves in Figures 18 and 19, which are for the two orientations and four path models with no caldera. The response curves for the two events differ by about half an order of magnitude, which is consistent with the peak motion ratios we attributed to radiation pattern effects.

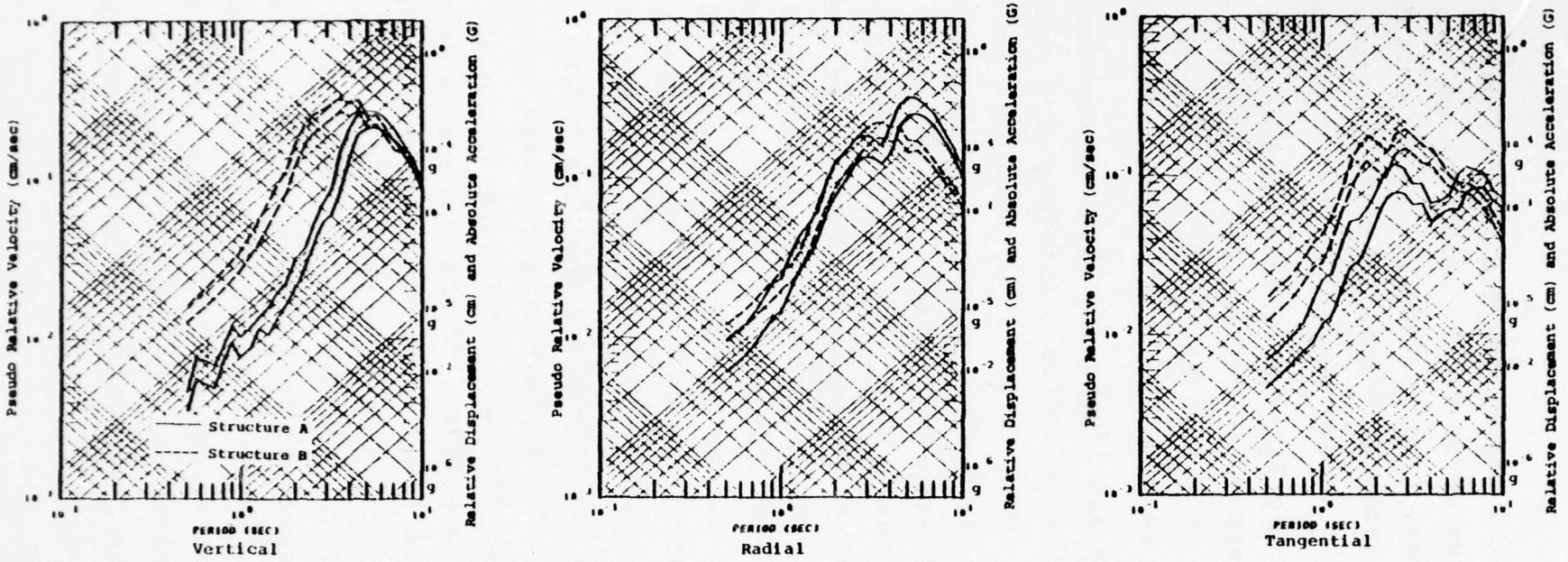

Figure 18. The response spectra for the Yellowstone earthquake Orientation 1 seismograms at Wing V Site 1 are shown for four path models. The two curves for each of Structures A and B correspond to the two Q models given by $f_Q = 1$ and $f_Q = 2$. (The $f_Q = 2$ curves lie above the $f_Q = 1$ curves.) The damping factor is 0.05 of critical.

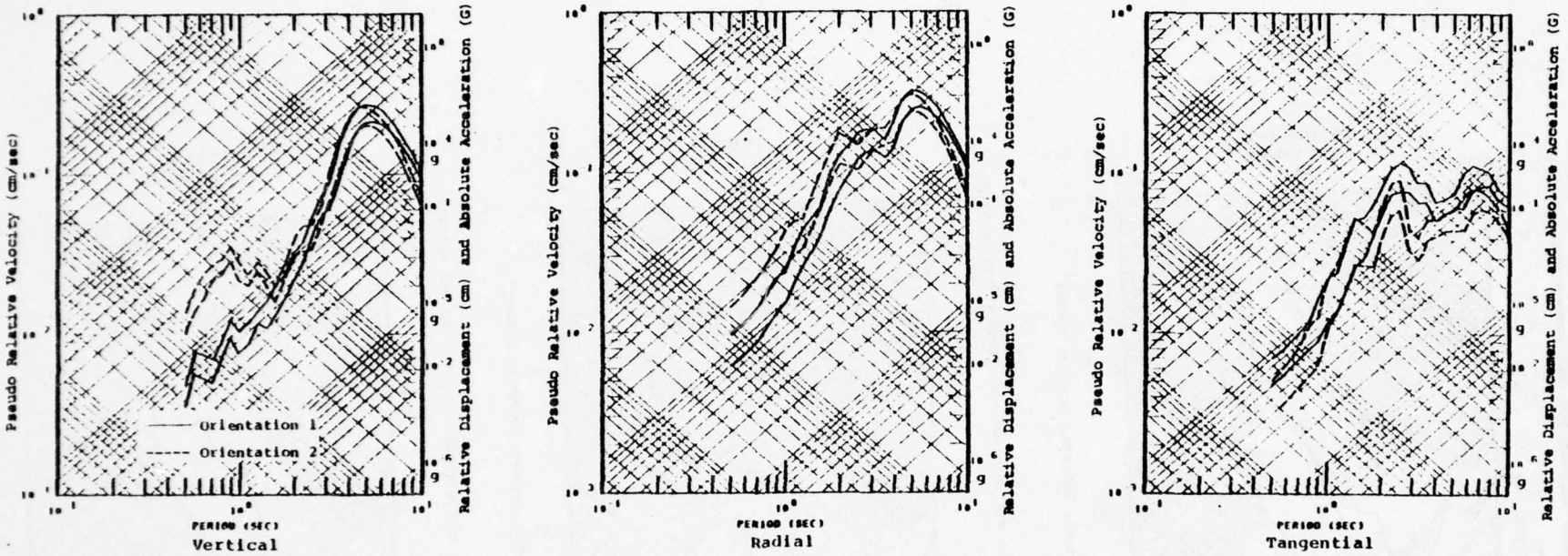

Figure 19. The response spectra at Wing V Site 1 are shown for two orientations of the Yellowstone earthquake. The path models for each orientation are Structure A, f_Q = 1 and 2.

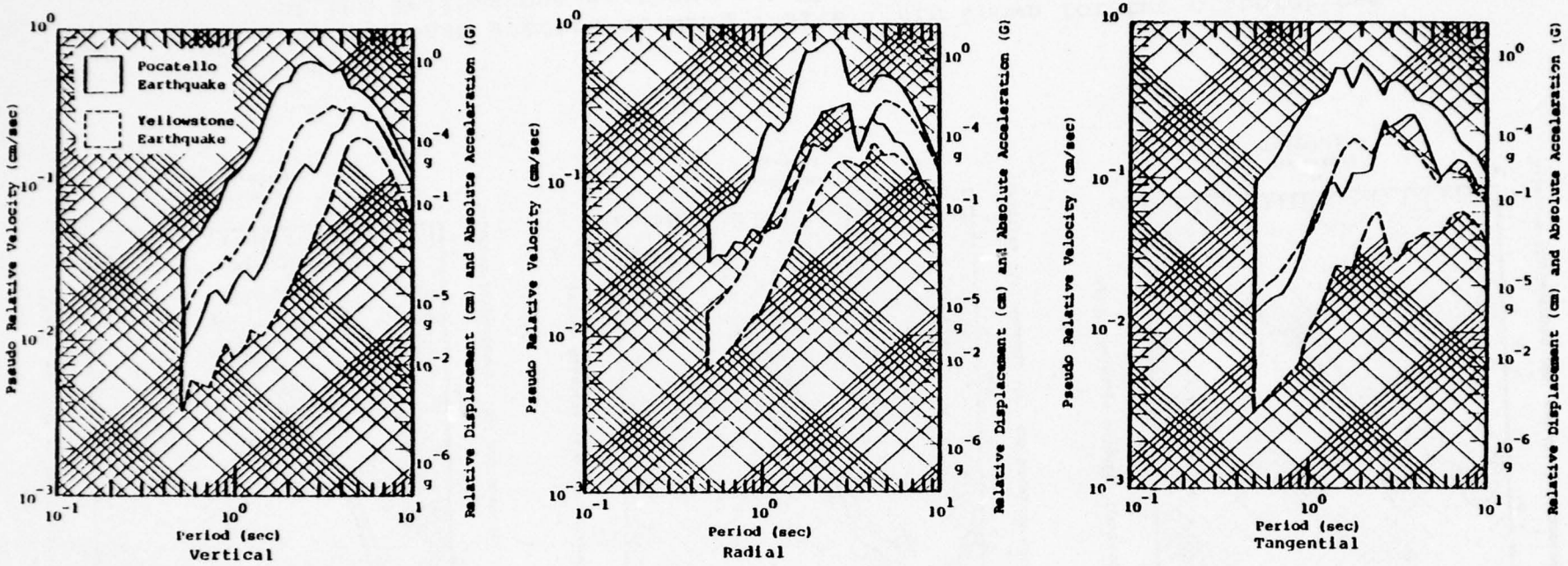

Figure 20. The range of response spectra at Wing V Site 1 determined by different path models (no caldera) and different Yellowstone earthquake orientations are shown for the Pocatello Valley and Yellowstone Park earthquakes. The Pocatello range is that determined by the curves in Figures 7 through 9 and the Yellowstone range by the curves in Figures 18 and 19.

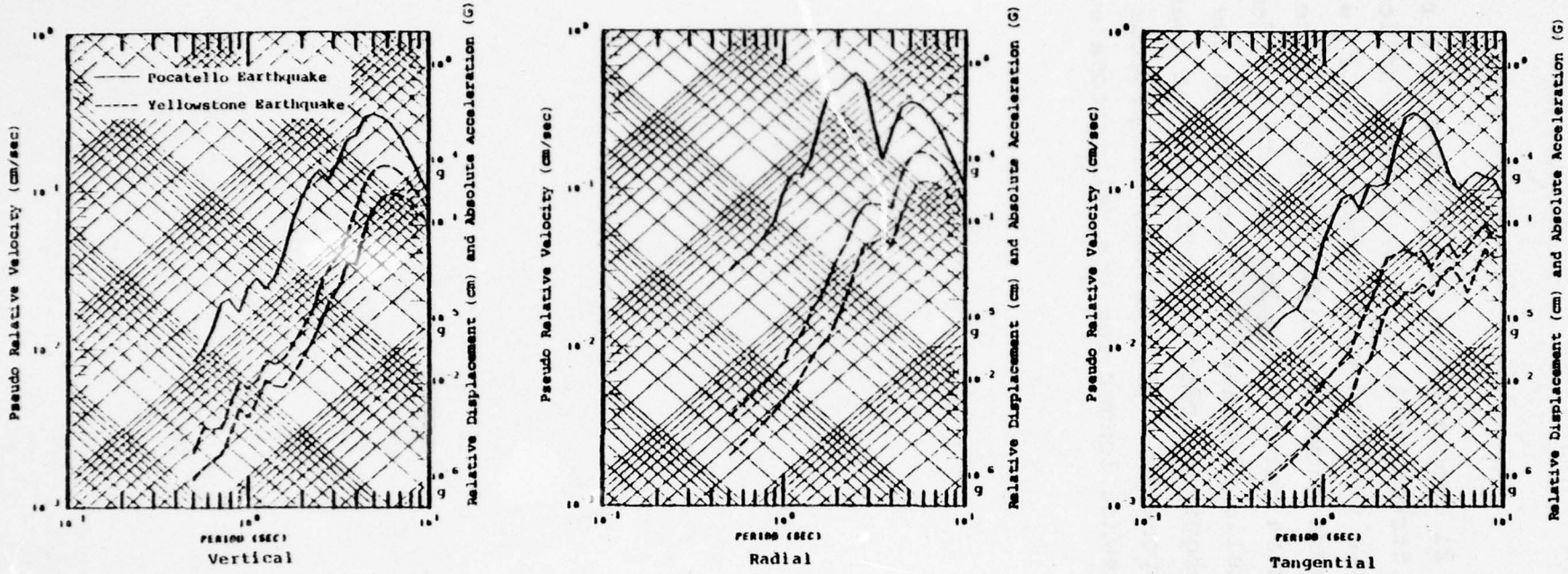

Figure 21. The response spectra at Wing V Site 1 from the Pocatello and Yellowstone earthquakes are compared. The path model for each curve is Structure A, with a Q/10 (top) and Q/20 caldera in the Yellowstone-Wing V path.

Figure 21 compares the Pocatello-Site 1 response spectra obtained with Structure A, $f_Q = 1$, and the Yellowstone-Site 1 response spectra obtained with Structure A, $f_Q = 0.53$ and 0.34. Thus, this figure shows the differences that are attributable to both radiation pattern and low caldera Q effects. We see that the Pocatello responses are larger than the Yellowstone responses by about an order of magnitude, at least for the horizontal components. In addition, the periods of peak response are somewhat longer for the Yellowstone event.

IV. EFFECTS OF SITE TOPOGRAPHY ON EARTHQUAKE GROUND MOTIONS

4.1 INTRODUCTION

An important feature of the Wing V ground motions is that they appeared to be much stronger at some sites than at others. This dichotomy is illustrated in Figure 22. Why were ground motions stronger at some sites than at others?

There are basically four possible causes for systematic ground motion differences like those shown in Figure 22.

1. The differences are due to the source radiation pattern. This seems most unlikely for the small azimuthal variations in this case. The distance attenuation from west to east is a stronger effect, yet many of the easterly silos experienced stronger ground motions.

2. The differences are due to deep structure (several kilometers and more) which causes the waves to be focused or channeled. This is certainly a possible explanation as this effect has been observed elsewhere (e.g., Haddon and Husebye, 1978).

3. The differences are due to characteristics of the local geology; for example, the depth of the sediment. There is no question that the local site geology affects the ground motion. There are very many (probably hundreds) papers devoted to this subject in the earthquake engineering literature (e.g., see recent summary papers by Donovan, 1978 and Cluff, 1978). Perhaps the observed effects can be explained on this basis. We have insufficient data to attempt to do so at this time.

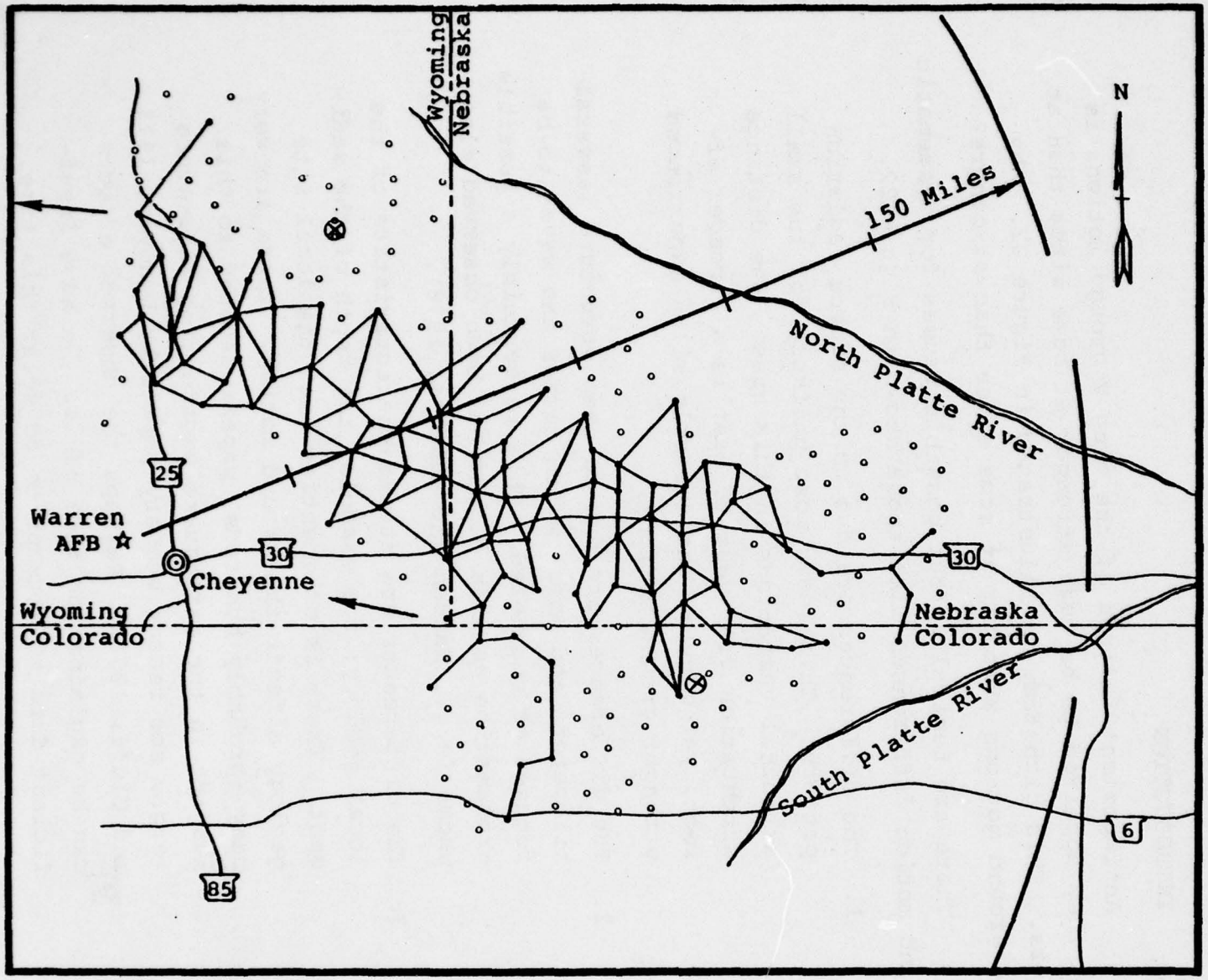

Figure 22. The Wing V silos are plotted. The closed circles indicate silos at which the ground motions were the largest. Our Sites 1 and 2 and the azimuth to the Pocatello Valley earthquake epicenter are indicated as in Figure 1. (Figure provided by R. A. Gray, private communication.)

4. The differences are due to the surface topography. A general observation is that the larger ground motions occurred on plateaus while the smaller ground motions were observed in lower lying valleys (R. A. Gray, private communication). In this section we are primarily concerned with this effect.

The ground motion simulations of the previous section were done with plane-layered earth models. They take no account of site differences other than those due to range and azimuth variations. Thus, our synthetic seismograms may be viewed as estimates for the "average" ground motions. The four effects listed above then modify this average ground motion.

In this section, we briefly discuss the current state of knowledge of the effects of local topographic features. In our research program we did no calculations to study this effect. Therefore, we will discuss results obtained by others. We shall see that the knowledge of topographic effects is really quite meager. Only a few calculations have been made, many for problems of unrealistic simplicity. This is an area of research in which work is just beginning.

4.2 SUMMARY OF PREVIOUS STUDIES

Several authors (Boore, 1972; Bouchon, 1973; Wong and Jennings, 1975) have shown that the large accelerations recorded at Pacoima Dam were due in part to the local topography. Local amplification may have increased the ground motions by as much as 50 percent. In Figure 23 we show the geometries considered by these authors. The most realistic is that of Wong and Jennings (1975). Pacoima Dam is located near the top of the ridge on the right side of the canyon.

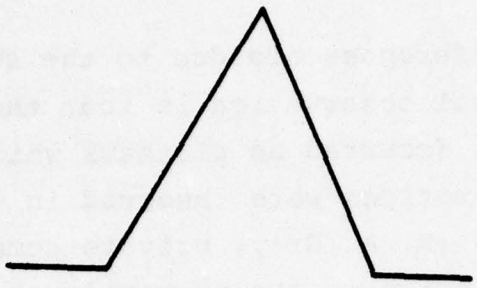

Boore (1972)

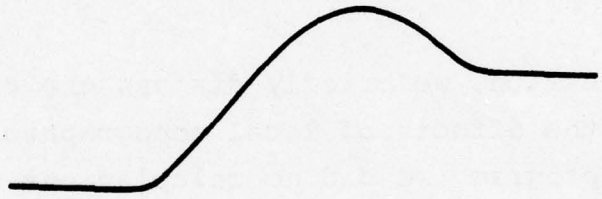

Bouchon (1973)

Wong and Jennings (1975)

Figure 23. Configurations used as approximations to the Pacoima Dam topography.

Boore (1972) examined the effect of a triangular hill on incident plane SH waves. He found the maximum response to occur at the crest, with response increasing as the slopes steepen. The maximum effect on the peak amplitudes was about 75 percent and for cases simulating the Pacoima Dam configuration about 25-50 percent. Frequencies with wavelengths comparable or smaller than the dimensions of the hill appeared to be most affected. Bouchon (1973) analyzed a smoothed hill and valley configuration with incident P, SV and SH motion and reached very similar conclusions.

Wong and Jennings (1975) used a more accurate approximation for the actual topographic configuration of the Pacoima Dam site. Their study showed that peak responses can vary by factors similar to those found by previous authors, but found variations in Fourier spectral response as large as a factor of six for wavelengths shorter than the canyon width. Their results suggest that details in the actual configuration may add complications which cannot be simulated by the simplified models, particularly at the high frequencies. The spectral responses were found to be extremely sensitive to the incident angles of incoming motion and the precise location of the observer. Response spectra were affected only at high frequencies.

The most detailed study of topographic effects is that of Sills (1978). This study examined the response of a semi-circular canyon, semi-circular hill, a Gaussian-shaped mountain and a smoothed ridge with adjacent valley. Each case was examined for various angles of incident SH motion, and different observer locations. The analysis of the semi-circular canyon and hill show strong amplifications and deamplifications at the edges of the structures. The displacement amplitudes were found to be highly dependent upon position, frequency, and angle of incidence (Figure 24). The response of the Gaussian-shaped mountain tended to be relatively much simpler.

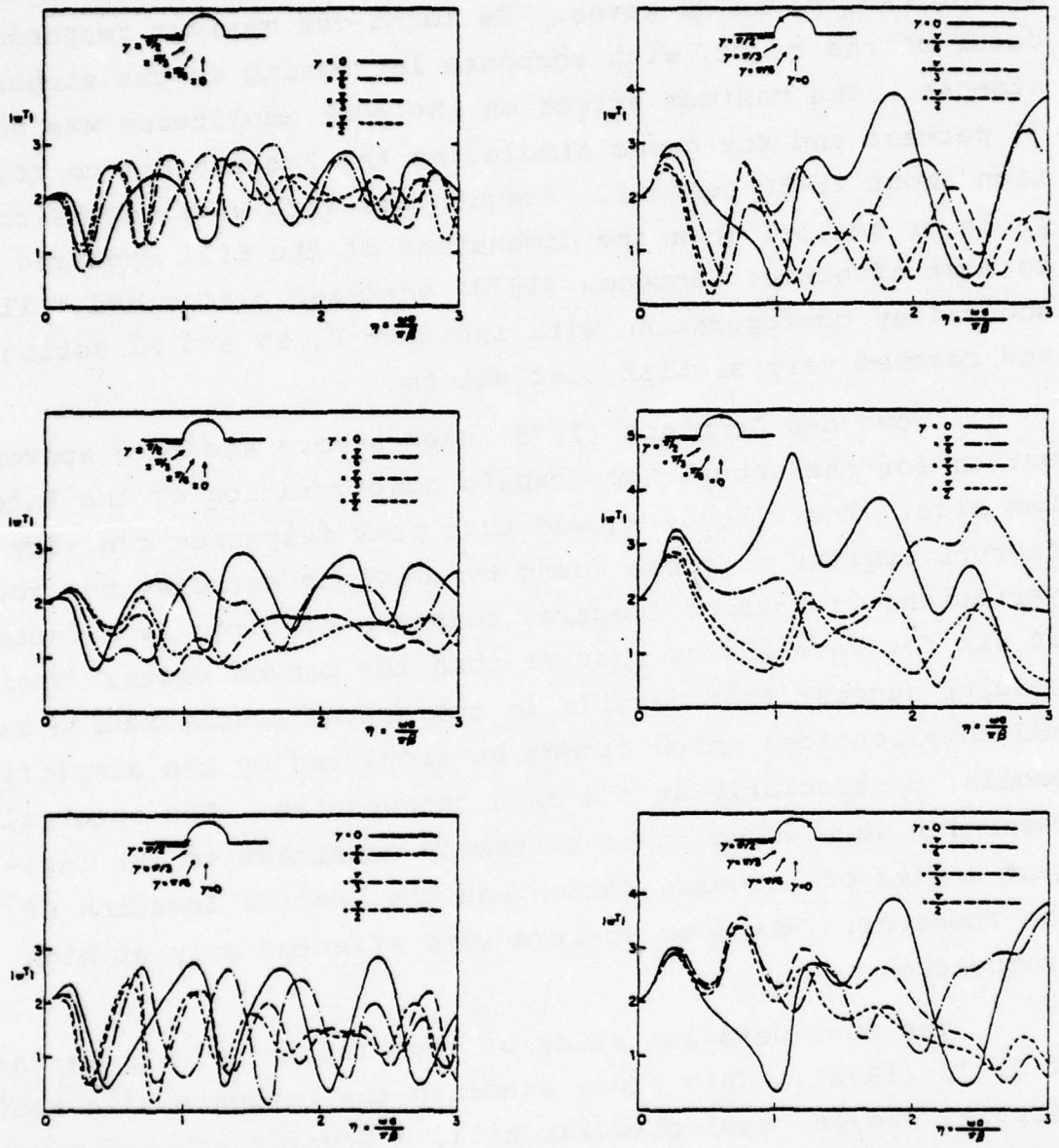

Figure 24. The spectral response relative to flat topography (w^T) is shown at six positions near a semi-circular hill. For each position, the responses for four angles of incidence (γ) are plotted versus normalized frequency (η). The radius of the hill is denoted as a and the shear velocity of the medium as β (from Sills, 1978).

Near-normal incidences tended to give a larger response than horizontal incidences. Motion at the crest of the hill was actually deamplified by horizontally incident motion (Figure 25). The ridge-valley configuration response was strongly dependent upon the direction of incoming motion. The response on the top of the ridge was considerably larger for motion incident on the ridge side as compared to incidence from the valley side.

A major conclusion drawn by Sills is that simple generalizations of the dependence of ground motion on the topographic relief is virtually impossible at this time. The circumstances at a particular site must be examined on an individual basis. The response tends to be very sensitive to all the variables involved.

4.3 LOCAL TOPOGRAPHY AND WING V

We have made some rather general observations about the potential effect of topographic features on ground motions. How do these apply to Wing V? First, we refer back to Figure 22. The largest sharp elevation changes in the Wing V area are less than 1,000 feet. The low ground motion sites to the north are differentiated from nearby high ground motion sites by elevation changes of this order. However, the low ground motion sites to the south do not appear to be characterized by topographical changes of nearly this magnitude.

The frequencies affected by surface topography are generally those with wavelengths comparable to or less than the dimensions of the dominant feature. Further, these effects are rather local in that they do not seem to be important several wavelengths from the feature. The wavelengths are proportional to period; for three second waves the wavelengths are about 10 km. Thus, the dimensions of the topographic features expected to have some influence are quite a lot larger than the scale of sharp topographic variations.

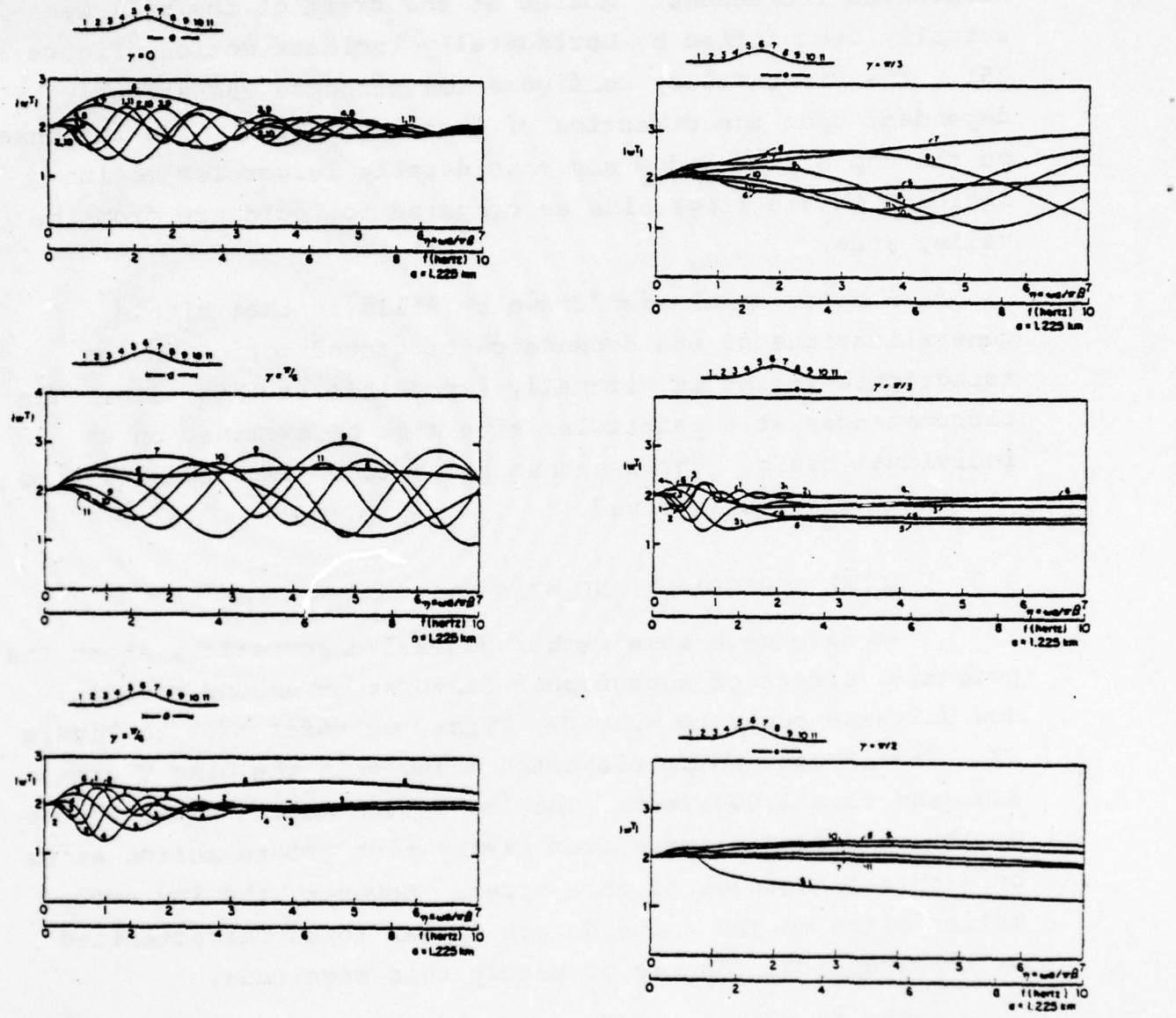

Figure 25. The spectral response relative to flat topography on a Gaussian-shaped hill (from Sills, 1978).

We conclude that the observed ground motion differences are not likely to be due to changes in the surface topography. Changes in the deep (several kilometers and more) and/or shallow geology seem much more likely to produce the observed effects.

AD-A069 727 SYSTEMS SCIENCE AND SOFTWARE LA JOLLA CALIF F/G 8/11
SYNTHESIS OF REGIONAL GROUND MOTION FROM WESTERN U. S. EARTHQUA--ETC (U)
MAR 79 W L RODI, T C BACHE, H J SWANGER F19628-77-C-0004
UNCLASSIFIED SSS-R-79-3988 AFGL-TR-79-0080 NL

2 OF 3
AD
A069727

We conclude that the observed ground motion differences are not likely to be due to changes in the surface topography. Changes in the deep (several kilometers and more) and/or shallow geology seem much more likely to produce the observed effects.

V. GROUND MOTIONS AT 150 AND 250 KM FROM WESTERN UNITED STATES EARTHQUAKES

5.1 INTRODUCTION

In previous sections we have been concerned about the ground motion at specific locations from specific events. Now we take a more general perspective and estimate the expected ground motions at ranges of 150-250 km from typical western U. S. earthquakes. The Pocatello Valley and Yellowstone events are assumed to typify the earthquakes of interest and our sources are based on our models for these events.

There are many parameters that influence earthquake ground motion. They include the dynamic source characteristics (stress drop, source dimension, rupture velocity, fault complexity, etc.), the source orientation and the focal depth. There is also the station range and azimuth and the characteristics of the travel path. An exhaustive study of the effects of these many parameters was not attempted. Rather, our objective is to characterize the major features of the ground motions at 150-250 km and give some initial estimates of the dependence on azimuth, crustal structure, source depth and event magnitude.

The source model we use for most of the calculations in this section is the Pocatello Valley earthquake model we used in Section II for inferring ground motions at Wing V. The model is described in Section 1.3 of this report and by Day, et al., (1978). The 1975 Pocatello Valley earthquake was a shallow magnitude 6 event whose source spectrum, radiation pattern and depth we believe to be typical of other past, and likely future, large earthquakes in the western U. S. Its inferred rupture history is similar to that inferred by Bache and Barker (1978) for the 1971 San Fernando earthquake. We do not entirely fix the source model in our calculations in this section. Seismograms from a shallower source and for a similar source of larger magnitude are compared to the seismograms from the Pocatello Valley source model.

We compute ground motions with three path structure models. Two of the models are Structures A and B, which we used in Sections II and III and which are listed in Table 1 (Section 2.3). Structure A is a model of the northern Colorado Plateau inferred by Keller, et al. (1976) and Structure B is the same model with the 2 km sedimentary layer replaced by basement material.

The third path model, which we call Structure C, is a model of the crustal structure in the southern Basin and Range, inferred by Bache, et al. (1978). This model was derived from the Rayleigh waves from Nevada Test Site explosions recorded at Tucson, Arizona. We actually use a simplified five-layer version of the multilayer model given by Bache, et al. In addition, we replaced their Q_β model by one more similar to the Q_β structures of Structures A and B. The parameters of Structure C are listed in Table 6.

In Sections II and III we showed seismograms obtained with two Q structures, but we do not do that in this section. Our calculations with standard and doubled Q values showed that the Q-dependence of the ground motions at 150 and 250 km is rather small compared to that at distances greater than 600 km. Therefore, all of the seismograms, peak motions and response spectra shown in this section were obtained with the standard Q structures listed in Table 1 for Structures A and B and Table 6 for Structure C. These models represent our best estimates of western U. S. crustal Q's.

As in previous sections, we present our ground motion synthesis results in the form of synthetic seismograms, peak motion values, and response spectra. All synthetic seismograms are shown in Appendix B. In this section we only show the velocity seismograms for they typically display the main features of both the low and high frequency motion.

TABLE 6

MODEL C, BASIN AND RANGE CRUSTAL MODEL
FROM BACHE, et al., (1978)

LAYER THICKNESS (km)	DEPTH (km)	P VELOCITY (km/sec)	S VELOCITY (km/sec)	DENSITY (gm/cm^3)	Q_β
1	1	3.21	1.89	2.33	75
11	12	5.96	3.52	2.78	350
9	21	6.11	3.61	2.80	375
10	31	6.37	3.76	2.84	400
∞	∞	7.90	4.42	3.20	650

5.2 EFFECTS OF SOURCE RADIATION PATTERN

In Section 3.4 we saw that the radiation patterns for our earthquake source model were close to double-couple patterns at low frequencies and were strongly asymmetric at high frequencies because of source directivity effects. The free-field radiation patterns for the horizontal take-off angle were shown in Figure 13 and these are appropriate for the epicentral distances considered in that section. The relative contributions from other take-off angles, however, may be more important at the shorter distances considered here. The surface-wave radiation patterns shown in Figure 12 were evaluated for a distance of 650 km. In Figure 26 we show the analogous patterns for a distance of 200 km.

Each pattern in Figure 26 is an azimuthal plot of the spectral displacement amplitude of the multimode surface-wave. The radiation patterns are oriented geographically. For the Pocatello Valley earthquake model, the strike is N45°E and the horizontal projection of the rupture (slip) direction is S89°E. The radiation patterns at 200 km are very similar to those at 650 km, except they have larger amplitudes and slightly altered shapes because the individual surface wave modes interfer differently at the two distances. However, these surface wave patterns do not include the P wave contributions which are much more important at ranges of 150 and 250 km than they were for the ranges considered in Sections II and III.

To see how the radiation patterns of this source model affect the ground motions at 150 and 250 km, we computed synthetic seismograms with Structure A for each distance and two azimuths: 90° and 216° from north. The two azimuths are marked on Figure 26 and we see that one is on a high and the other on a low of the high frequency surface wave radiation. Comparing Figures 26 and 12, we also see that 90° and 216° were the azimuths of Wing V Site 1 with respect to the Pocatello

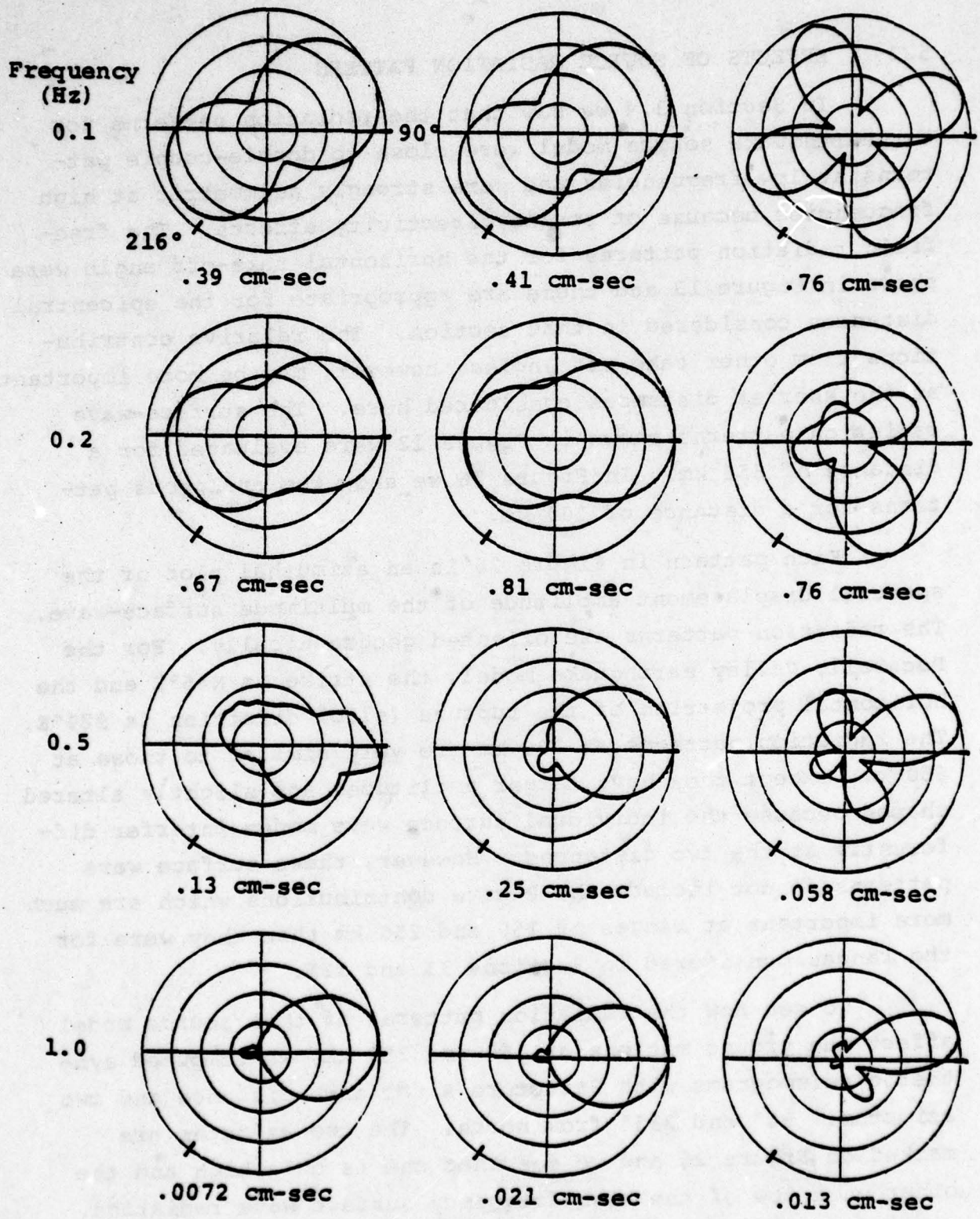

Figure 26. The surface wave radiation patterns from the Pocatello Valley earthquake model at an epicentral distance of 200 km are shown in the same format as in Figure 12.

and Yellowstone earthquakes, the latter corrected for the 95° difference between the strikes of the two events.

Figure 27 compares the three-component velocity seismograms for azimuths of 90° and 216° at a distance of 150 km. At both azimuths the P waves, which arrive near the time t = 30 sec, are the biggest arrivals and contain the highest frequencies. The fundamental mode Rayleigh wave is the next biggest phase, beginning at about t = 55 sec on the vertical and radial components. The smallest phases on each component are the Lg and S waves between about t = 40 sec and t = 55 sec.

At 150 km the P waves have about the same amplitude at 90° and 216° azimuths. The fundamental mode Rayleigh and Love waves are somewhat bigger at 90° than at 216°. However, the greatest azimuthal variation is in the horizontal components of Lg, which are much bigger at 90°.

Figure 28 compares the velocity seismograms for the two azimuths at a distance of 250 km. The P waves attenuate rapidly with distance and are a much smaller arrival at 250 km. In addition, we see a large azimuthal variation in the P waves, which are much bigger and contain more high frequencies at 90° than at 216°. This is distinctly different from the variation at 150 km (Figure 27), where the amplitude and frequency content of the P waves at the two azimuths are similar. The azimuthal dependence of the Lg, S and surface waves at 250 km, on the other hand, is similar to that at 150 km. However, the P wave phases on the records include energy from many different source take-off angles arriving at nearly the same time. This is especially true at 150 km. Thus, a single take-off angle radiation pattern plot like that in Figure 13 does not explain the computed azimuthal variation of the P waves.

In Table 7 we compare the peak displacements, velocities and accelerations from the synthetic seismograms at the two

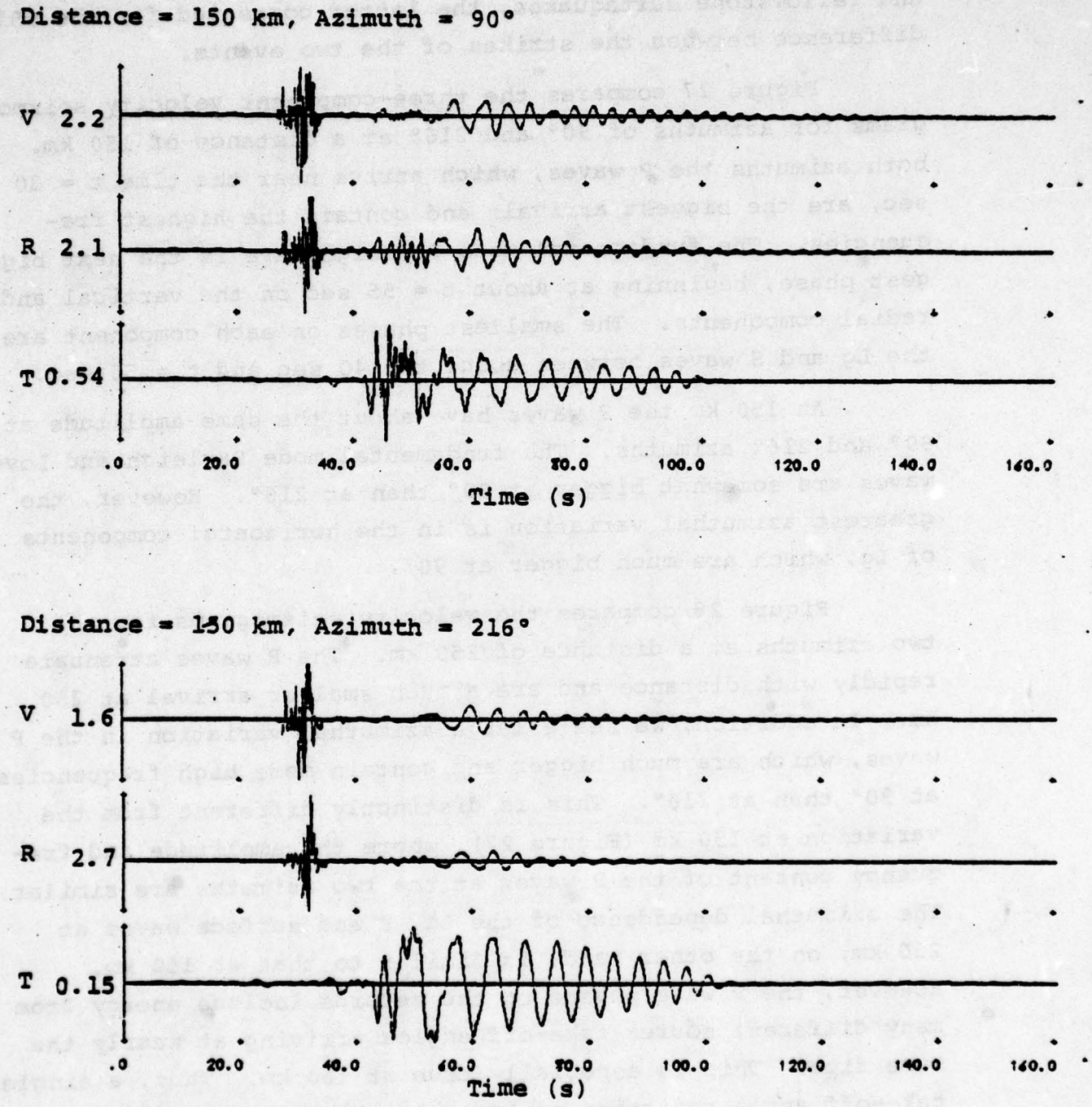

Figure 27. The velocity seismograms at a distance of 150 km and azimuths of 90° and 216° from the Pocatello earthquake model. Both sets of seismograms were computed with the Structure A path model. The time scale is seconds after origin time. The height of the vertical axis in units of cm/sec is noted beside each trace.

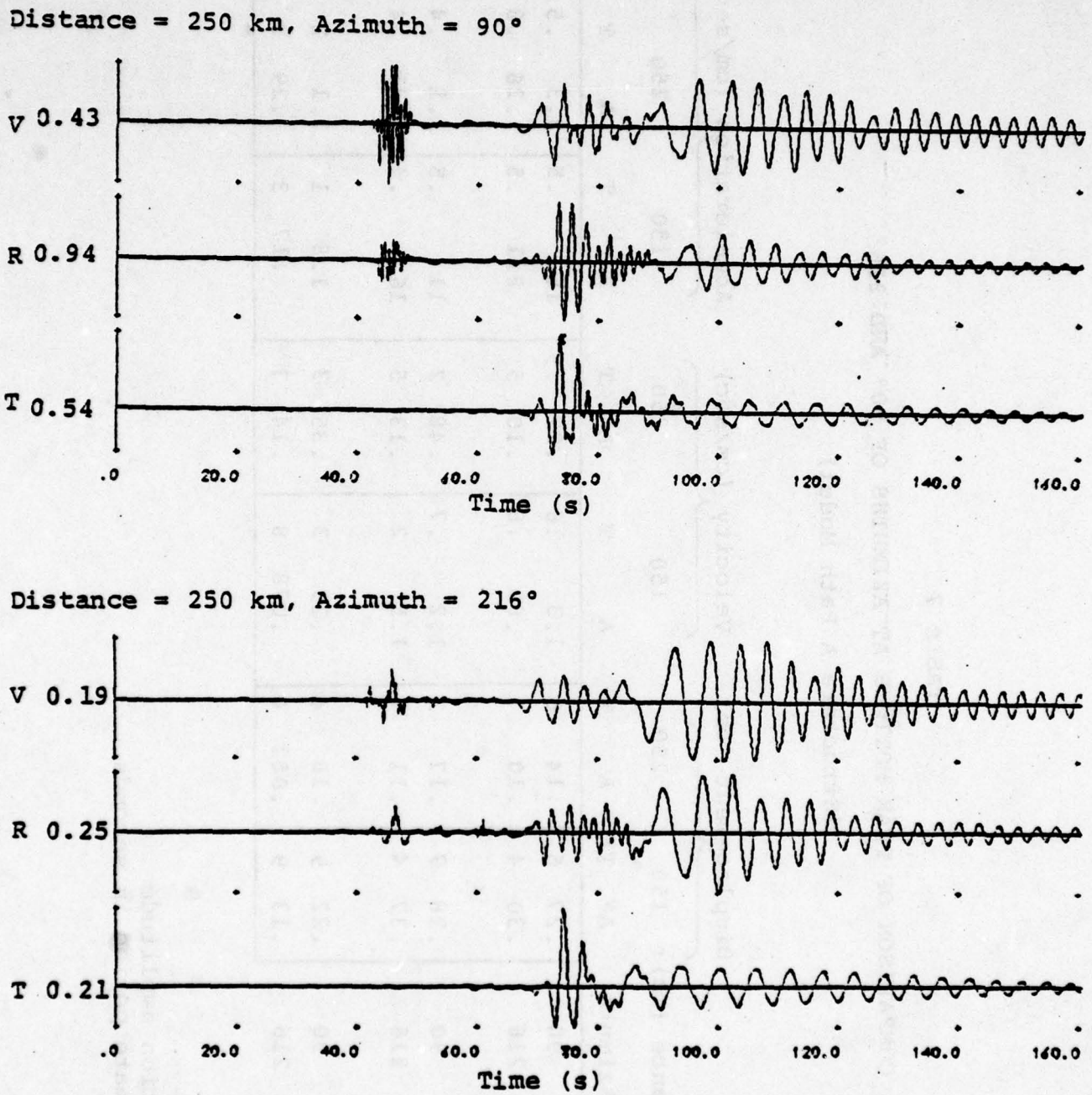

Figure 28. The velocity seismograms at a distance of 250 km and azimuths of 90° and 216° from the Pocatello earthquake model. The path model is Structure A.

TABLE 7

COMPARISON OF PEAK MOTIONS AT AZIMUTHS OF 90° AND 216°

(Structure A Path Model)

		Displacement (cm)				Velocity (cm/sec)				Acceleration (cm/sec^2)			
Distance (km):		150		250		150		250		150		250	
Component	Azimuth	A*	T*	A	T	A	T	A	T	A	T	A	T
V	90	.27	6	.14	6	1.3	.6	.22	.9	15	.5	2.3	.5
	216	.30	4	.10	7	.89	.8	.10	5	8.1	.5	.26	.8
R	90	.28	7	.17	2	1.2	.7	.48	2	11	.5	2.1	.4
	216	.37	4	.11	7	1.5	2	.13	5	16	.4	.31	.4
T	90	.22	9	.18	4	.29	3	.35	3	1.8	1	1.1	2
	216	.13	9	.082	4	.078	8	.14	3	.17	3	.29	3

*A = Peak motion amplitude
T = Approximate period in seconds

distances and azimuths. Also listed are the approximate periods of the peak motions. Periods less than one second invariably indicate that the peak motion is due to the P wave. The peak motion values in Table 7 are plotted in Figure 29.

The accelerations at 250 km show the largest radiation pattern effect in Table 7 and Figure 29. The values at 90° are a factor of 5 to 10 larger than those at 216°. For the tangential motions the peaks at 90° are always larger than those at 216° with the difference being greater for higher frequency motions. The radial and vertical motions behave alike. The longer period displacements exhibit little radiation pattern effect. For velocities and accelerations, the 250 km values behave like the tangential peak motions. At 150 km the radiation pattern effects are not very strong even at high frequencies.

These radiation pattern effects can be seen in the response spectra for each distance and azimuth. Figures 30, 31 and 32, respectively, show the response spectra for the vertical, radial and tangential components of our synthetic seismograms. In each figure the responses at 90° and 216° are compared for distances of 150 and 250 km. For all three components at 250 km, and for the tangential component at 150 km, the response curves for 90° are up to an order of magnitude higher than those for 216°, with the difference being greatest at short resonant periods. The response curves for the radial and vertical components at 150 km are higher than for the other cases and show little azimuthal dependence.

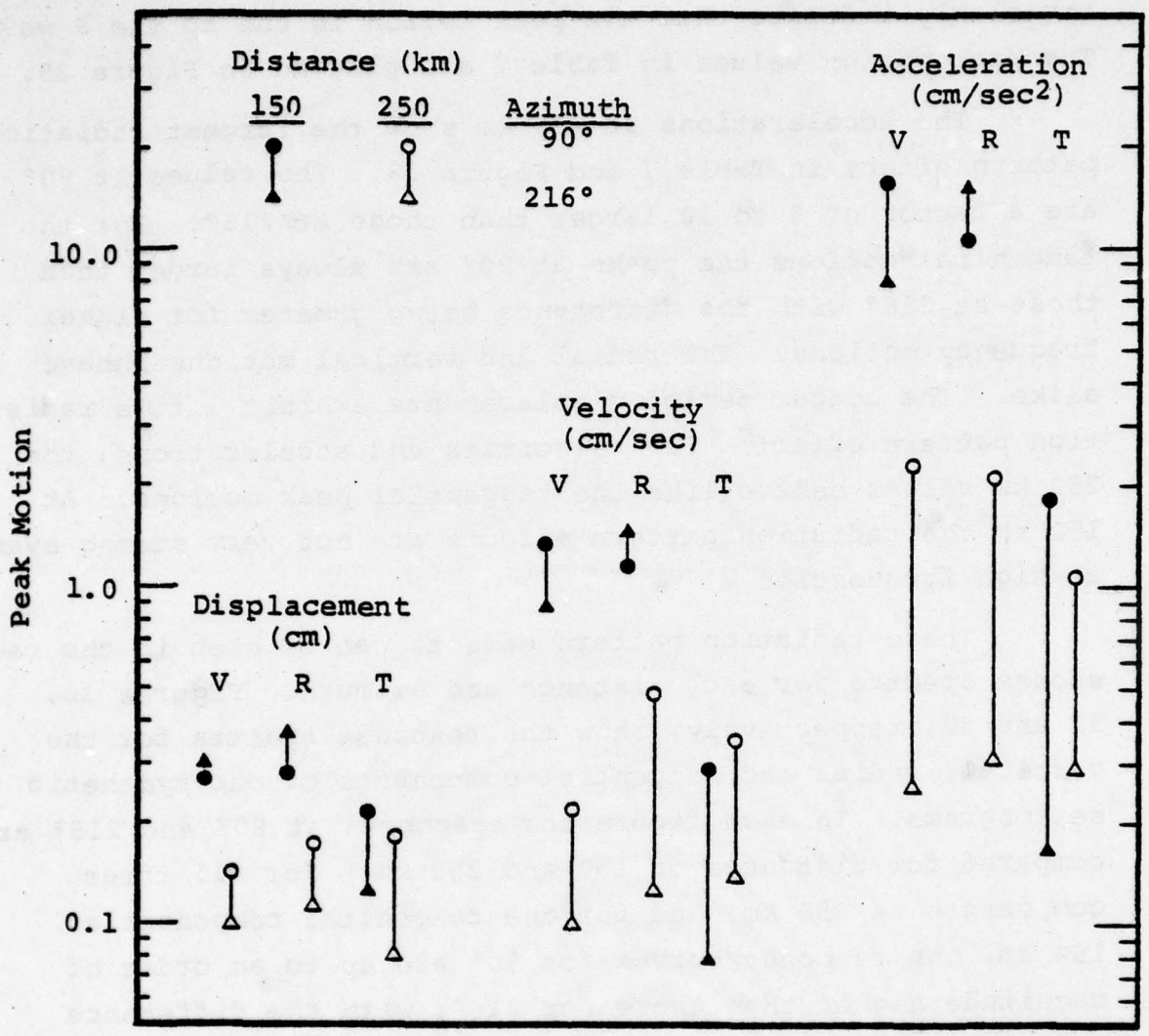

Figure 29. The peak motions at azimuths of 90° and 216° are compared for two distances. The values plotted are from Table 7.

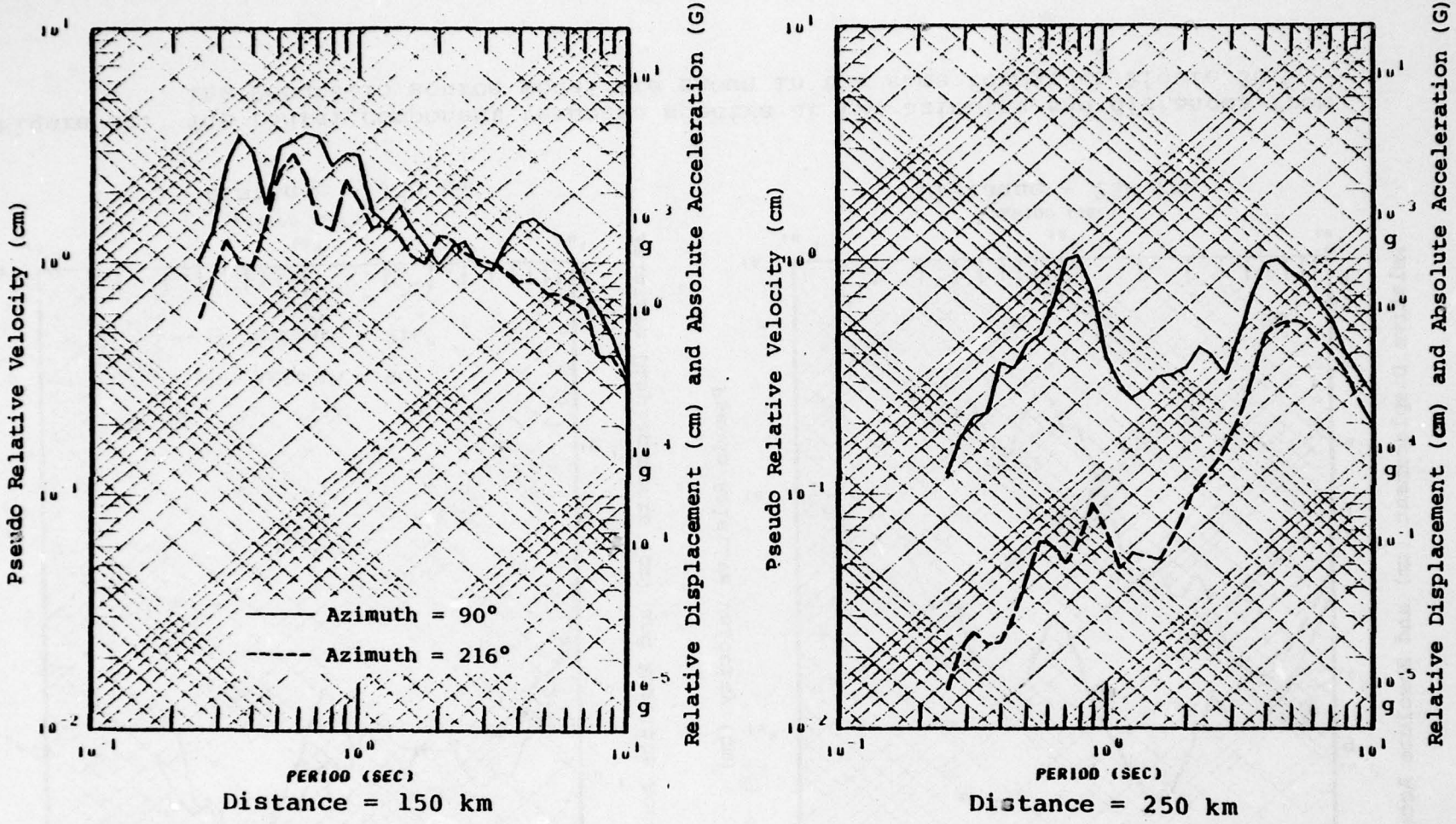

Figure 30. The vertical component response spectra at two azimuths from the Pocatello source model are compared for two epicentral distances. The path model is Structure A (f_Q = 1). The damping factor is 0.05 of critical.

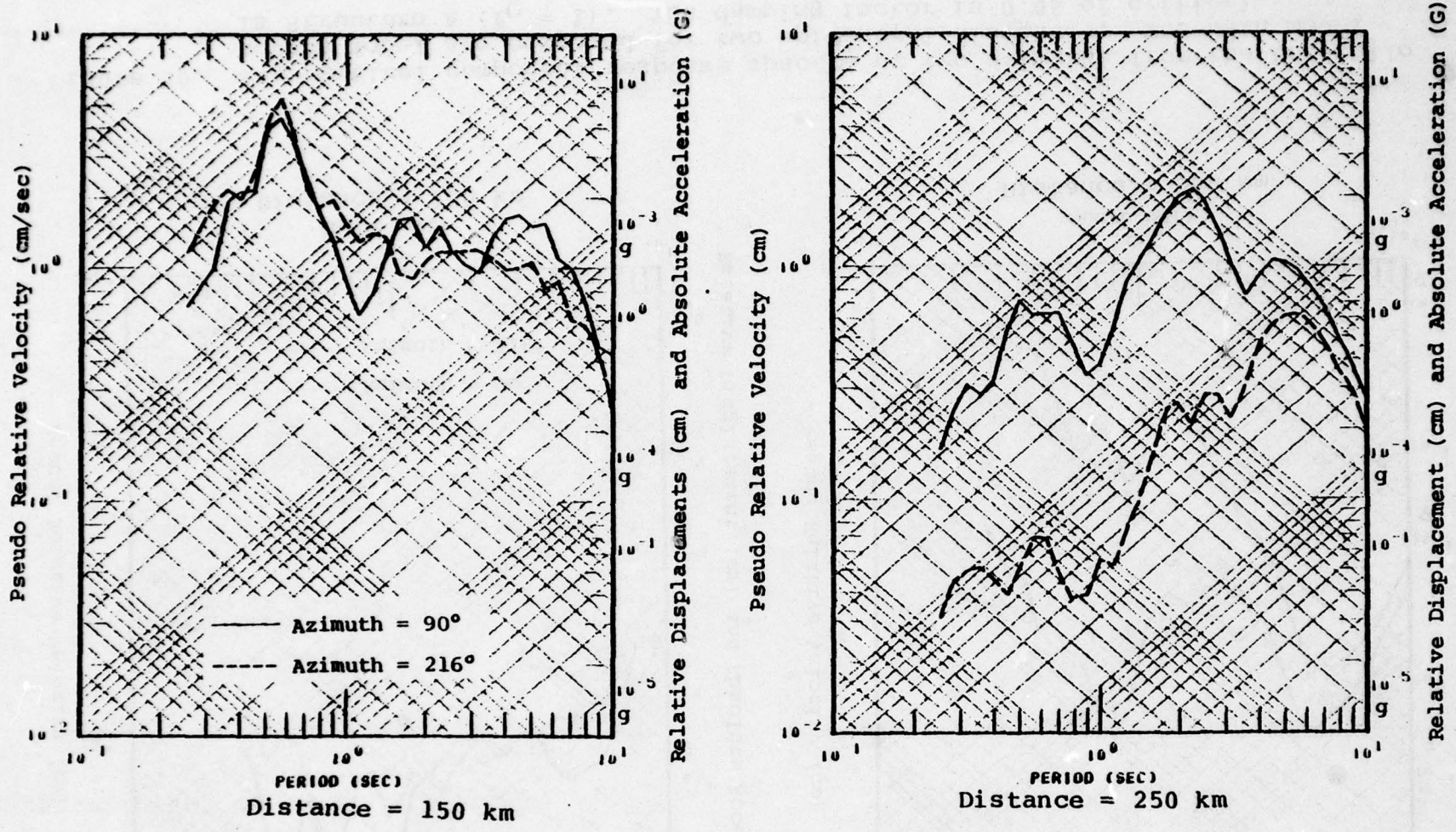

Figure 31. The radial component response spectra at two azimuths and distances from the Pocatello source model are shown in the same format as Figure 30.

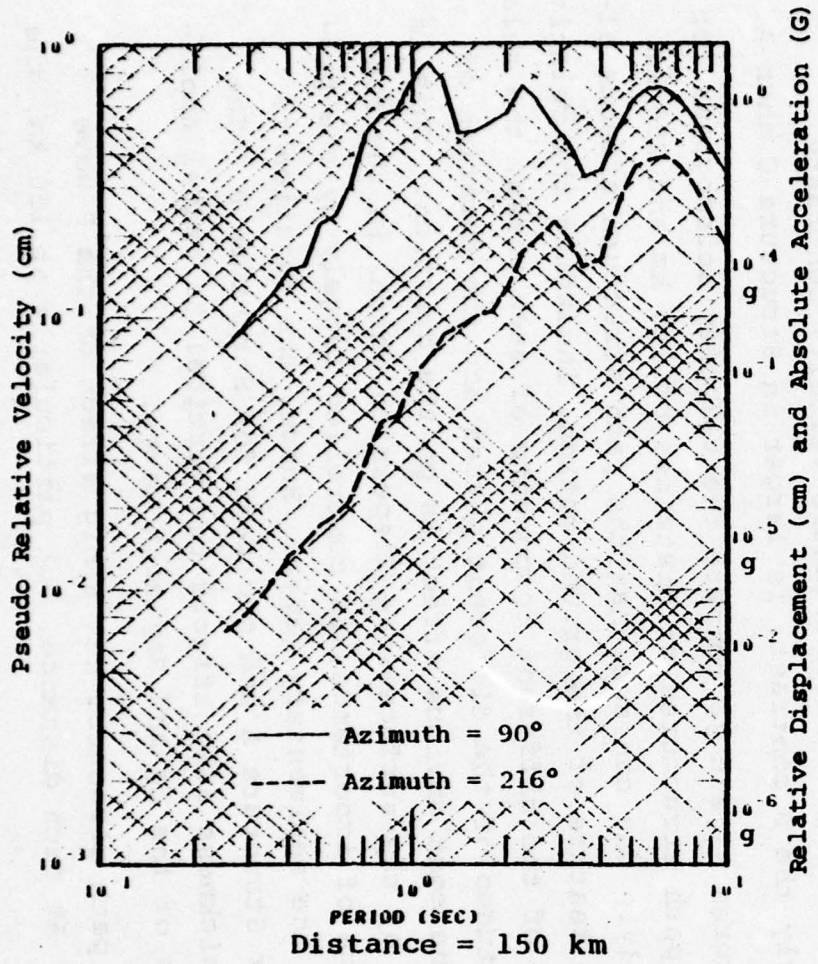

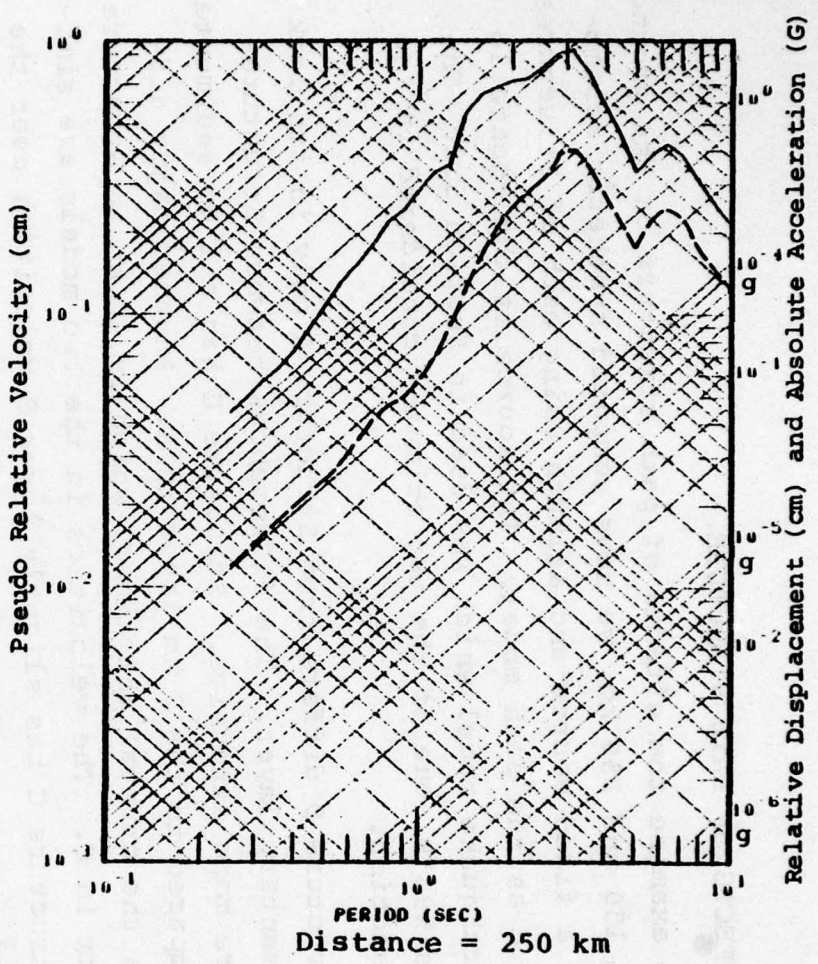

Figure 32. The tangential component response spectra at two azimuths and distances from the Pocatello source model are shown in the same format as Figure 30.

5.3 EFFECTS OF PATH STRUCTURE

To examine the effects of path structure on the ground motion at 150 and 250 km, we have computed synthetic seismograms for a fixed source and azimuth using each of Structures A, B, and C as the path model. The source is the Pocatello Valley earthquake model which was used in Section 5.2. The azimuth is N90°E, one of the two azimuths considered in the previous section.

Structure B differs from Structure A only in its lack of a sedimentary layer. The differences between Structures C and A are more extensive. Structure C has a 1 km sedimentary layer, compared to the 2 km layer in A. Another major difference is the crustal thickness, which is 40 km in Structure A and 31 km in C. The velocities in the two models are similar but Structure C has slightly lower P velocities near the surface and lower P and S velocities at the base of the crust. Therefore, the crust-mantle velocity contrasts, particularly the P contrast, is larger in Structure C than A.

Figures 33 and 34 compare the velocity seismograms for the three path structures at distances of 150 km and 250 km, respectively. One can see that the path structure affects almost every feature of the ground motion, including the relative amplitudes of the different components of each phase, the relative amplitudes of the different phases and the duration of motion. The most obvious effect is on the duration. This is determined by the surface-wave dispersion which, in the frequency range of importance, is controlled largely by the properties of the sedimentary layer. Hence, the duration is longest for Structure A and shortest for Structure B. The sediment thickness also affects the vertical to radial amplitude ratios of the Lg and Rayleigh waves.

The path structure has a big effect on the P wave amplitude. At each distance, but particularly at 150 km, the

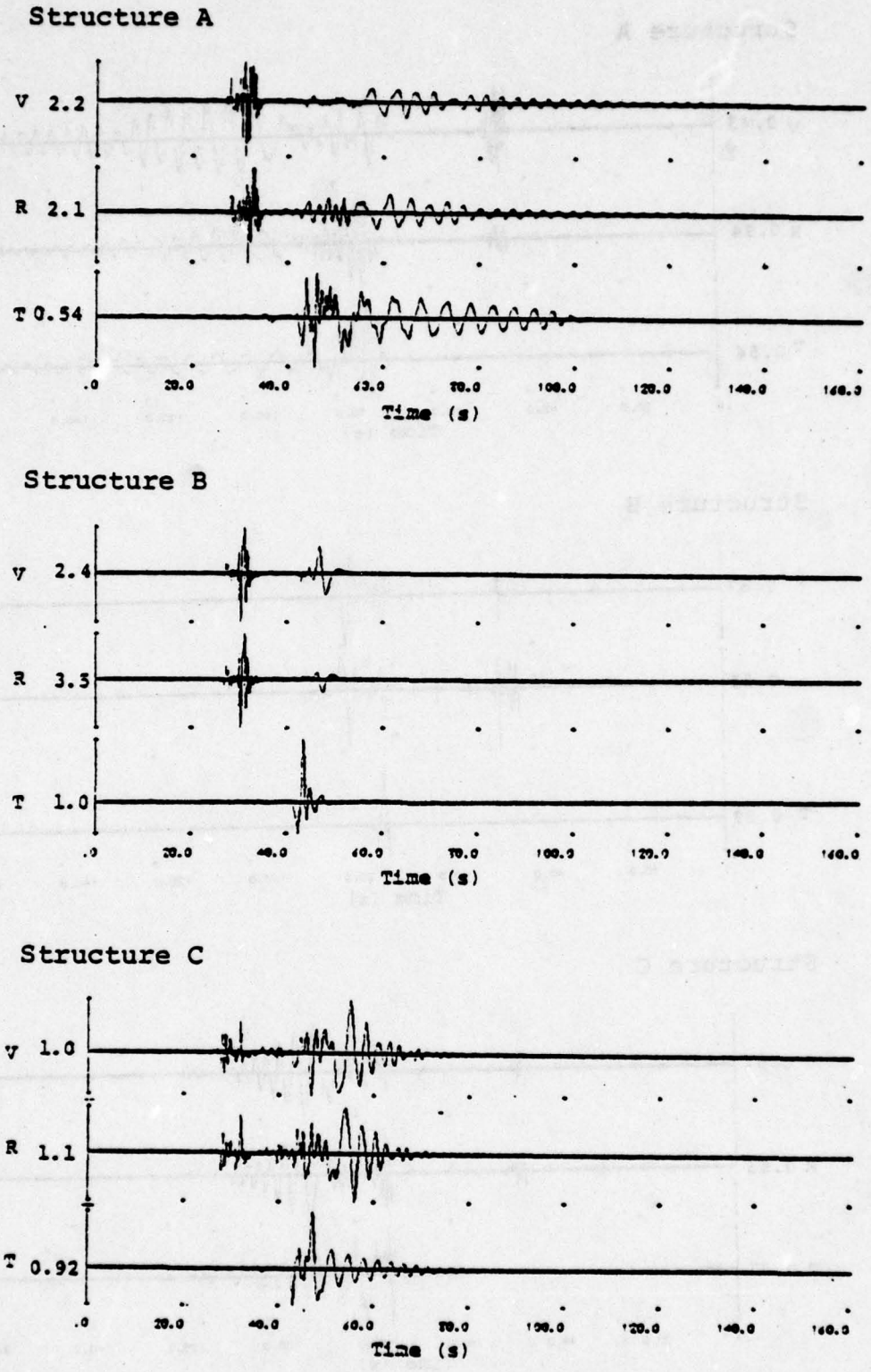

Figure 33. Velocity seismograms at 150 km and 90° from the Pocatello earthquake model computed with three path structure models.

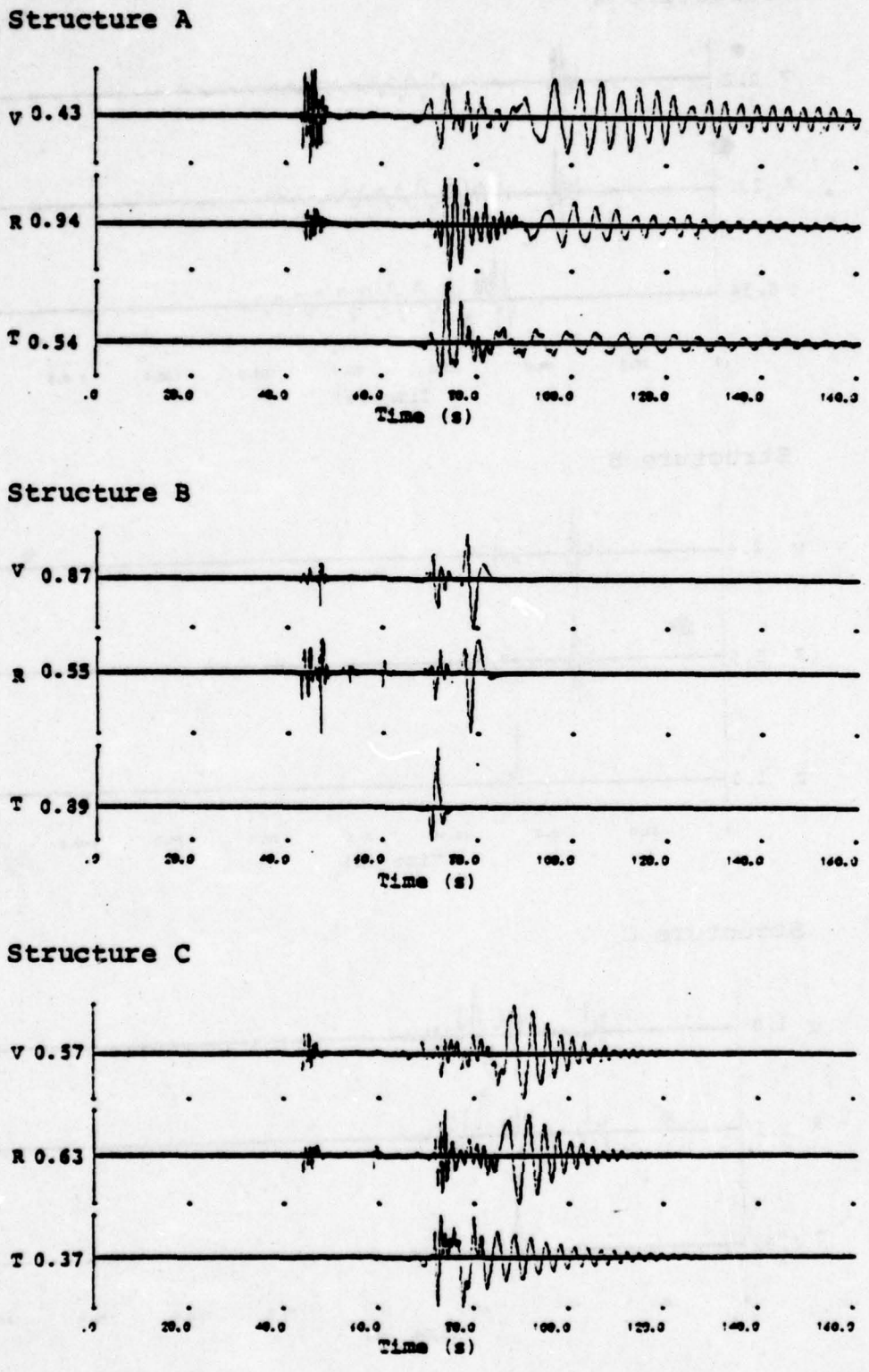

Figure 34. Velocity seismograms at 250 km and 90° from the Pocatello earthquake model computed with three path structure models.

P waves for Structure C are smaller than those for Structures A and B. This is apparently related to differences between the deep crustal structures of the models rather than to the sediment thicknesses. However, there is a late arriving P phase that is more pronounced in Structure C than in the other models. This phase arrives at t = 40 seconds at 150 km and t = 60 seconds at 250 km and is most prominent in the acceleration records (Appendix B). It is similar to the Pn phase but its crustal legs are S waves rather than P waves. This phase was also large at 216° in Structure A so it is not clear what path or source properties control its amplitude.

The peak motions resulting from the three path structures are compared in Table 8 and Figure 35. At both 150 km and 250 km there is roughly a factor of 2 variation among the peak displacements from different path models, with Structure A producing the smallest values. At 250 km, the dependence of peak velocity and peak acceleration on path structure is not much greater than this. At 150 km, though, Structure C produces very low peak vertical and radial velocities and accelerations because of its smaller P waves.

In Figures 36 through 38 the response spectra from the three path structures are compared. The most pronounced dependence on structure is seen at short resonant periods in the vertical and radial response curves at 150 km. Here the response curves of Structures A and B are much higher than the Structure C curves because of the larger P waves resulting from A and B.

5.4 EFFECTS OF SOURCE DEPTH

The depth of the Pocatello source model we have used in the previous examples is 8.7 km. This is the depth to the bottom of the fault, where rupture begins. Here we investigate the effect of decreasing the source depth to 5 km. We consider the effect on the ground motions at 250 km and N90°E with Structure C as the path model.

TABLE 8

COMPARISON OF PEAK MOTIONS FROM THREE PATH STRUCTURE MODELS

(Azimuth = 90°)

		Displacement (cm)				Velocity (cm/sec)				Acceleration (cm/sec^2)			
Distance (km) =		150		250		150		250		150		250	
Component	Structure	A	T	A	T	A	T	A	T	A	T	A	T
V	A	.27	6	.14	6	1.3	.6	.22	.9	15	.5	2.3	.5
	B	.45	4	.29	4	1.2	.9	.46	4	12	.6	2.8	.4
	C	.46	5	.26	7	.57	4	.30	5	2.4	.6	1.3	.6
R	A	.28	7	.17	2	1.2	.7	.48	2	11	.5	2.1	.4
	B	.56	6	.21	5	1.9	.9	.36	.5	17	.6	4	.4
	C	.41	6	.28	6	.57	3	.32	5	2.9	.6	1.8	1
T	A	.22	9	.18	4	.29	3	.35	3	1.8	1	1.1	2
	B	.30	4	.24	3	.68	2	.57	3	3.1	.9	1.5	.9
	C	.35	5	.16	8	.56	4	.20	2	1.2	2	1.0	1

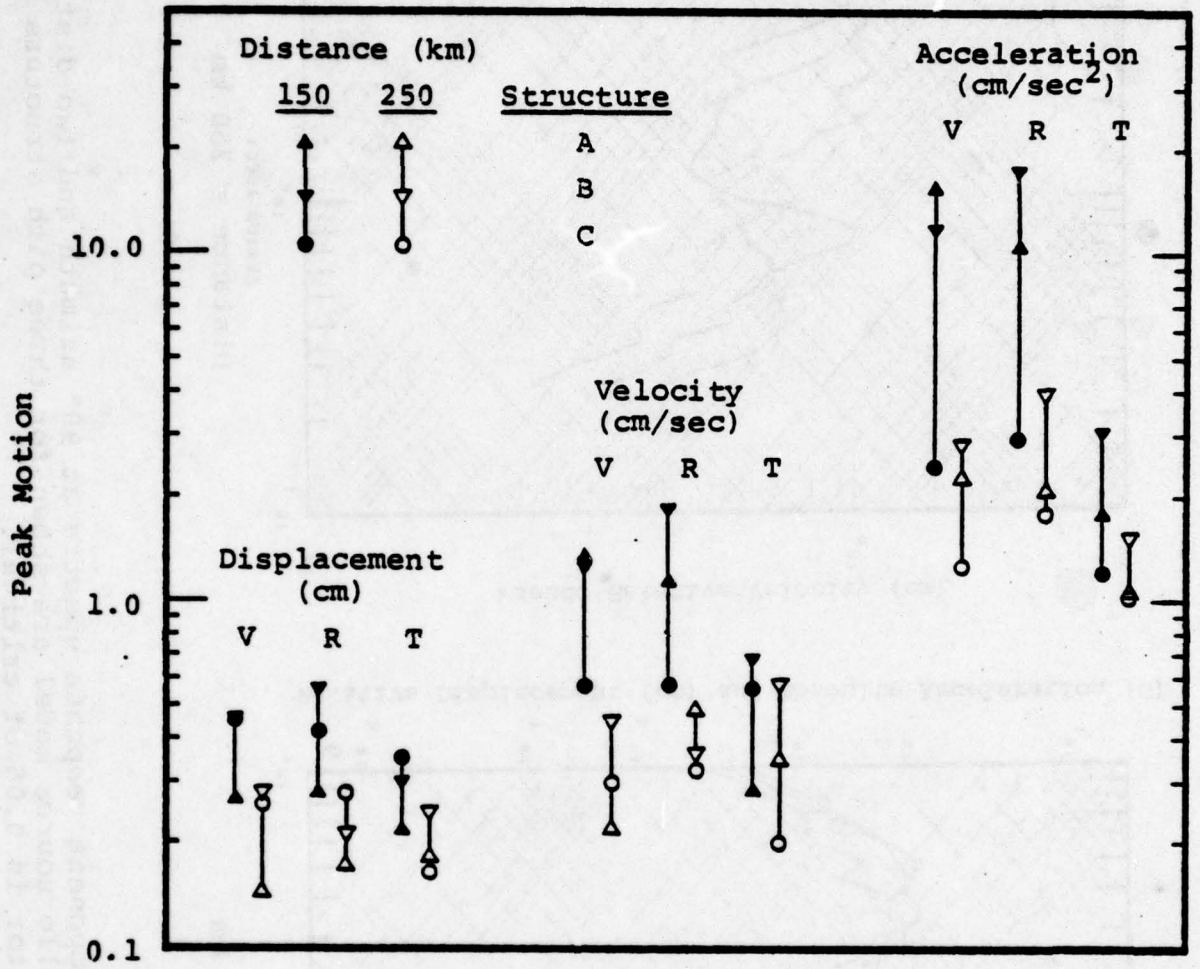

Figure 35. Comparison of peak motions at two distances from three path structure models (from Table 8).

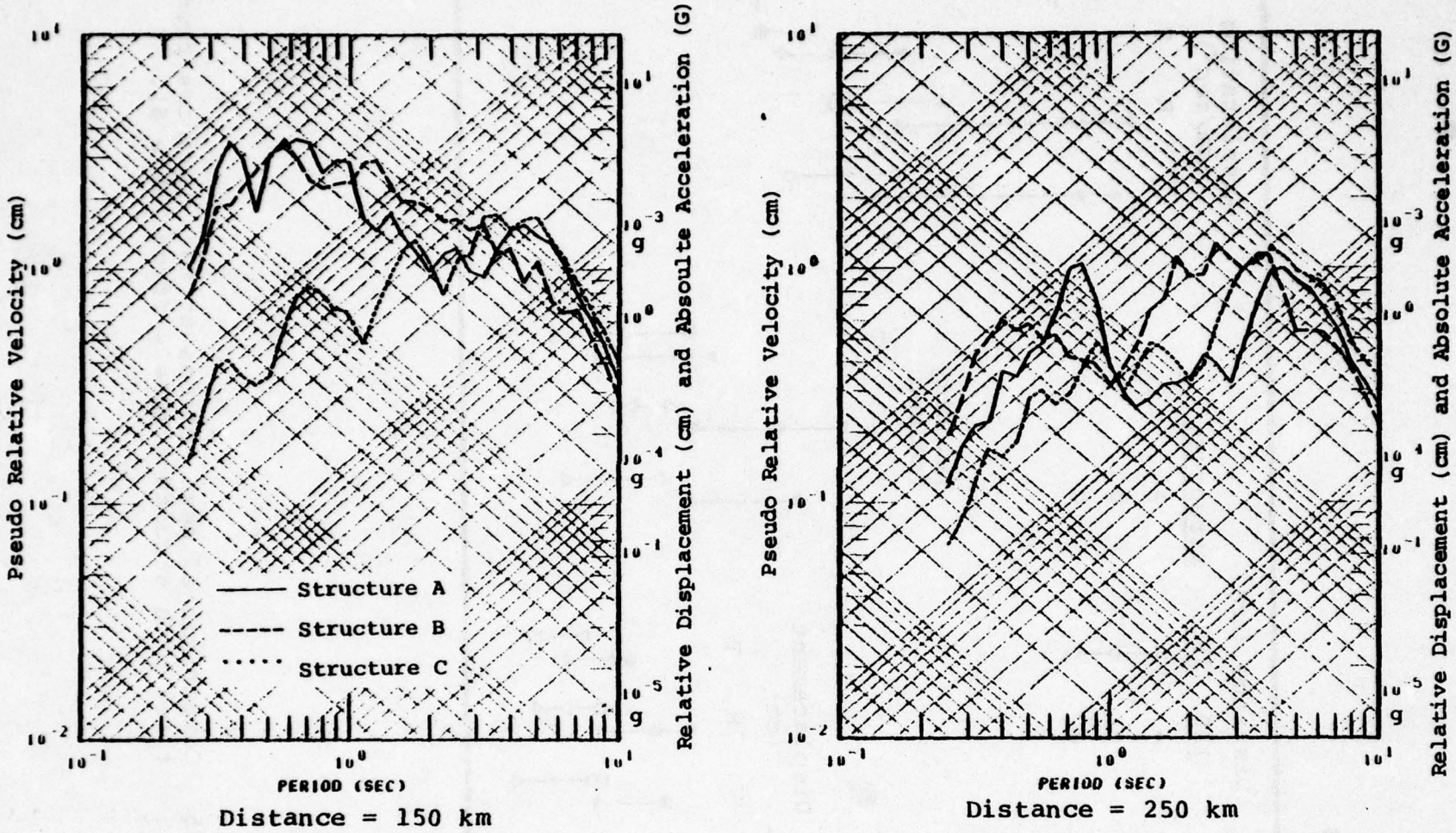

Figure 36. The vertical component response spectra at 90° azimuth and two distances from the Pocatello source model are shown for three path structure models. The damping factor is 0.05 of critical.

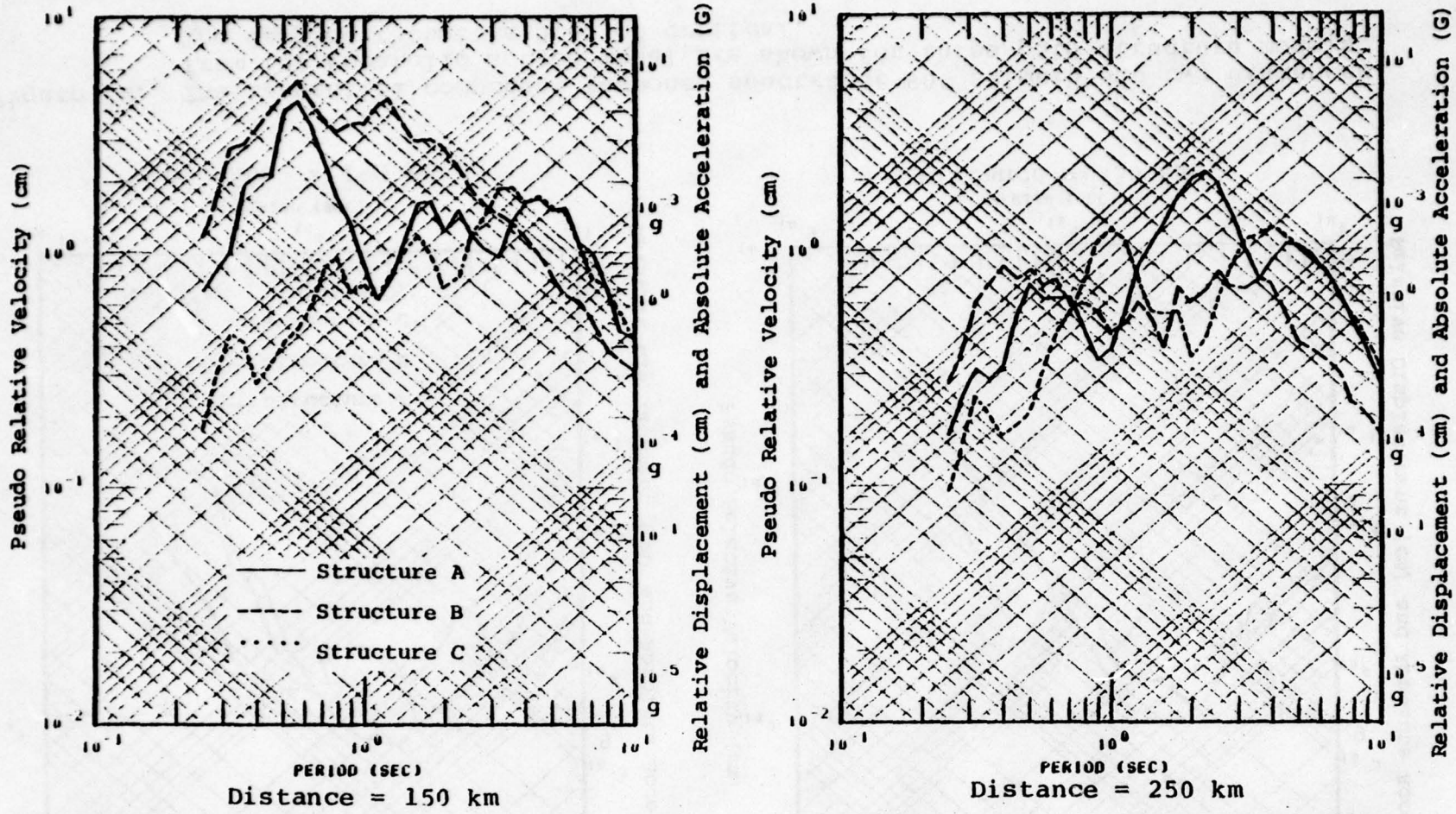

Figure 37. The radial component response spectra at 90° azimuth and two distances from the Pocatello source model are shown for three path structure models. The damping factor is 0.05 of critical.

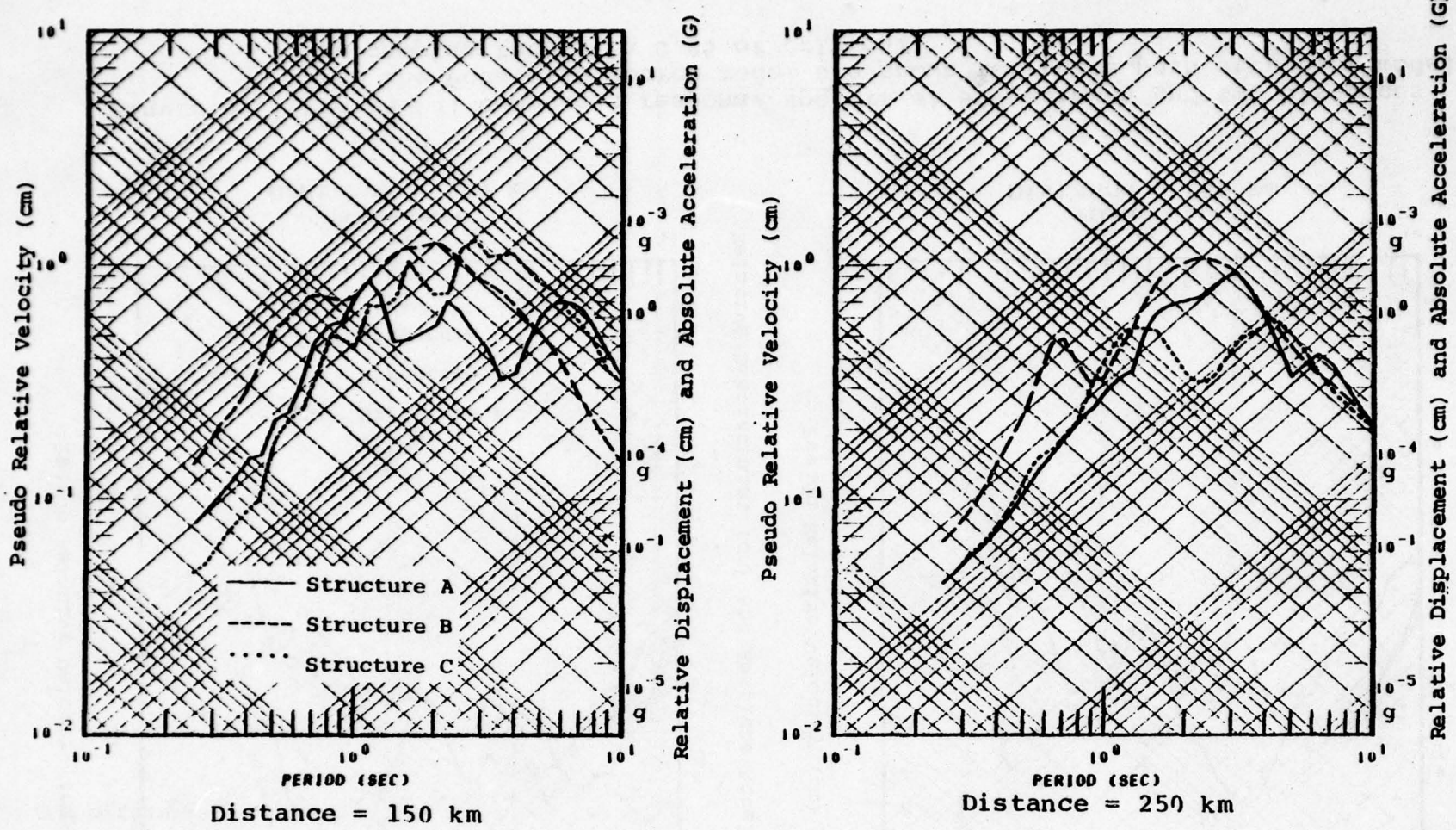

Figure 38. The tangential component response spectra at 90° azimuth and two distances from the Pocatello source model are shown for three path structure models. The damping factor is 0.05 of critical.

Figure 39 compares the velocity seismograms that result from the two source depths. The peak motions are listed in Table 9 and plotted in Figure 40. Figure 41 shows the response spectra.

The shallower source depth causes greater excitation of the short period fundamental mode surface waves. The amplitudes of Lg and P waves are reduced. As a result, the peak velocities, which for this path model and distance are determined by the short period surface waves, are about 50 percent larger for the shallower source depth. The peak accelerations are caused by P and Lg and these are about 30 percent smaller for the shallower depth. The peak displacements are due to the longer period surface waves and are not affected by the change in source depth. The principal effect of the shallower depth on the response spectra is an increase in the responses at periods near 3 seconds.

5.5 EFFECTS OF EVENT MAGNITUDE

A new source model was constructed by modifying the source parameters of our Pocatello Valley earthquake model to produce an earthquake source model having a magnitude one unit greater. To do so, we increased the stress drop and fault length and included bilateral rupture propagation. In the Pocatello Valley model, the rupture propagates upward from a depth of 8.7 km along a 7 km long fault. In the modified model, rupture begins at 8.7 km depth and propagates upward 9 km and downward 4 km. Thus, the total fault length is 13 km. The fault orientation was not changed. The resulting earthquake model has a moment ten times larger than that of the Pocatello Valley model. The M_s should then be one unit higher. However, the larger source has a lower "corner frequency" and thus the high frequency waves (controlling m_b) will be less than a factor of ten different.

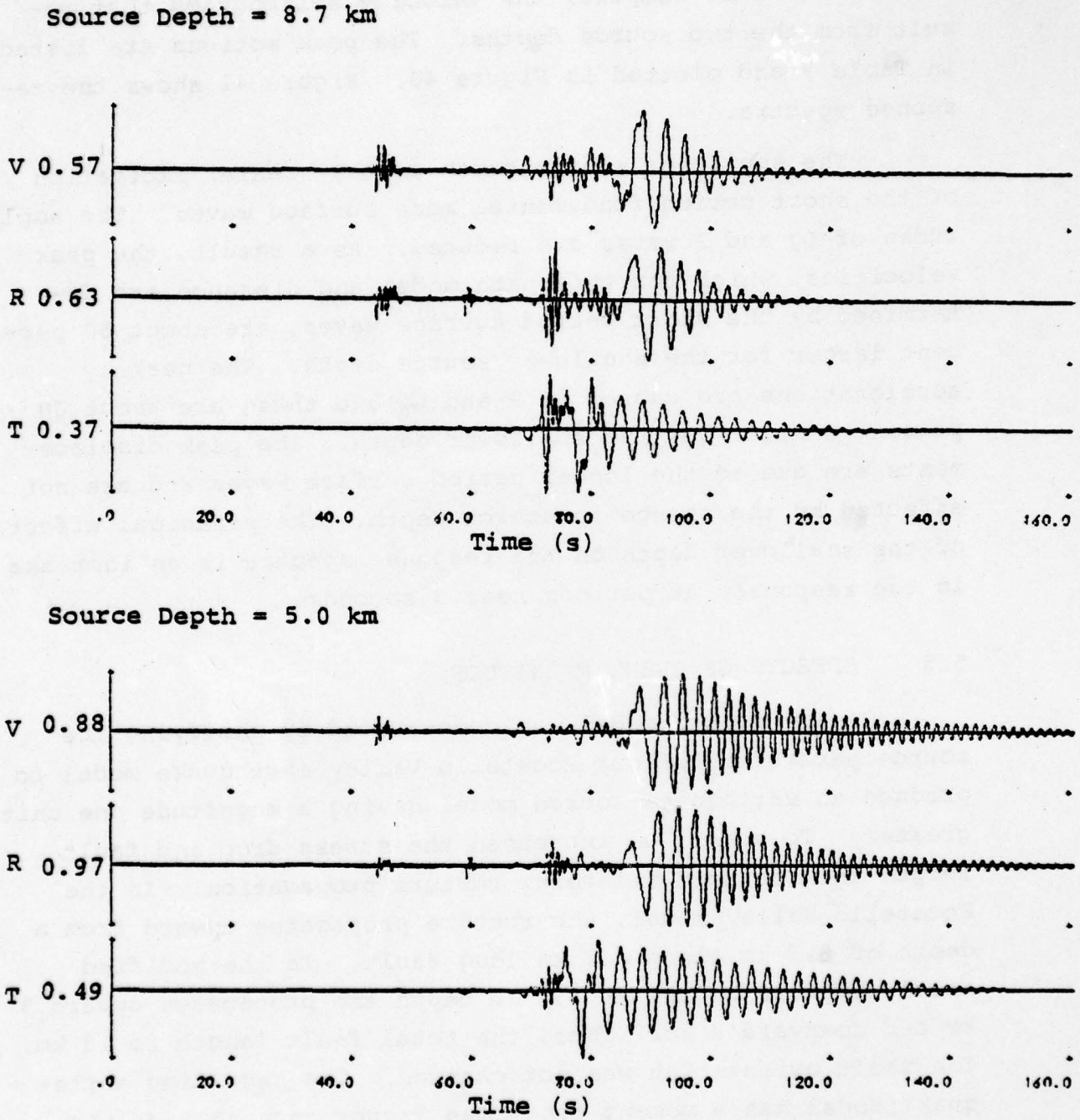

Figure 39. Velocity seismograms at 250 km and 90° from the Pocatello earthquake model at two source depths. The path model is Structure C.

TABLE 9

COMPARISON OF PEAK MOTIONS FROM SOURCE DEPTHS OF 8.7 AND 5.0 KM

(Structure C, Distance = 250 km, Azimuth = 90°)

Component	Source Depth	Displacement (cm)		Velocity (cm/sec)		Acceleration (cm/sec^2)	
		A	T	A	T	A	T
V	8.7	.26	7	.30	5	1.3	.6
	5	.30	5	.45	3	1.0	.6
R	8.7	.28	6	.32	5	1.8	1
	5	.29	4	.49	3	1.3	.4
T	8.7	.16	8	.20	2	1.0	1
	5	.18	7	.28	5	.65	2

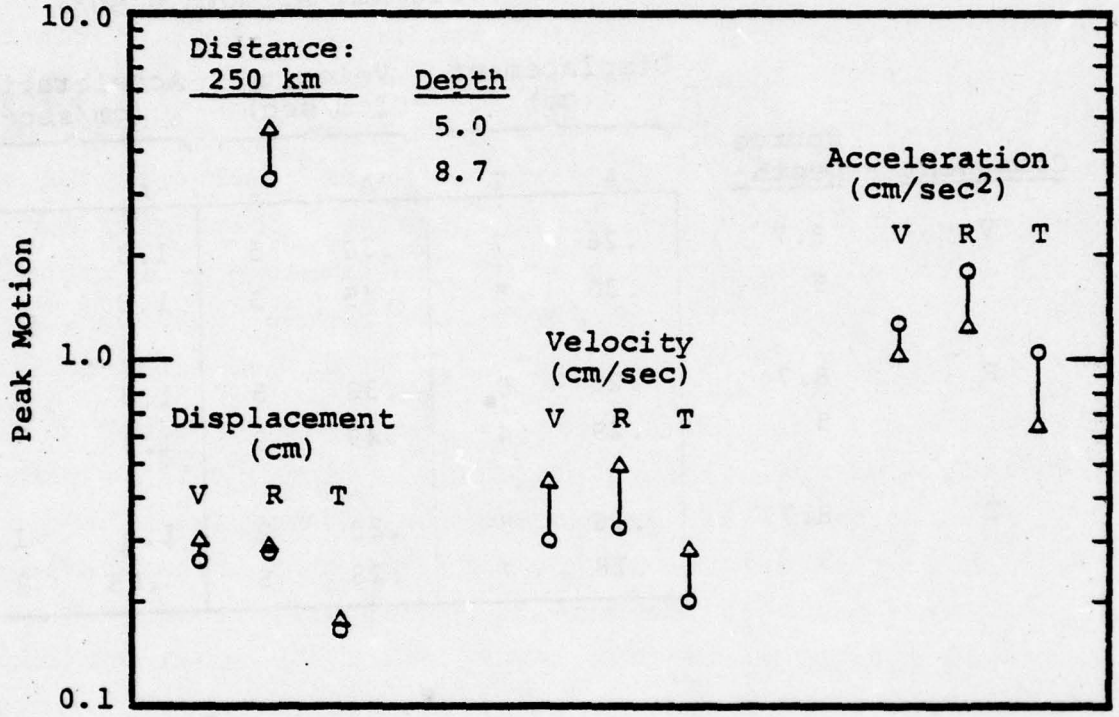

Figure 40. Comparison of peak motions from two source depths (from Table 9).

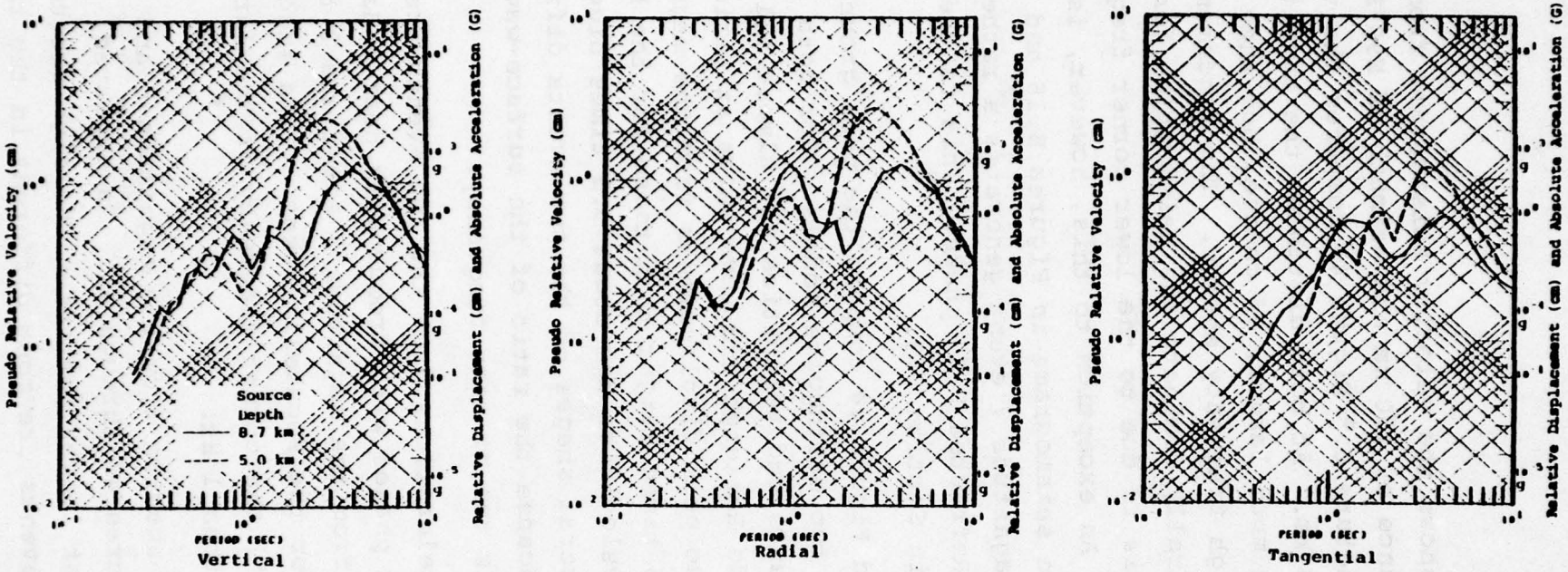

Figure 41. The response spectra at a distance of 250 km and azimuth of 90° from the Pocatello source model are compared for two source depths. The path model is Structure C with standard Q. The damping factor is 0.05 of critical.

Figure 42 shows the velocity seismograms from the two sources at a distance of 150 km and azimuth of N90°E. The path model is Structure C. Figure 43 compares the velocity seismograms at 250 km. At both distances the magnitude 7 ground motions are much larger, of course, but they also have relatively less high frequency energy. The fundamental mode surface waves generally dominate the seismograms for the magnitude 7 source. This is due to the lower corner frequency of the larger event. An exception to this, however, is apparent in the acceleration seismograms in Figures B.16 and B.17 of Appendix B. The magnitude 7 event generates a rather large high frequency "S-Refracted P-S" phase. This is the refracted wave we described in Section 5.3.

Table 10 and Figure 44 compare the peak ground motions resulting from the two earthquake models. For both sources, the peak displacements and velocities are almost all due to the fundamental mode Rayleigh and Love waves at periods from 5 to 8 seconds. The peak displacements from the magnitude 7 event are about 6.5 times larger than those for the Pocatello source. The peak velocities are about 5.5 times bigger. This shows that the spectral shapes of the two events differ even at these periods because the ratio of the surface-wave spectra of the two events is ten at zero frequency.

The peak accelerations from the two events are mostly due to the P and Lg phases with frequencies near 1 Hz. The peak accelerations from the magnitude 7 event are 2 to 3 times larger than those for the Pocatello event. This suggests that at this azimuth (90°) the corner frequency of the larger event is shifted to less than 1 Hz.

The response spectra from the magnitude 6 and 7 events are compared in Figures 45 through 48. As expected, the difference is greater at longer periods. The high frequency responses of the two events are most different in the radial component.

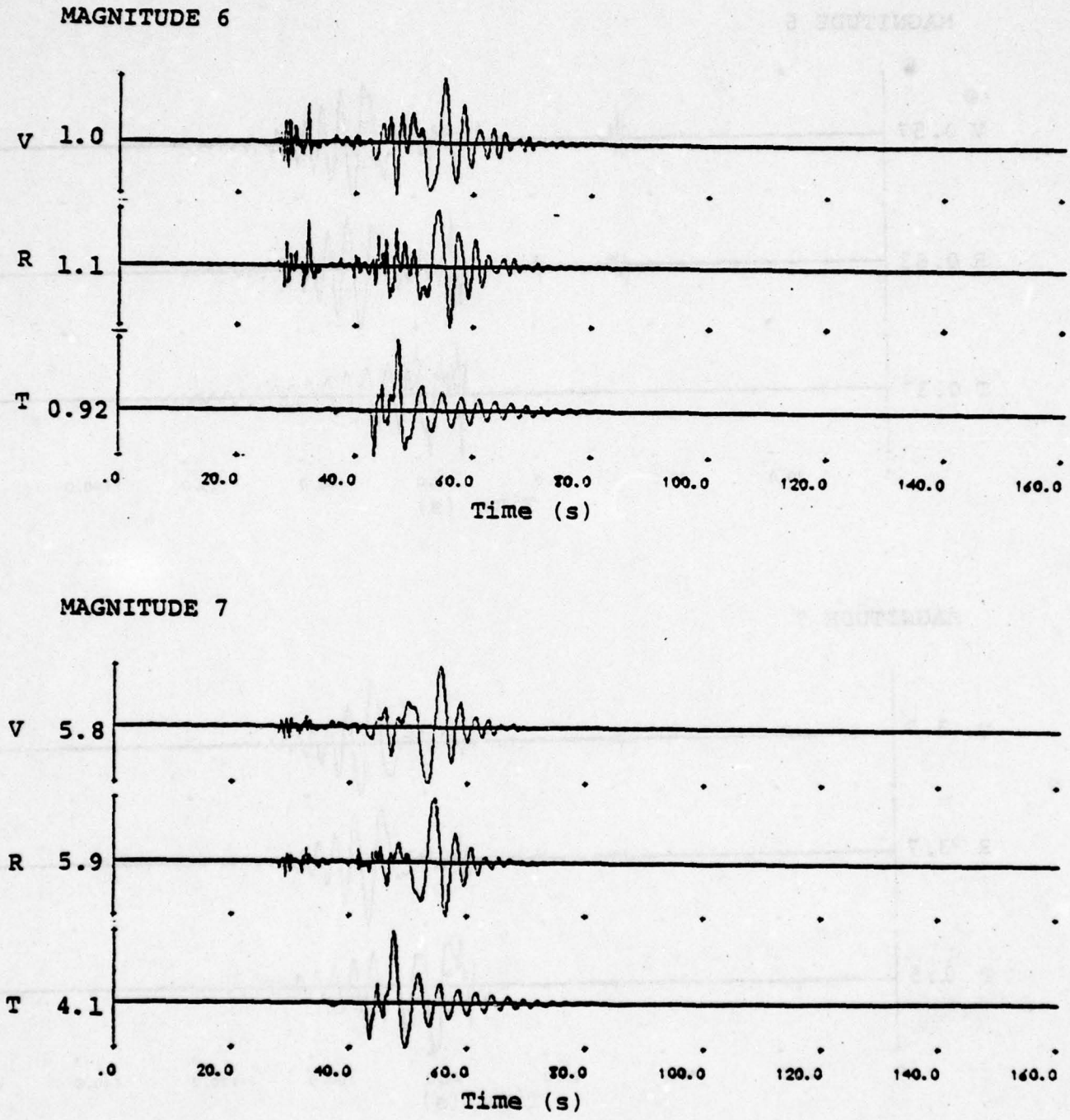

Figure 42. Velocity seismograms at 150 km and 90° from magnitude 6 and 7 earthquake models. The magnitude 6 source is the Pocatello earthquake model used in previous examples. Both sources have the same depth (8.7 km) and orientations. The path model is Structure C.

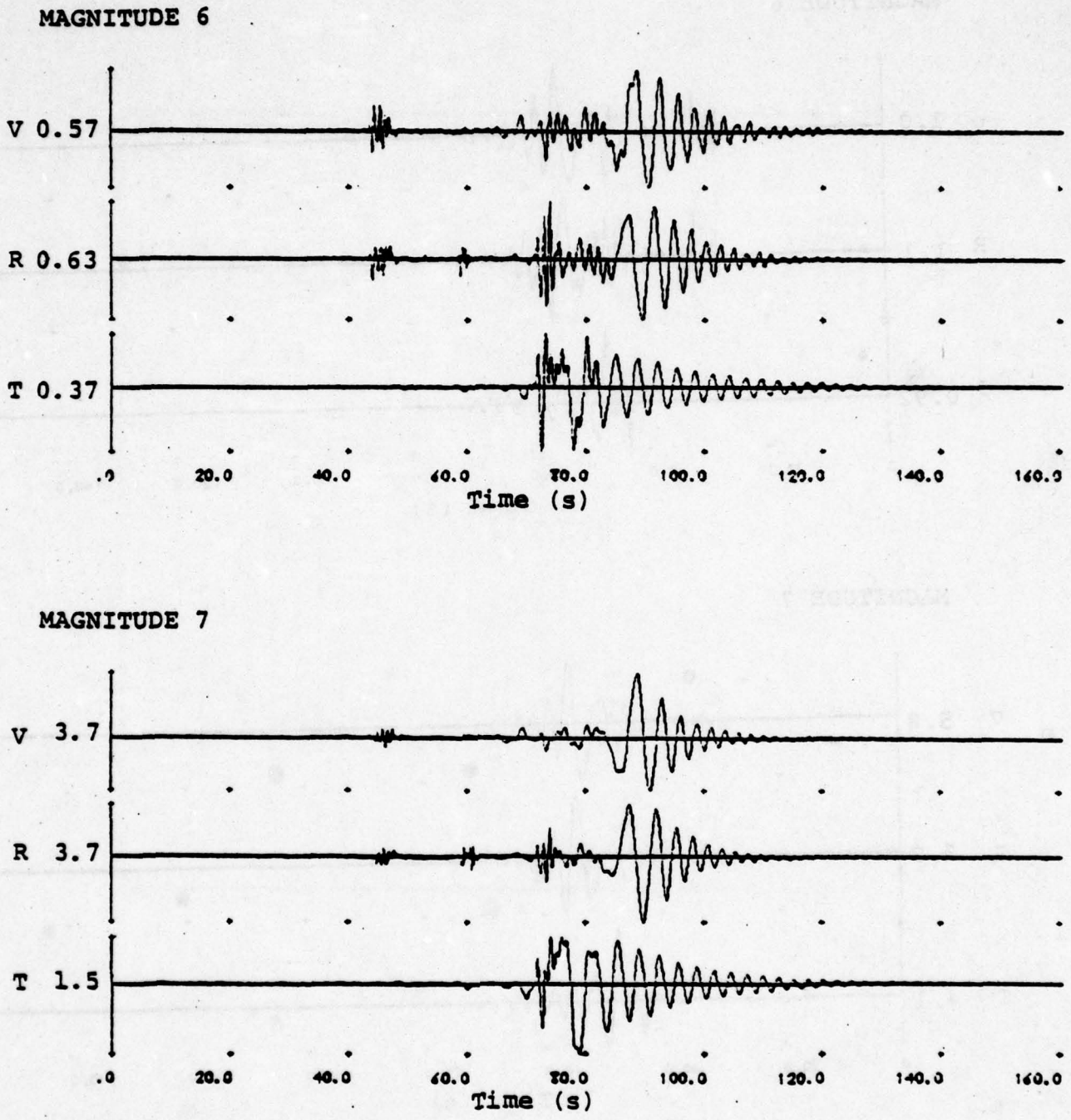

Figure 43. Velocity seismograms at 250 km and 90° from magnitude 6 and 7 earthquake models.

TABLE 10

COMPARISON OF PEAK MOTIONS FROM MAGNITUDE 6 AND 7 EARTHQUAKES

Structure C, Azimuth = 90°

		Displacement (cm)				Velocity (cm/sec)				Acceleration (cm/sec^2)			
Distance (km):		150		250		150		250		150		250	
Component	Magnitude	A	T	A	T	A	T	A	T	A	T	A	T
V	6	.46	5	.26	7	.57	4	.30	5	2.4	.6	1.3	.6
	7	3.0	6	1.8	7	3.0	4	2.0	6	6.1	.6	2.6	4
R	6	.41	6	.28	6	.57	3	.32	5	2.9	.6	1.8	1
	7	2.8	6	1.9	6	3.2	5	2.0	5	9.4	.4	6.4	.4
T	6	.35	5	.16	8	.56	4	.20	2	1.2	2	1.0	1
	7	1.8	5	1.1	8	2.5	5	.89	5	3.7	4	2.0	1

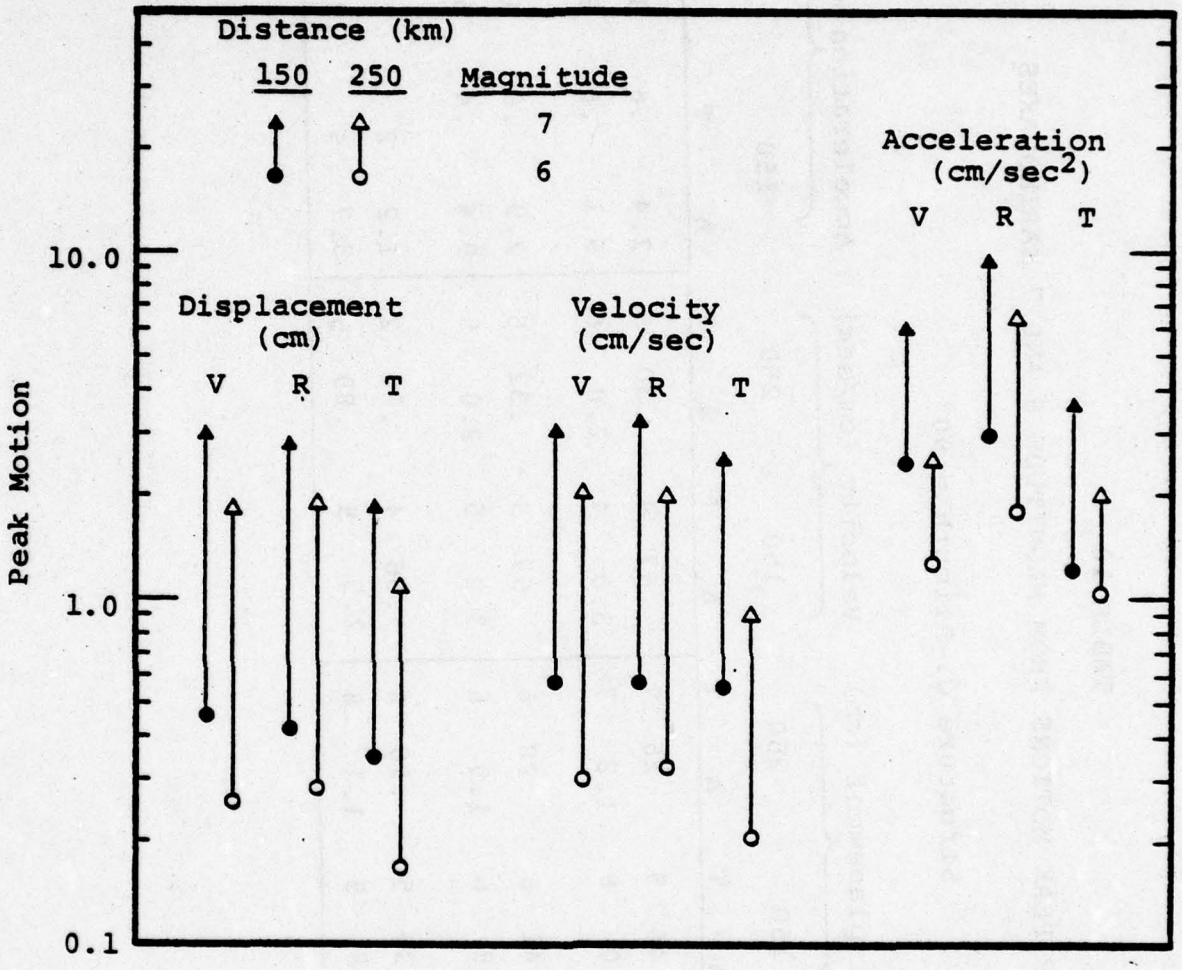

Figure 44. Comparison of peak motions from magnitude 6 and 7 earthquakes (from Table 10).

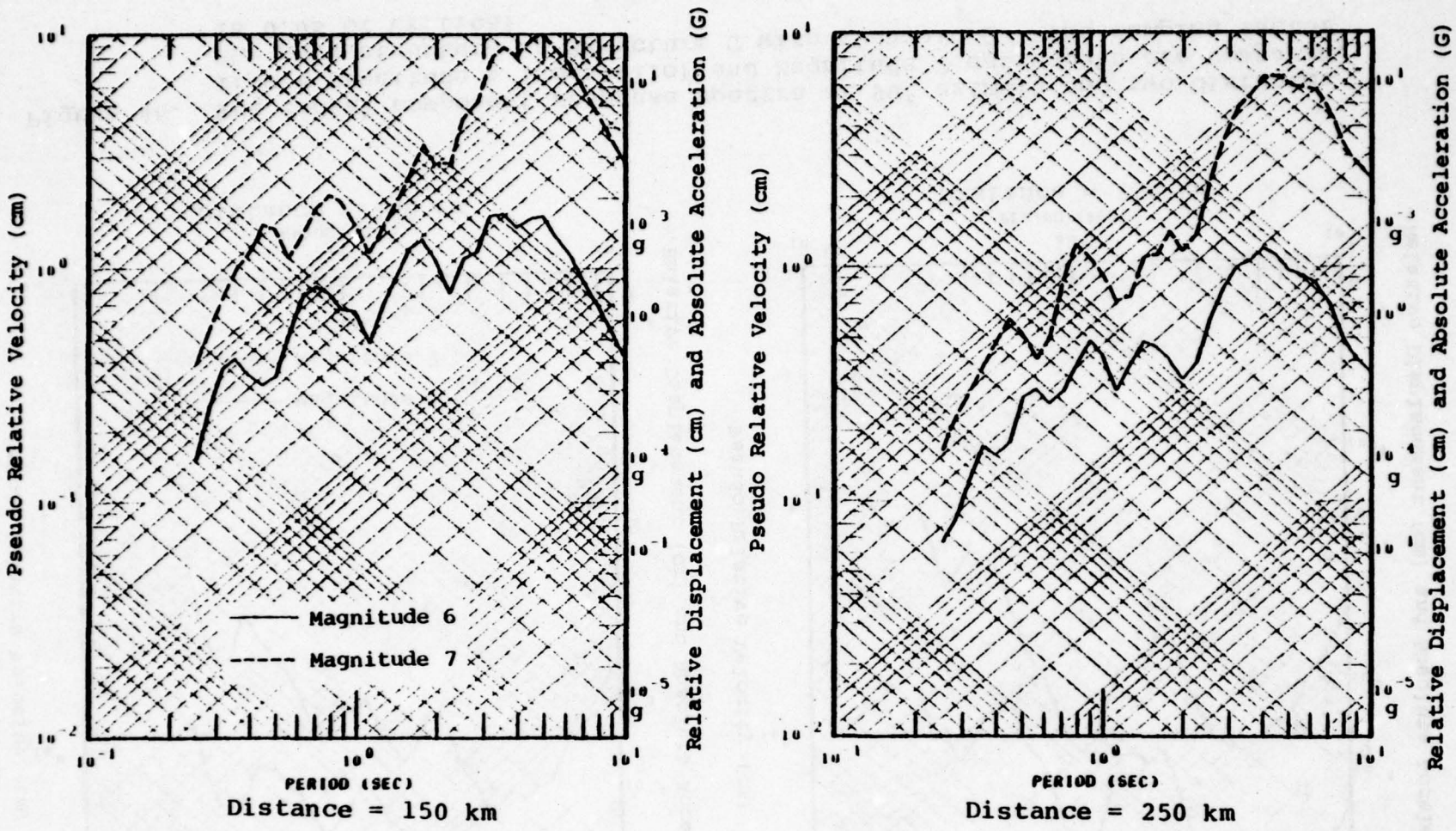

Figure 45. The vertical component response spectra at 90° azimuth and two distances from a Magnitude 6 (Pocatello) and a Magnitude 7 earthquake are compared. The path structure is Structure C with standard Q. The damping factor is 0.05 of critical.

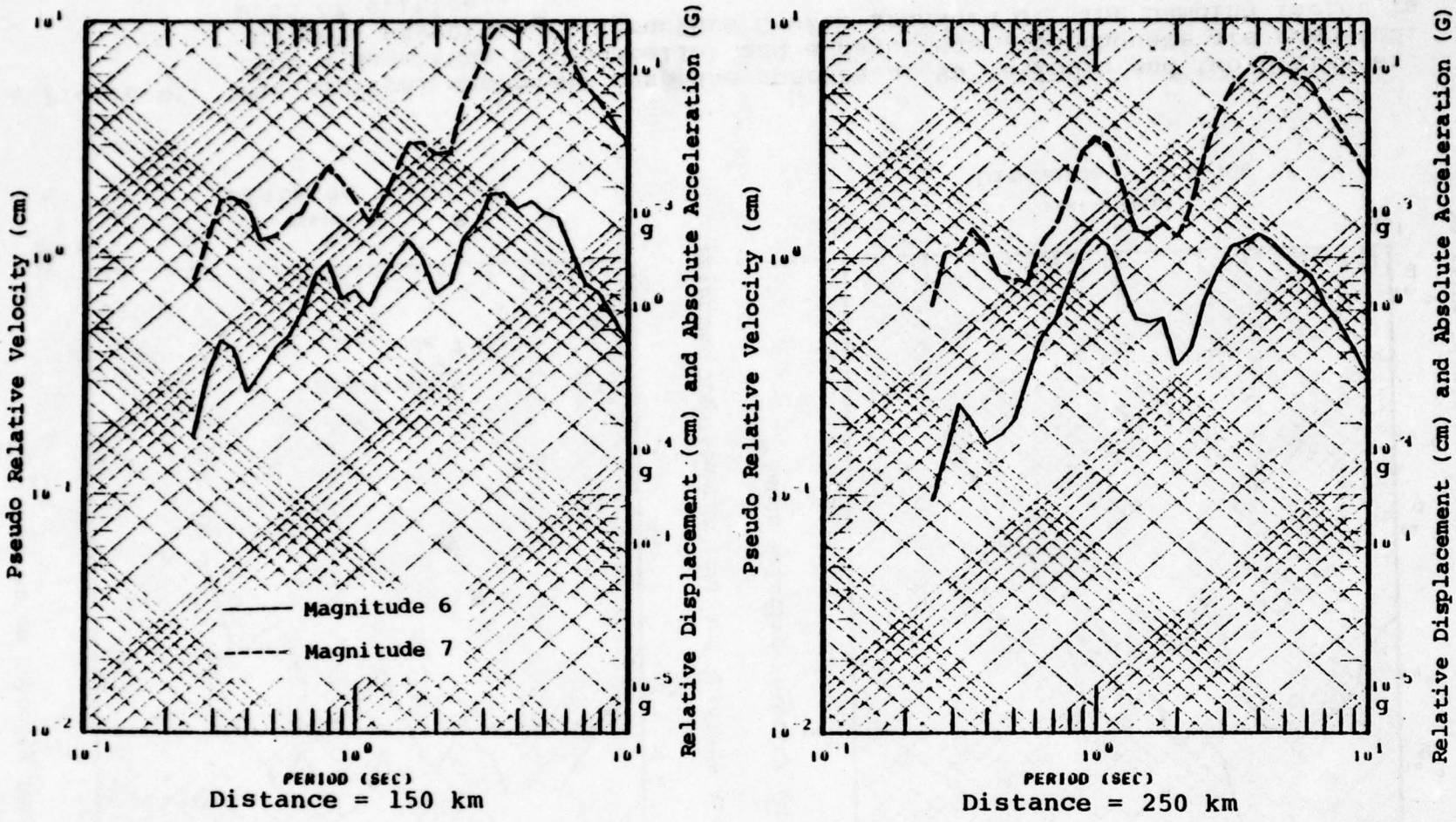

Figure 46. The radial component response spectra at 90° azimuth and two distances from a Magnitude 6 (Pocatello) and Magnitude 7 earthquake are compared. The path structure is Structure C with standard Q. The damping factor is 0.05 of critical.

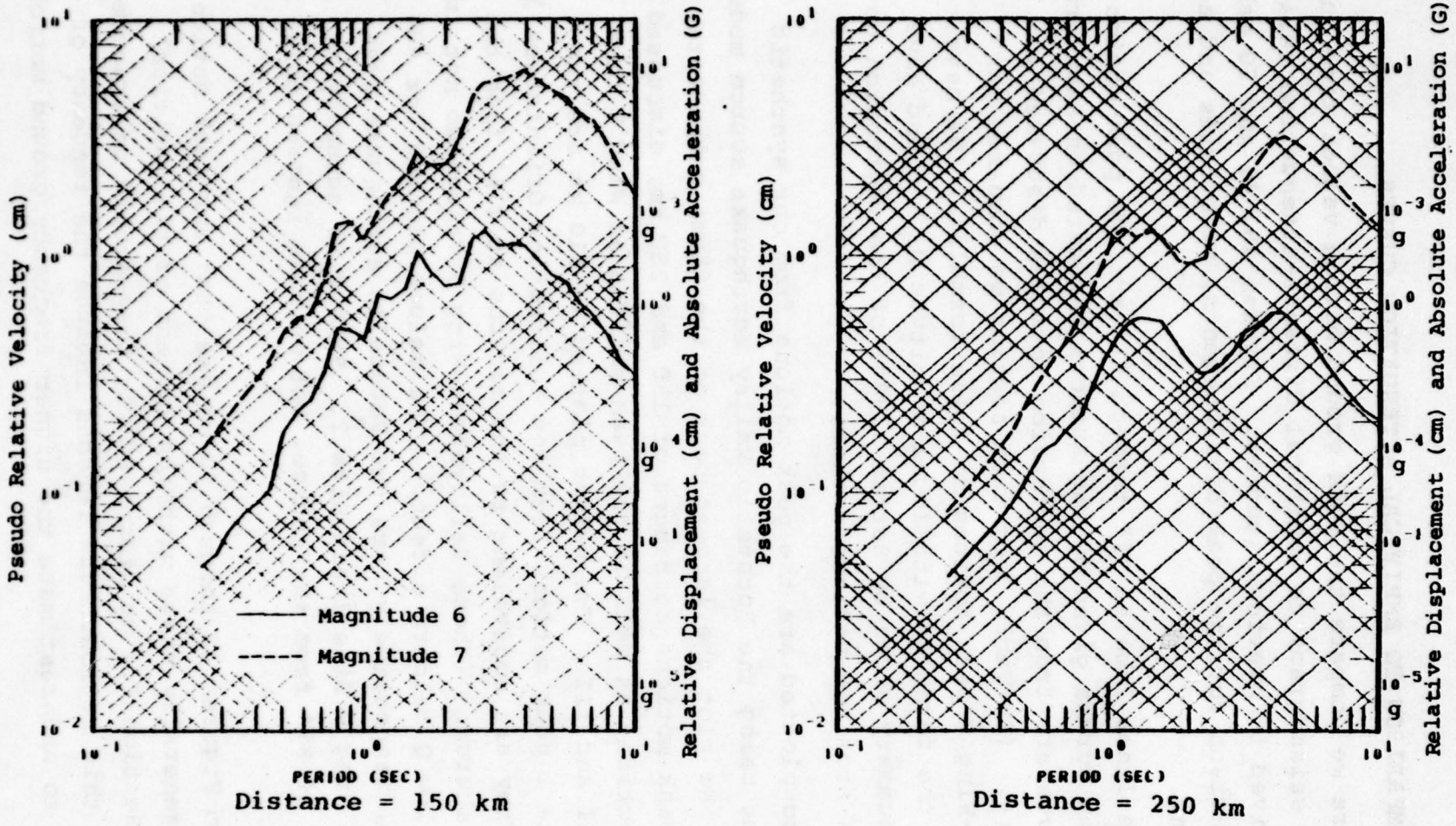

Figure 47. The tangential component response spectra at 90° azimuth and two distances from a Magnitude 6 (Pocatello) and Magnitude 7 earthquake are compared. The path structure is Structure C with standard Q. The damping factor is 0.05 of critical.

5.6 COMPARISON TO EMPIRICAL ATTENUATION CURVES

Here we compare the peak ground motion values from our synthetic seismograms to empirical distance-attenuation relations derived in previous studies. Figures 48, 49 and 50 make this comparison for the peak displacements, velocities and accelerations.

The lines labeled "1" through "7" are the peak motion attenuation curves given by the authors indicated on each graph. These curves are from the regression formulas discussed in Section 2.4. (In Table 3 of that section we compared our Pocatello-Wing V peak motions to these formulas.) We have evaluated the formulas with local magnitude $M_L = 6$ and have used the summary given by Battis (1978) of the regression coefficients from the various authors.

Also plotted are the peak motions from our synthetic seismograms using the Pocatello Valley earthquake source model ($m_b = 6$). We plot the largest peak of the three components. We show the peak motions at ranges of 150 and 250 km, discussed in this section, as well as the peak motions at Wing V from Sections II and III. The values plotted at 610 km are the Wing V Site 1 peak motions from the Yellowstone Orientation 1 source. They are equivalent to the motions at 216° from the Pocatello source. (These Yellowstone-Wing V values do not include the low Q caldera effect.) The values plotted for 680 and 768 km, respectively, are the Pocatello earthquake peak motions at Wing V Site 1 and Site 2. Site 2 is actually at an azimuth of 97° from the source, but we have ignored this difference.

From Figures 48 through 50 we see that our peak motion estimates generally agree with the low end of the empirical data. In Section 2.4 we discussed why they should be expected to plot in this region. The reasons include the tendency of our models to underestimate the higher frequency ground motions

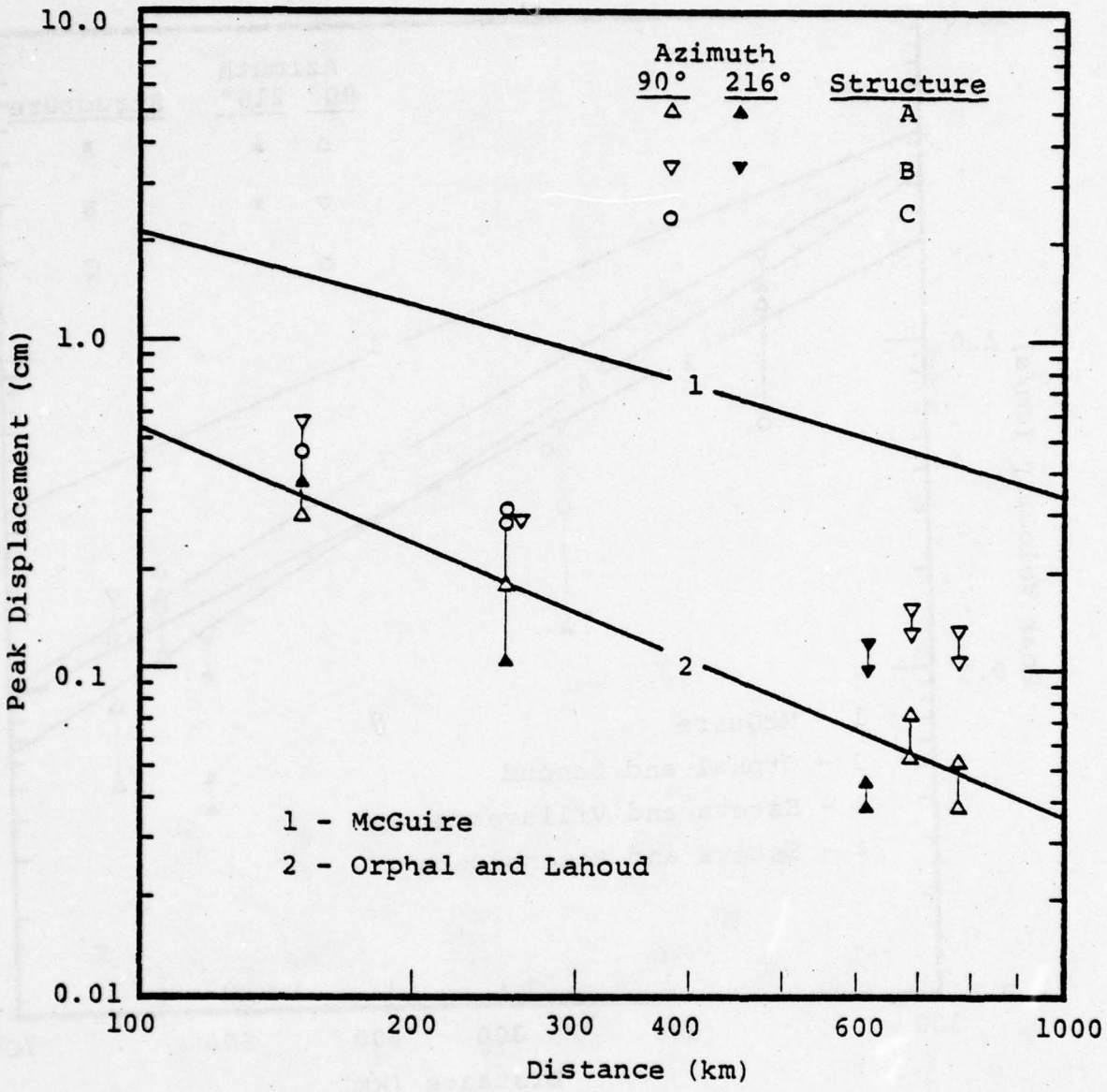

Figure 48. The peak displacements of the synthetic seismograms from the Pocatello source model are compared to the empirical attenuation curves of other authors. The peak motions are from both the Wing V synthetics (Table 2 in Section II and Tables 4 and 5 in Section III) and the synthetics for 150 and 250 km distances (Tables 7, 8 and 9 in Section V).

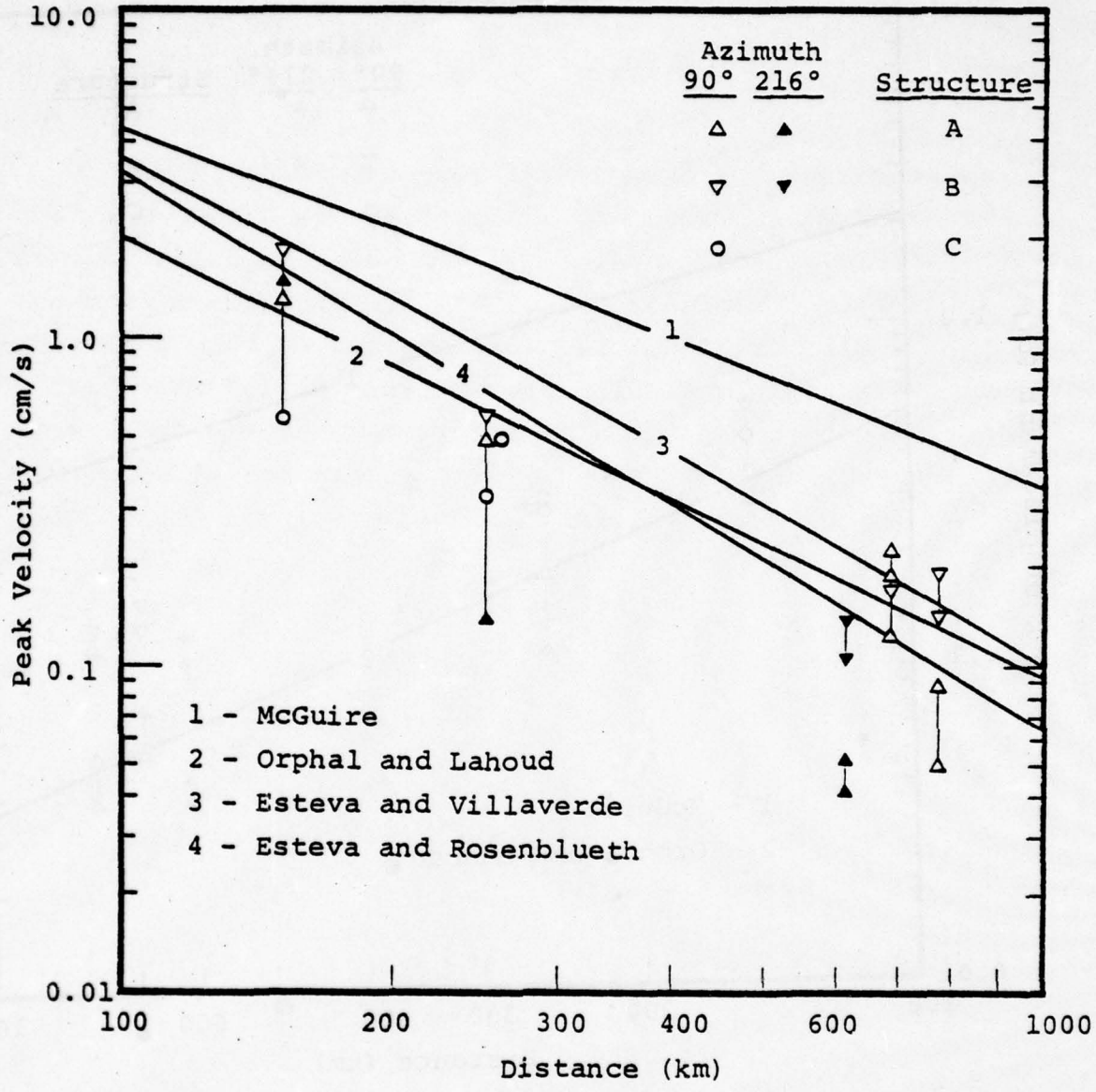

Figure 49. The peak velocities of the synthetic seismograms from the Pocatello source model are compared to the empirical attenuation curves of other authors. The peak motions are from the tables of this report listed in the caption of Figure 48.

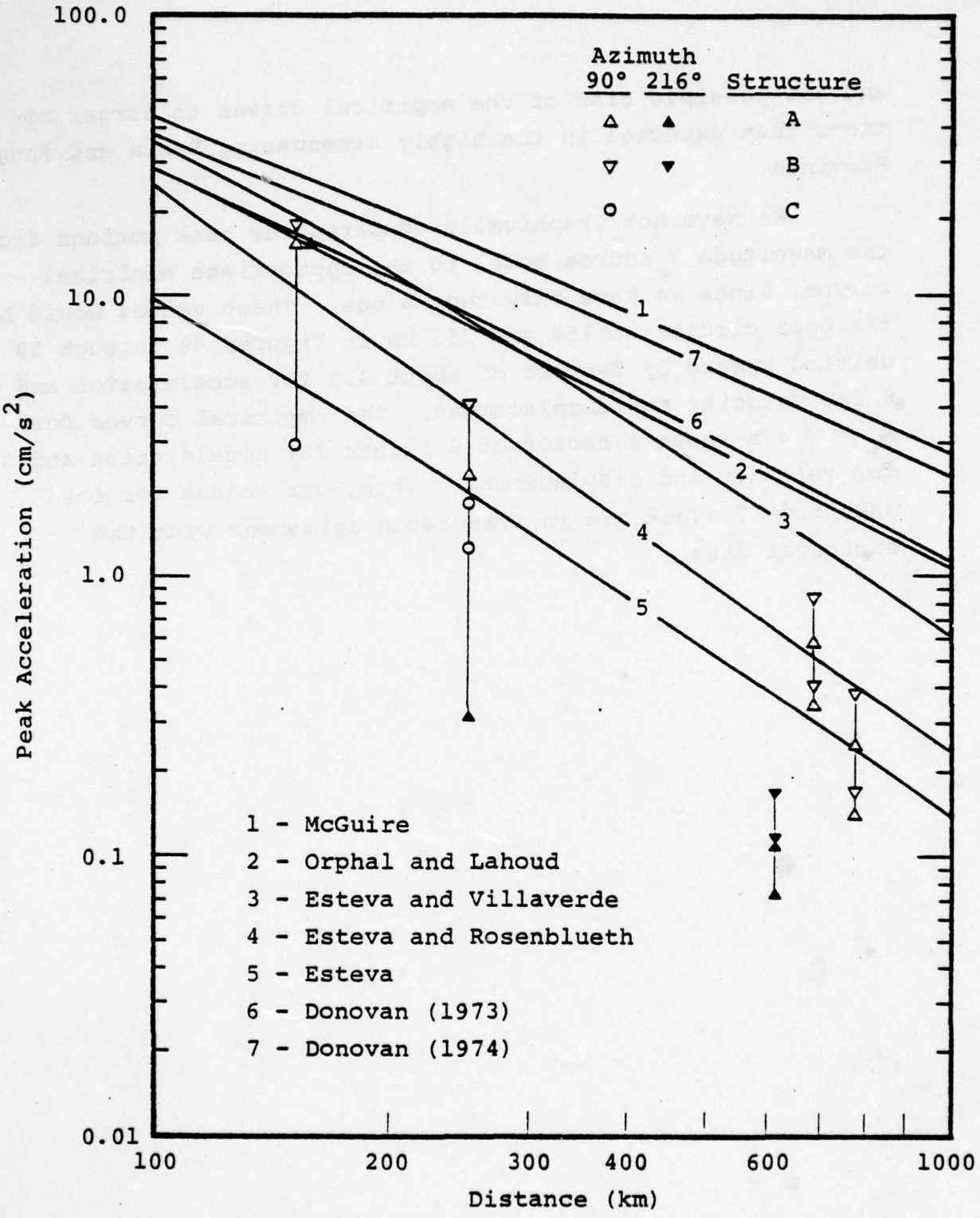

Figure 50. The peak accelerations of the synthetic seismograms from the Pocatello source model are compared to the empirical attenuation curves of other authors. The peak motions are from the tables of this report listed in the caption of Figure 4 .

and the possible bias of the empirical curves to larger motions than expected in the highly attenuating Basin and Range Province.

We have not graphically compared our peak motions from the magnitude 7 source model to the appropriate empirical curves, since we have only two values. These values would be the open circles at 150 and 250 km in Figures 48 through 50 shifted upward by factors of about 3.5 for acceleration and 6 for velocity and displacement. The empirical curves for M_L = 7 are about a factor of 2 higher for acceleration and 3 for velocity and displacement. Thus, our values for the magnitude 7 event are in reasonable agreement with the empirical data.

VI. SURFACE BURST INDUCED GROUND MOTION

6.1 INTRODUCTION

There are no data which provide a direct measurement of the characteristics of the ground motion induced by large surface bursts at distances relatively far from the area of impact (several km and greater). For this reason various investigators have turned to underground nuclear shot data (Cooper, 1972) and chemical explosions (Auld and Murphy, 1979) in order to develop a predictive methodology for distant surface burst ground motion.

On the other hand, earthquake data are plentiful for distances 10-100 km and well studied. Empirical relations linking ground motion characteristics with earthquake size and epicentral distances are numerous. Computational methods for simulation of ground motion characteristics are being employed with reasonable reliability.

Here we summarize briefly some of the important similarities and differences between ground motion induced by a large surface burst, and its associated airblast, and shallow earthquakes of moderate size. Without extensive computations, only qualitative results are possible, but these qualitative results may serve to suggest future theoretical and experimental work which might resolve many of the uncertainties.

6.2 POINT LOAD VERSUS DISLOCATION

We normally view an earthquake as a continuous series of dislocations where slip is induced by a relaxation of the local stress level. A surface burst might be viewed as a sum of surface point loads due to either the direct shock or the moving airblast. A dislocation radiates seismic energy in a distinct radiation pattern. In a whole space the radiation is four lobed and equivalent to a double couple force system

without torque. The double couple radiation pattern can be altered by many dislocations being summed to produce the final motion. In certain directions, the motion may be enhanced by directionized rupture effects. The radiation of energy from a vertical point load is axisymmetric. For a moving airblast, the effective propagation is also axisymmetric. The resulting motion should then show no azimuthal bias except due to near source inhomogeneities and path effects during the propagation.

Dislocation type sources are very effective generators of shear energy. For an isolated dislocation source the amplitude ratio of shear waves to compressional waves radiated is proportional to $(\alpha/\beta)^3$, where β is the media shear velocity and α is the compressional velocity. For most earthquakes this ratio is about a factor of five. As a consequence, ground motion from earthquakes at close distances (within 100 km) is dominated by shear waves and generally they produce surface motion which is primarily horizontal. (At larger distances, attenuation differences can make compressional and shear waves approximately equal in size.)

Point loads are generally less efficient at producing shear energy. In general, the ratio of compressional to shear wave amplitudes is proportional to $(\alpha/\beta)^2$. For earth materials at depth this ratio is usually about a factor of three. For near surface materials where surface burst loads are applied, this factor can be much larger and quite variable.

The axisymmetric nature of a surface burst load does not permit the formation of SH or Love waves in a laterally homogeneous medium. Earthquake ground motion is often dominated by this type of motion. Love waves might be generated by surface bursts when lateral inhomogeneities exist.

6.3 SURFACE SOURCE VERSUS BURIED SOURCE

Most energy radiated from earthquakes appears to originate at depths of several kilometers. As a consequence, most of the high frequency energy (wavelength small compared to the source depth) is in the form of body waves. Attenuation with distance due to geometrical spreading tends to decay at a rate proportional to distance in both peak amplitudes and spectral characteristics. Intrinsic attenuation makes the actual decay somewhat more rapid. The low frequencies (wavelengths comparable to a source depth) tend to propogate as surface waves (Rayleigh or Love waves). Peak amplitudes tend to decay as r^{-1} but spectral amplitudes will decay at $r^{-\frac{1}{2}}$ (neglecting intrinsic attenuation).

As a surface source, surface bursts will be very efficient generators of surface wave type motion at all frequencies. The excitation of a surface wave mode is a linear function of the characteristic mode shape with depth. Figure 51 shows the Rayleigh wave vertical mode shapes with depth for four periods in the Northern Colorado Plateau model used in a previous section. The normalized values plotted give an approximate measure of how an earthquake at a given depth will excite surface wave modes. As source depth increases, the excitation of short period surface waves is rapidly decreased. However, a surface source will excite all frequencies of a given mode.

At close distances one would predict that these high frequency surface waves will be an important factor in the observed motion, and the overall nature of the ground motion will be much different from that observed near earthquakes. At distances beyond a few kilometers, there are many reasons to suspect that the high frequency surface waves generated by surface bursts will not be important in determining the characteristics of induced ground motion. High frequency waves

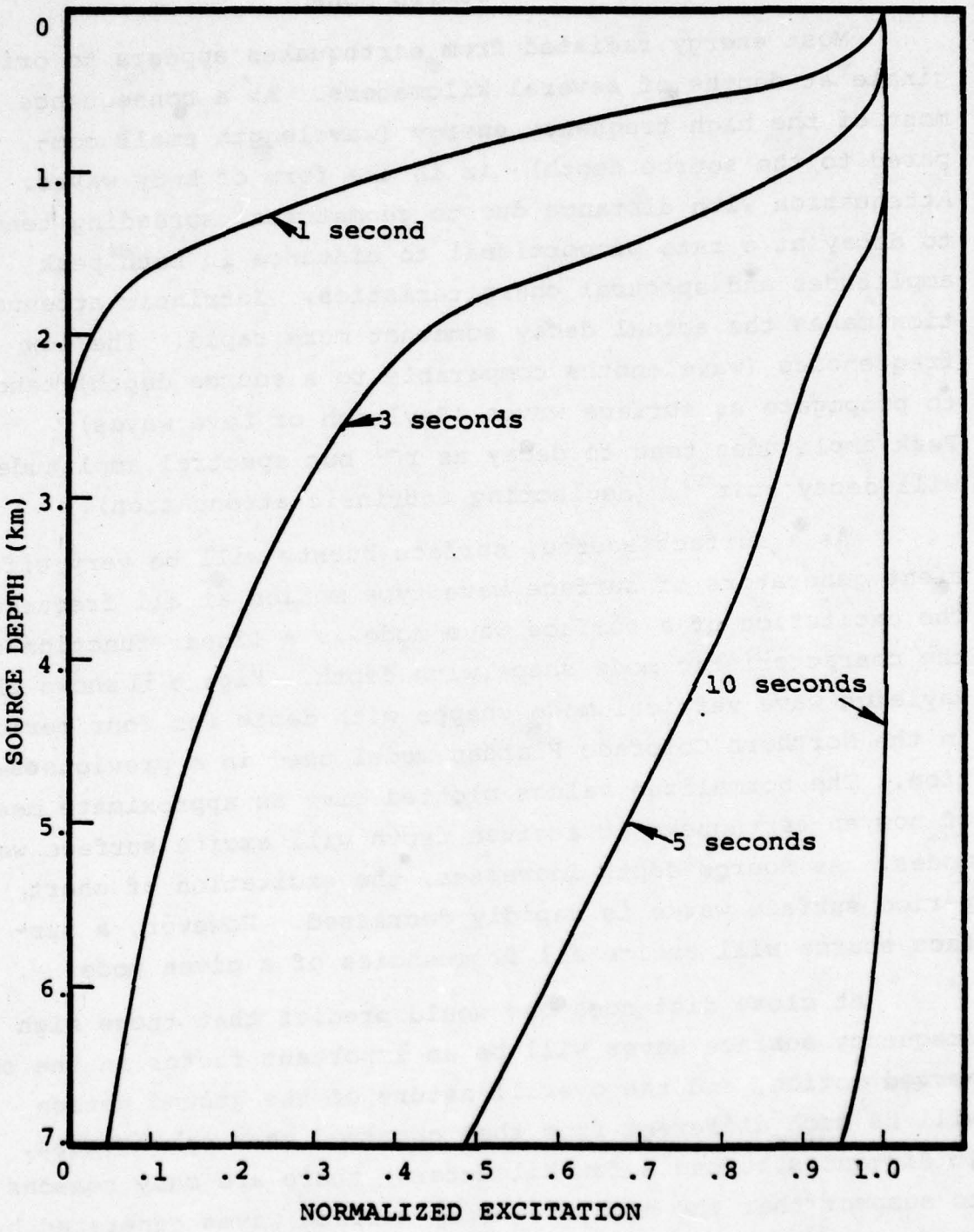

Figure 51. The depth dependence of the fundamental mode Rayleigh wave excitation for a vertical point force -- Northern Colorado Plateau model.

in near surface materials may be degraded by numerous mechanisms. Near the source high strains may cause nonlinear effects in surface soils which absorb much of the energy propagating outward. Even in the linear realm, intrinsic attenuation in near surface materials can be quite severe. Near surface materials tend to be rather heterogeneous laterally over dimensions of kilometers, so that coherent wave-guide propagation may not be possible over such distances. At these moderate distances the controlling mechanism in the induced ground motion will probably be the shallowest earth materials which remain relatively homogeneous over the propagation path.

6.4 SPECTRAL EXCITATION

The effective source spectral excitation of seismic waves is controlled by the characteristics of the associated rupture process. The typical earthquake source displacement spectrum (as observed in the far-field, beyond a few wavelengths) is generally flat at low frequencies and decays at a rate of inverse frequency to the second or third power at high frequencies. The frequencies where the change in trends occur are generally known as the corner frequencies and are a function of the characteristic times associated with the rupture process. For moderate to large earthquakes, the corner frequencies are generally less than one hertz.

For a surface burst the spectral excitation will also be associated with the specific dynamics of the event. The direct shock occurs over a time scale much shorter than the periods of wave motion of interest. In theory, the radiated amplitude spectrum would then be flat over the frequencies of interest. However, in practice this may not be the case due to crater formation. Although Auld and Murphy (1979) have identified the airblast originating at the crater radius as the source of the Rayleigh wave ground motion from chemical surface explosions, it is still not well understood what

proportion of energy is used in crater formation and how much is radiated from a high yield nuclear explosion. The spectral excitation associated with the direct shock and subsequent crater formation is not clear at this time and cannot be resolved until a better understanding of cratering is obtained.

The effective seismic radiation due to airblast loading from large yield nuclear surface bursts is predictable with available modeling techniques (Cherry, et al., 1978). We can view the airblast as a surface load moving cylindrically from the direct shock. Sometimes analogies are made between airblast induced motion and air-coupled Rayleigh waves often observed in seismic exploration experiments. This is a somewhat deceptive comparison. Air-coupled Rayleigh waves are excited by a pressure load moving at a constant velocity (the sound speed). This uniformly moving load will efficiently excite a Rayleigh wave with a horizontal phase velocity at or near the sound speed. The airblast associated with a large surface burst is actually a shock wave with a highly non-uniform propagation velocity. In general, no single Rayleigh wave horizontal phase velocity will be preferentially excited as in the trans-sonic case.

Brode (1968) describes the specific nature of the airblast in terms of an overpressure time history as a function of distance. The peak overpressure P_s is related to distance from the direct shock and yield by the expression

$$\Delta P_s = \frac{3300W}{r^3} + \frac{192W^{1/2}}{r^{3/2}} \text{ psi}$$

with the yield W in MT and the distance r in kilofeet. The particular time history at any given distance can be approximated by the form

$$\Delta P(t) = \Delta P_s \ (1-\tau) \ (- ae^{-\alpha\tau} + be^{-\beta\tau} + ce^{-\gamma\tau})$$

with $\tau = (t - t_s)/D_p^+$ while D_p^+ is the duration of the positive pressure loading and t_s is the shock arrival time. The coefficients a, b, c, α, β, and γ control the decay of the pressure load at times after the arrival. All of the parameters above are functions of the peak overpressure and, hence, are functions of yield and distance. At small distances the overpressure loading decays very rapidly with time. As distance increases, the duration of loading increases.

The relative excitation of seismic energy due to overpressure loading at any given distance and azimuth will be a linear function of the spectral overpressure. The spectral overpressure is simply the Fourier transform of the time history which is

$$\Delta\bar{P}(\omega) = D_p^+ \Delta P_s e^{-i\omega t_s} \left[\frac{a}{\alpha + i\omega D_p}\left[1 - \frac{1}{\alpha + i\omega D_p}\right]\right.$$

$$\left. + \frac{b}{\beta + i\omega D_p}\left[1 - \frac{1}{\beta + i\omega D_p}\right] + \frac{c}{\gamma + i\omega D_p}\left[1 - \frac{1}{\gamma + i\omega D_p}\right]\right],$$

where ω is angular frequency. Figure 52 shows the amplitude of spectral overpressures as a function of distance for a few frequencies using the pressure dependent values of the coefficients plotted in Brode (1968). At small distances the spectral response decays very slowly with frequency implying the response will resemble that of an impulse. At distances greater than 1 km the response decays at a rate of about ω^{-1} implying the response will resemble that of a step load in overpressure.

The seismic response will be proportional to the spectral overpressure loading integrated over the spectral extent of the airblast. Because of the cylindrical symmetry of the loading, it can be shown that the effective source contribution of the airblast will be the Fourier-Bessel transform of

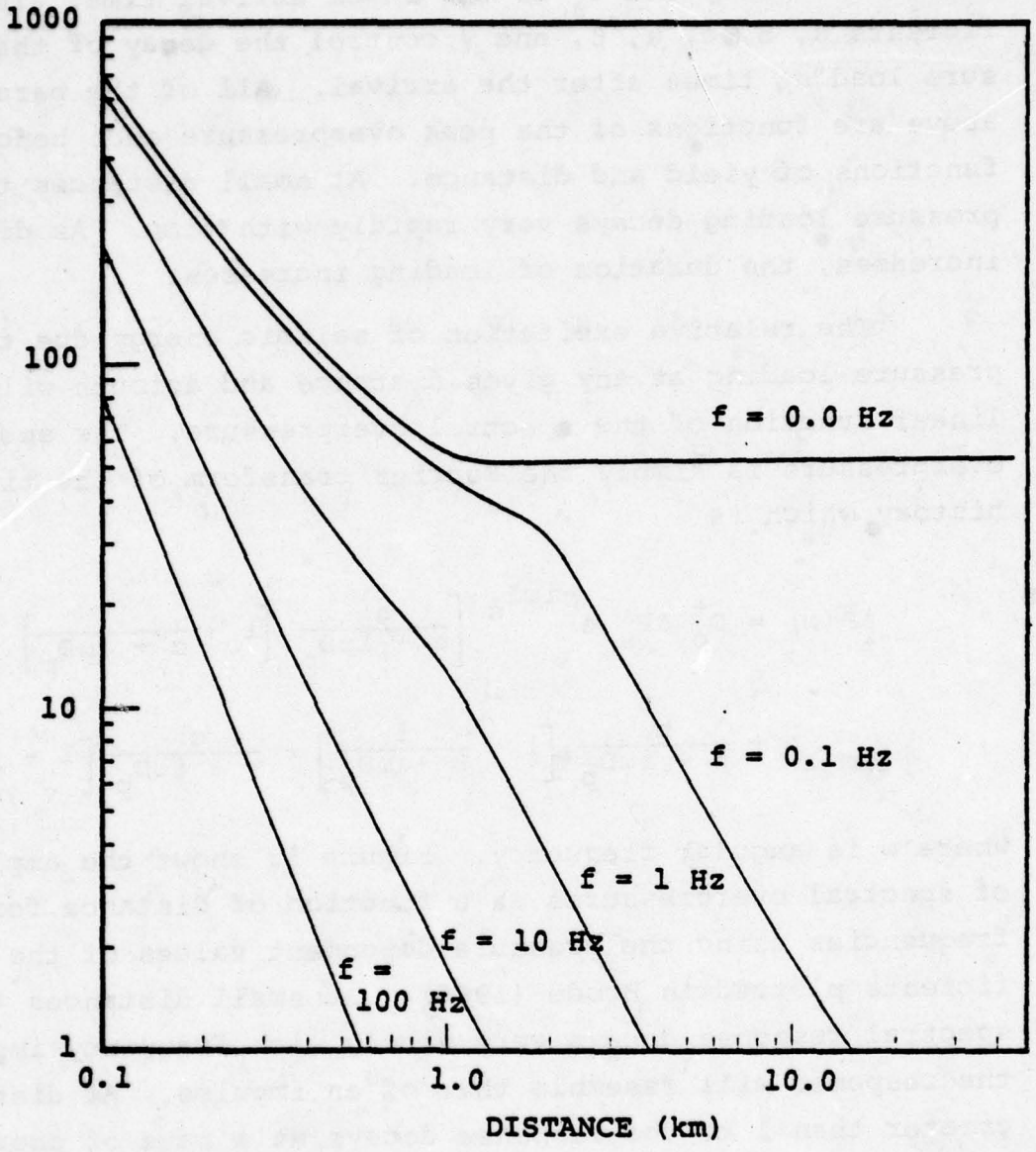

Figure 52. Spectral overpressure, psi/second, as a function of distance from blast.

the blast loading with distance. The equivalent seismic source function can be expressed as

$$S(\omega,k) = 2\pi \int_0^\infty r\, \Delta P\ (r,\omega)\ J_0\ (kr)\ dr$$

where the transform variable k is a horizontal wave number. The horizontal wave number k is often more conveniently expressed by

$$k = \frac{\omega}{c}$$

where c is a horizontal phase velocity. The contribution of the airblast to surface wave motion is directly proportional to the functions $S(\omega,k)$ for the ω and k appropriate to a given mode. In the far-field the body wave contributions will be proportional asymptotically to the values of $S(\omega,k)$ for an appropriate choice of horizontal phase velocity.

At a given yield W, the source function can be represented by

$$S_1 = A\ f_1^{-n}$$

where S has units of L^3, f is frequency and n is a monotonically increasing function of frequency such that

$$0 \leq n \leq 3\ .$$

At a new yield, W_2, cube root scaling gives

$$S_2 = \frac{W_2}{W_1}\ f_2^{-n}$$

such that f_2 scales into f_1, i.e.,

$$f_2 = \left(\frac{W_2}{W_1}\right)^{1/3} f_1 .$$

Therefore,

$$S_2 = \left(\frac{W_2}{W_1}\right)^{(1 - n/3)} S_1 .$$

The exact details of the source function S should be computed numerically including all the phase information associated with the moving airblast. Such computations are quite straightforward, but they have not been completed at this time. A very preliminary analysis suggests that the corner frequency for a 1 MT airblast occurs at about 0.5 Hz. Therefore, at this frequency $0 < n < 1$ and the yield exponent is expected to be approximately 0.8.

REFERENCES

Anderson, D. L. and C. B. Archambeau (1964), "The Anelasticity of the Earth," JGR, 69, pp. 2071-2084.

Anderson, D. L. and R. S. Hart (1978), "Q of the Earth," JGR, 83, pp. 5869-5882.

Arabasz, W. J., W. D. Richins and C. J. Langer (1975), "Detailed Characteristics of March 1975 Idaho-Utah Border Earthquake Sequence," EOS, 56, p. 1022.

Archambeau, C. B. (1968), "General Theory of Elastodynamic Source Fields," Rev. Geophys. 6, pp. 241-288.

Auld, H. E. and J. R. Murphy (1979), "Surface Wave Calculations," DNA Strategic Structure Division Biennial Review Conference, SRI International, Menlo Park, California.

Bache, T. C. and D. G. Harkrider (1976), "The Body Waves Due to a General Seismic Source in a Layered Earth Model: 1. Formulation of the Theory," BSSA, 66, pp. 1805-1819.

Bache, T. C. and T. G. Barker (1978), "The San Fernando Earthquake--A Model Consistent with Near-Field and Far-Field Observations at Long and Short Periods," Systems, Science and Software Report SSS-R-78-3552, January.

Bache, T. C., W. L. Rodi and D. G. Harkrider (1978), "Crustal Structures Inferred from Rayleigh-Wave Signatures of NTS Explosions," BSSA, 68, pp. 1399-1413.

Battis, J. C. (1978), "Geophysical Studies of Missile Basing: Seismic Risk Studies in the Western United States," Interim Scientific Report No. 2, AFOSR Contract No. F44620-76-C-0063, Texas Instruments, Incorporated, Dallas, Texas.

Battis, J. C. and K. Hill (1977), "Analysis of Seismicity and Tectonics of the Central and Western United States," Interim Scientific Report No. 1, AFOSR Contract No. F44620-76-C-0063, Texas Instruments, Incorporated, Dallas, Texas.

Boore, D. M. (1972), "A Note on the Effect of Simple Topography on Seismic SH Waves," BSSA, 62, pp. 275-284.

Bouchon, M. (1973), "Effect of Topography on Surface Motion," BSSA, 63, pp. 615-632.

Brode, H. L. (1968), "Review of Nuclear Weapons Effects," Annual Review of Nuclear Science, 18, pp. 153-202.

Cherry, J. T., S. M. Day, N. Rimer, W. L. Rodi and H. L. Swanger (1978), "Rayleigh Waves in MX Valleys," Systems, Science and Software Report SSS-R-79-3874, October.

Cluff, L. S. (1978), "Geologic Considerations for Seismic Microzonation," Proceedings of the 2nd International Conference on Microzonation, San Francisco, California, p. 135.

Cooper, H. F., Jr. (1972), "Some Comments on Seismic Data from Underground Explosions at the Nevada Test Site," R & D Associates Report RDA-TR-077-DNA, June.

Day, S. M., T. C. Bache, T. G. Barker and J. T. Cherry (1978), "A Source Model for the 1975 Pocatello Valley Earthquake," Systems, Science and Software Scientific Report SSS-R-79-3893 to Air Force Geophysics Laboratory, December.

Donovan, N. C. (1973), "A Statistical Evaluation of Strong Motion Data Including the February 9, 1971 San Fernando Earthquake," Paper presented to the Fifth World Conference on Earthquake Engineering, Rome, Italy.

Donovan, N. C. (1978), "Soil and Geologic Effects on Site Response," Proceedings of the 2nd International Conference on Microzonation, San Francisco, California, p. 55.

Eaton, G. P., R. L. Christiansen, H. M. Iyer, A. M. Pitt, D. R. Mabey, H. R. Blank, Jr., I. Zietz and M. E. Gettings (1975), "Magma Beneath Yellowstone National Park," Science, 188, pp. 787-796.

Esteva, L. and E. Rosenblueth (1963), "Espectros de Temblores a Distancias Moderadas y Grandes," Bol. Soc. Mex. Ing. Sism., 2, pp. 1-18.

Esteva, L. (1970), "Seismic Risk and Seismic Design Input for Nuclear Power Plants," in Seismic Design for Nuclear Power Plants, edited by R. J. Hansen, pp. 438-483.

Evoy, J. A. (1978), "Precision Gravity Reobservations and Simultaneous Inversion of Gravity and Seismic Data for Subsurface Structure of Yellowstone," Masters Thesis, University of Utah, Salt Lake City, Utah.

Ewing, W. M., W. S. Jardetzky and F. Press (1957), Elastic Waves in Layered Media, McGraw-Hill, New York.

Haddon, R. A. W. and E. S. Husebye (1978), "Joint Interpretation of P-Wave Time and Amplitude Anomalies in Terms of Lithospheric Heterogeneities," Geophys. J. R. Astr. Soc., 55, pp. 19-43.

Harkrider, D. G. (1964), "Surface Waves in Multilayered Media, I. Rayleigh and Love Waves from Buried Sources in a Multilayered Elastic Half-Space," BSSA, 54, pp. 627-679.

Harkrider, D. G. (1970), "Surface Waves in Multilayered Media, II. Higher Mode Spectra and Spectral Ratios from Point Sources in Plane-Layered Earth Models," BSSA, 60, pp. 1937-1987.

Helmberger, D. V. (1974), "Generalized Ray Theory for Shear Dislocations," BSSA, 64, pp. 45-64.

Herrmann, R. B. (1977), "Research Study of Earthquake Generated SH Waves in the Near-Field and Near-Regional Field," Final Report, Contract DACW39-76-C-0058, Waterways Experiment Station, Vicksburg, Mississippi.

Keller, G. R., R. B. Smith, L. W. Braile, R. Heaney and D. H. Shurbert (1976), "Upper Crustal Structure of the Eastern Basin and Range, Northern Colorado Plateau and Middle Rocky Mountains from Rayleigh-Wave Dispersion," BSSA, 66, pp. 869-876.

Knopoff, L., F. Schwab and E. Kausel (1973), "Interpretation of Lg," Geophys. J. R. astr. Soc., 33, pp. 389-404.

Laster, S. J., J. G. Foreman and A. F. Linville (1965), "Theoretical Investigation of Modal Seismograms for a Layer Over a Half-Space," Geophysics, 30, pp. 571-596.

McGuire, R. K. (1974), "Seismic Structural Response Risk Analysis, Incorporating Peak Response Regressions on Earthquake Magnitude and Distance," Department of Civil Engineering, Research Report R74-51, Massachusetts Institute of Technology, Cambridge, Massachusetts.

Minster, J. B. (1973), "Elastodynamics of Failure in a Continuum," Ph.D. Thesis, California Institute of Technology, Pasadena, California.

Mitchell, B. J. (1973), "Surface Wave Attenuation and Crustal Anelasticity in Central North America," BSSA, 63, pp. 1057-1071.

Mitchell, B. J. (1975), "Regional Rayleigh Wave Attenuation in North America," JGR, 80, pp. 4904-4916.

O'Neill, M. E. and J. H. Healy (1973), "Determination of Source Parameters of Small Earthquakes from P-Wave Rise Time," BSSA, 63, pp. 599-614.

Orphal, D. and J. Lahoud (1974), "Prediction of Peak Ground Motion from Earthquakes," BSSA, 64, pp. 1563-1574.

Page, R. A., D. M. Boore, W. B. Joyner and H. W. Coulter (1972), "Ground Motion Values for Use in the Seismic Design of the Trans-Alaska Pipeline System", U. S. Geological Survey, Circular 672, Washington, D. C.

Panza, G. F., F. A. Schwab and L. Knopoff (1972), "Channel and Crustal Rayleigh Waves," Geophys. J. R. Astr. Soc., 30, pp. 273-280.

Panza, G. F. and G. Calcagnile (1975), "Lg, Li and Rg from Rayleigh Modes," Geophys. J. R. Astr. Soc., 40, pp. 475-487.

Pitt, A. M., C. S. Weaver and W. Spence (1979), "The Yellowstone Park Earthquake of June 30, 1975," BSSA, 69, pp. 187-205.

Sills, L. B. (1978), "Scattering of Horizontally-Polarized Shear Waves by Surface Irregularities," Geophys. J. R. Astr. Soc., 54, pp. 319-348.

Smith, R. B., R. T. Shuey, R. O. Freidline, R. M. Otis and L. B. Alley (1974), "Yellowstone Hot Spot: New Magnetic and Seismic Evidence," Geology, 2, pp. 451-455.

Strick, E. (1970), "A Predicted Pedestal Effect for Pulse Propagation in Constant-Q Solids," Geophysics, 35, pp. 387-403.

Swanger, H. J. and D. M. Boore (1978), "Simulation of Strong-Motion Displacements Using Surface-Wave Modal Superposition," BSSA, 68, pp. 907-922.

Tsai, Y. B. and K. Aki (1969), "Simultaneous Determination of the Seismic Moment and Attenuation of Seismic Surface Waves," BSSA, 59, pp. 275-288.

Turnbull, L. S., Jr., D. Sum and J. Shaub (1973), "Determination of Seismic Source Parameters from Frequency Dependent Rayleigh and Love Wave Radiation Patterns," Semi Annual Technical Report No. 1- Part C, Texas Instruments Report No. ALEX(02)-TR-73-01-PART C, AFOSR Contract Number F44620-73-C-0055, Texas Instruments, Incorporated, Dallas, Texas.

Warren, D. H. and J. H. Healy (1973), "Structure of the Crust in the Conterminous United States," In: S. Mueller (ed.), The Structure of the Earth's Crust, Based on Seismic Data. Tectonophysics, 20(1-4), pp.203-213.

Wong, H. L. and P. C. Jennings (1975), "Effects of Canyon Topography on Strong Ground Motion," BSSA, 65, pp. 1239-1257.

APPENDIX A

SYNTHETIC POCATELLO VALLEY AND YELLOWSTONE PARK EARTHQUAKE SEISMOGRAMS AT WING V

The figures in this appendix show the Pocatello and Yellowstone-Wing V seismograms on which the results in Sections II and III are based. Figures A.1 through A.8 show the three-component displacement seismograms for the two earthquakes obtained with various path structures. The corresponding velocity seismograms are shown in Figures A.9 through A.16 and the acceleration seismograms in Figures A.17 - A.24.

The ordering of the figures is as follows:

Figure Numbers	Source	Path Model	Wing V Site
A.1, 9, 17	Pocatello	B, f_Q = 1 & 2	2
2, 10, 18	Pocatello	A, f_Q = 1 & 2	2
3, 11, 19	Pocatello	B, f_Q = 1 & 2	1
4, 12, 20	Pocatello	A, f_Q = 1 & 2	1
5, 13, 21	Yellowstone (Orientation 1)	B, f_Q = 1 & 2	1
6, 14, 22	Yellowstone (Orientation 1)	A, f_Q = 1 & 2	1
7, 15, 23	Yellowstone (Orientation 1)	A, f_Q = 0.34 & 0.53	1
8, 16, 24	Yellowstone (Orientation 2)	A, f_Q = 1 & 2	1

Sites 1 and 2 at Wing V are located on Figure 1 (Section 2.1). The path structures A and B with f_Q = 1 are listed in Table 1 (Section 2.3). The Q scaling factor, f_Q, is defined in Sections 2.3.1 and 3.2. Values of f_Q less than 1 account for the low Q caldera in the Yellowstone-Wing V path. The two orientations of the Yellowstone Park earthquake are defined in Section 3.3.

The time scale for each plot is seconds after event origin time. The number to the left of each vertical axis is the height of the vertical axis in units of either cm, cm/sec or cm/sec^2.

STRUCTURE B, f_Q = 2 (high Q)

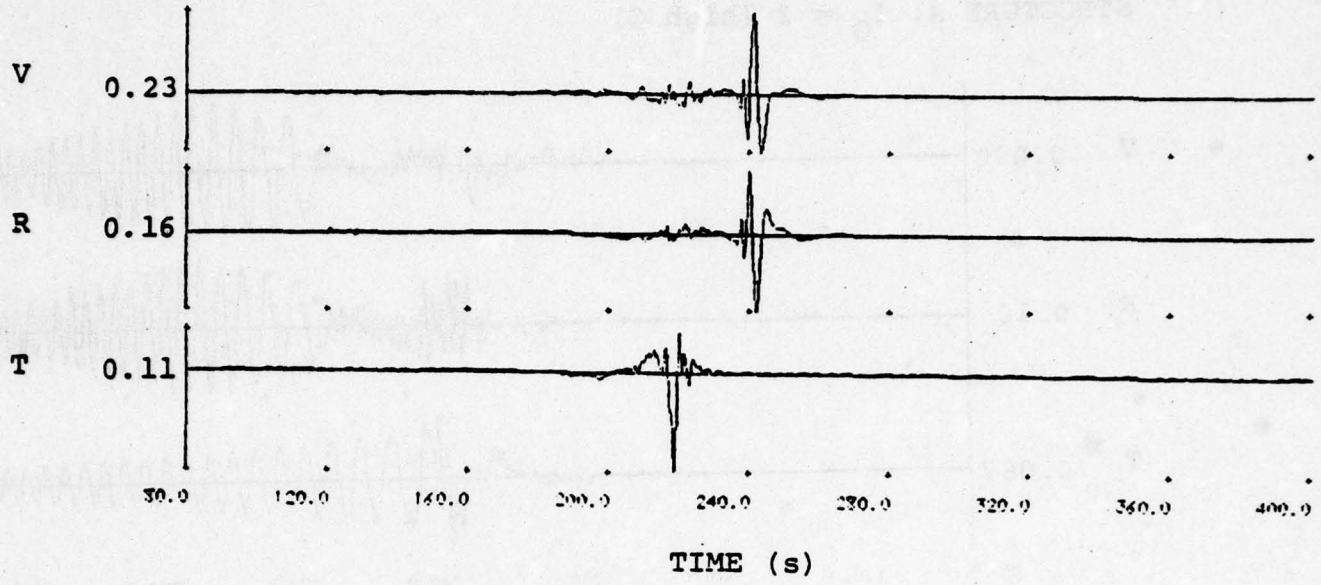

STRUCTURE B, f_Q = 1 (low Q)

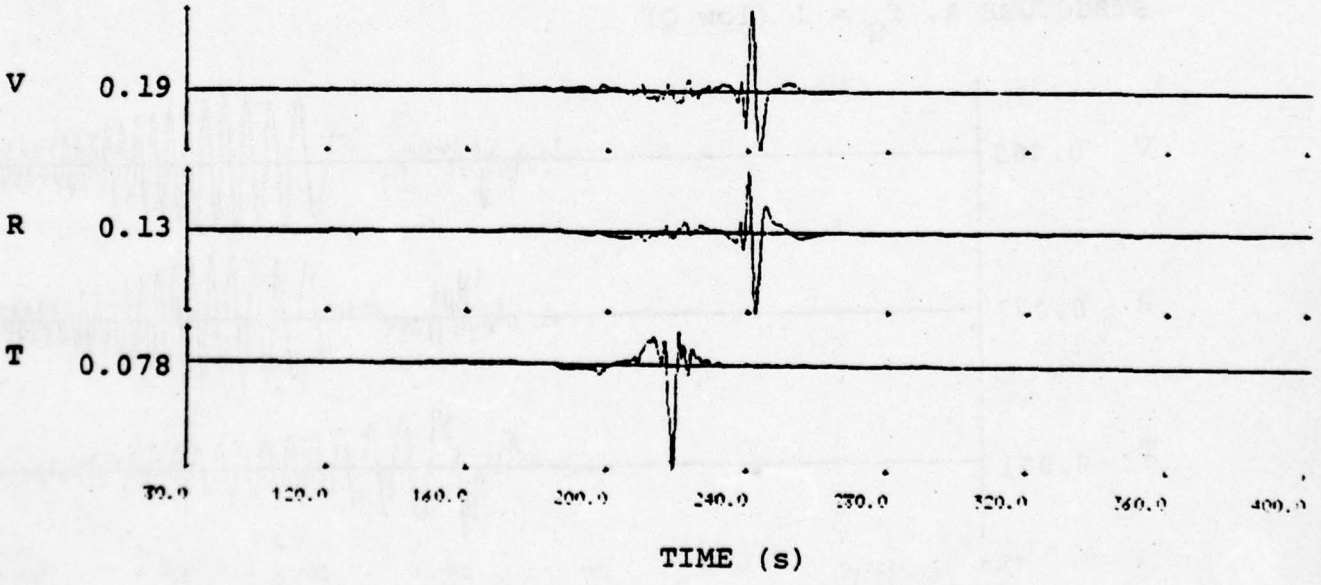

Figure A.1. Displacement seismograms at Wing V Site 2 from Pocatello earthquake using Structure B path model.

STRUCTURE A, f_Q = 2 (high Q)

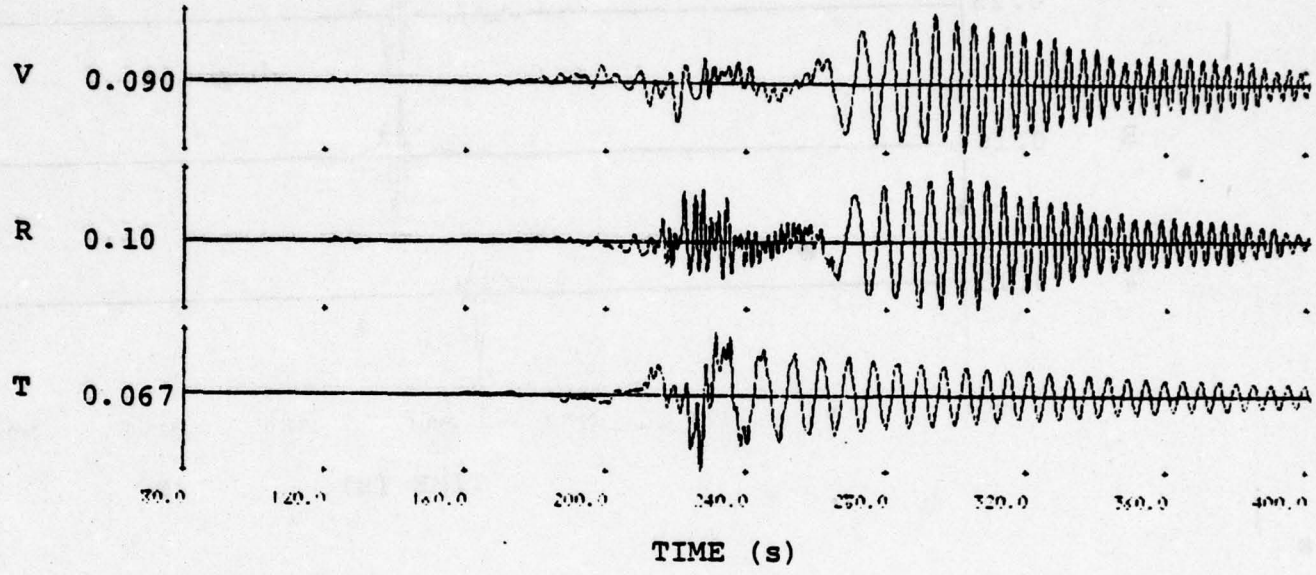

STRUCTURE A, f_Q = 1 (low Q)

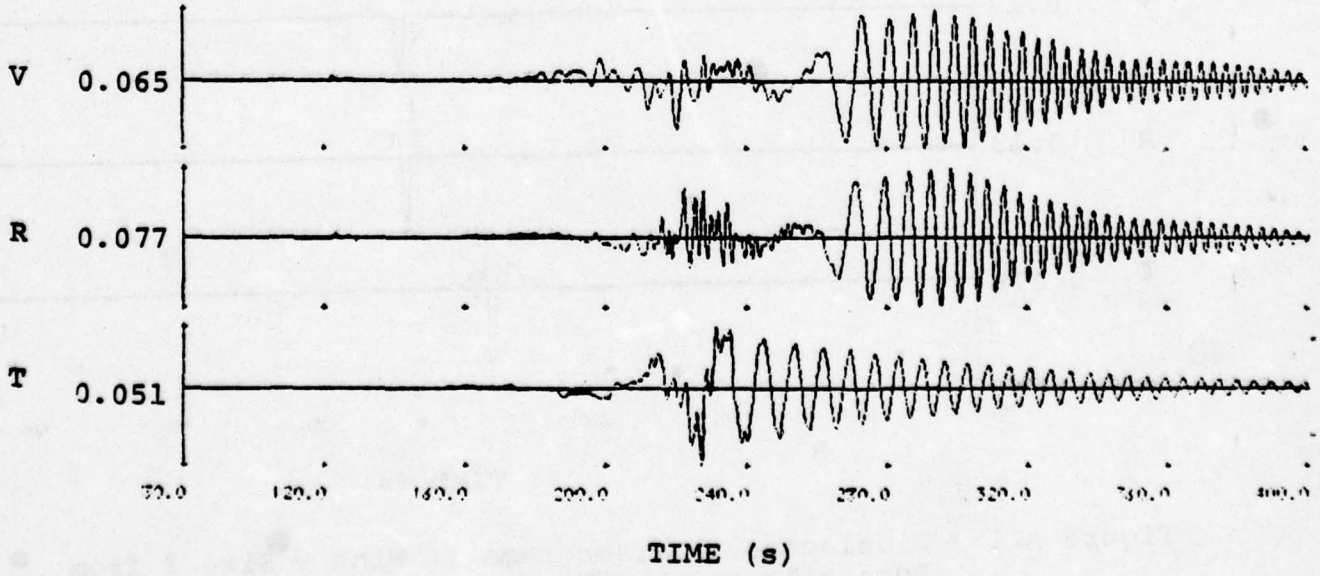

Figure A.2. Displacement seismograms at Wing V Site 2 from Pocatello earthquake using Structure A path model.

STRUCTURE B, f_Q = 2 (high Q)

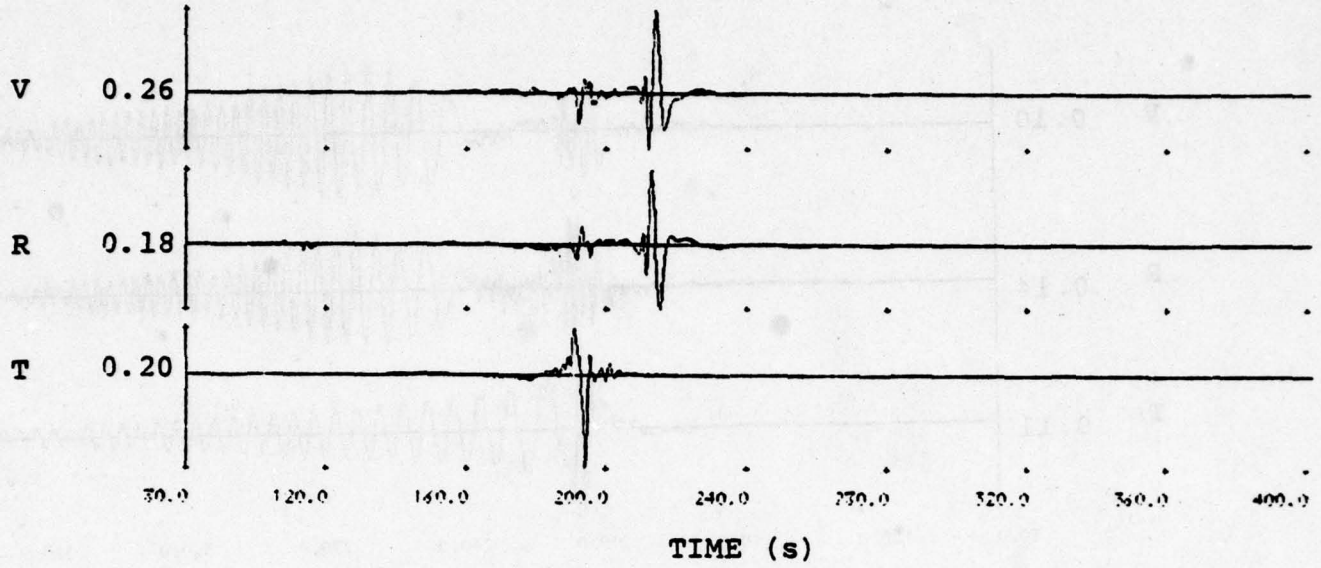

STRUCTURE B, f_Q = 1 (low Q)

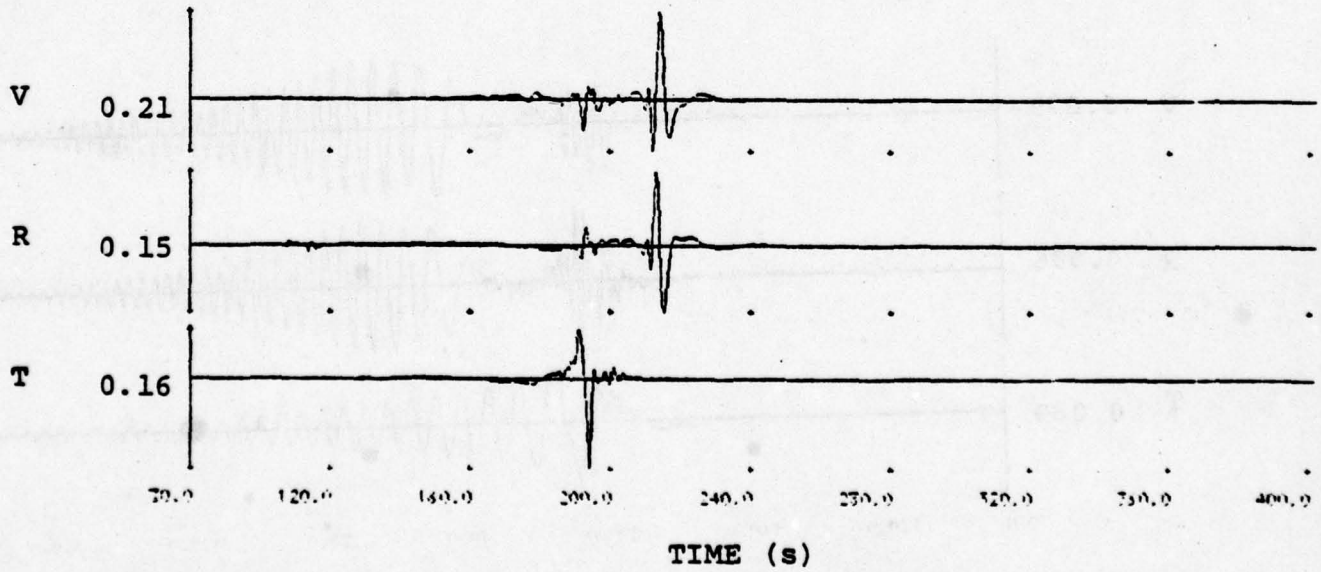

Figure A.3. Displacement seismograms at Wing V Site 1 from Pocatello earthquake using Structure B path model.

STRUCTURE A, f_Q = 2 (high Q)

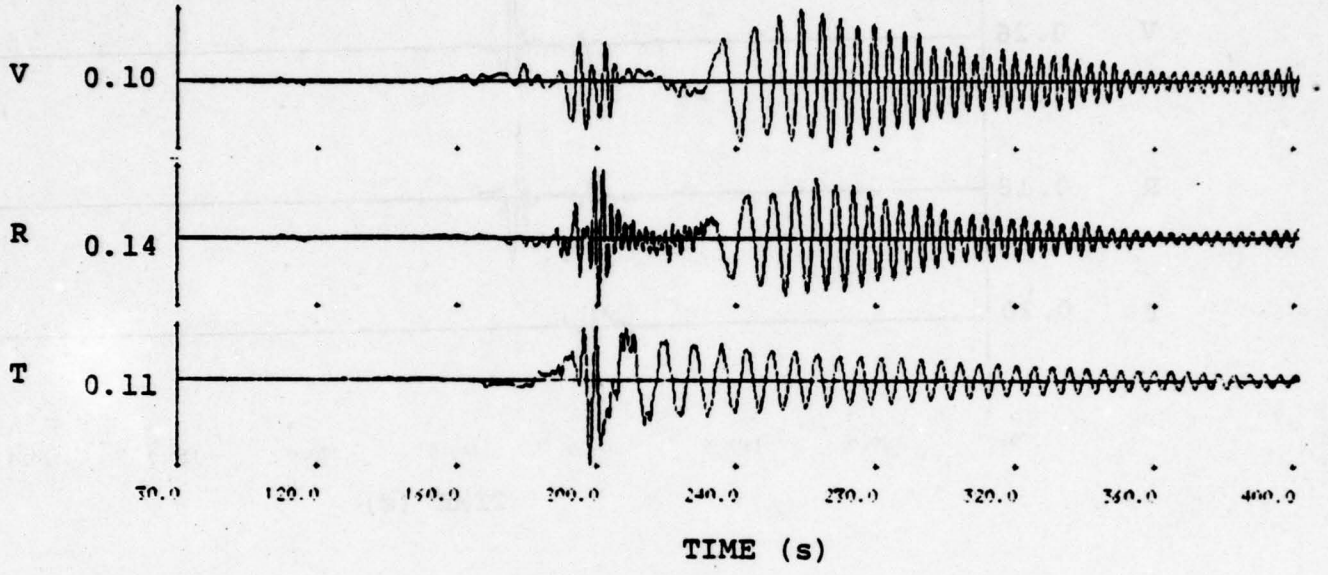

STRUCTURE A, f_Q = 1 (low Q)

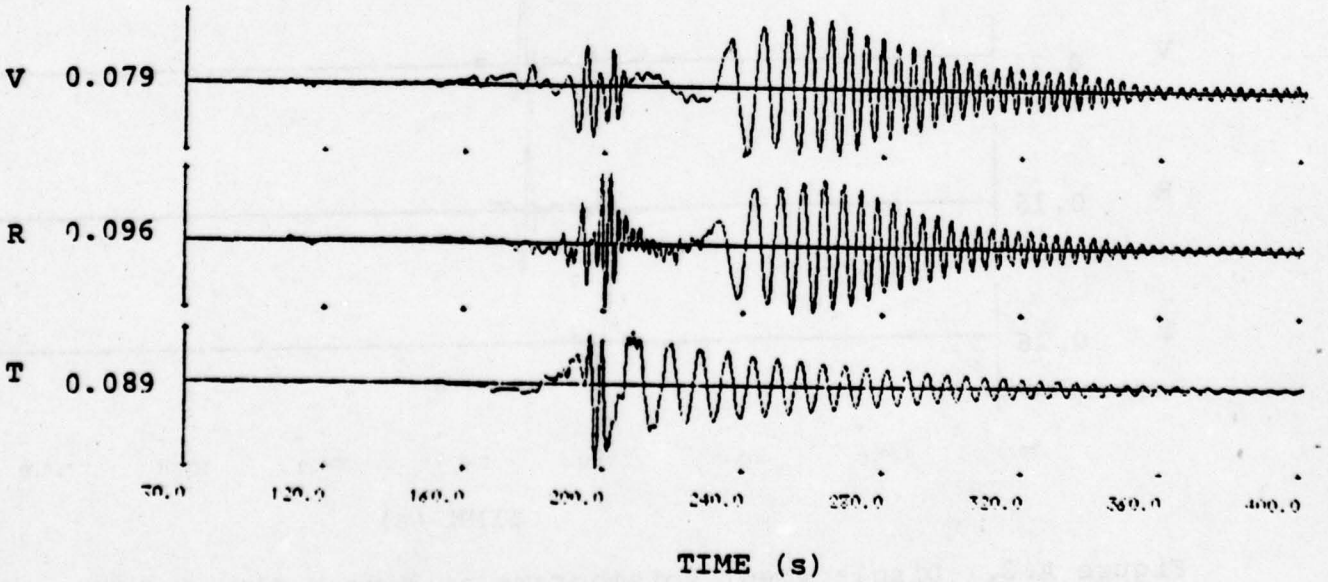

Figure A.4. Displacement seismograms at Wing V Site 1 from Pocatello earthquake using Structure A path model.

STRUCTURE B, f_Q = 2 (high Q)

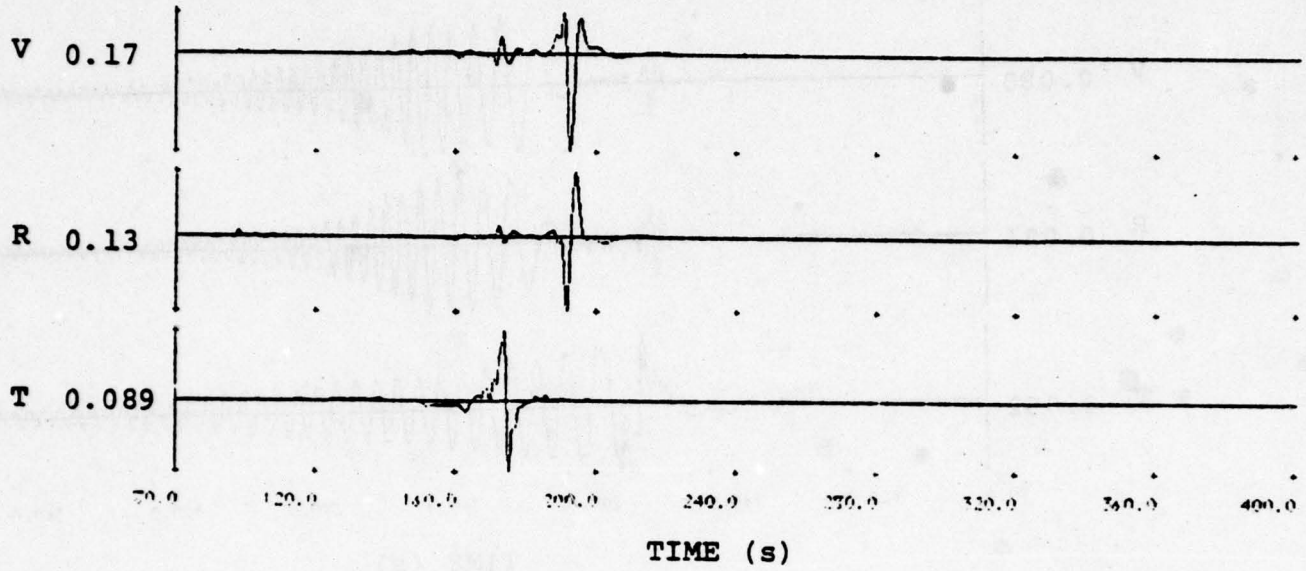

STRUCTURE B, f_Q = 1 (low Q)

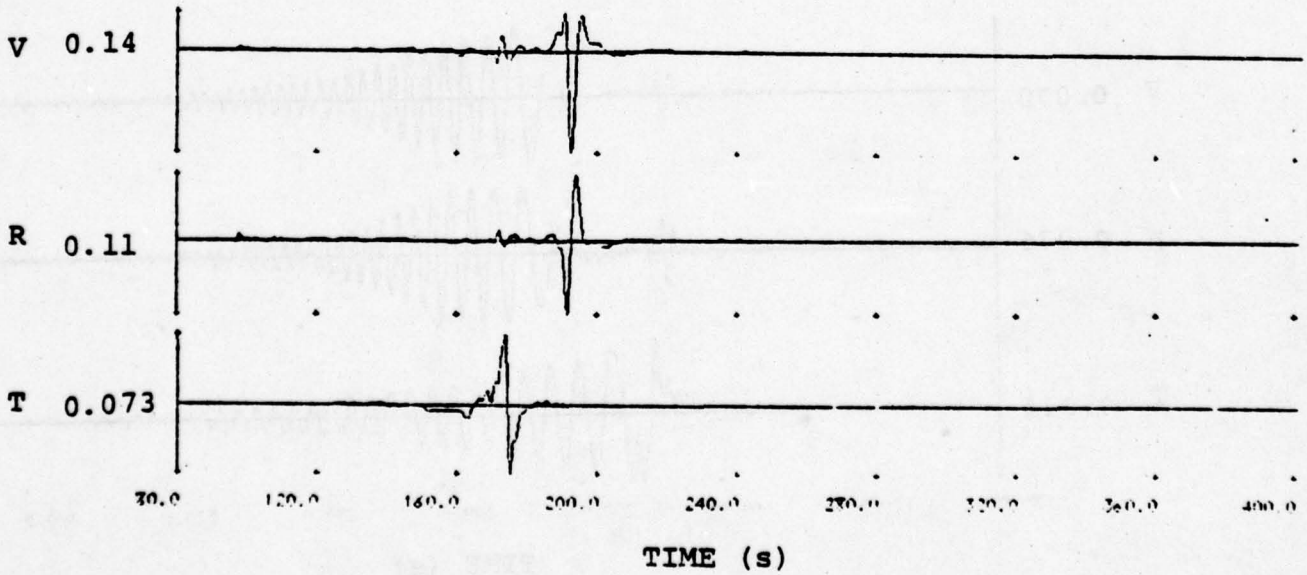

Figure A.5. Displacement seismograms at Wing V Site 1 from Yellowstone (Orientation 1) earthquake using Structure B path model.

STRUCTURE A, f_Q = 2 (high Q)

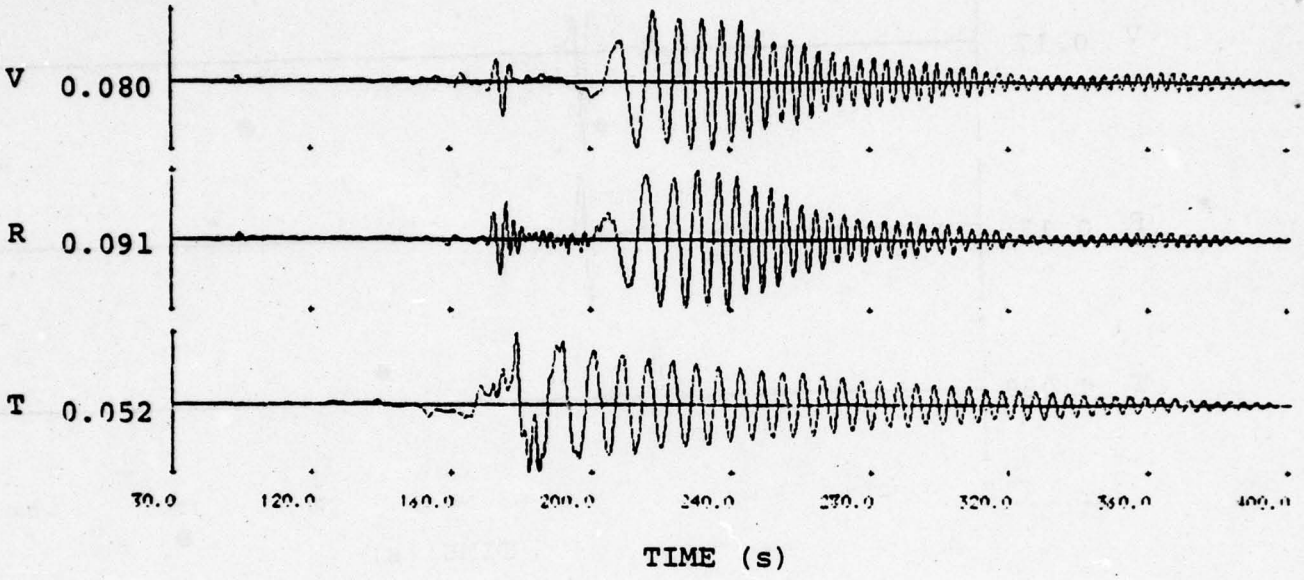

STRUCTURE A, f_Q = 1 (low Q)

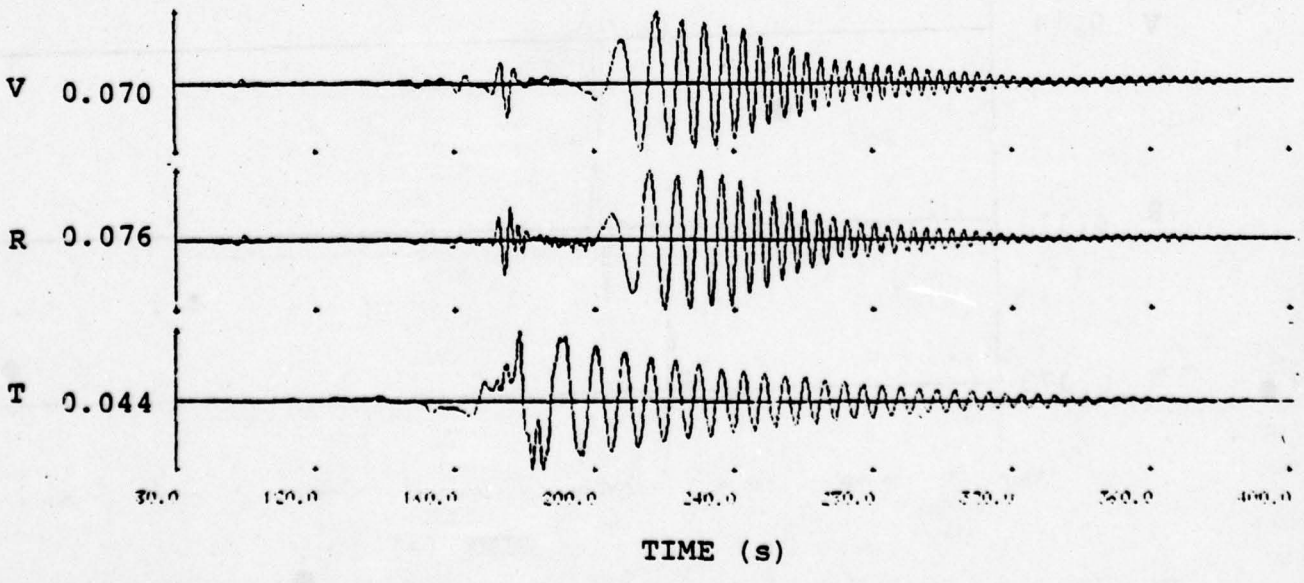

Figure A.6. Displacement seismograms at Wing V Site 1 from Yellowstone (Orientation 1) earthquake using Structure A path model.

STRUCTURE A, f_Q = 0.53 (low Q with Q/10 in caldera)

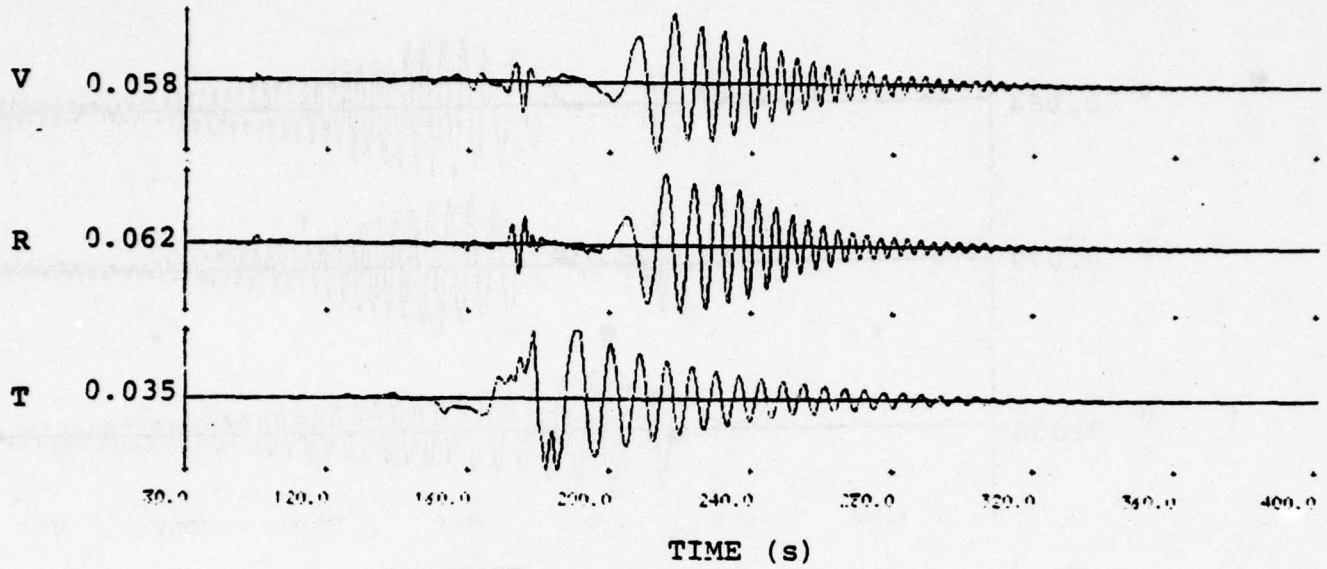

STRUCTURE A, f_Q = 0.34 (low Q with Q/20 in caldera)

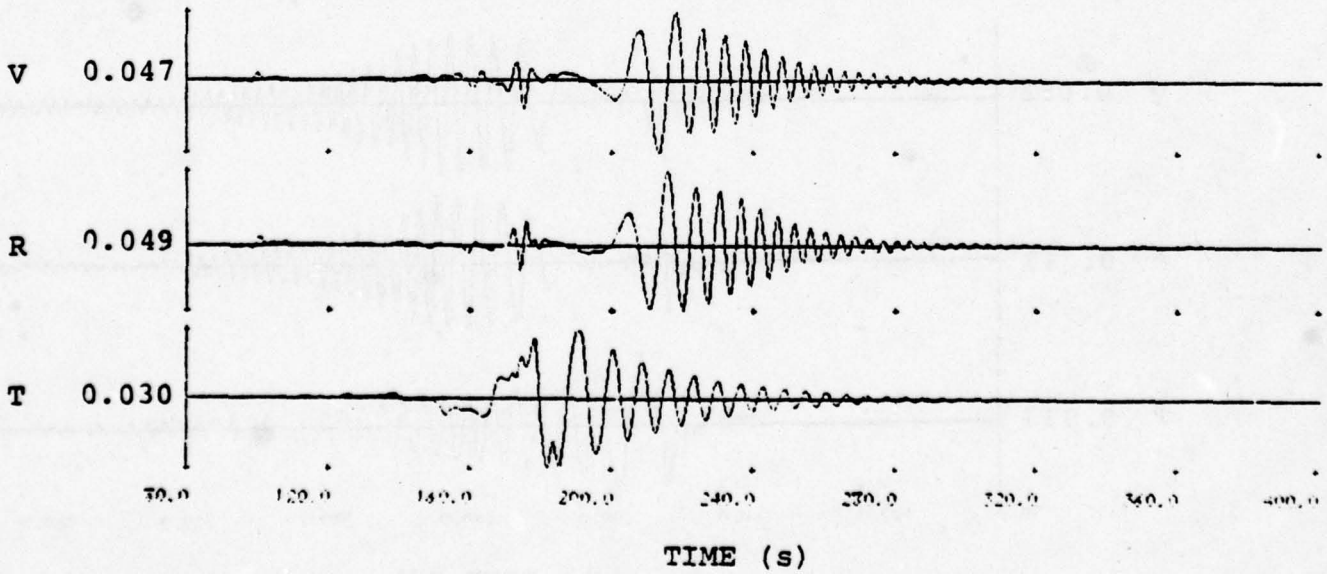

Figure A.7. Displacement seismograms at Wing V Site 1 from Yellowstone (Orientation 1) earthquake using Structure A path model with low Q calderas.

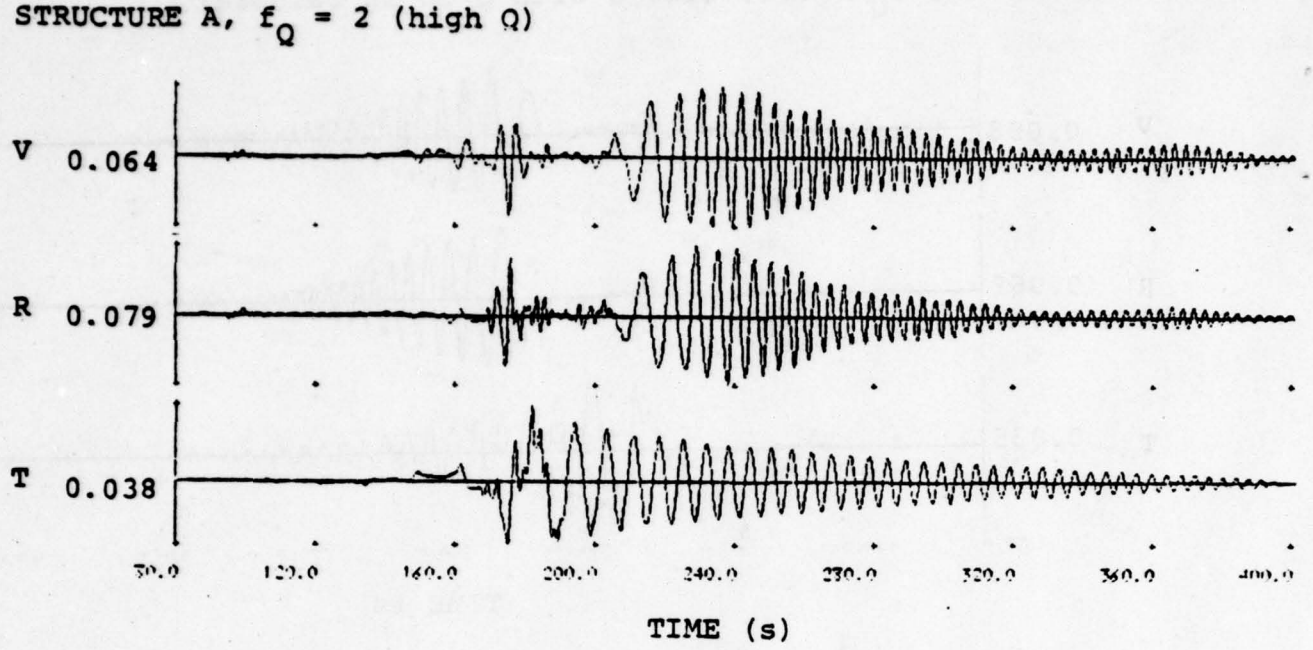

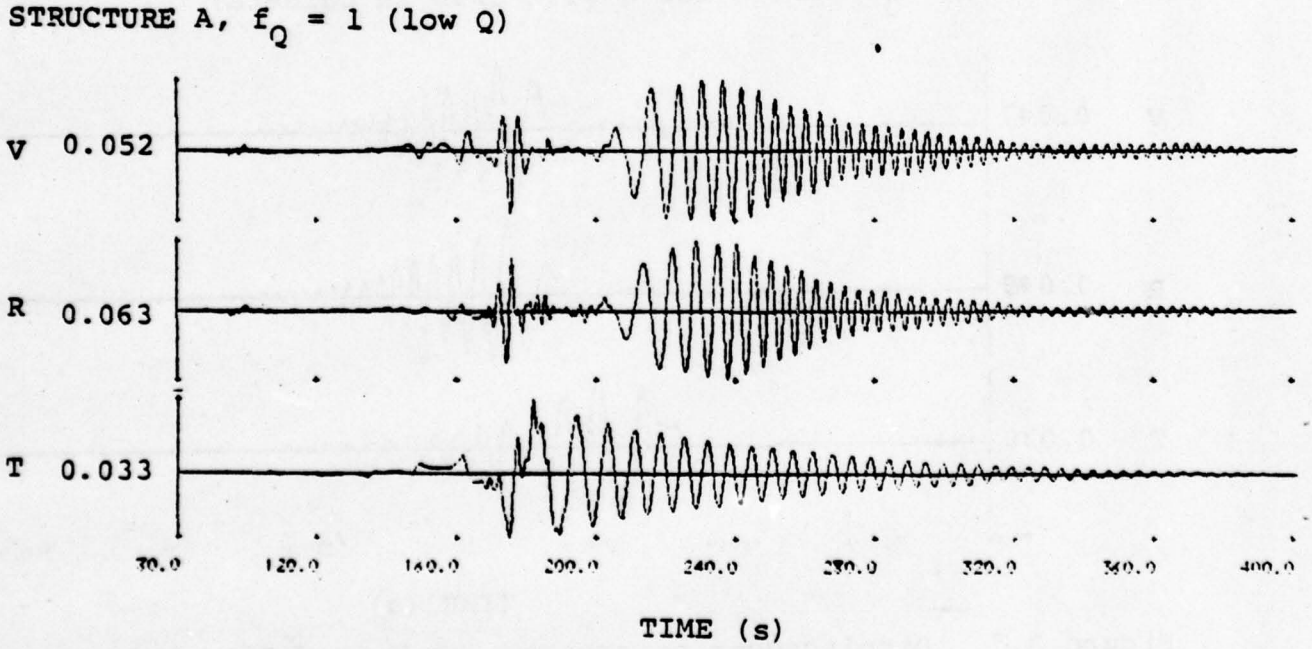

Figure A.8. Displacement seismograms at Wing V Site 1 from Yellowstone (Orientation 2) earthquake using Structure A path model.

STRUCTURE B, f_Q = 2 (high Q)

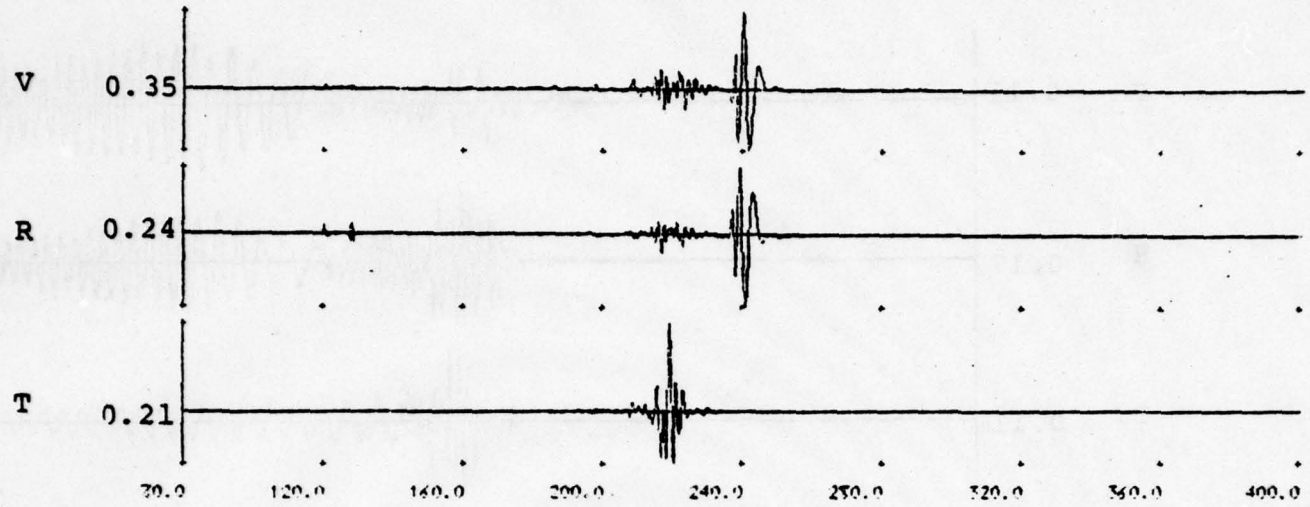

STRUCTURE B, f_Q = 1 (low Q)

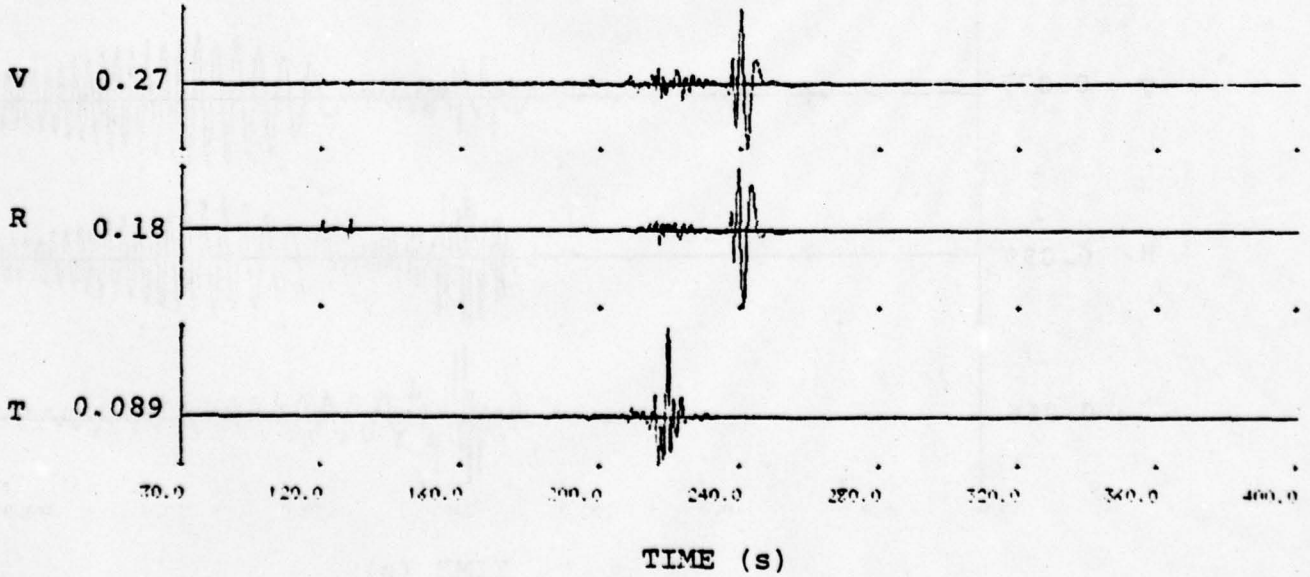

Figure A.9. Velocity seismograms at Wing V Site 2 from Pocatello earthquake using Structure B path model.

STRUCTURE A, f_Q = 2 (high Q)

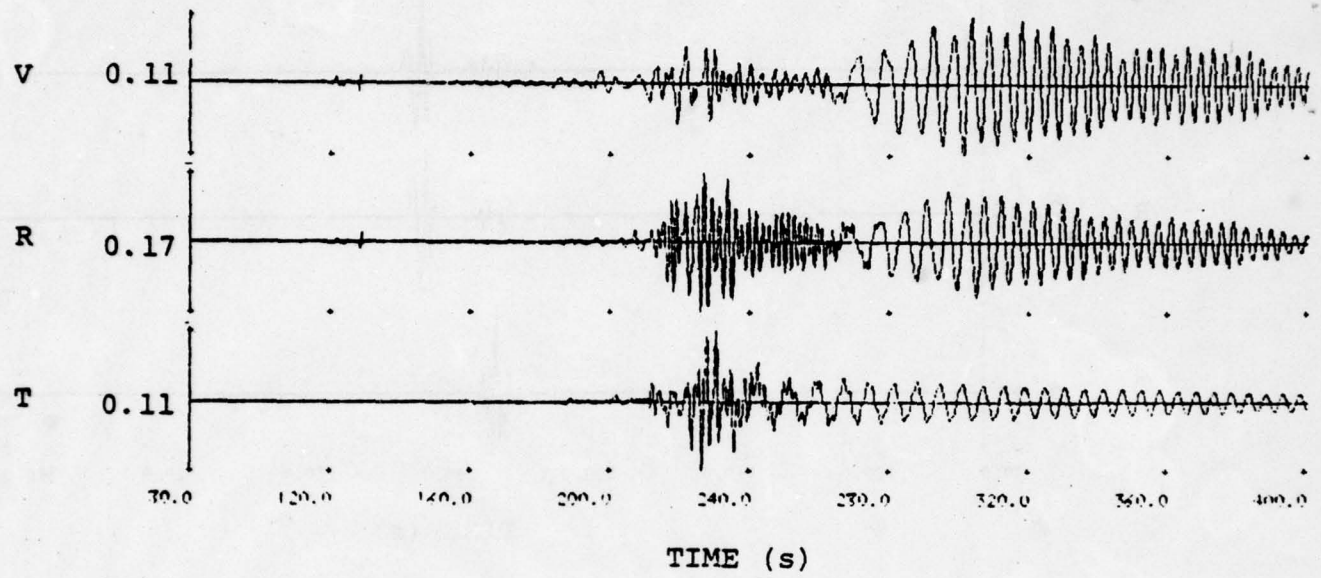

STRUCTURE A, f_Q = 1 (low Q)

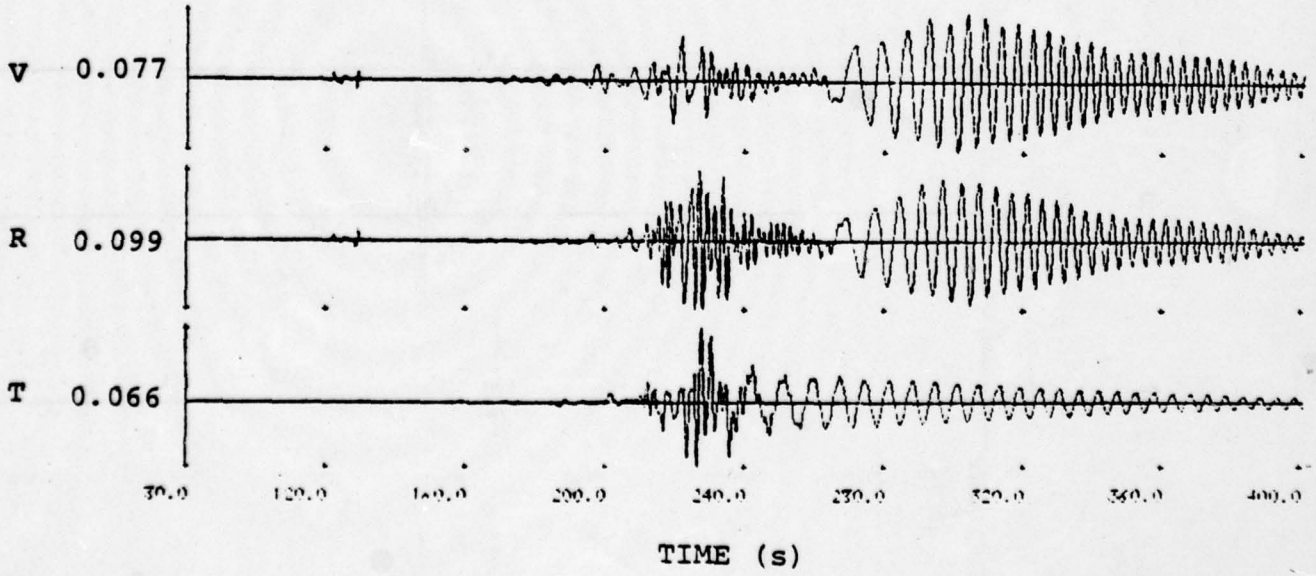

Figure A.10. Velocity seismograms at Wing V Site 2 from Pocatello earthquake using Structure A path model.

STRUCTURE B, f_Q = 2 (high Q)

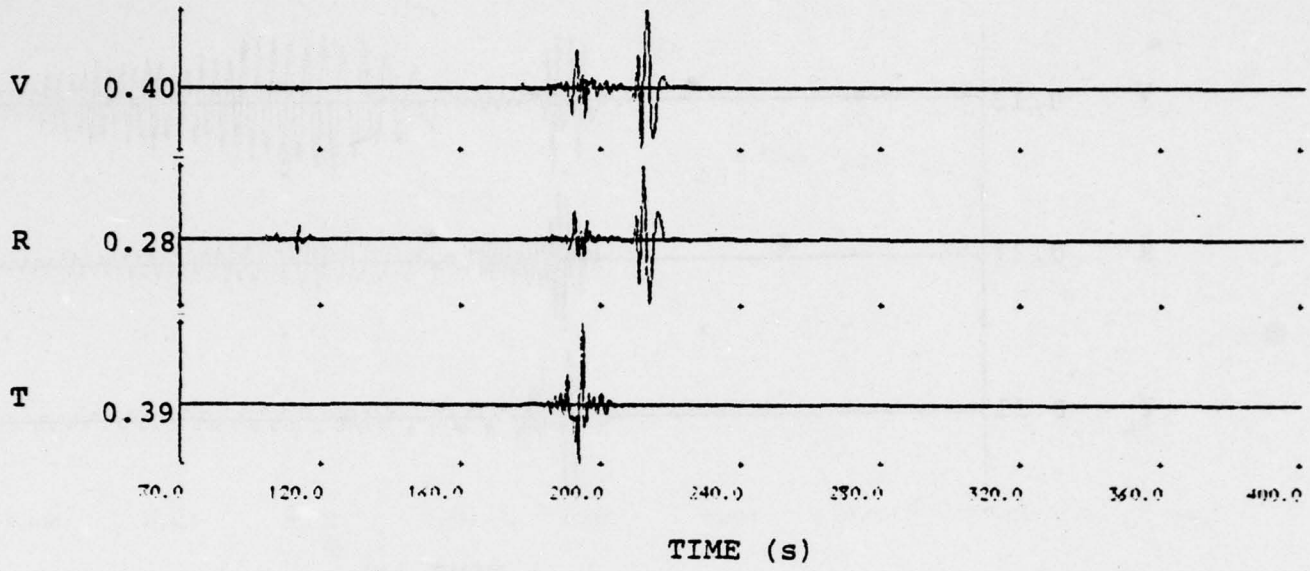

STRUCTURE B, f_Q = 1 (low Q)

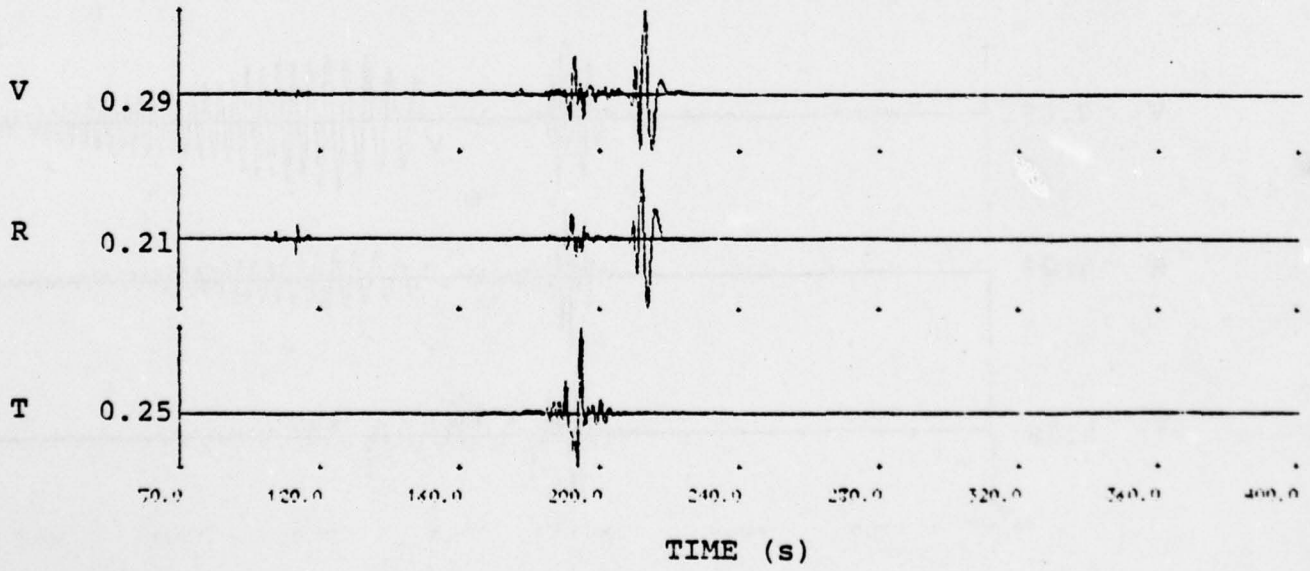

Figure A.11. Velocity seismograms at Wing V Site 1 from Pocatello earthquake using Structure B path model.

STRUCTURE A, f_Q = 2 (high Q)

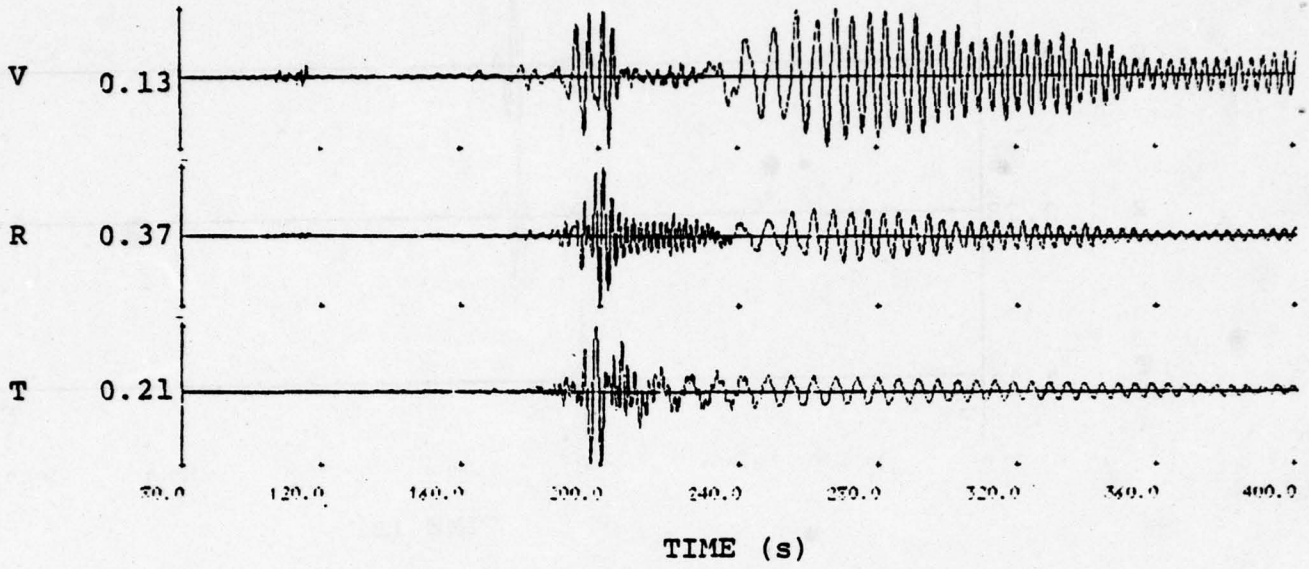

STRUCTURE A, f_Q = 1 (low Q)

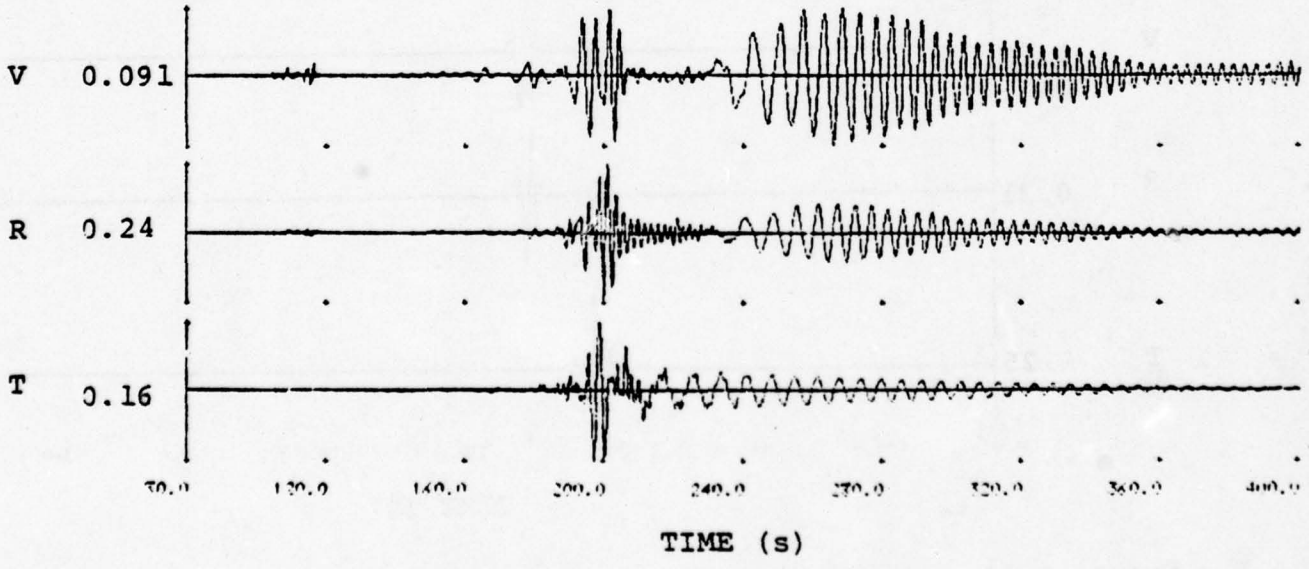

Figure A.12. Velocity seismograms at Wing V Site 1 from Pocatello earthquake using Structure A path model.

STRUCTURE B, f_Q = 2 (high Q)

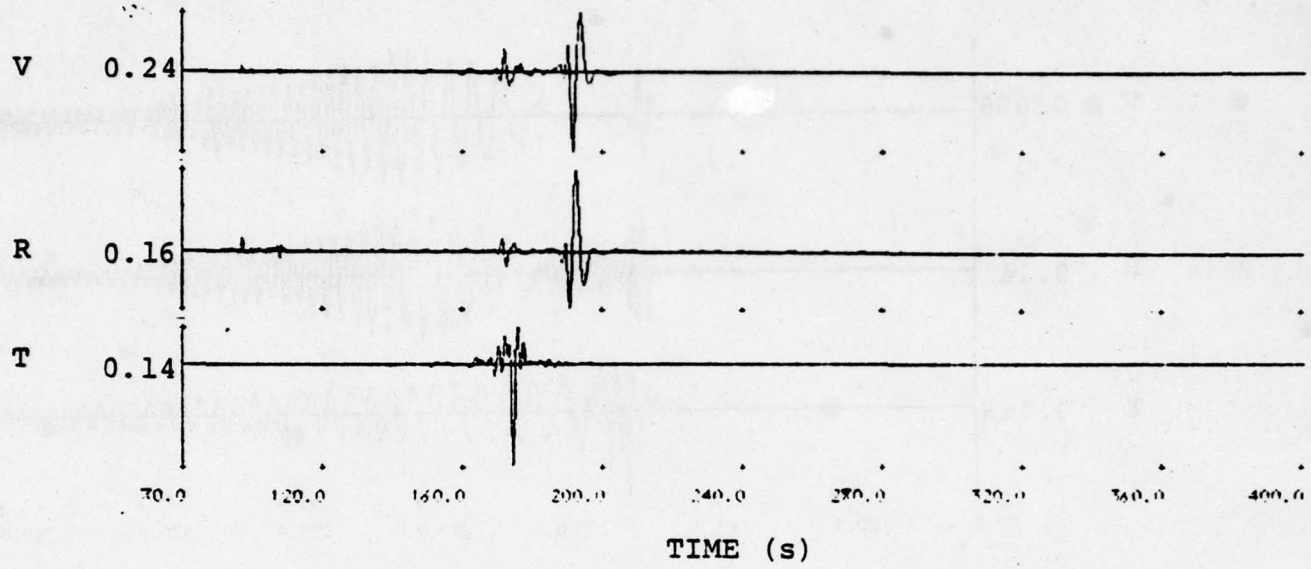

STRUCTURE B, f_Q = 1 (low Q)

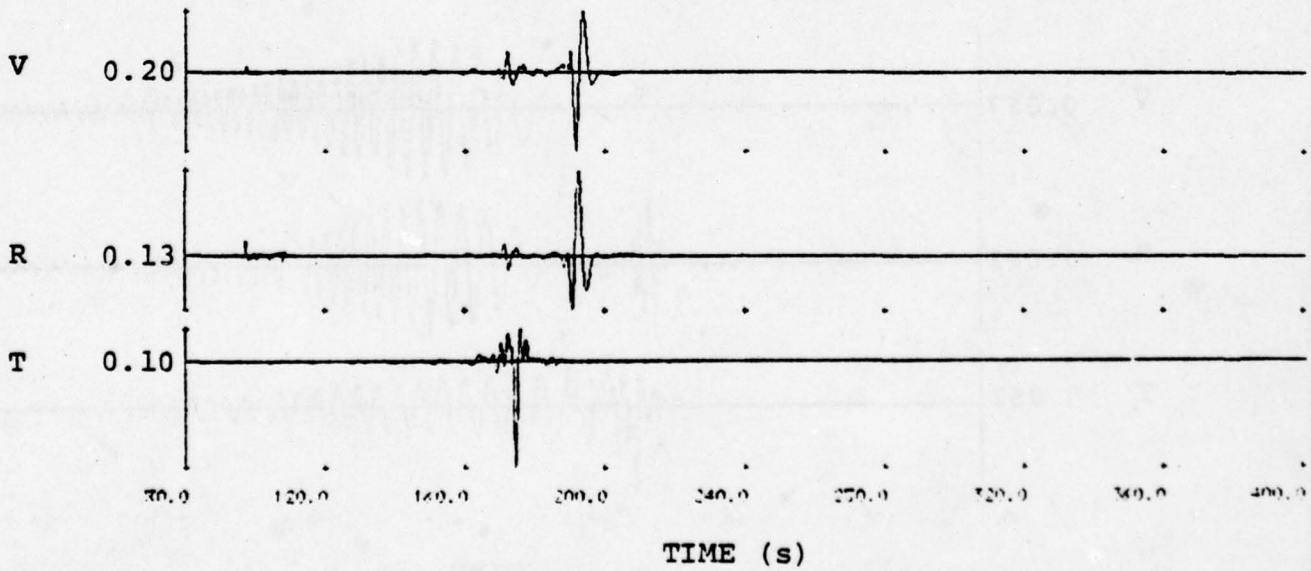

Figure A.13. Velocity seismograms at Wing V Site 1 from Yellowstone (Orientation 1) earthquake using Structure B path model.

STRUCTURE A, f_Q = 2 (high Q)

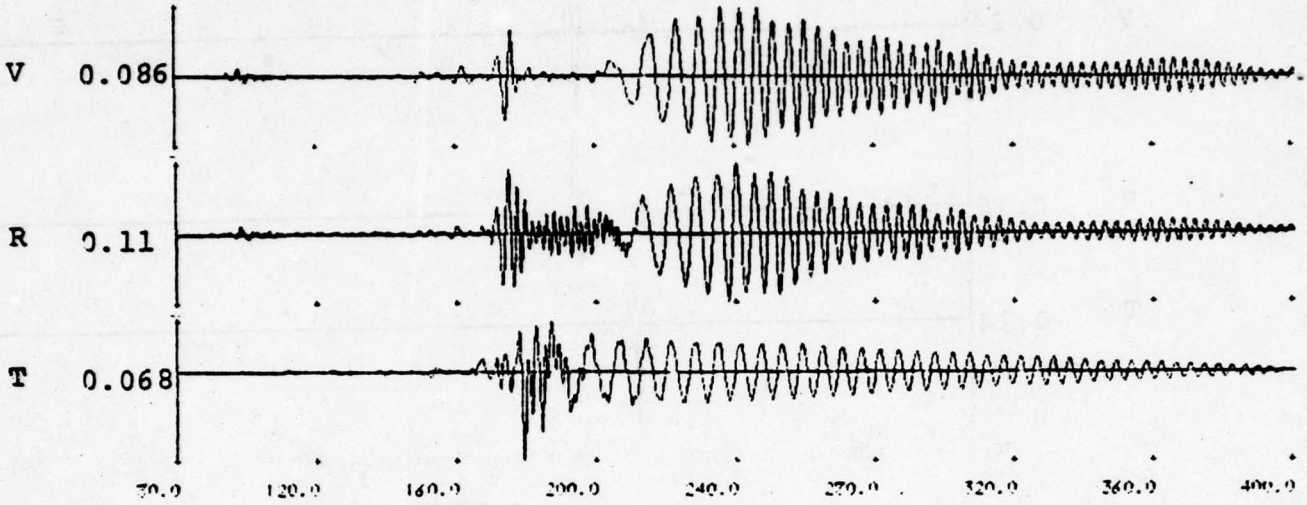

STRUCTURE A, f_Q = 1 (low Q)

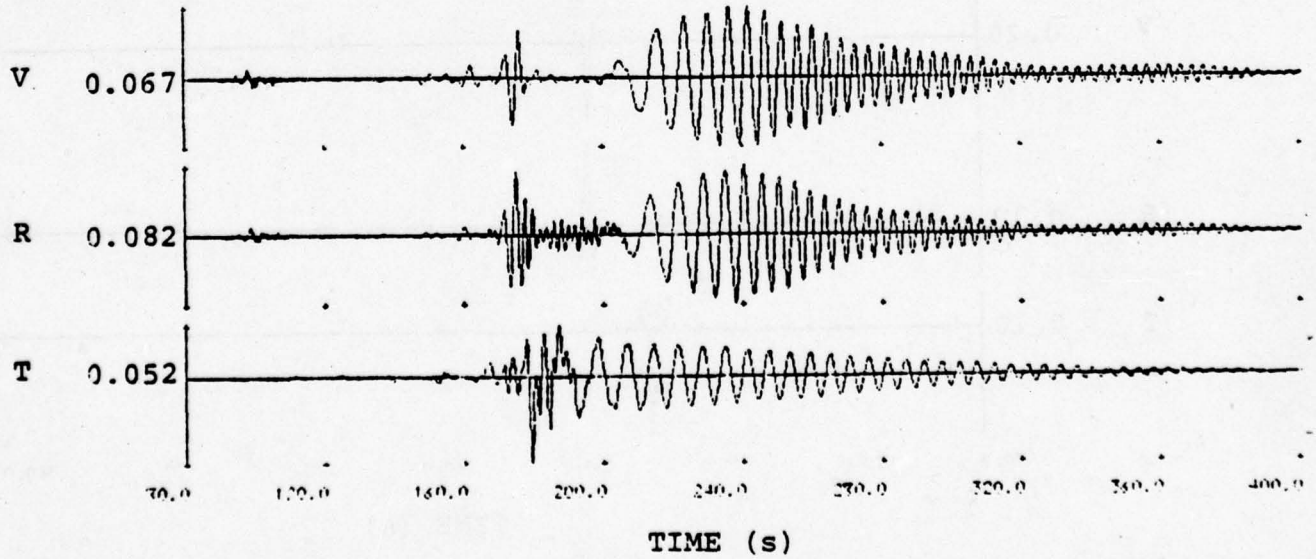

Figure A.14. Velocity seismograms at Wing V Site 1 from Yellowstone (Orientation 1) earthquake using Structure A path model.

STRUCTURE A, f_Q = 0.53 (low Q with A/10 in caldera)

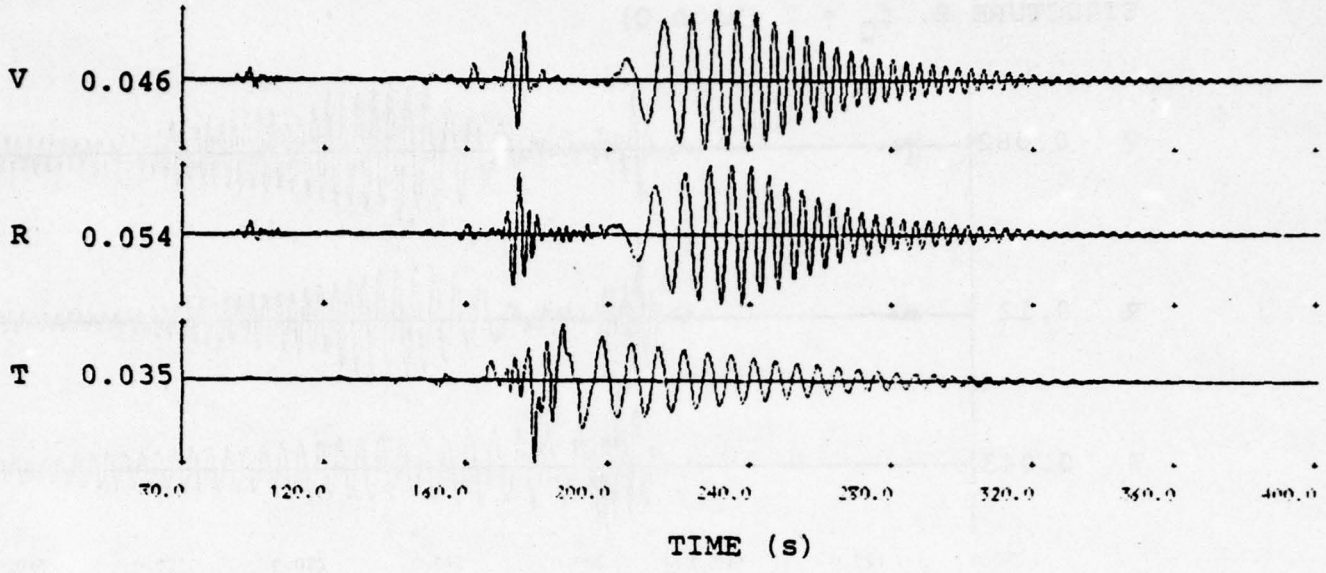

STRUCTURE A, f_Q = 0.34 (low Q with Q/20 in caldera)

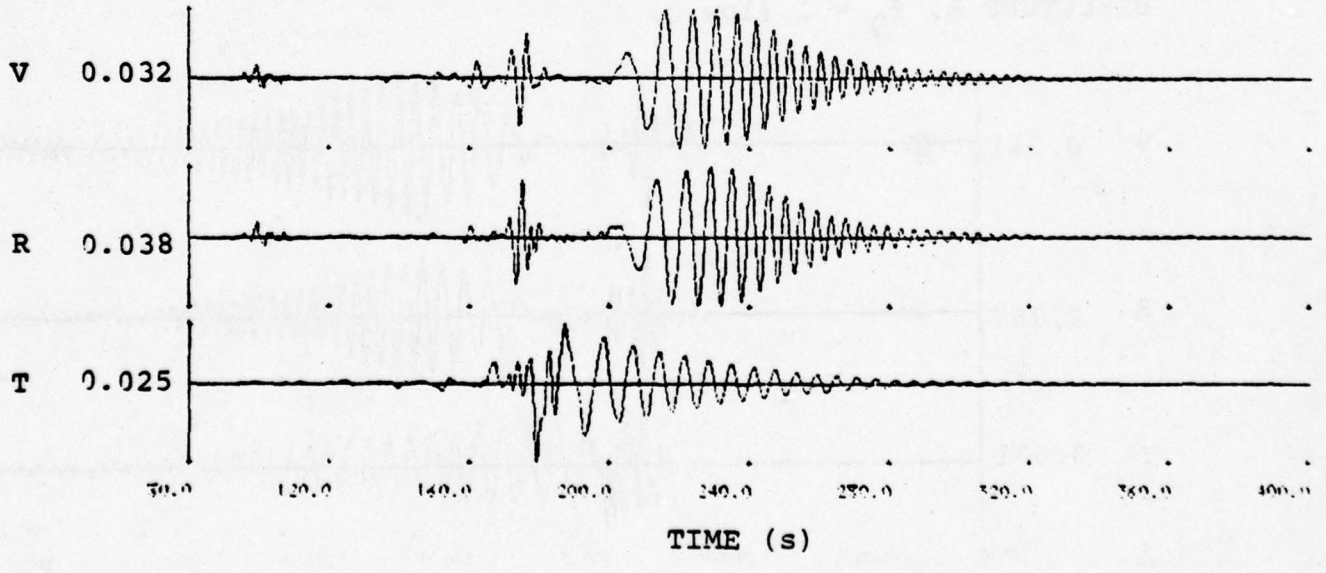

Figure A.15. Velocity seismograms at Wing V Site 1 from Yellowstone (Orientation 1) earthquake using Structure A path model with low Q calderas.

STRUCTURE B, f_Q = 2 (high Q)

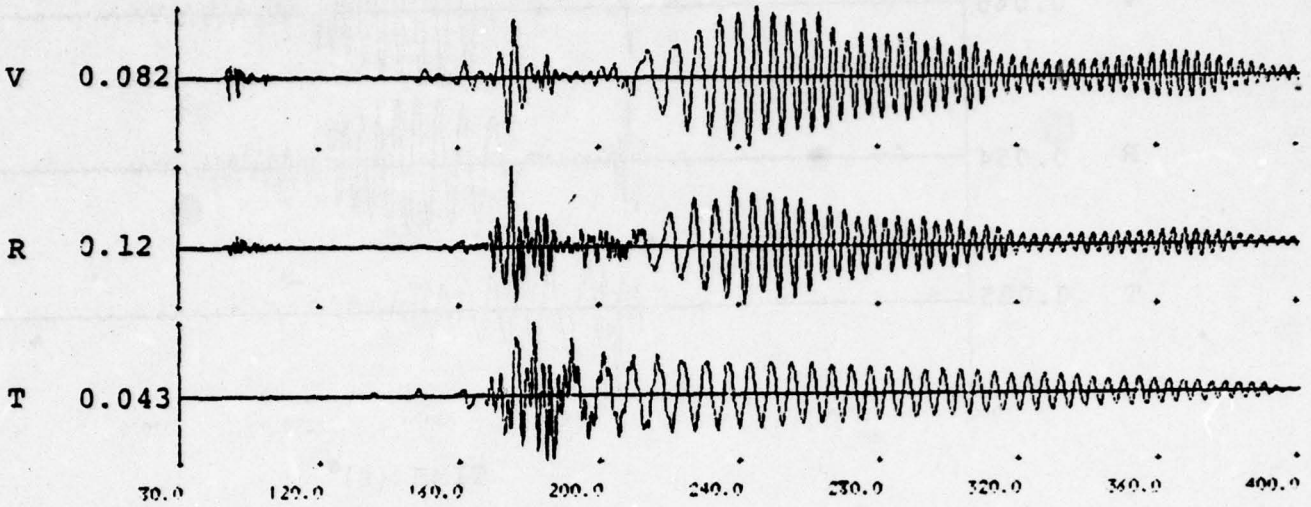

STRUCTURE A, f_Q = 1 (low Q)

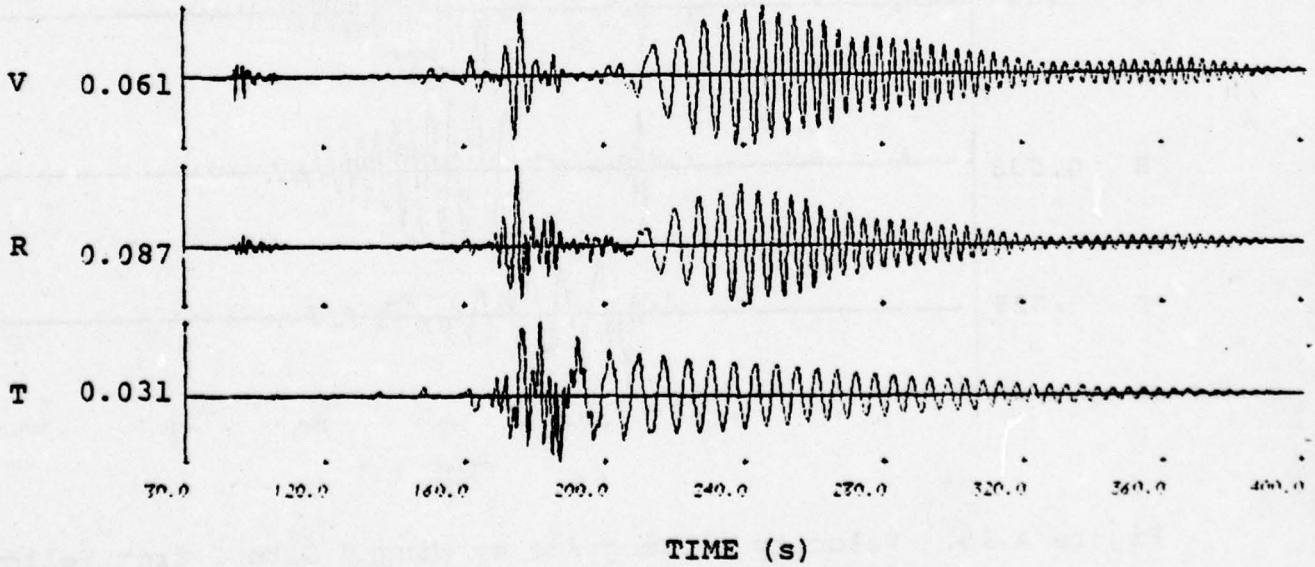

Figure A.16. Velocity seismograms at Wing V Site 1 from Yellowstone (Orientation 2) earthquake using Structure A path model.

STRUCTURE B, f_Q = 2 (high Q)

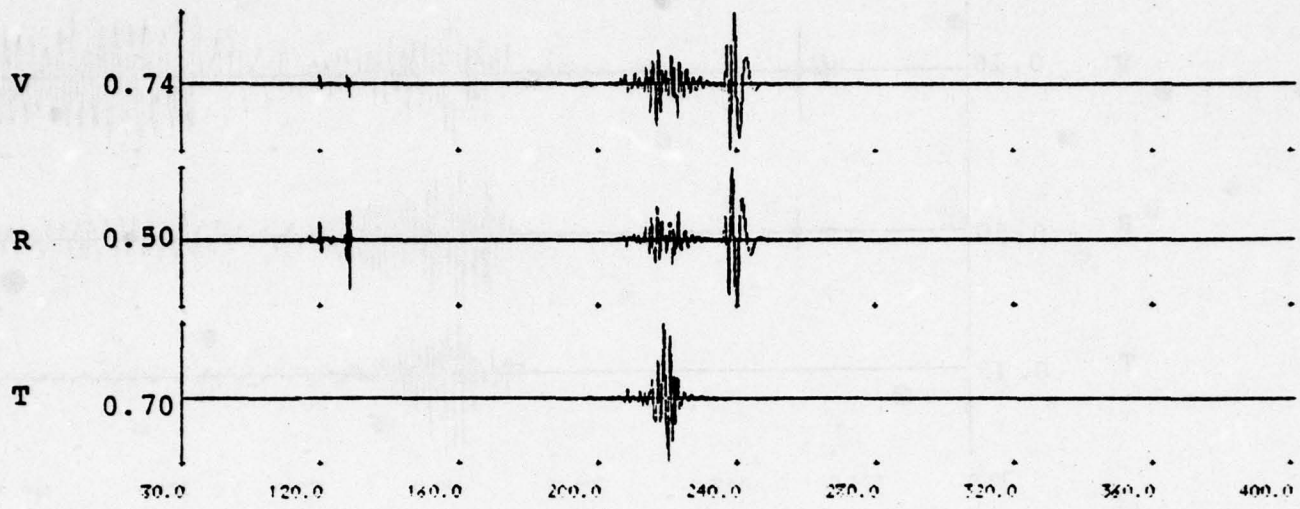

STRUCTURE B, f_Q = 1 (low Q)

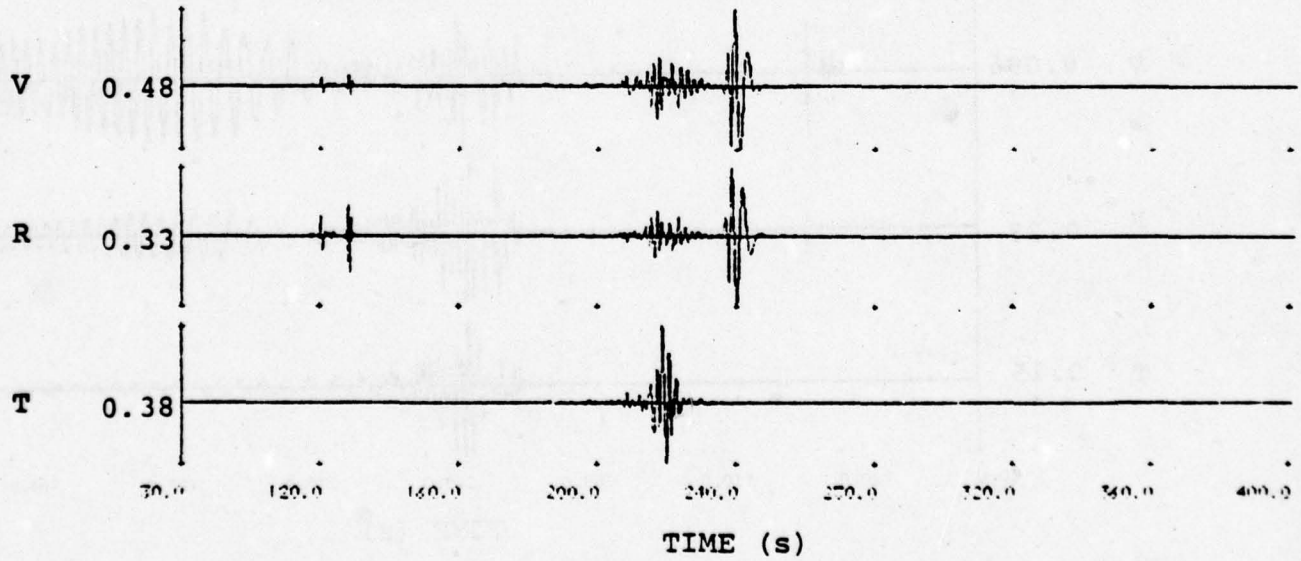

Figure A.17. Acceleration seismograms at Wing V Site 2 from Pocatello earthquake using Structure B path model.

STRUCTURE A, f_Q = 2 (high Q)

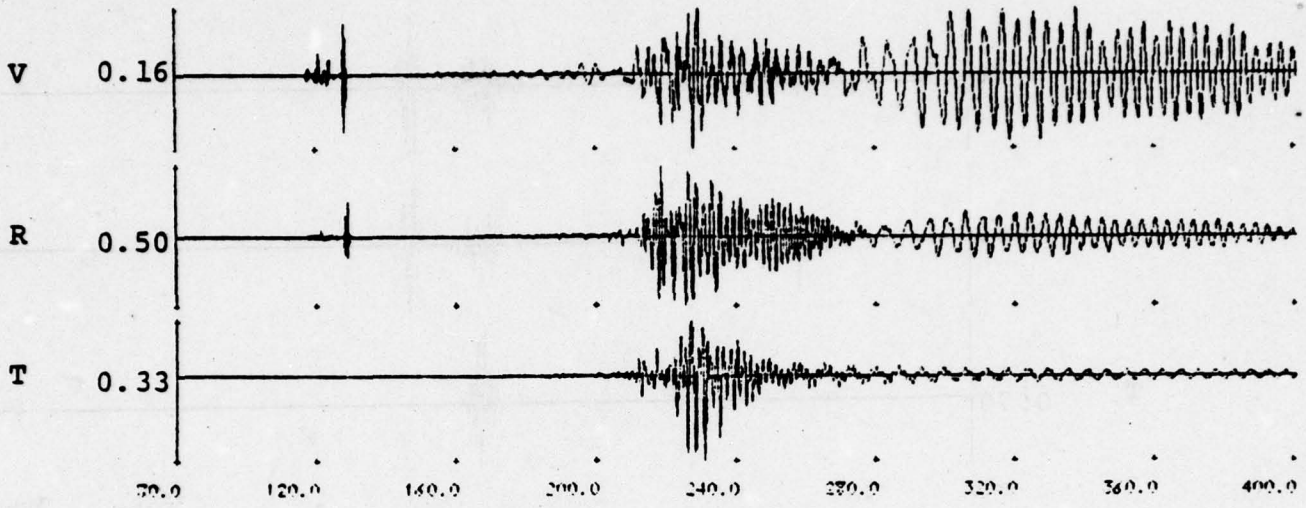

STRUCTURE A, f_Q = 1 (low Q)

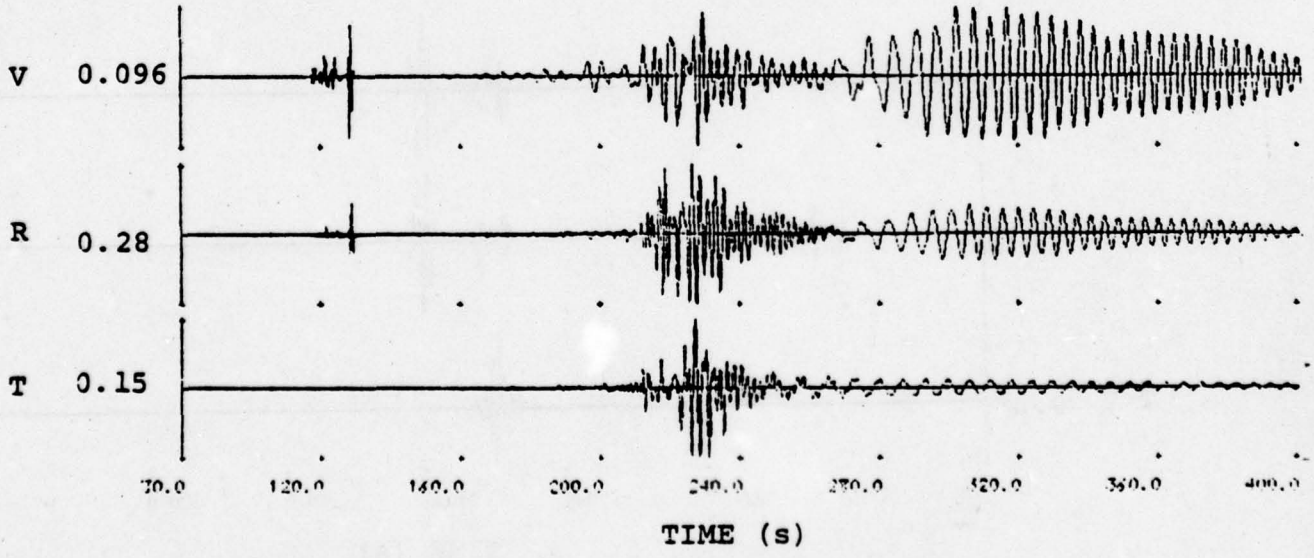

Figure A.18. Acceleration seismograms at Wing V Site 2 from Pocatello earthquake using Structure A path model.

STRUCTURE B, f_Q = 2 (high Q)

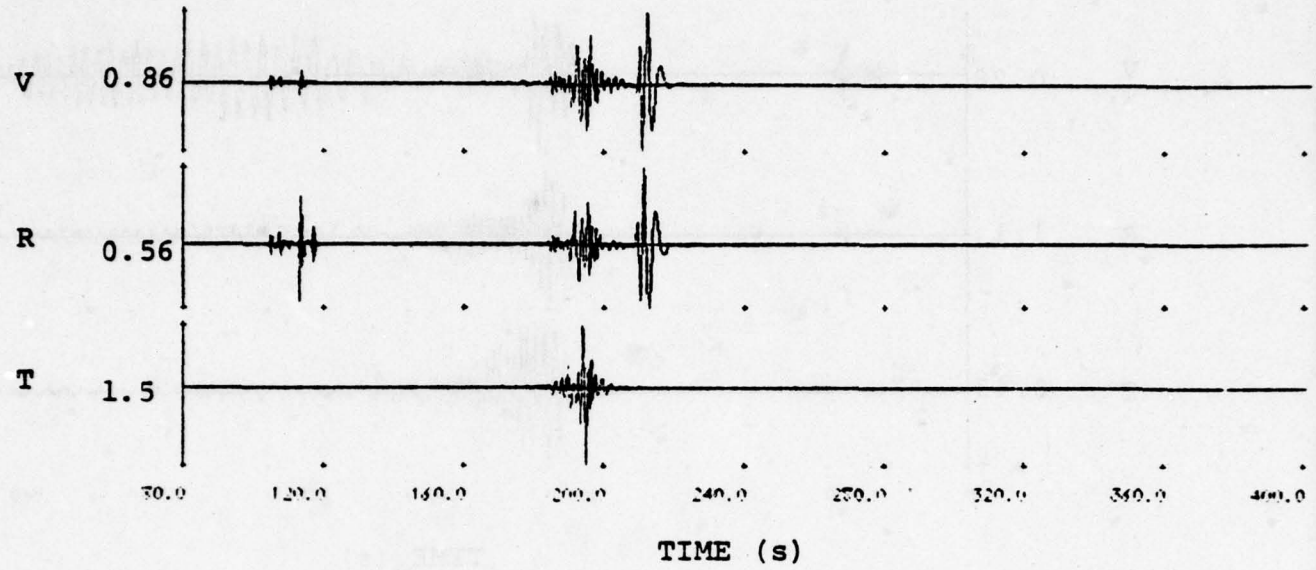

STRUCTURE B, f_Q = 1 (low Q)

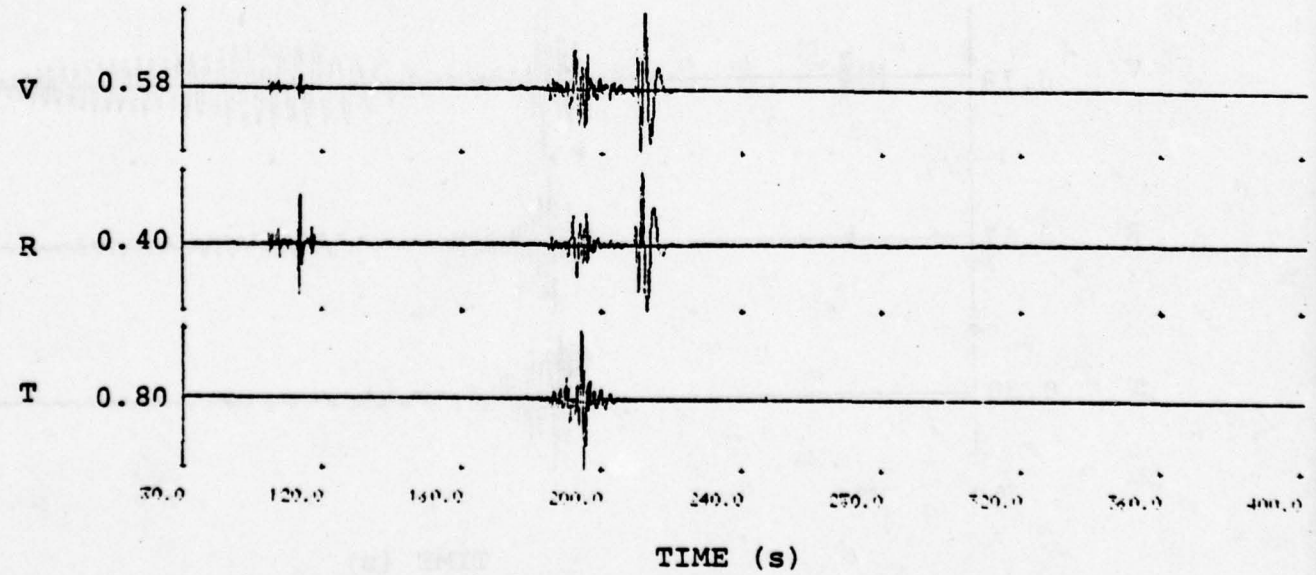

Figure A.19. Acceleration seismograms at Wing V Site 1 from Pocatello earthquake using Structure B path model.

STRUCTURE A, f_Q = 2 (high Q)

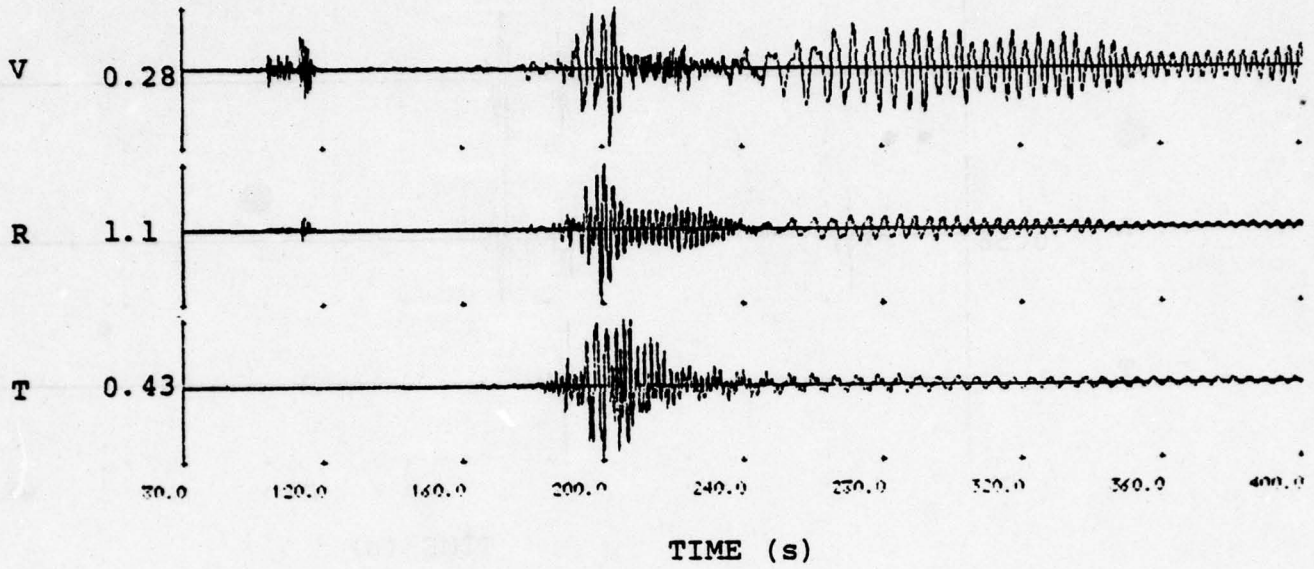

STRUCTURE A, f_Q = 1 (low Q)

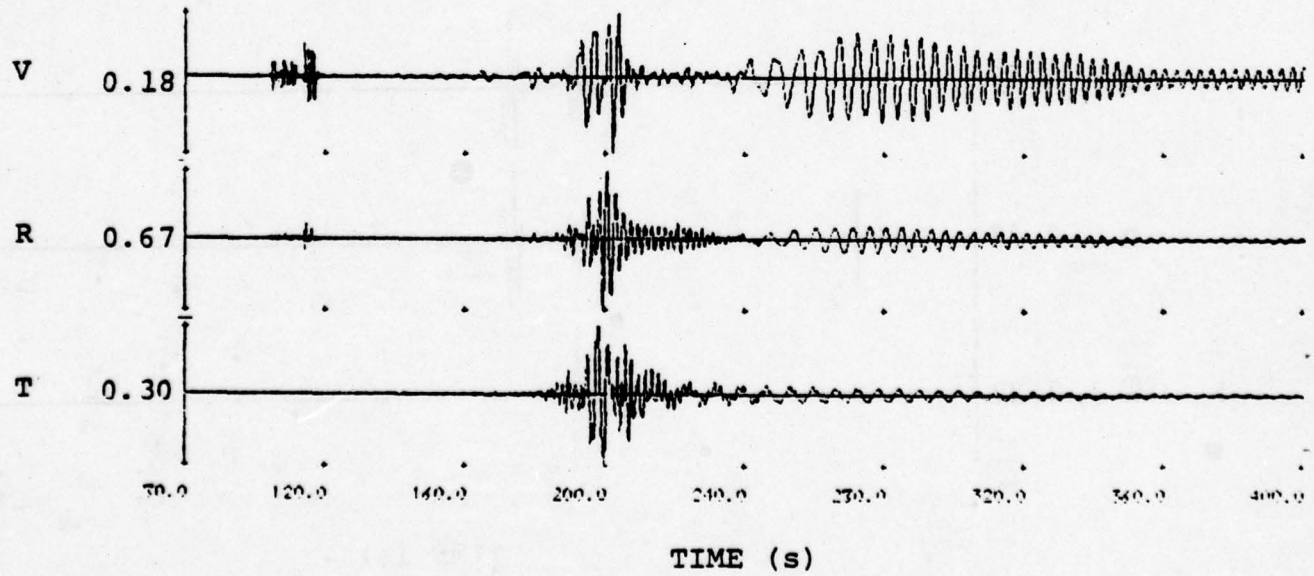

Figure A.20. Acceleration seismograms at Wing V Site 1 from Pocatello earthquake using Structure A path model.

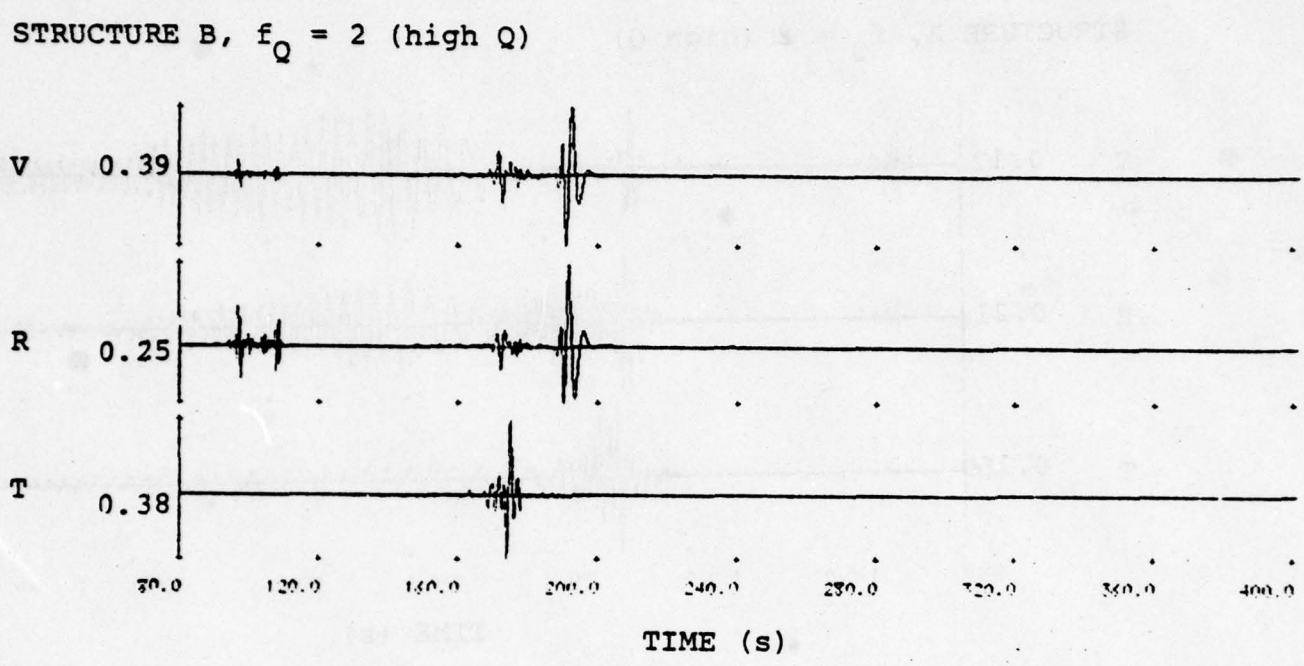

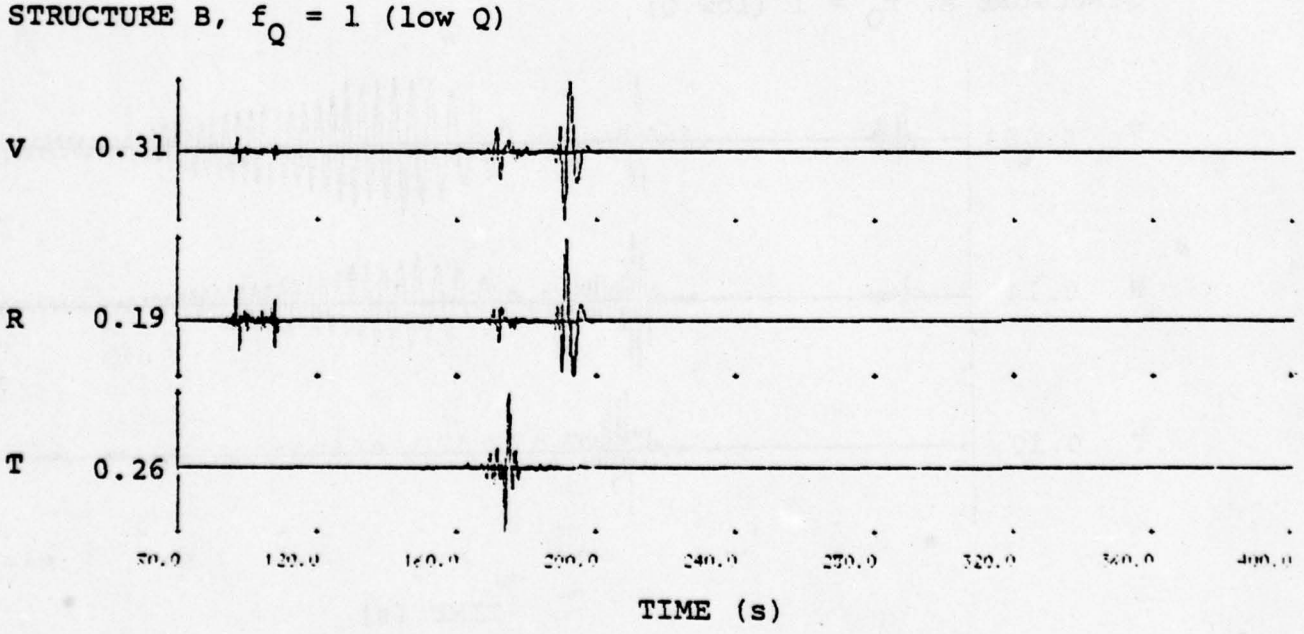

Figure A.21. Acceleration seismograms at Wing V Site 1 from Yellowstone (Orientation 1) earthquake using Structure B path model.

STRUCTURE A, f_Q = 2 (high Q)

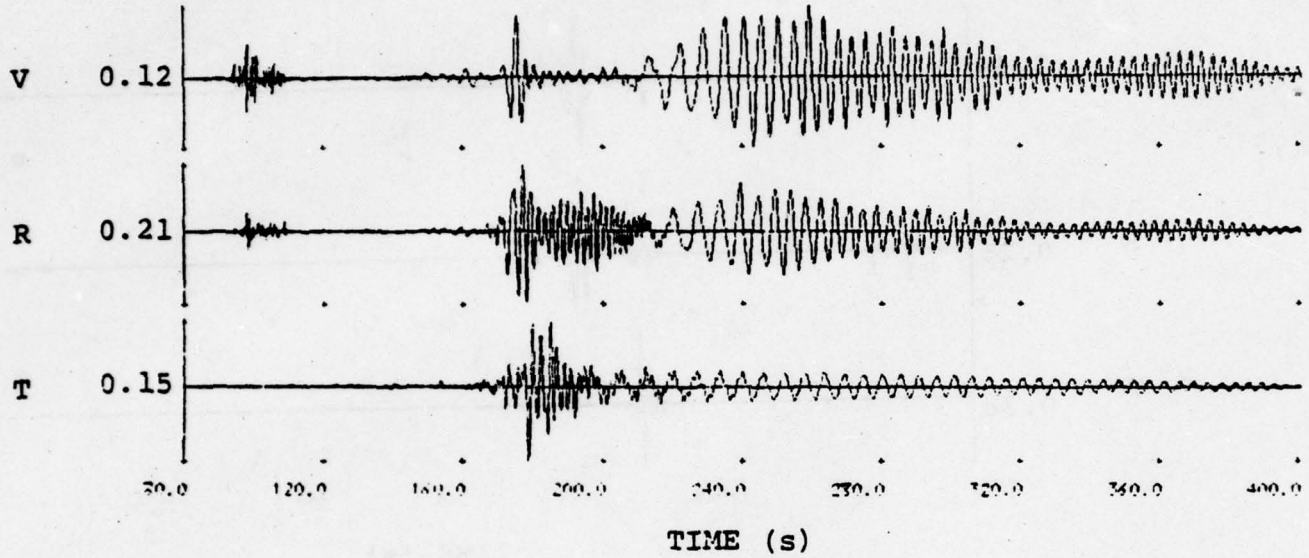

STRUCTURE A, f_Q = 1 (low Q)

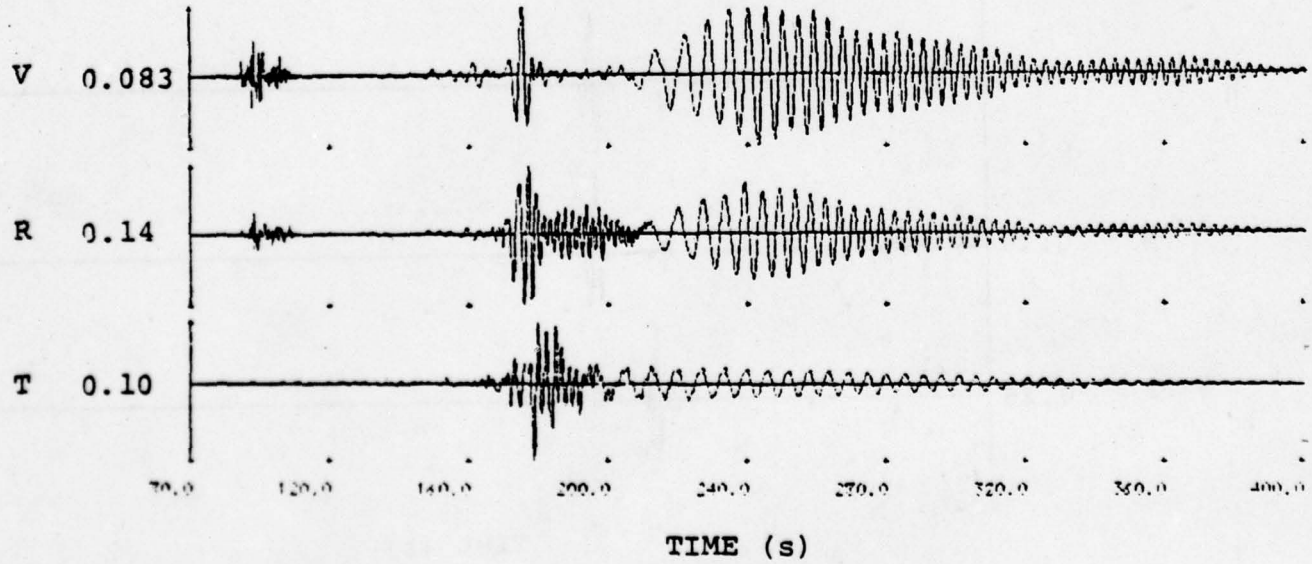

Figure A.22. Acceleration seismograms at Wing V Site 1 from Yellowstone (Orientation 1) earthquake using Structure A path model.

STRUCTURE A, f_Q = 0.53 (low Q with Q/10 in caldera)

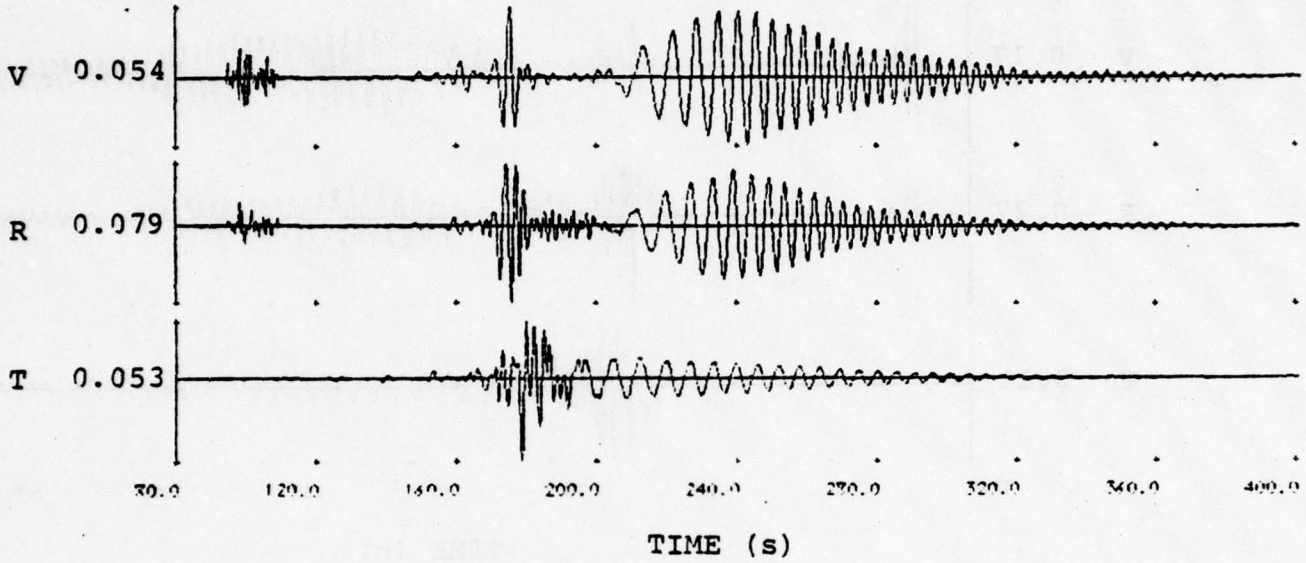

STRUCTURE A, f_Q = 0.34 (low Q with Q/20 in caldera)

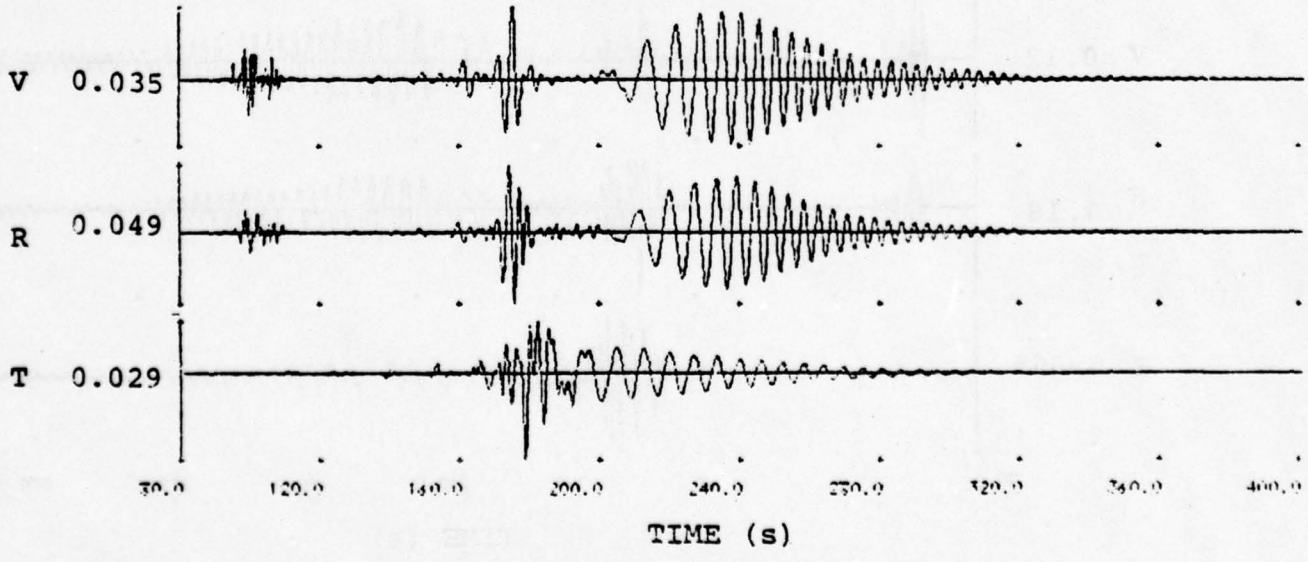

Figure A.23. Acceleration seismograms at Wing V Site 1 from Yellowstone (Orientation 1) earthquake using Structure A path model with low Q calderas.

STRUCTURE A, f_Q = 2 (high Q)

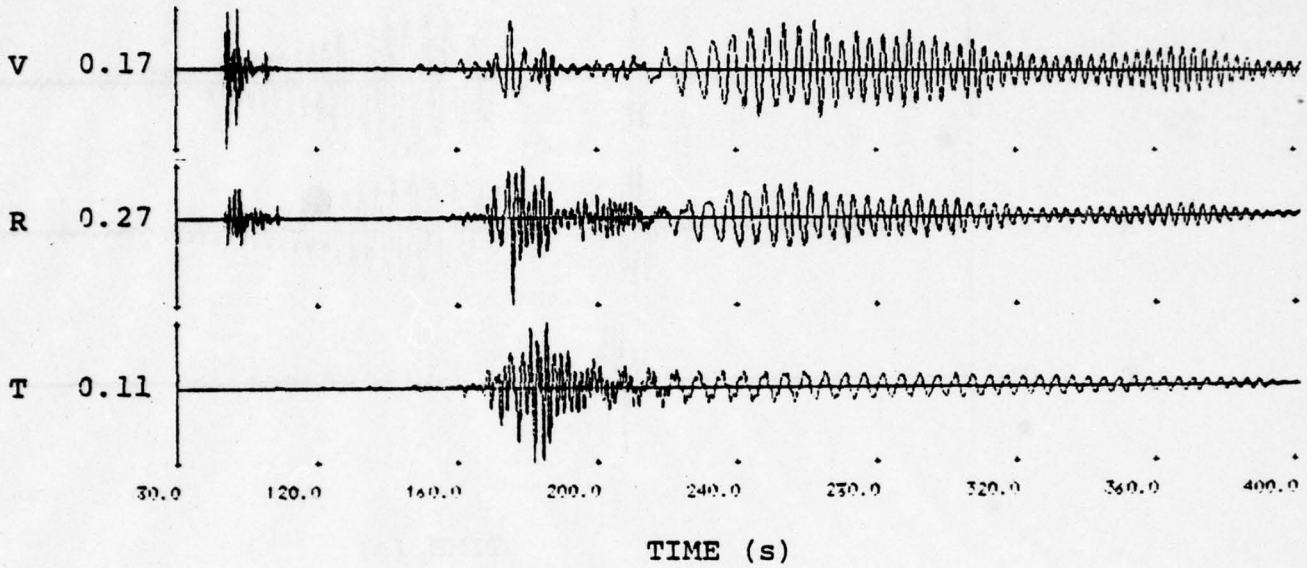

STRUCTURE A, f_Q = 1 (low Q)

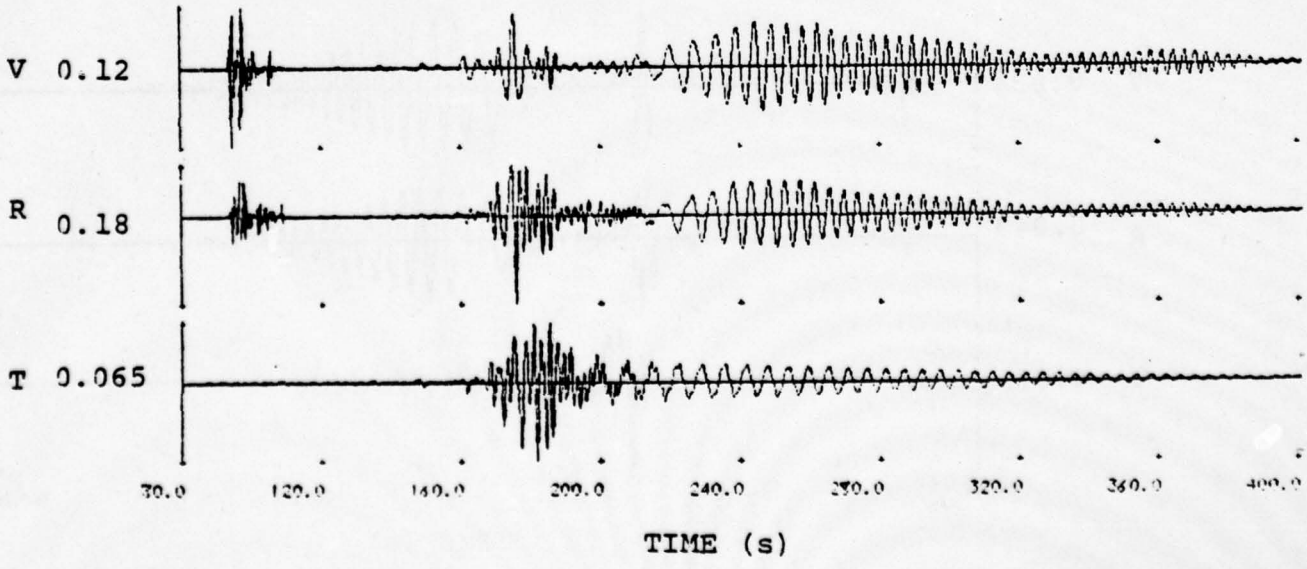

Figure A.24. Acceleration seismograms at Wing V Site 1 from Yellowstone (Orientation 2) earthquake using Structure A path model.

APPENDIX B

SYNTHETIC SEISMOGRAMS FOR EPICENTRAL DISTANCES OF 150 AND 250 KM

The figures in this appendix show the synthetic seismograms at distances of 150 and 250 km, discussed in Section V. Figures B.1 through B.6 are the three-component displacement seismograms, B.7 through B.12 the corresponding velocity seismograms, and B.13 through B.18 the acceleration seismograms. The ordering of the figures is as follows:

Figure Numbers	Source Model	Source Depth	Path Model	Azimuth (Clockwise from North)
B.1, 7, 13	Pocatello	8.7	A	90°
2, 8, 14	Pocatello	8.7	A	216°
3, 9, 15	Pocatello	8.7	B	90°
4, 10, 16	Pocatello	8.7	C	90°
5, 11, 17	Magnitude 7	8.7	C	90°
6, 12, 18	Pocatello	5.0	C	90°

The Pocatello source model is described in Section 1.3 of this report. The path models Structure A and B are listed in Table 1 (Section 2.3) and Structure C is listed in Table 6 (Section 5.1). For all three structures, the Q factor f_Q was set to one.

The time scale for each plot is seconds after event origin time. The number to the left of the vertical axis is the height of the vertical axis in units of either cm, cm/sec or cm/sec^2.

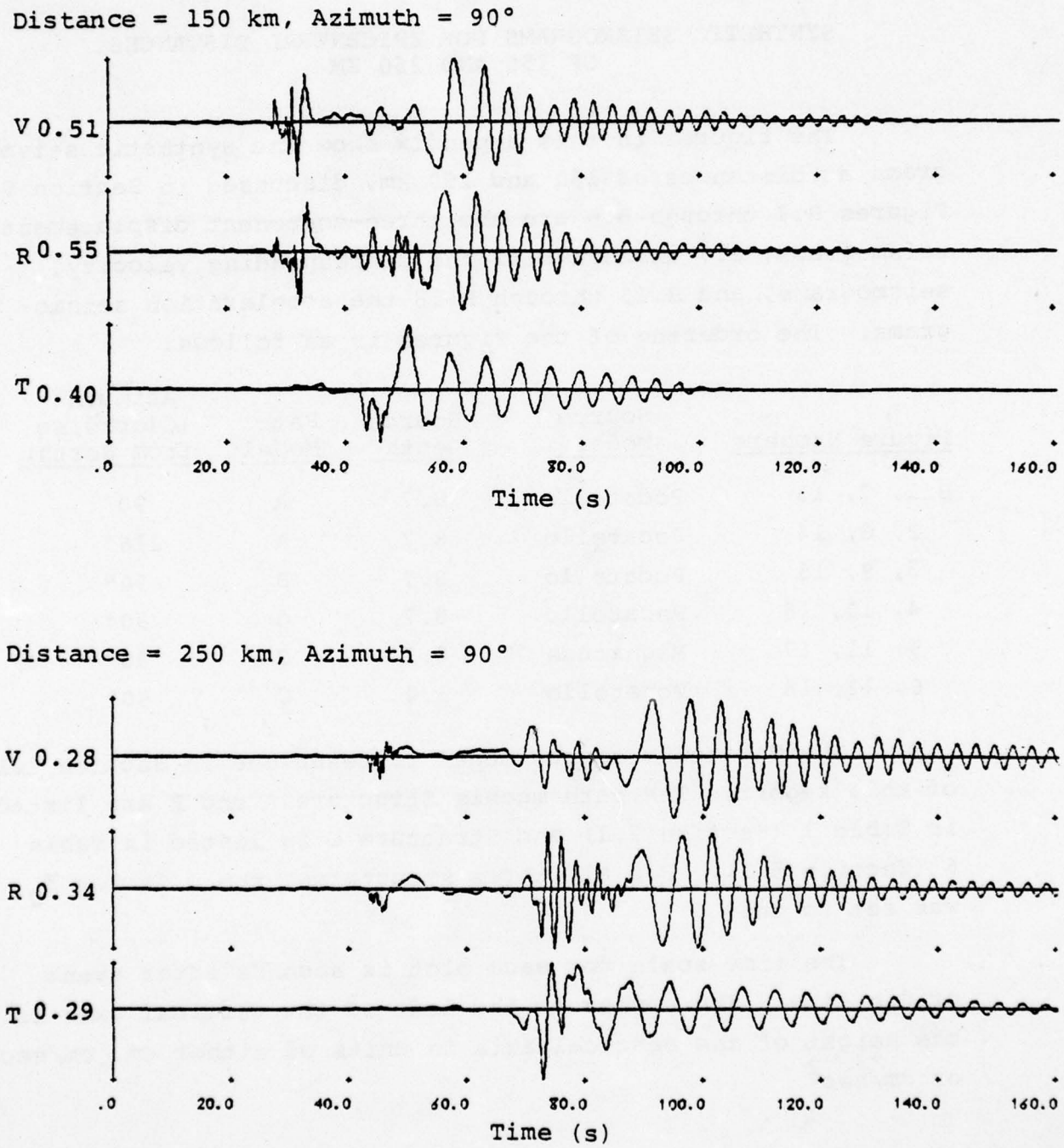

Figure B.1. Displacement seismograms from Pocatello source model and Structure A path model.

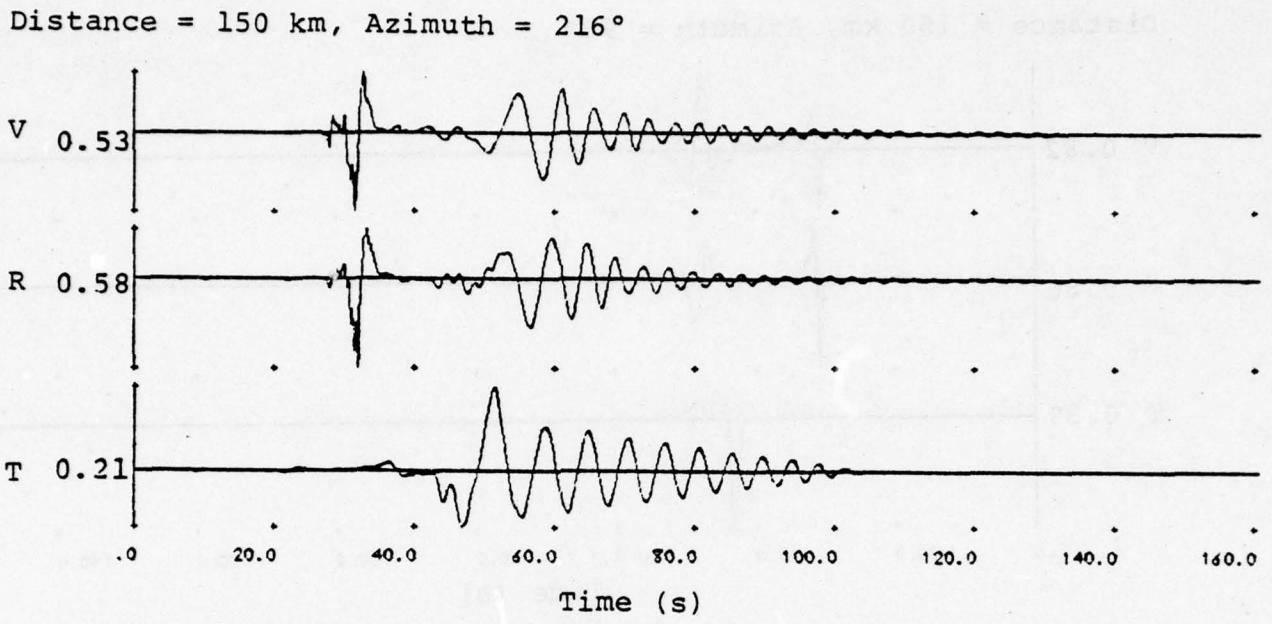

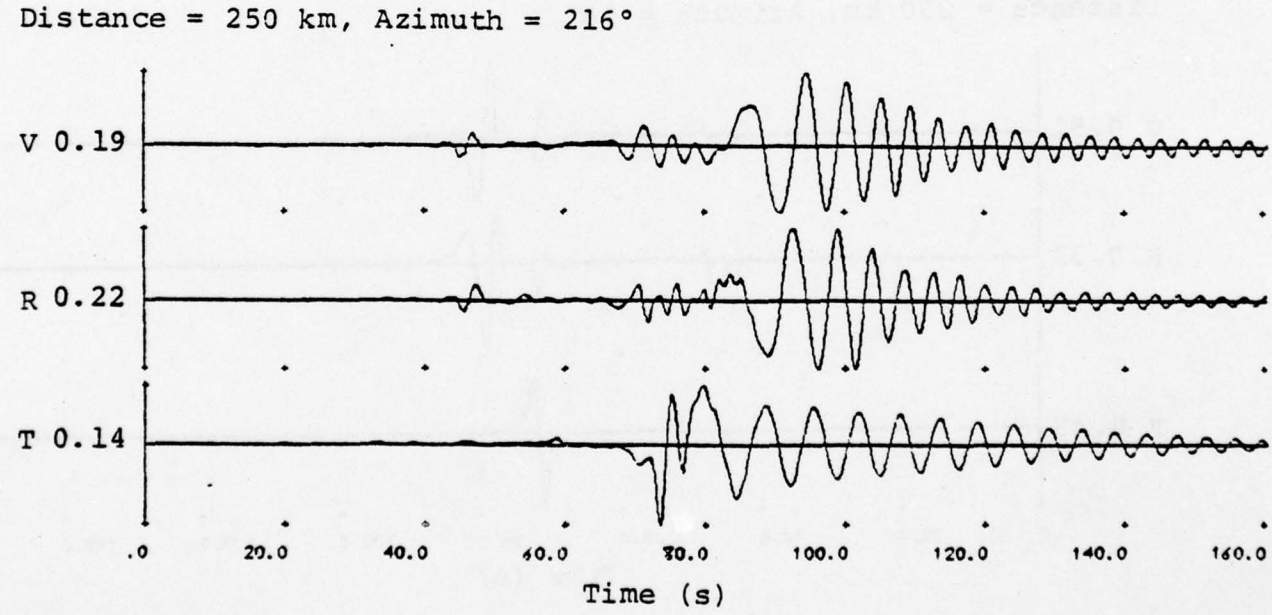

Figure B.2. Displacement seismograms from Pocatello source model and Structure A path model.

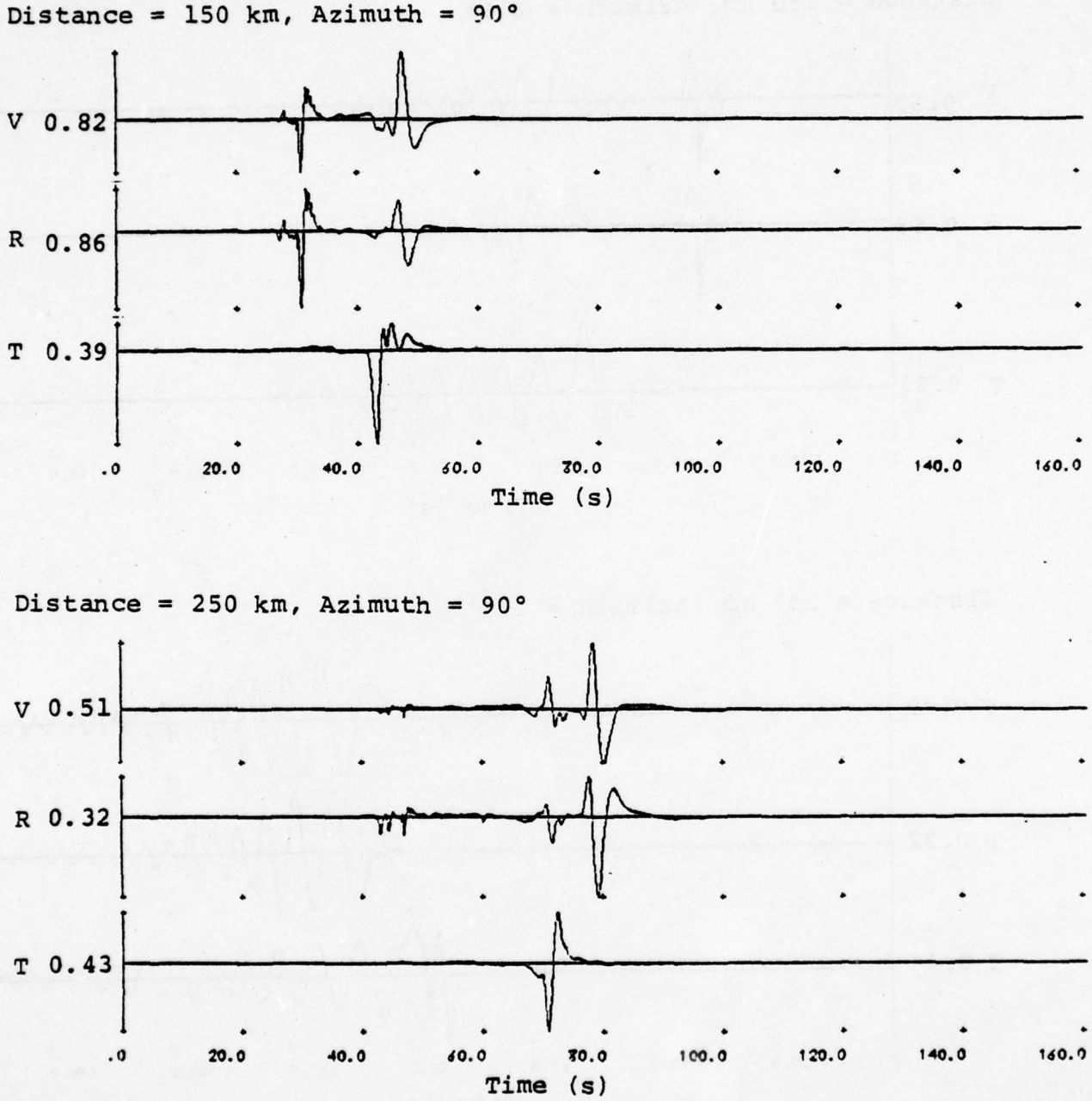

Figure B.3. Displacement seismograms from Pocatello source model and Structure B path model.

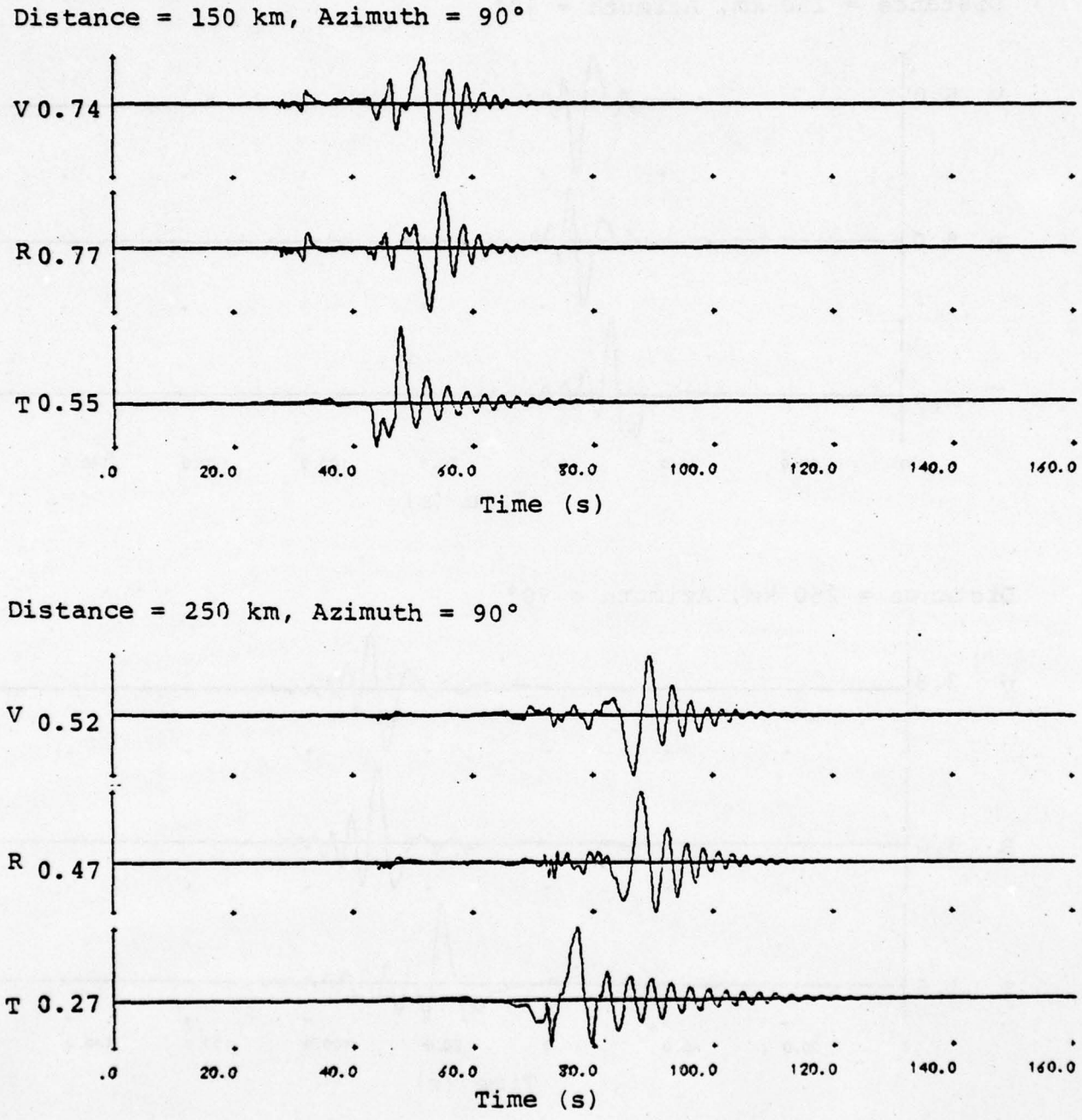

Figure B.4. Displacement seismograms from Pocatello source model and Structure C path model.

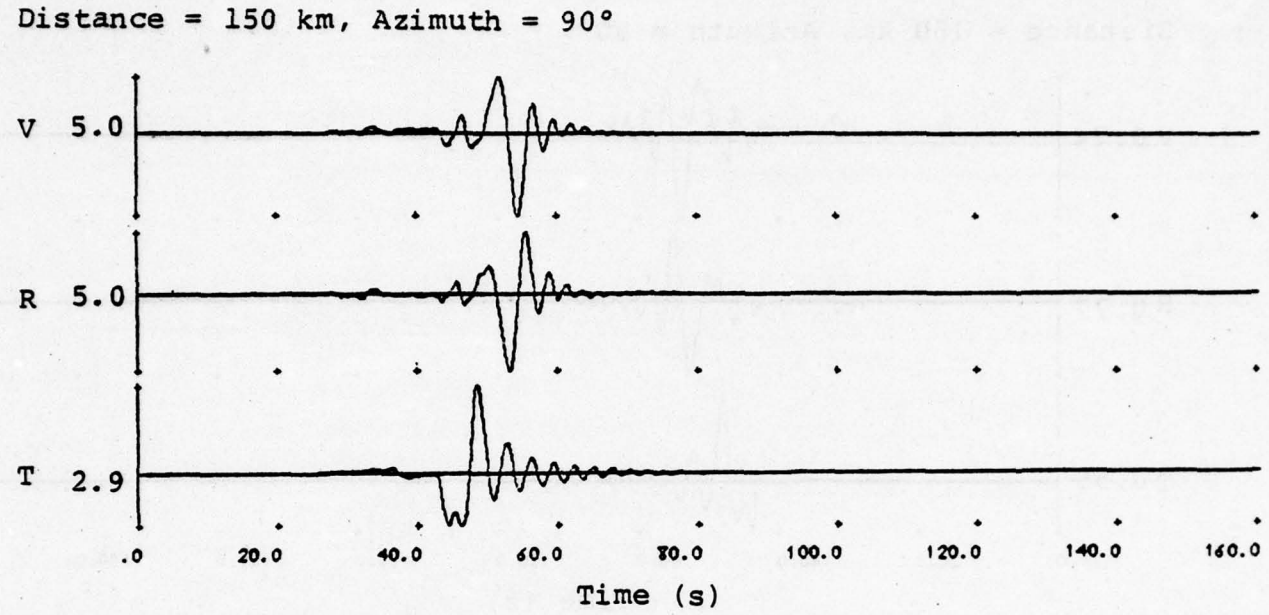

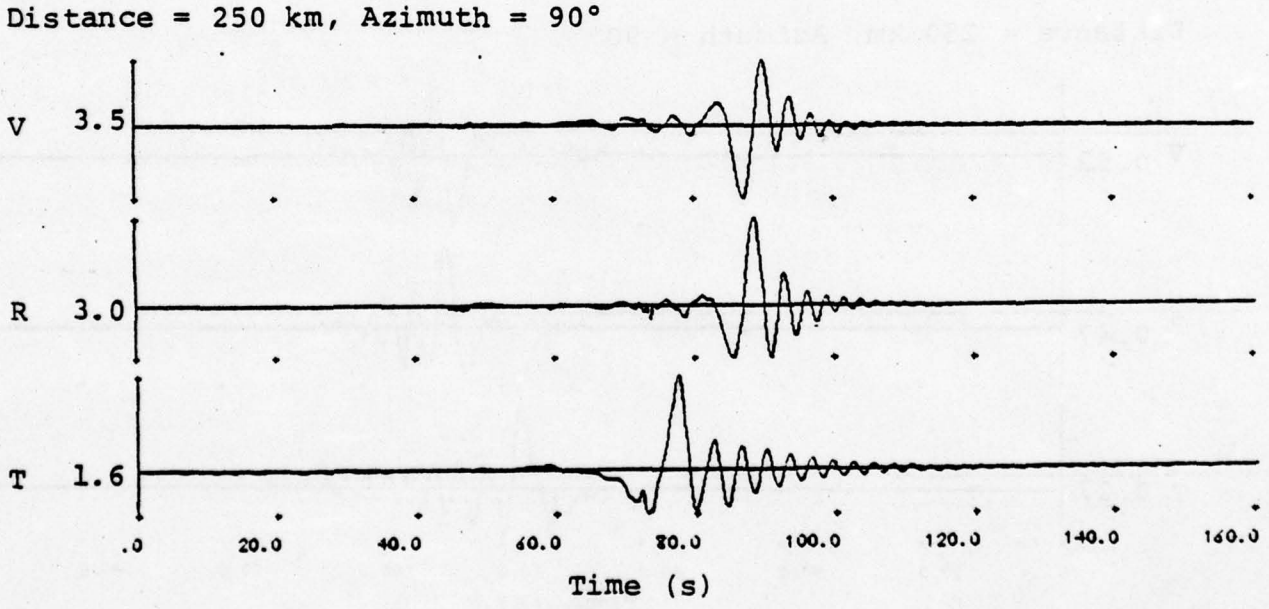

Figure B.5. Displacement seismograms from M_S = 7 source model and Structure C path model.

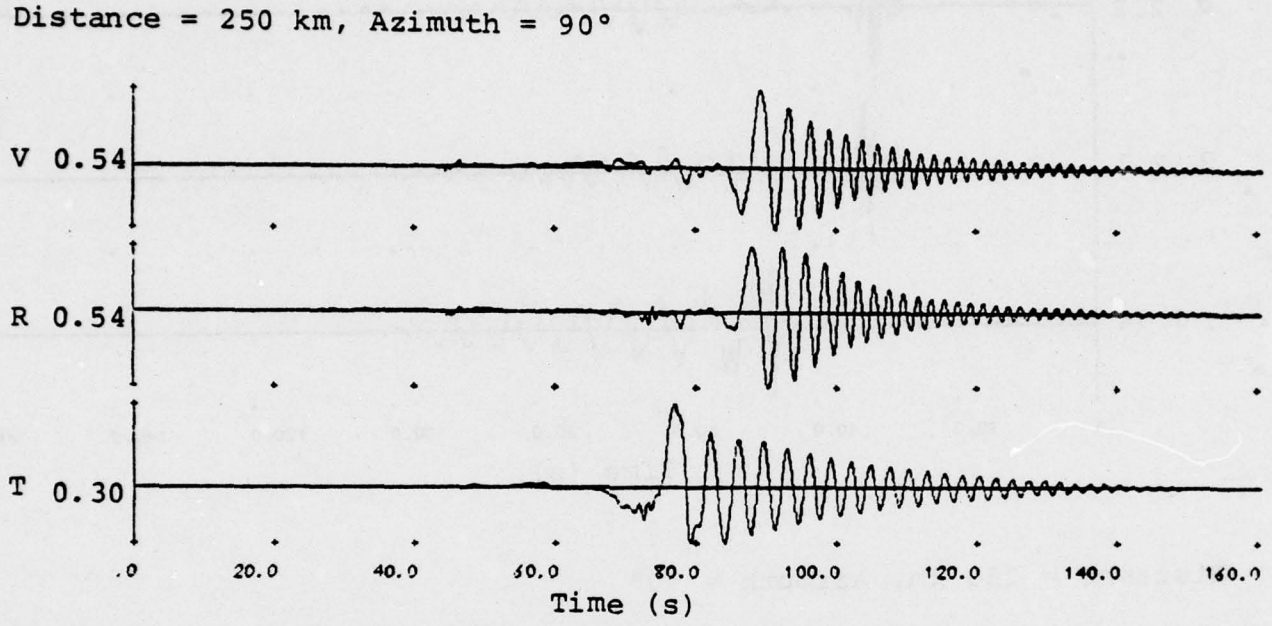

Figure B.6. Displacement seismograms from Pocatello source model at a depth of 5.0 km and Structure C path model.

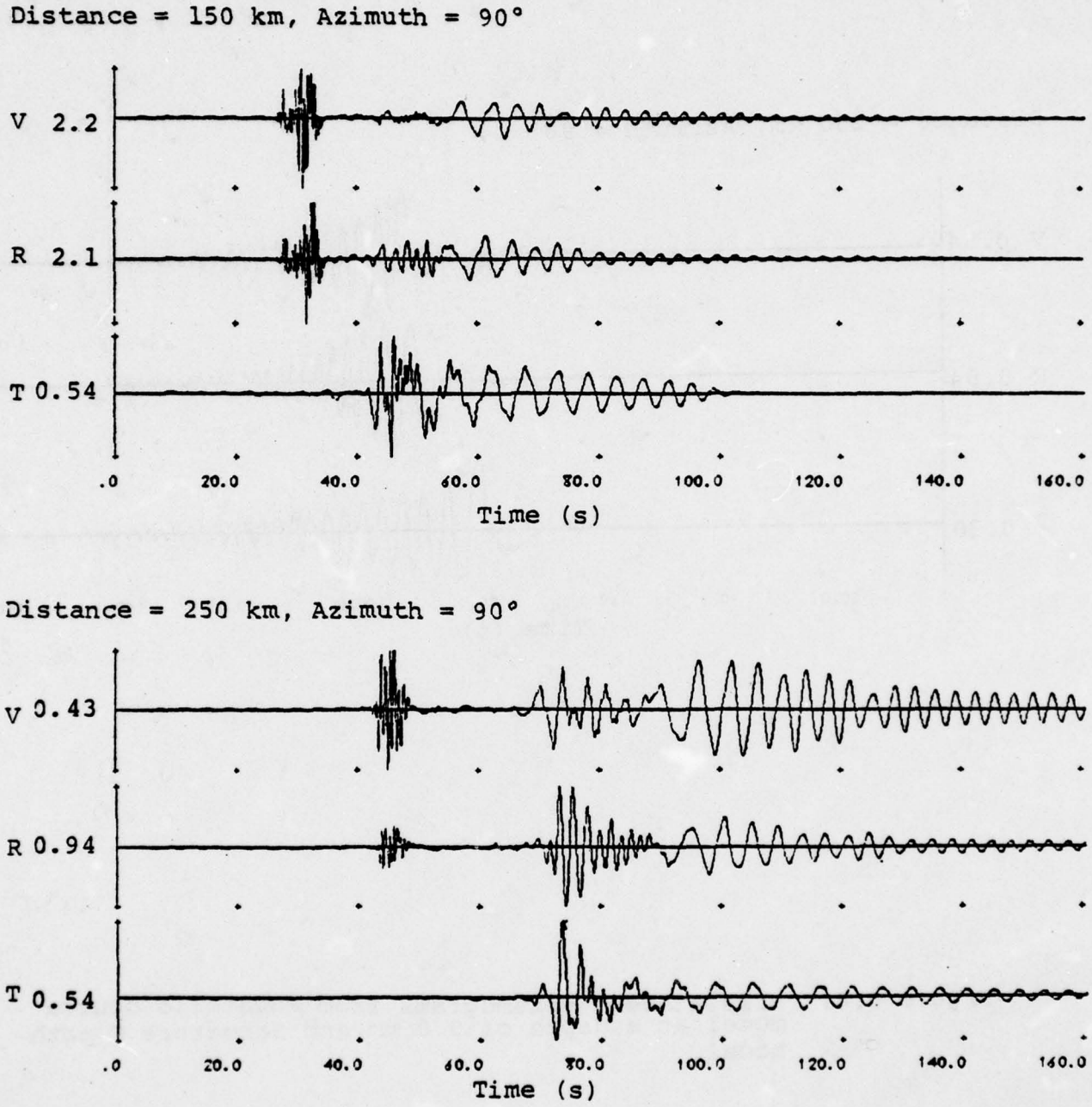

Figure B.7. Velocity seismograms from Pocatello source model and Structure A path model.

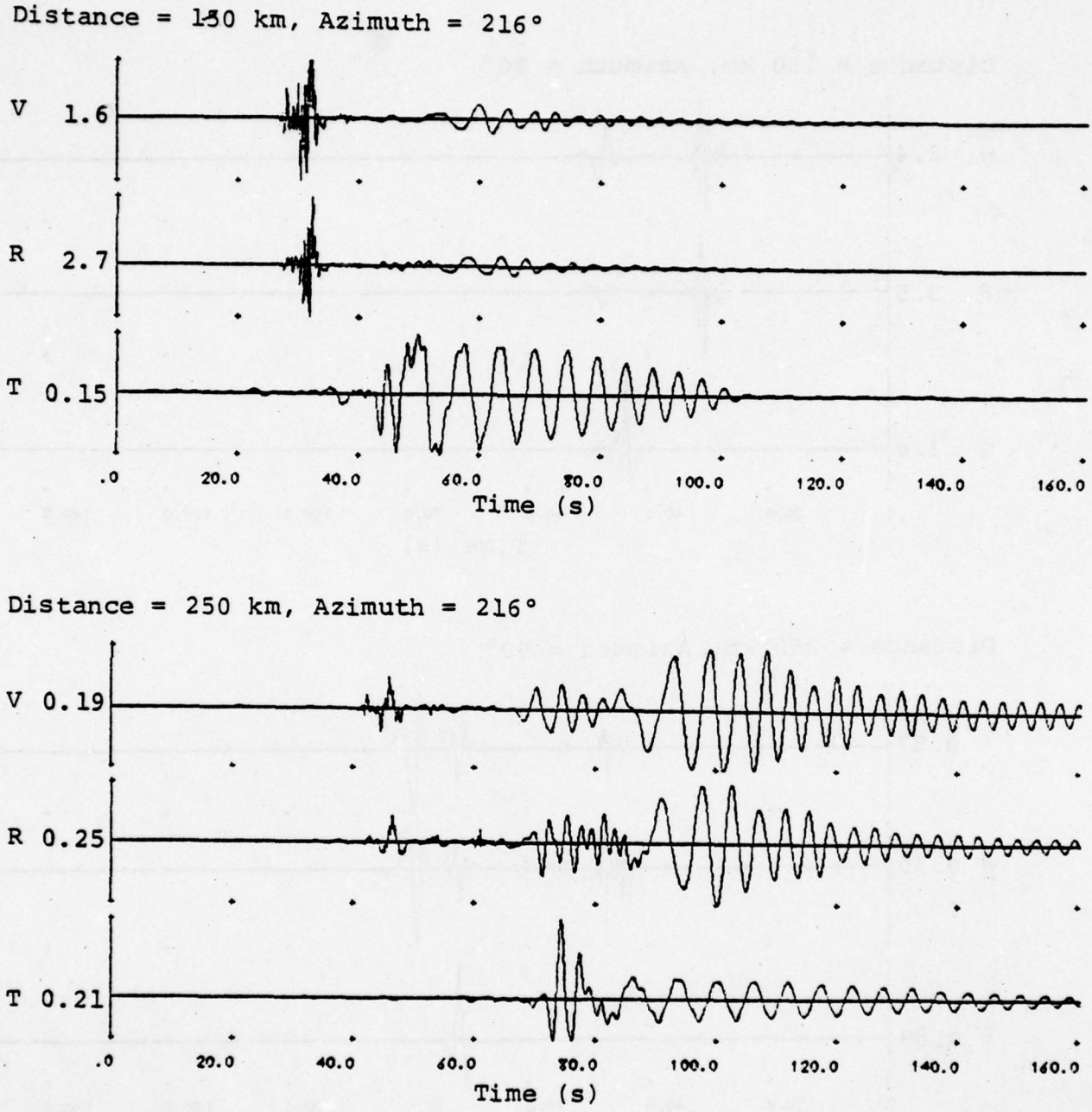

Figure B.8. Velocity seismograms from Pocatello source model and Structure A path model.

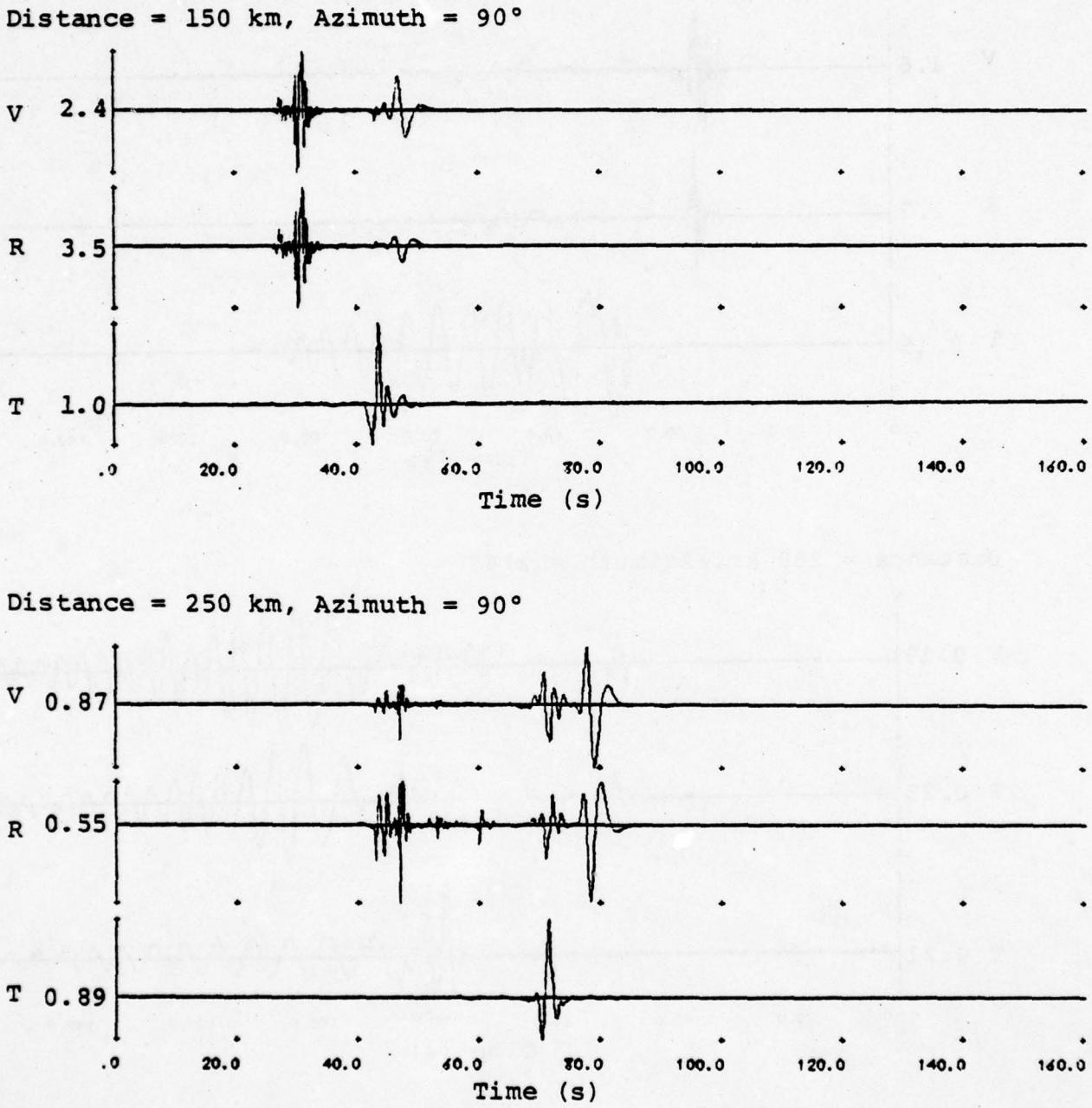

Figure B.9. Velocity seismograms from Pocatello source model and Structure B path model.

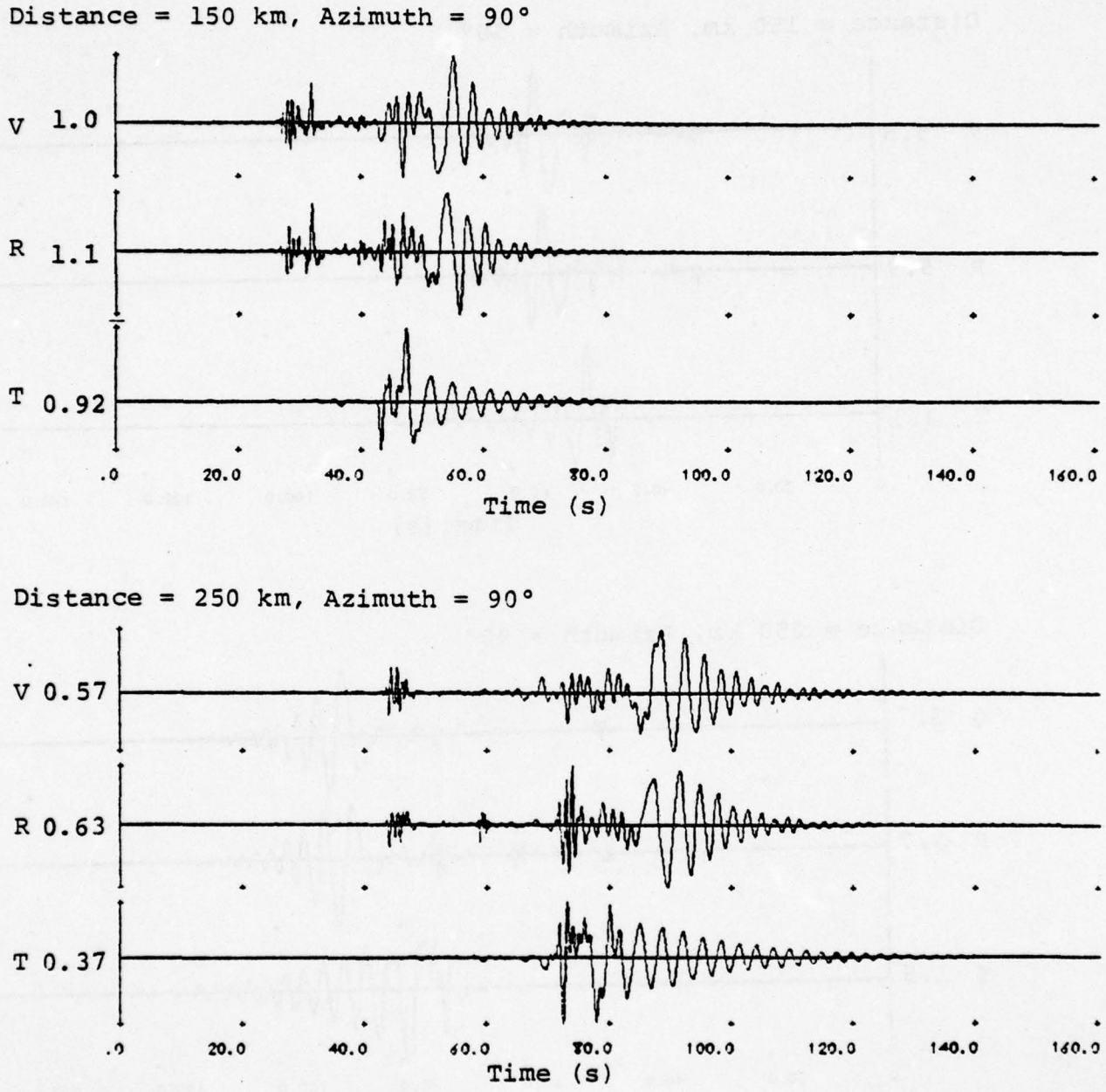

Figure B.10. Velocity seismograms from Pocatello source model and Structure C path model.

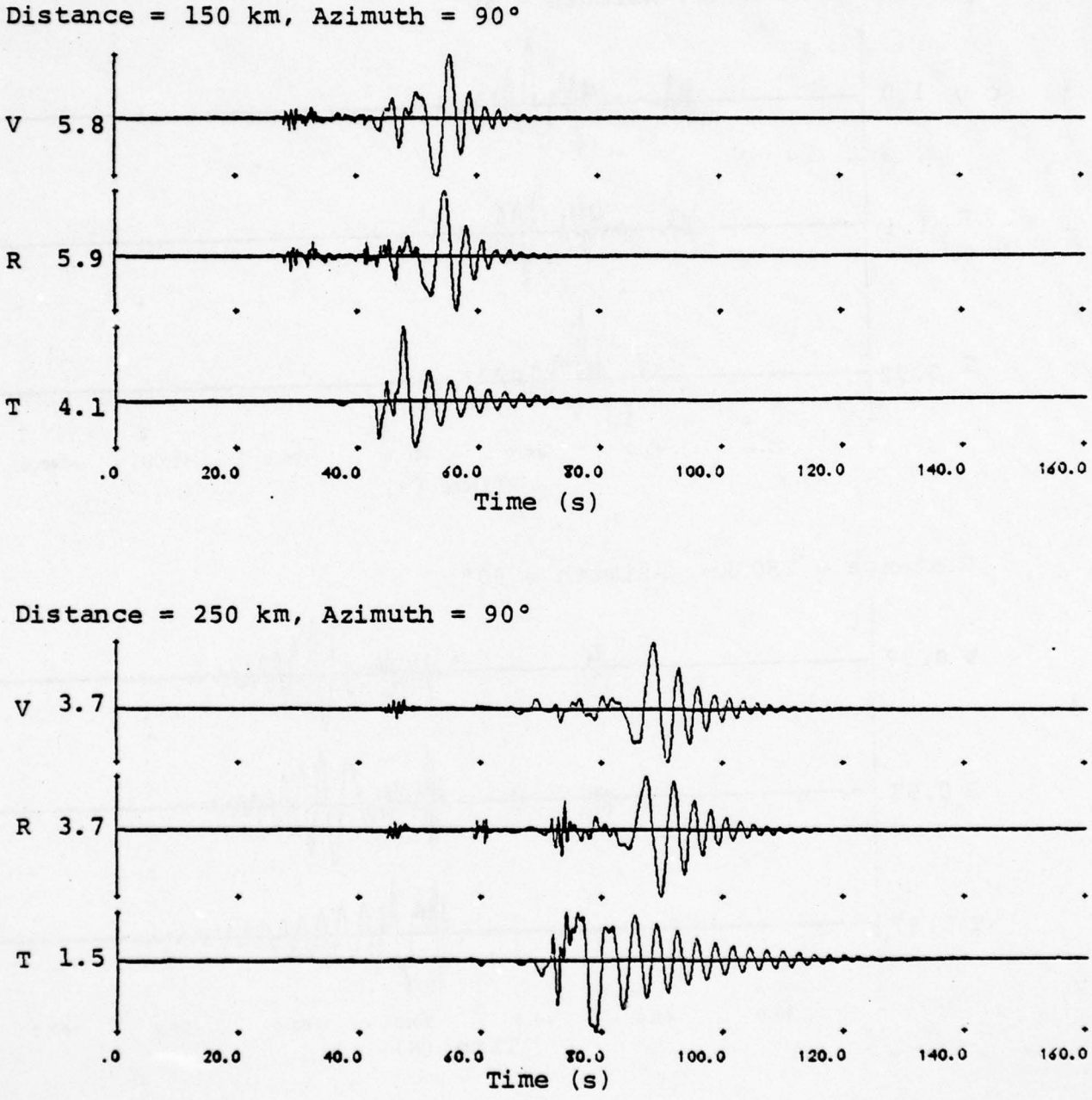

Figure B.11. Velocity seismograms from M_S = 7 source model and Structure C path model.

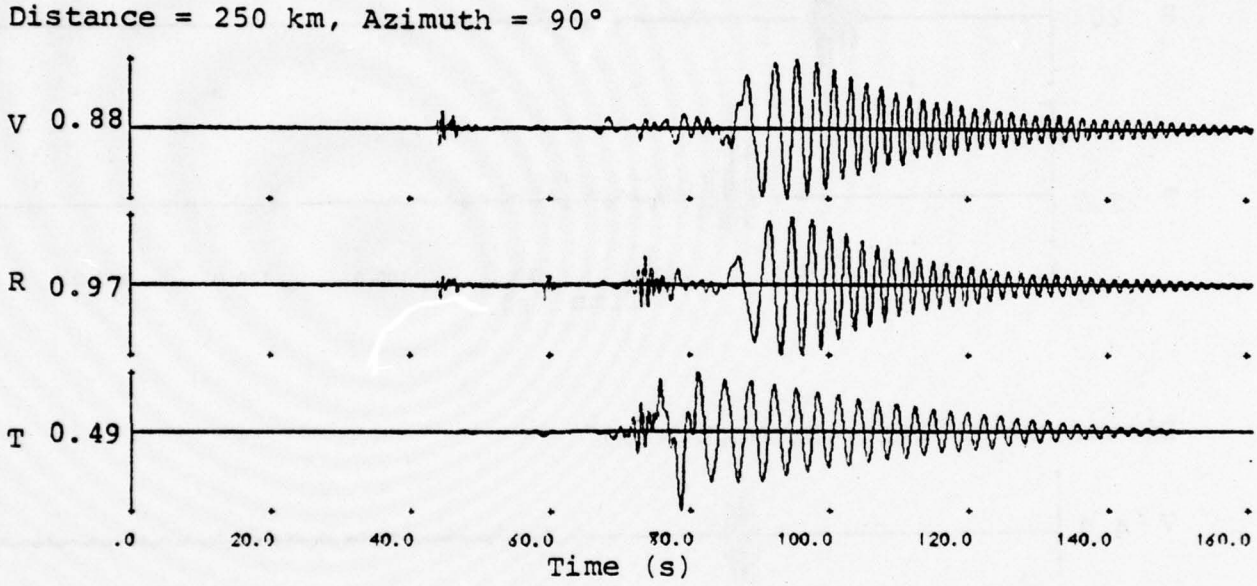

Figure B.12. Velocity seismograms from Pocatello source model at a depth of 5.0 km and Structure C path model.

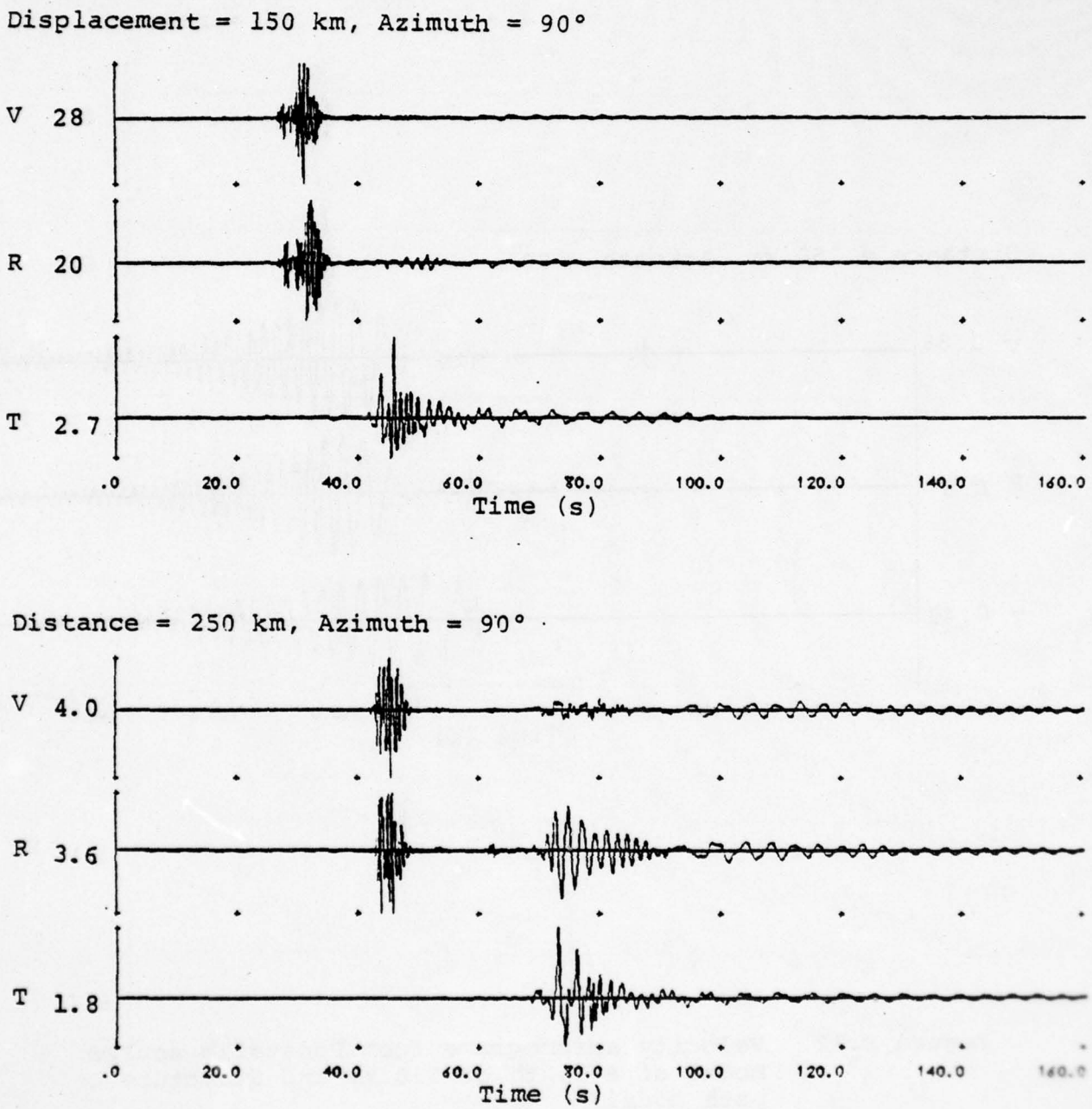

Figure B.13. Acceleration seismograms from Pocatello source model and Structure A path model.

AD-A069 727 SYSTEMS SCIENCE AND SOFTWARE LA JOLLA CALIF F/G 8/11
SYNTHESIS OF REGIONAL GROUND MOTION FROM WESTERN U. S. EARTHQUA--ETC(U)
MAR 79 W L RODI, T C BACHE, H J SWANGER F19628-77-C-0004
UNCLASSIFIED SSS-R-79-3988 AFGL-TR-79-0080 NL

3 OF 3
AD
A069 727

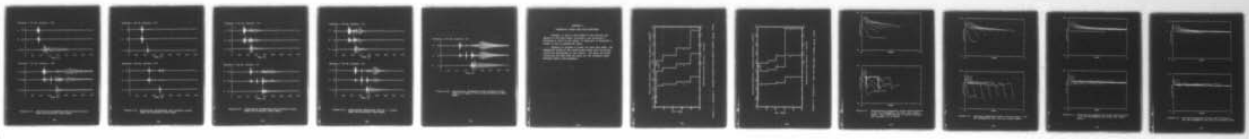

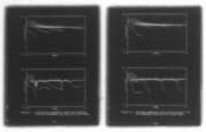

END
DATE
FILMED
7 -79
DDC

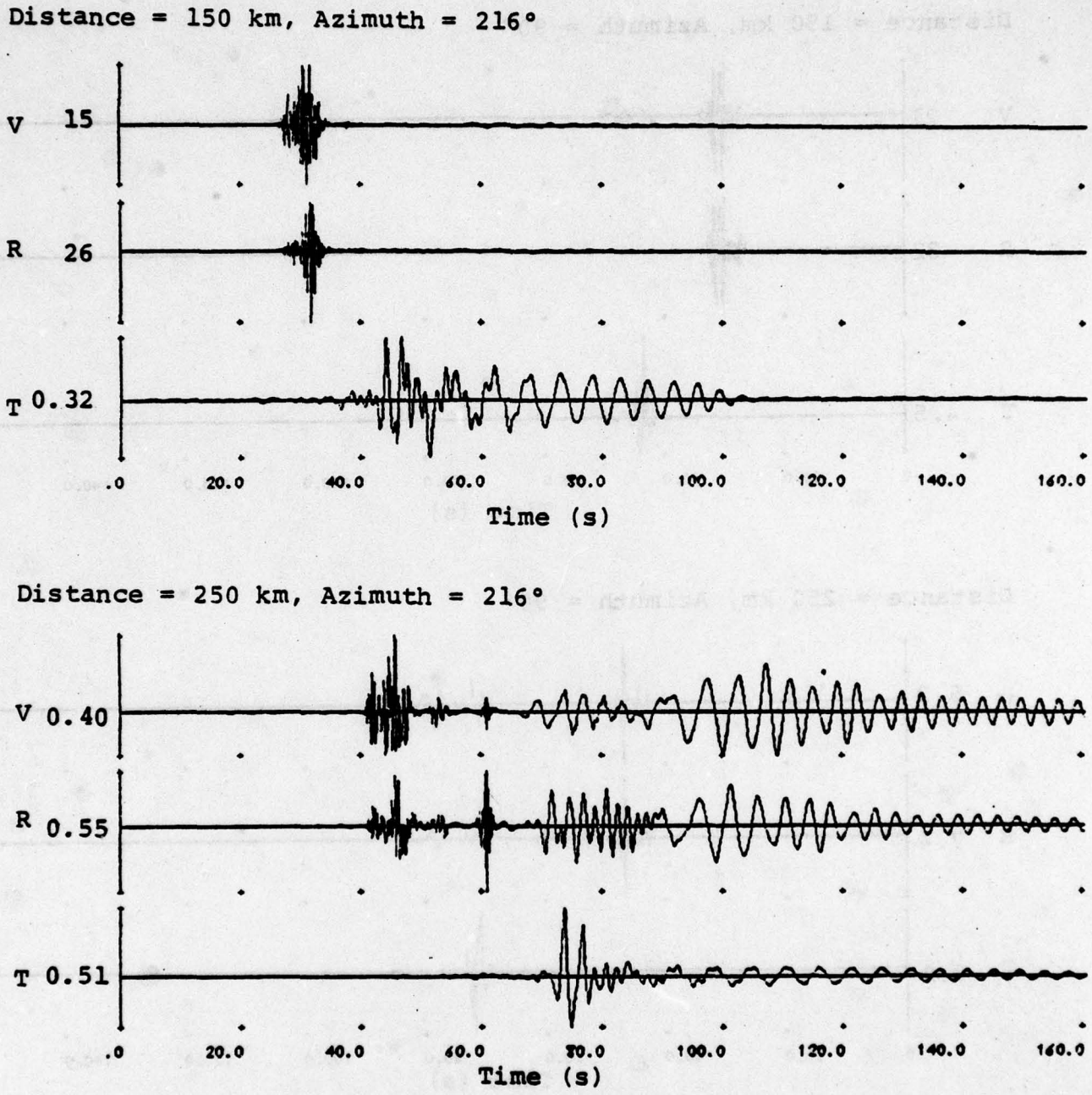

Figure B.14. Acceleration seismograms from Pocatello source model and Structure A path model.

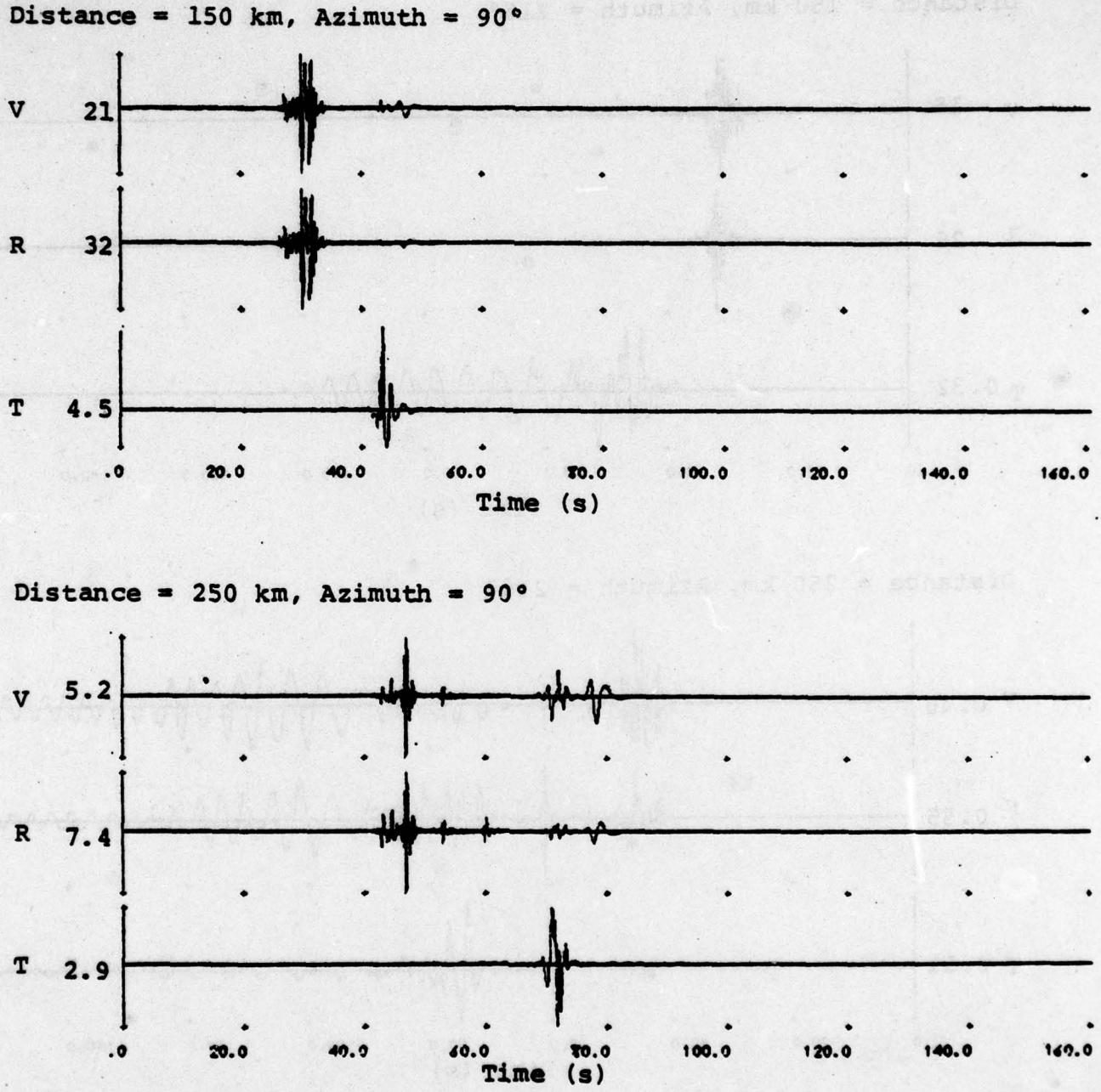

Figure B.15. Acceleration seismograms from Pocatello source model and Structure B path model.

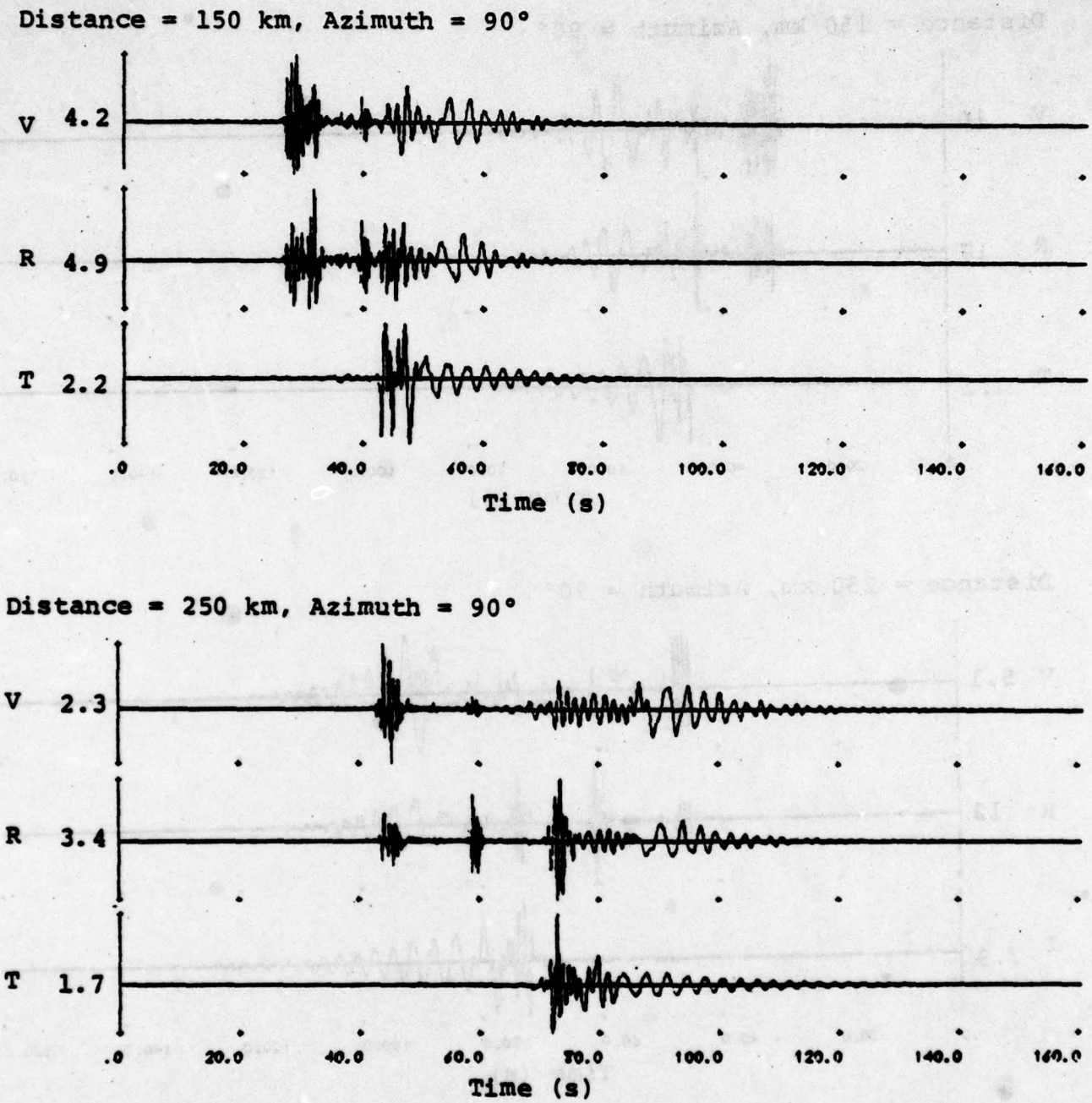

Figure B.16. Acceleration seismograms from Pocatello source model and Structure C path model.

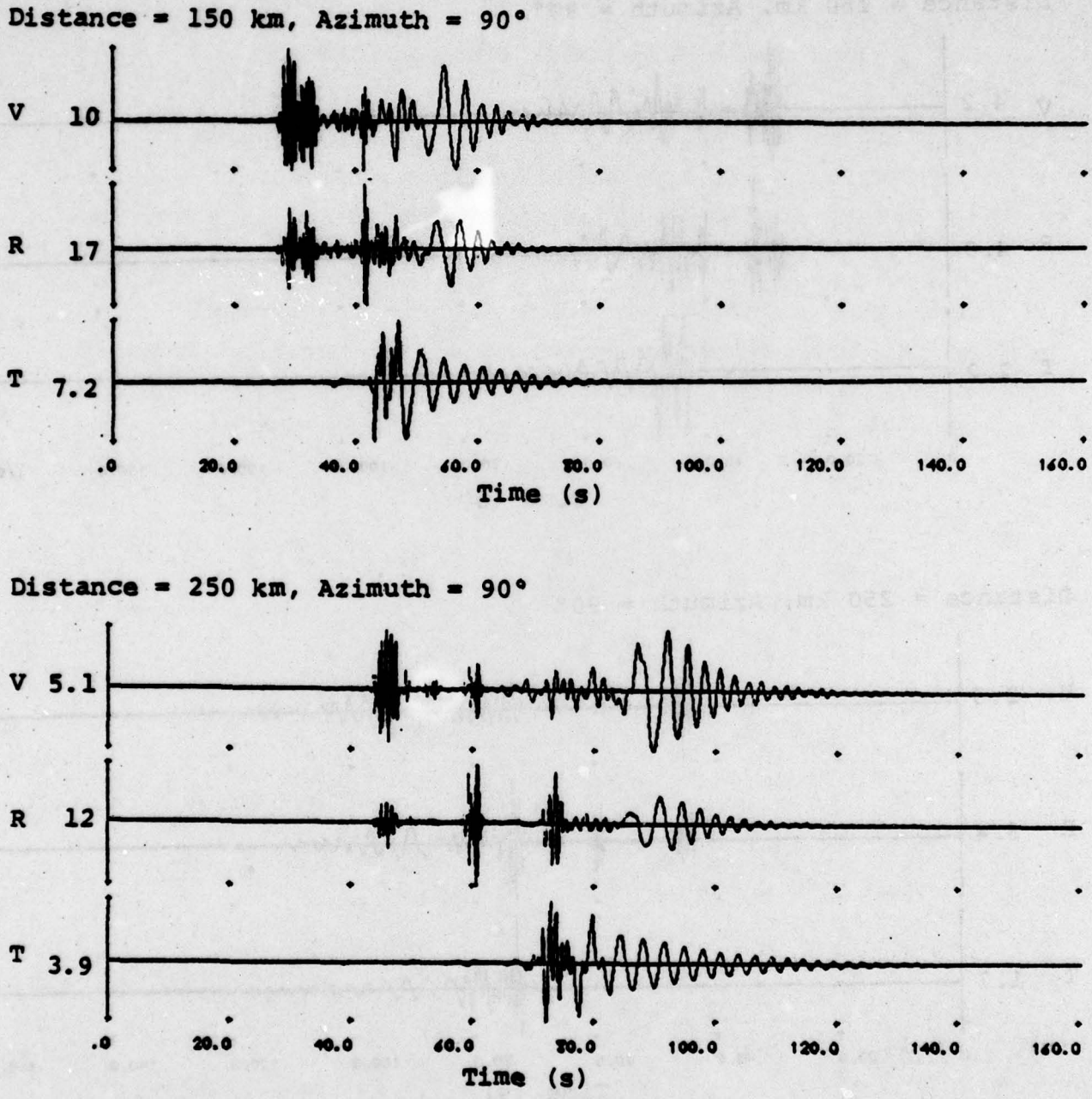

Figure B.17. Acceleration seismograms from M_S = 7 source model and Structure C path model.

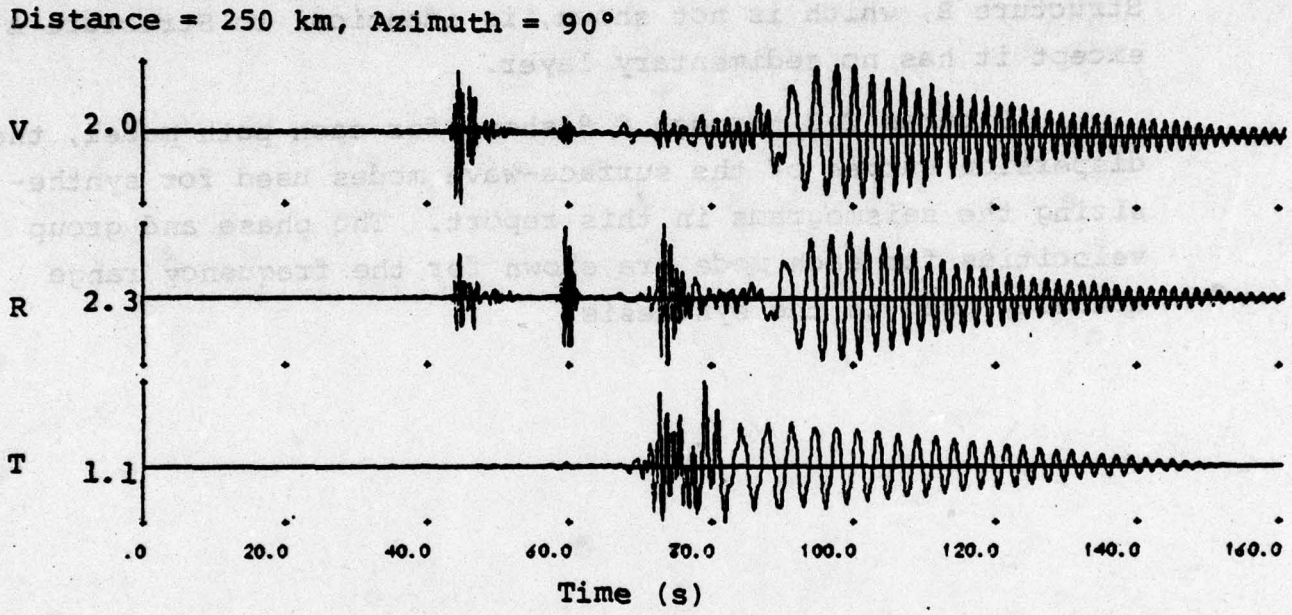

Figure B.18. Acceleration seismograms from Pocatello source model at a depth of 5.0 km and Structure C path model.

APPENDIX C

DISPERSION CURVES FROM PATH STRUCTURES

Figures C.1 and C.2 are graphs of the velocity and density of the path models Structure A and Structure C. Structure B, which is not shown, is identical to Structure A except it has no sedimentary layer.

Figures C.3 through C.8 show, for each path model, the dispersion curves of the surface-wave modes used for synthesizing the seismograms in this report. The phase and group velocities for each mode are shown for the frequency range actually used in the synthesis.

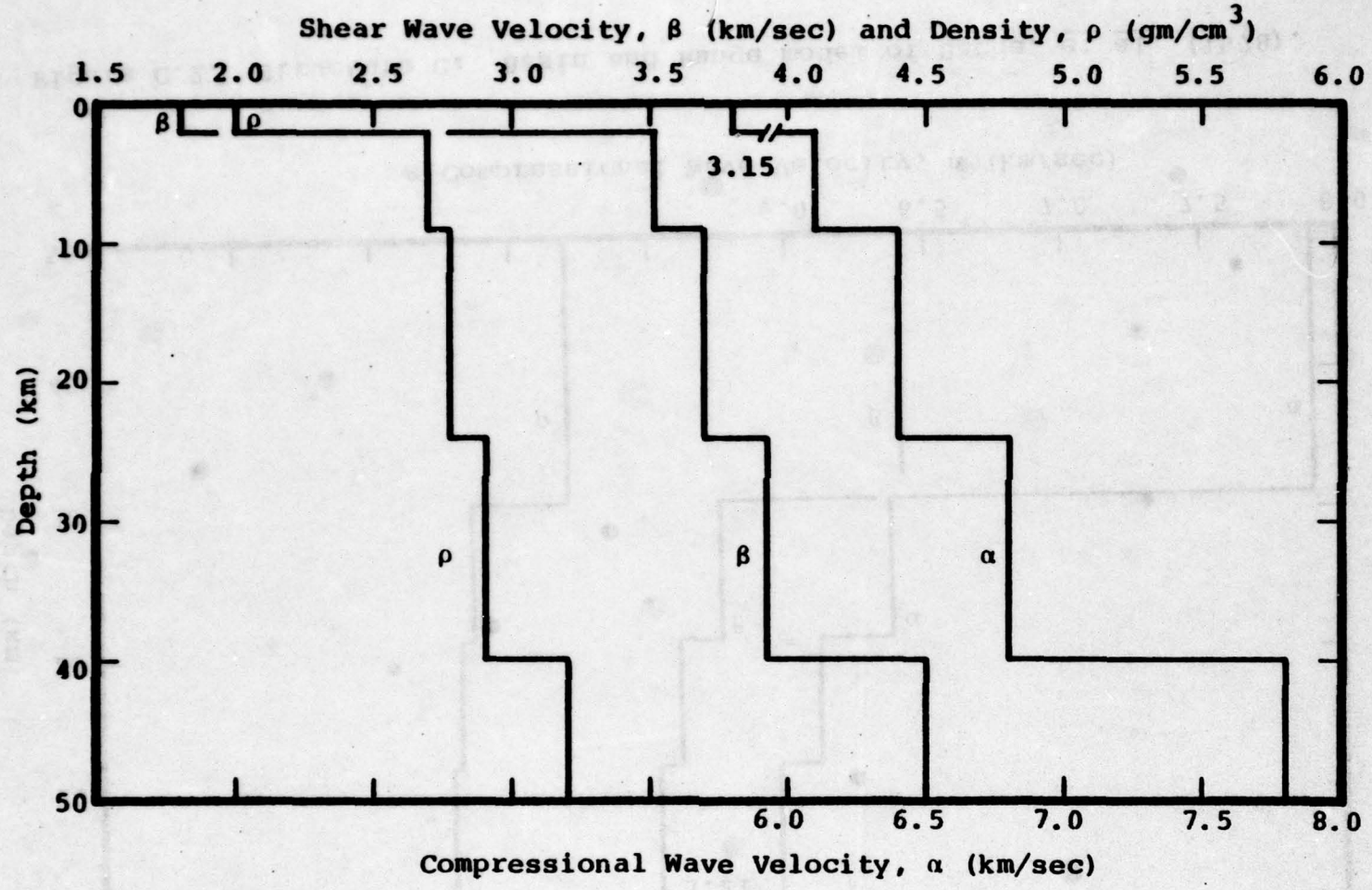

Figure C.1. Structure A: Northern Colorado Plateau model of Keller, et al. (1976).

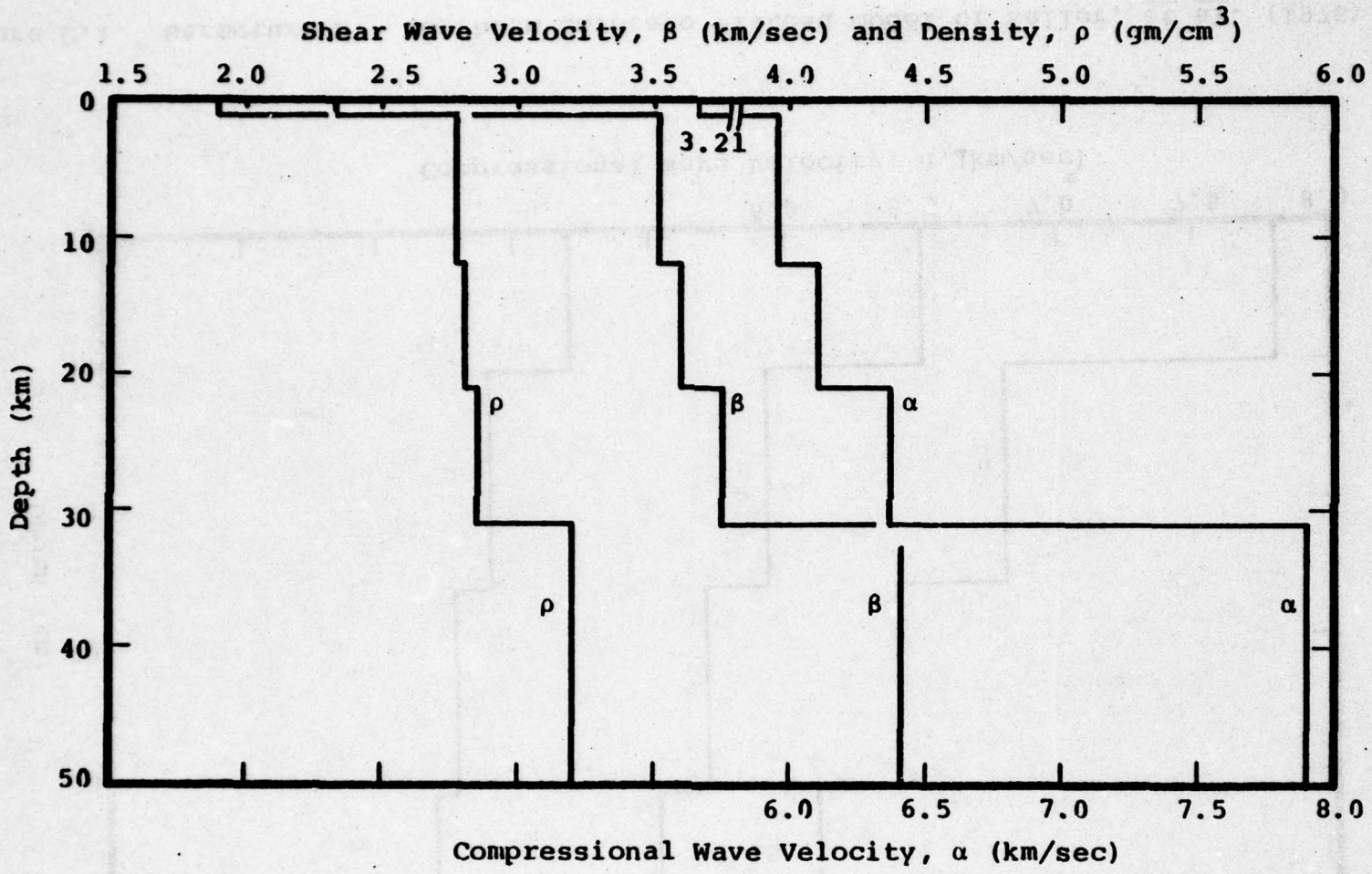

Figure C.2. Structure C: Basin and Range model of Bache, et al. (1978).

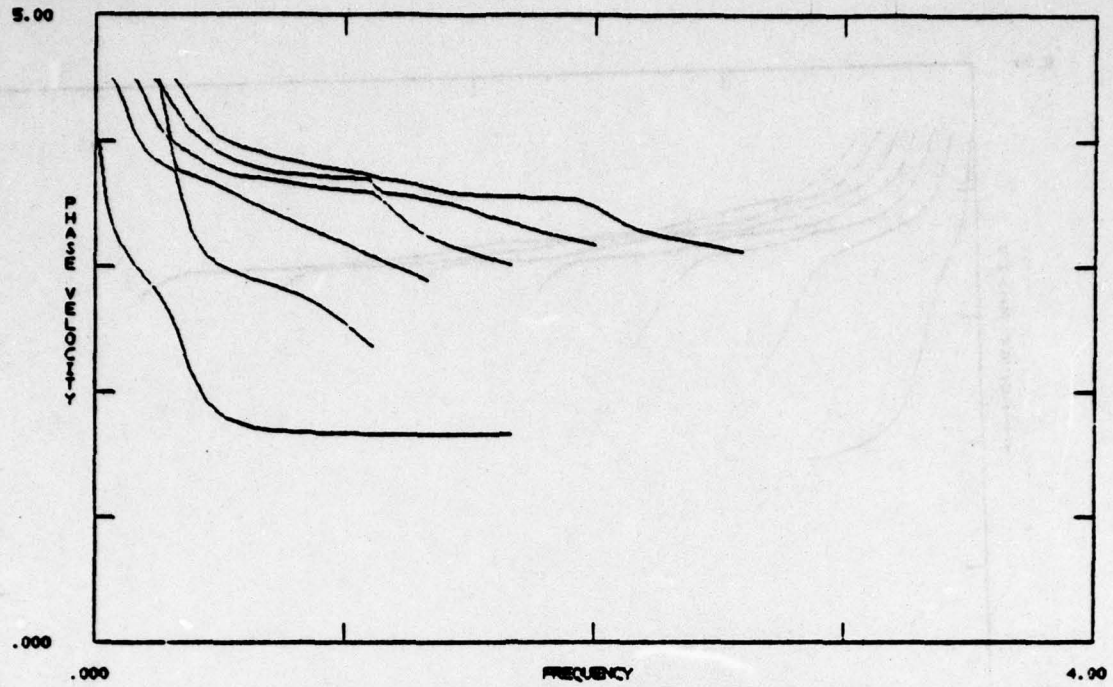

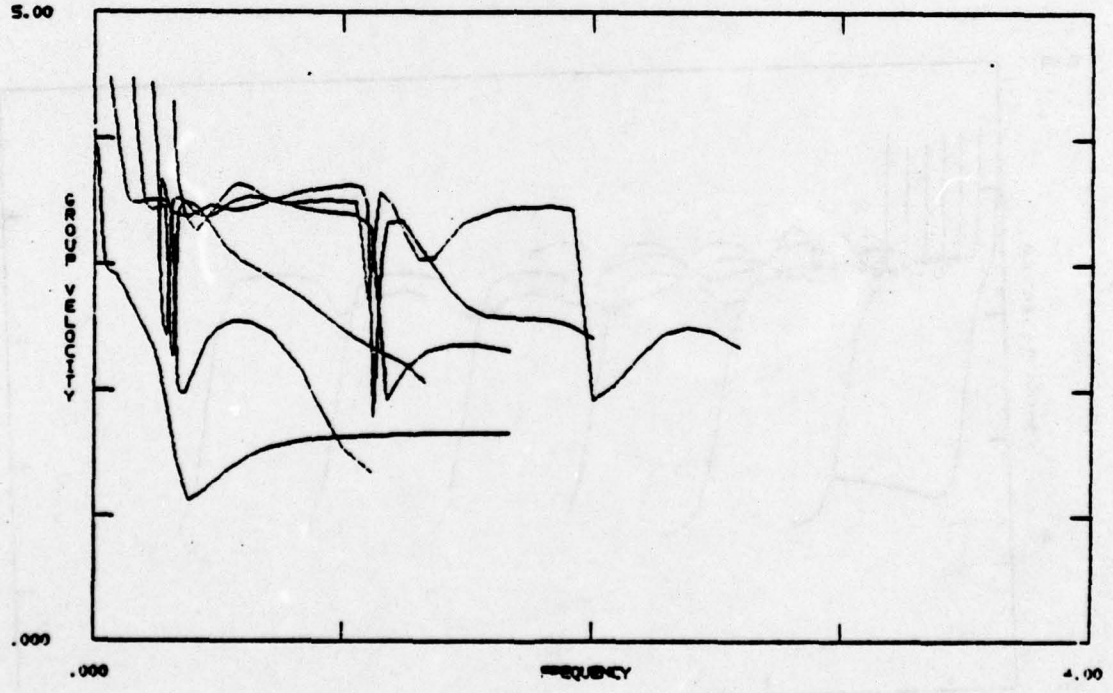

Figure C.3. Rayleigh-wave dispersion curves from Structure A for the fundamental and first five higher modes. The velocities are in units of km/sec and frequency is in hertz.

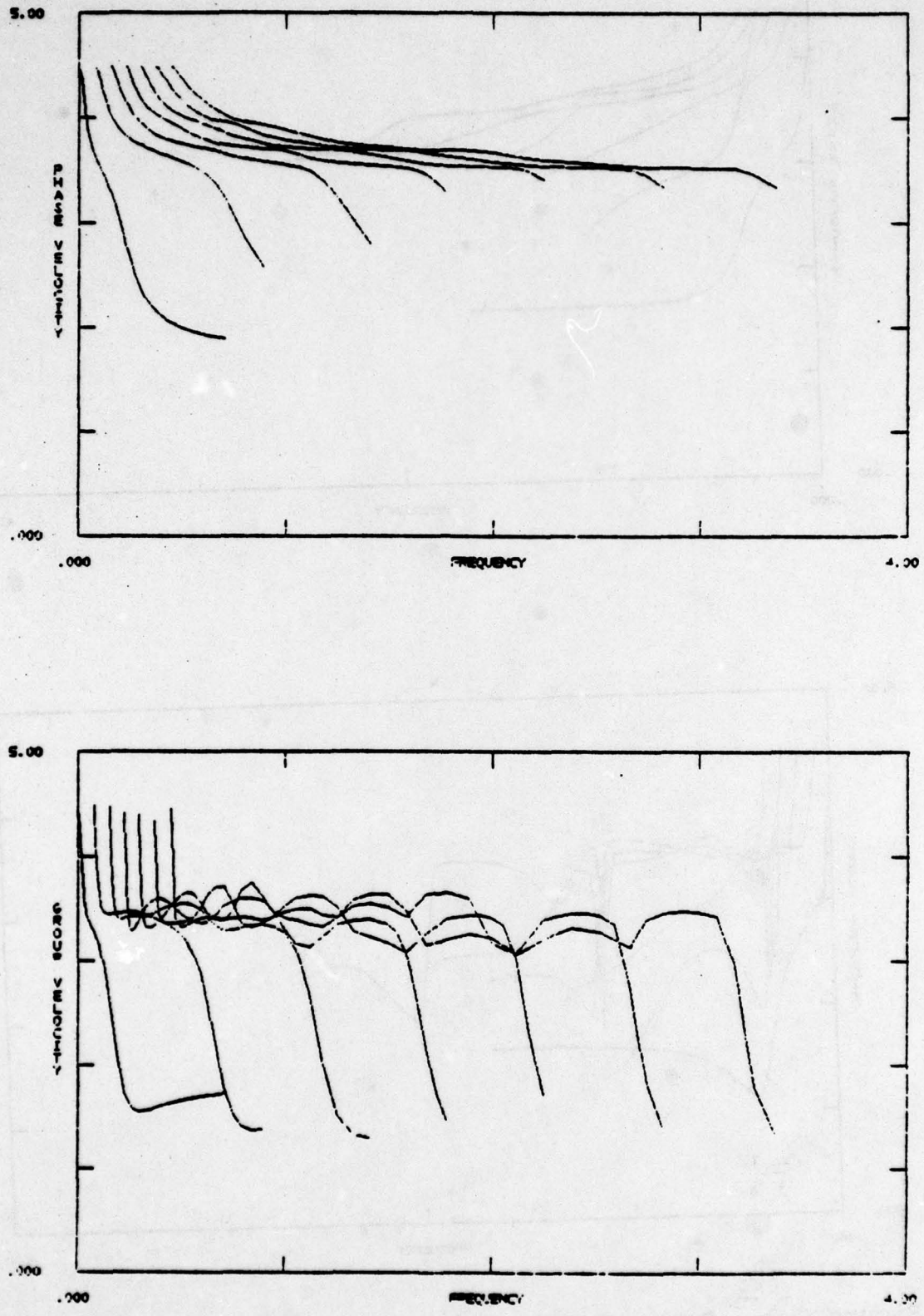

Figure C.4. Love-wave dispersion curves from Structure A for the fundamental and first six higher modes.

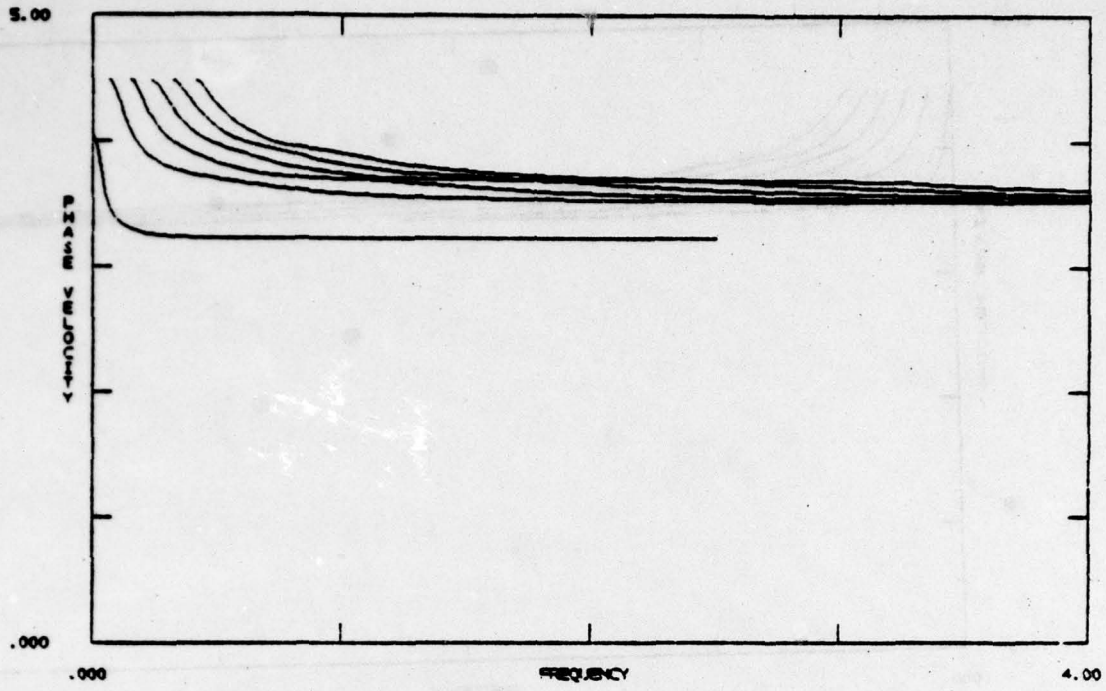

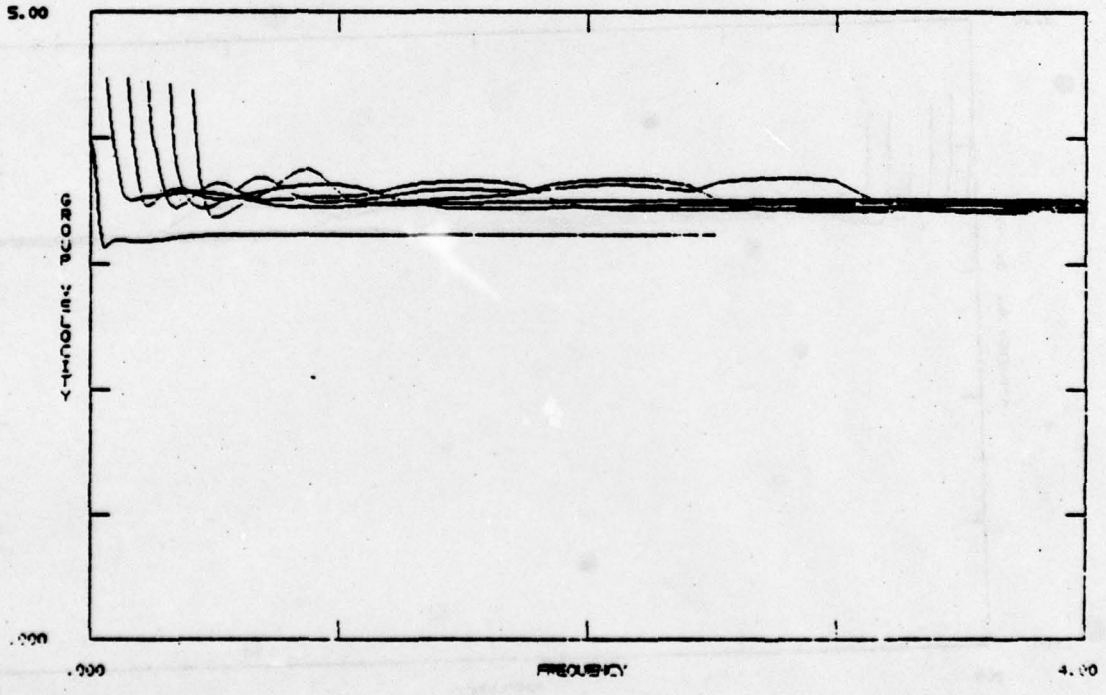

Figure C.5. Rayleigh-wave dispersion curves from Structure B for the fundamental and first five higher modes.

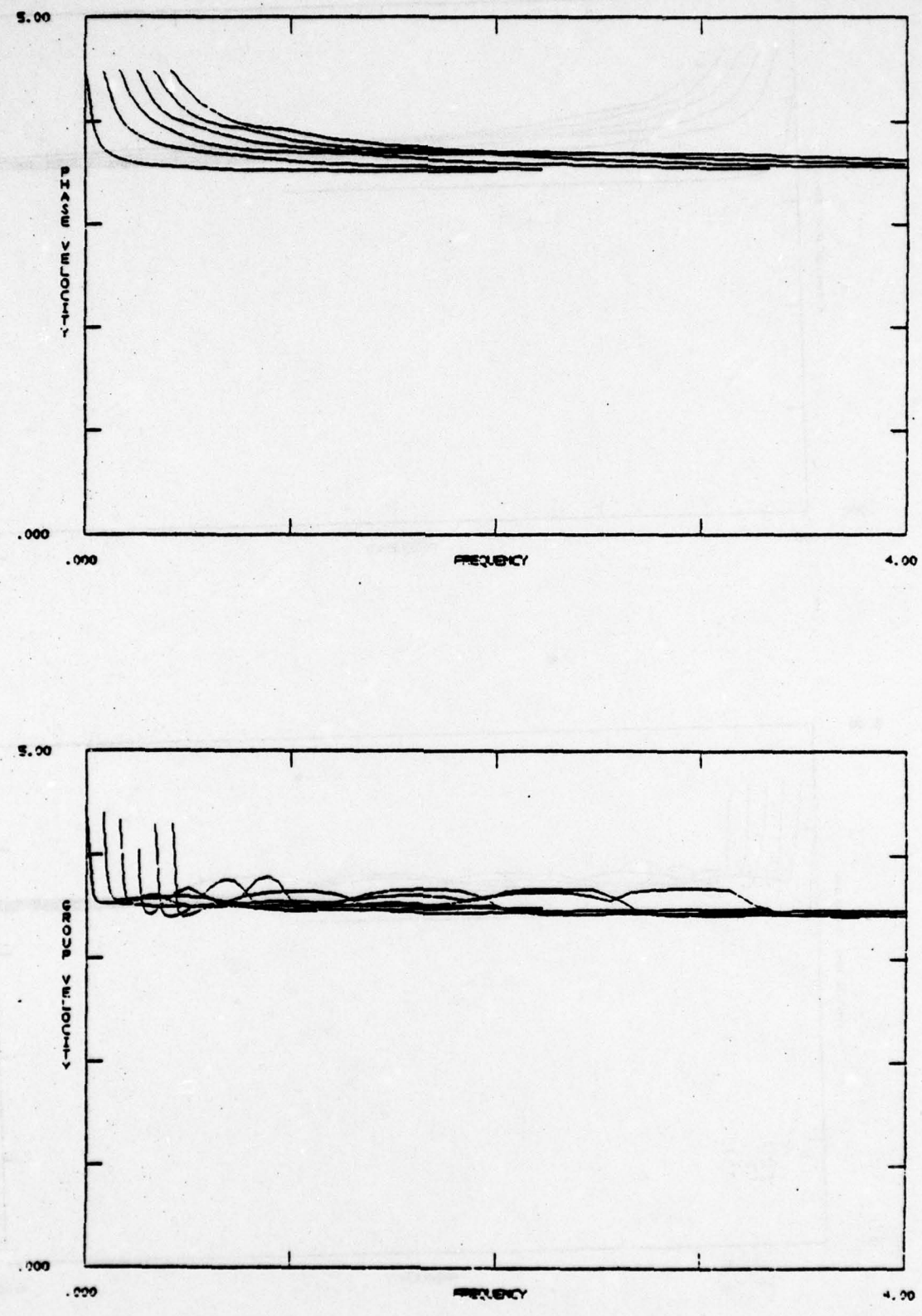

Figure C.6. Love-wave dispersion curves from Structure B for the fundamental and first five higher modes.

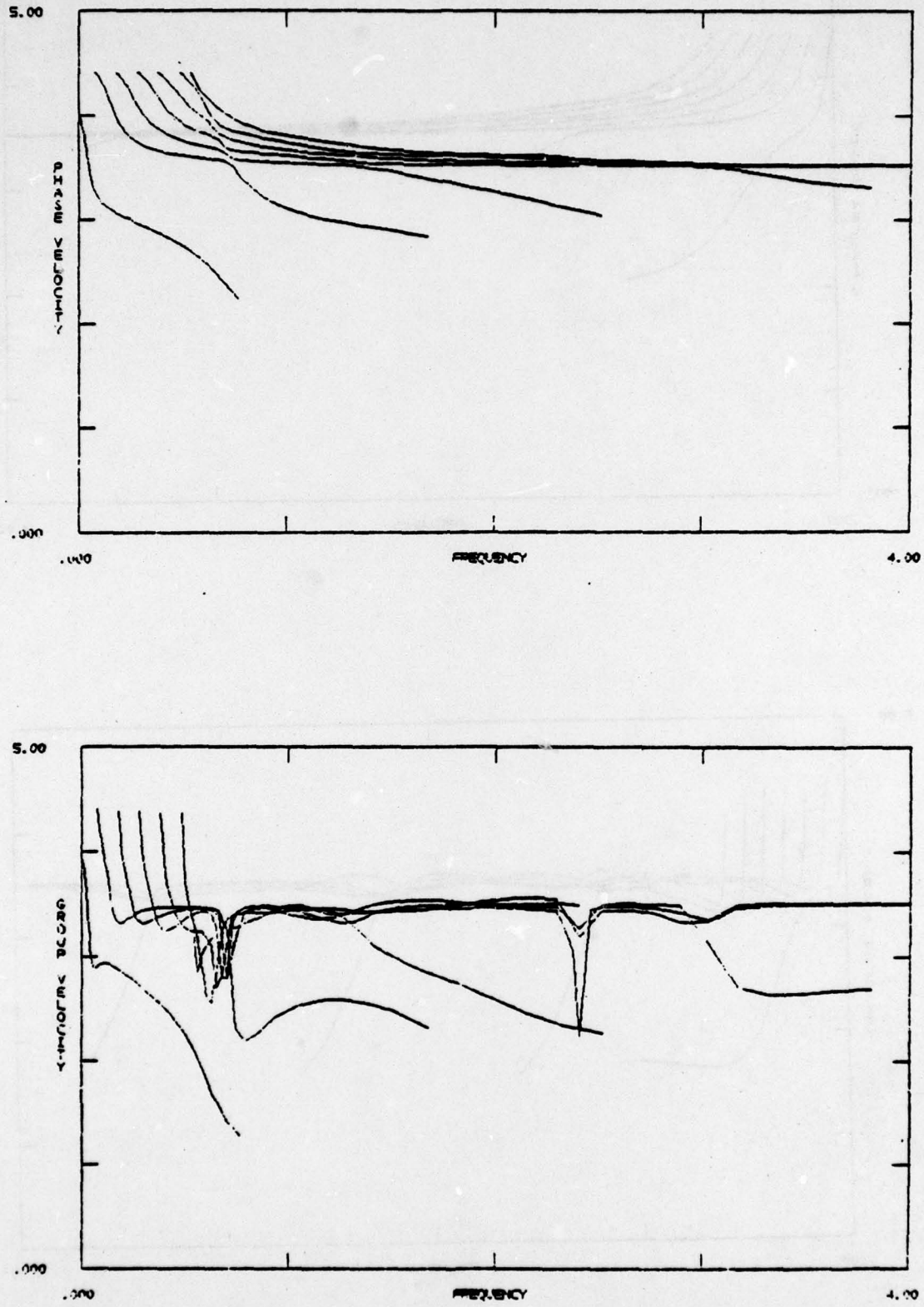

Figure C.7. Rayleigh-wave dispersion curves from Structure C for the fundamental and first six higher modes.

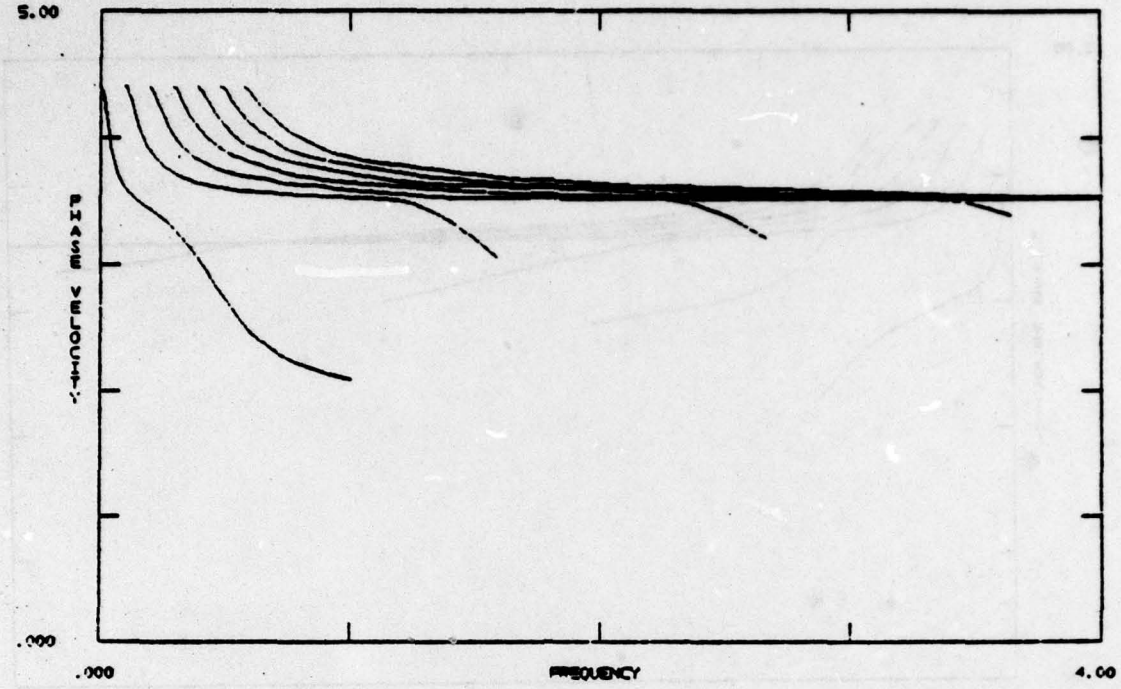

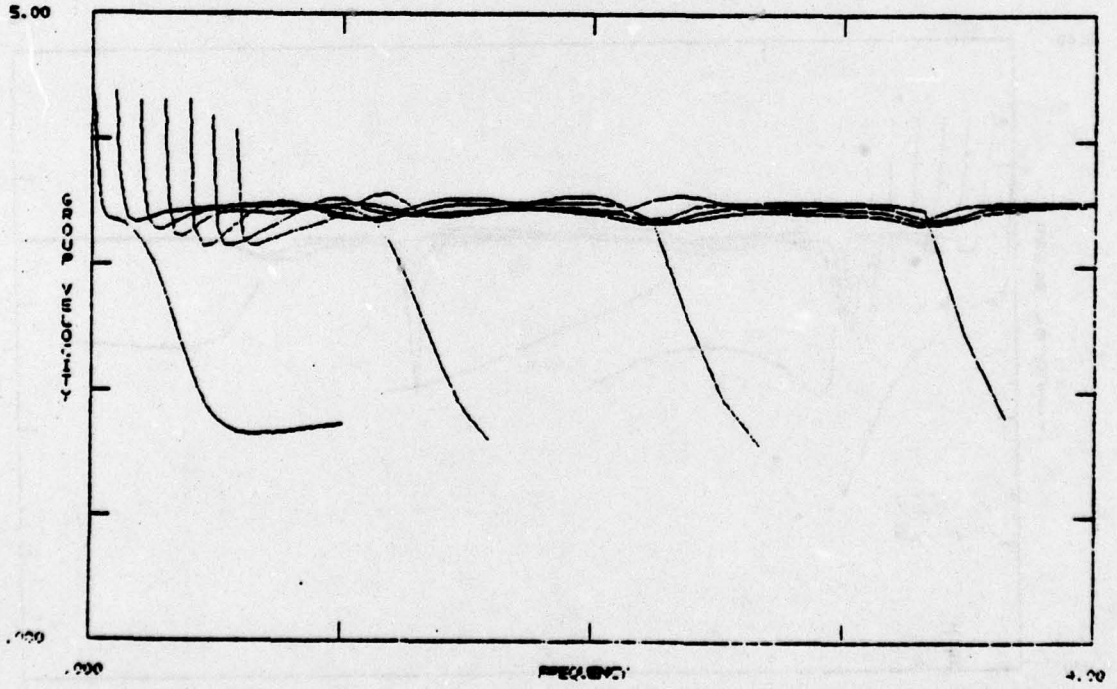

Figure C.8. Love-wave dispersion curves from Structure C for the fundamental and first six higher modes.